ENCLOSURE 2

MFN 07-452

NEDO-32177, Revision 3, August 2007, *TRACG Qualification*,

Non-Proprietary Version

IMPORTANT NOTICE

This is a non-proprietary version of Enclosure 1 to MFN 07-452, which has the proprietary information removed. Portions of the enclosure that have been removed are indicated by an open and closed brackets as shown here [[   ]]

Licensing Topical Report

TRACG Qualification

J.G.M. Andersen
Y.K. Cheung
J. R. Fitch
J. M. Healzer
C.L. Heck
L.A. Klebanov
J.C. Shaug
B.S. Shiralkar

Legal Notice

This document was prepared by GE-Hitachi Nuclear Energy Americas LLC (GEH). The use of this information for any purpose(s) other than that for which it is intended, is not authorized; and with respect to any unauthorized use, GEH makes no representation or warranty, expressed or implied, as to the completeness, accuracy, or usefulness of the information contained in this document, or that its use may not infringe privately owned rights, and assumes no responsibility for liability or damage of any kind that may result from such use of this information.

Non-Proprietary Notice

This is a non-proprietary version of the document NEDE-32177P, Revision 3, which has the proprietary information removed. Portions of the document that have been removed are indicated by an open and closed double brackets as shown here [[   ]].

Acknowledgments

CONTENTS

CONTENTS

CONTENTS

CONTENTS

LIST OF FIGURES

LIST OF FIGURES

LIST OF FIGURES

LIST OF FIGURES

LIST OF FIGURES

LIST OF FIGURES

LIST OF FIGURES

LIST OF FIGURES

LIST OF FIGURES

LIST OF FIGURES

LIST OF FIGURES

LIST OF FIGURES

LIST OF FIGURES

LIST OF FIGURES

LIST OF TABLES

LIST OF TABLES

LIST OF TABLES

Abstract

This document provides a description of the qualification of the TRACG code. TRACG is a computer code that can be applied to prediction of boiling water reactor transients ranging from simple operational transients to design basis loss-of-coolant accidents, stability events and anticipated transients without scram. TRACG incorporates a two-fluid thermal-hydraulic model for the reactor vessel and the primary coolant system and a three-dimensional kinetics model for the reactor core. This document describes the qualification of TRACG against separate effects test data, component performance tests, integral system effects tests and plant data. The scope of the TRACG qualification in Revision 3 is limited to cover BWR/2 to 6, ABWR and ESBWR.

1.0   INTRODUCTION

TRACG is a General Electric (GE) proprietary version of the original Transient Reactor Analysis Code (TRAC) [1-1, 1-2]. It is a best-estimate code for analysis of Boiling Water Reactor (BWR) transients ranging from simple operational transients to design basis Loss-Of-Coolant Accidents (LOCAs) and Anticipated Transients Without Scram (ATWS). This report describes the qualification of TRACG against test facility data from separate effects tests, component performance tests, integral effects tests and plant data.

1.1   SCOPE AND CAPABILITIES

TRACG is based on a multi-dimensional two-fluid model for the reactor thermal hydraulics and a three-dimensional neutron kinetics model.

The two-fluid model used for the thermal hydraulics solves the conservation equations for mass, momentum and energy for the gas and the liquid phases. Thus, TRACG does not assume thermal or mechanical equilibrium between the phases. The gas phase may consist of a mixture of steam and non-condensable gases, and the liquid phase may contain dissolved boron. The thermal-hydraulic model includes a multi-dimensional formulation for one component, designated by the mnemonic VSSL, and a one-dimensional formulation for all other components.

The conservation equations for mass, momentum and energy are closed through a set of constitutive correlations for interfacial shear and heat transfer at the gas/liquid and fluid/wall interfaces. The constitutive correlations are flow regime dependent and are assigned to a given interface on the basis of a single flow regime map that is used consistently throughout the code.

In addition to the basic-thermal hydraulic models, TRACG contains a set of component models for such specific BWR components as recirculation pumps, jet pumps, fuel channels, steam separators and dryers.

The kinetics model is consistent with the GE BWR core simulator PANACEA [1-3, 1-4]. It solves a modified one-group diffusion model with six delayed neutron precursor groups. Feedback from the thermal-hydraulic model includes control rod position, moderator density, fuel temperature and boron concentration.

TRACG also contains a control system model capable of simulating the BWR control systems regulating such major parameters as pressure, level and recirculation flow.

The TRACG structure is based on a modular approach. The TRACG thermal-hydraulic model contains modules for such basic components as pipes (PIPE), pumps (PUMP), valves (VLVE), tees (TEE), channels (CHAN), jet pumps (JETP), steam separators (special version of TEE), and the multi-dimensional vessel (VSSL). System simulations are constructed using the component modules as building blocks with no practical restriction on the number of components that may be combined. The number of components, the individual component descriptions and the component interconnections are specified through code input. By appropriate combination of the component modules, TRACG can be used to simulate a wide range of systems, from simple separate effects test facilities to complex BWR plant simulations.

1.2 BACKGROUND

TRAC was originally developed for analysis of Pressurized Water Reactors (PWRs) by Los Alamos National Laboratory (LANL). The first PWR version of TRAC was called TRAC-P1A [1-5]. The development of a BWR version of TRAC started in 1979 as a cooperative effort between GE and Idaho National Engineering Laboratory (INEL). The objective of this cooperation was the development of a version of TRAC capable of simulating BWR Loss-of-Coolant Accidents (LOCAs). The main tasks consisted of modifying the basic models in TRAC for BWR applications and developing models for BWR-specific components. At GE this work was jointly funded by GE, the Nuclear Regulatory Commission (NRC) and the Electric Power Research Institute (EPRI) under the REFILL/REFLOOD and FIST programs. The work culminated in the mid 1980s with the development of TRAC-BD1/MOD1 at INEL [1-6] and TRACB04 at GE [1-7 through 1-13]. These were the first major versions of TRAC having BWR LOCA capability. As a result of the joint development effort, the basic structure and component models in these two BWR TRAC versions were virtually identical. During this phase of development, TRACG was extensively qualified against separate effects test data, component performance data and integral system effects tests simulating BWR LOCAs and transients. Detailed documentation of the qualification is contained in References 1-7, 1-8, 1-9 and 1-13.

The next phase of development of the TRACG BWR version, begun in 1985, focused on the objective of upgrading the capabilities of the code to include transient and ATWS applications. During this phase, the major accomplishments were the implementation of the three-dimensional kinetics model, development of an implicit numerical integration scheme for the thermal-hydraulic model and an improved simulation of the BWR fuel. The result of this development activity, which extended throughout the 1990s, was the code version designated as TRACG. During this phase, TRACG was extensively qualified against transient and stability data from test facilities [1-14] and BWR plants [1-15, 1-16] as well as rod drop tests. A comprehensive description of these qualification studies was provided in Reference 1-17. TRACG was further qualified against a wide range of systems effect, component performance and integral system effects tests performed in support of the development of the ESBWR [1-18, 1-19].

1.3 TRACG QUALIFICATION

As described above, an essential element at each major step of the evolutionary process that has led to the current version of TRACG is the performance of a comprehensive set of qualification studies in which the predictions of the code are compared with test data. This process ensures that the overall predictive capability of the code is maintained as models are upgraded to address findings from previous qualification studies and new features are added to encompass a broader range of applications and to facilitate code usage. The current revision of this report continues that process. It provides a systematic documentation of TRACG qualification that includes an update of most of the qualification studies documented in the previous revision [1-17] along with a substantial set of new cases that extend and enhance the scope of the qualification.

Qualification cases have been added in each of the major qualification categories. (A detailed discussion of these categories is provided in Section 2.) In the separate effects category, the additional cases: (1) extend the range of the void fraction qualification to lower pressures and larger diameter geometries; (2) provide a qualification basis for TRACG prediction of core spray heat transfer; and (3) extend the fuel bundle pressure drop and critical power qualifications to

include the current 10x10 fuel design. In the component category, a set of qualification cases has been added to evaluate the capability of the TRACG mechanistic core spray distribution model. In the integral systems category, qualification studies using data from the ROSA, FIX and GIST test facilities have been added to provide additional support for TRACG LOCA applications. Finally, in the BWR plant category, qualification studies utilizing stability data from Peach Bottom and Nine Mile Point have been added to support the application of TRACG for prediction of plant stability.

1.4 REFERENCES

[1-1]   J. A. Borkowski, et al., TRAC-BF1/MOD1: An Advanced Best Estimate Program for BWR Accident Analysis, NUREG/CR–4356, Idaho National Engineering Laboratory, August 1992.

[1-2]   TRAC-PF1/MOD2 Code Manual: Vol. I Theory Manual (draft), Vol.II User's Guide, Vol. III Programmer's Manual and Vol. IV Developmental Assessments Manual (draft), LA-12301-M (NUREG/CR-5673), Los Alamos National Laboratory, July 1993.

[1-3]   Steady State Nuclear Methods, NEDE-30130PA, April 1985.

[1-4]   S. Richards (NRC) to G. Watford (GE), Amendment 26 to GE Licensing Topical Report NEDE-24011-P-A, "GESTAR II" - Implementing Improved GE Steady State Methods (TAC No. MA6481), MFN-035-99, November 10, 1999.

[1-5]   R. J. Pryor, et al., TRAC-P1A: An Advanced Best Estimate Computer Program for PWR LOCA Analysis, Los Alamos Scientific Laboratory, NUREC/CRA-0665, May 1979.

[1-6]   D. D. Taylor, et al., TRAC-BD1/MOD1: An Advanced Best Estimate Program for Boiling Water Reactor Transient Analysis, Volumes 1-4, NUREG/CR-3633, Idaho National Engineering Laboratory, April 1984.

[1-7]   J. G. M. Andersen, K. H. Chu and J. C. Shaug, BWR REFILL/REFLOOD Program, Task 4.7 - Model Development, Basic Models for the BWR Version of TRAC, GEAP-22051, NUREG/CR-2573, EPRI NP-2375, April 1983.

[1-8]   Y. K. Cheung, V. Parameswaran. and J. C. Shaug, BWR REFILL/REFLOOD Program, Task 4.7 - Model Development, TRAC-BWR Component Models, GEAP-22052, NUREG/CR-2574, EPRI NP-2376, April 1983.

[1-9]   Md. Alamgir, et al., BWR REFILL/REFLOOD Program Task 4.8 - TRAC-BWR Model Qualification for BWR Safety Analysis, Final Report, GEAP-30157, NUREG/CR-2571, EPRI NP-2377, October 1983.

[1-10] J. G. M. Andersen and C. L. Heck, BWR Full Integral Simulation Test (FIST) Program, TRAC-BWR Model Development, Volume 1 - Numerical Methods, GEAP-30875-1, NUREG/CR-4127-1, EPRI NP-3987-1, November 1985.

[1-11] K. H. Chu, J. G. M. Andersen, Y. K. Cheung and J. C. Shaug, BWR Full Integral Simulation Test (FIST) Program, TRAC-BWR Model Development, Volume 2 – Models, GEAP-30875-2, NUREG/CR-4127-2, EPRI NP-3987-2, October 1985.

[1-12] Y. K. Cheung, J. G. M. Andersen, K. H. Chu and J. C. Shaug, BWR Full Integral Simulation Test (FIST) Program, TRAC-BWR Model Development, Volume 3 - Developmental Assessment for Plant Application, GEAP-30875-3, NUREG/CR-4127-3, EPRI NP-3987-3, October 1985.

[1-13] W. A. Sutherland, Md. Alamgir, J. A. Findlay and W. S. Hwang, BWR Full Integral Simulation Test (FIST) Program, Phase II Test Results and TRAC-BWR Model Qualification, GEAP-30876, NUREG/CR–4128, EPRI NP-3988, October 1985.

[1-14] J. G. M. Andersen, et al., Time Domain Stability Analysis with TRACG – Sensitivity to Numerical Method and Qualification to Data, BWR Instability Symposium, Idaho Falls, Idaho, 1989.

[1-15] J. G. M. Andersen, J. K. Garrett and J. C. Shaug, TRACG Analysis of BWR Plant Stability Data, Proceedings from the International Workshop on Boiling Water Reactor Stability, Brookhaven, New York, October 1990.

[1-16] J. G. M. Andersen and J. C. Shaug, TRACS - Best Estimate Simulation in Real Time, SCS Eastern Multiconference, Nashville, Tennessee, April 1990.

[1-17] J. G. M. Andersen, et al., TRACG Qualification, NEDE-32177P, Rev. 2, January 2000.

[1-18] Fitch, J. R., et al., TRACG Qualification for SBWR, NEDC-32725P, Rev. 1 August 2002.

[1-19] Fitch, J. R., et al., TRACG Qualification for ESBWR, NEDC-33080P, Rev. 1, May 2005.

2.0 QUALIFICATION STRATEGY

2.1 SUMMARY

The qualification of TRACG follows a systematic approach consisting of the following major qualification categories:

- *Separate effects tests.* These are well controlled tests that are specifically directed at the qualification of basic models and phenomena. They include: (1) void fraction data to assess interfacial shear and subcooled boiling models; (2) heat transfer data; (3) flow limitation data such as counter current flow limitation (CCFL) and critical flow; (4) pressure drop data to assess wall friction models; (5) critical power data; (6) rod drop test data (from the SPERT test reactor) to assess kinetics modeling; and (7) thermal-hydraulic stability data to assess modeling of such phenomena as density wave propagation. Section 3 contains a detailed description of TRACG qualification against separate effects tests. It is also appropriate to note, in this context, that the TRACG boron reactivity model has been qualified against reactor physics models in the TRACG model report [2-32].

- *Component performance tests.* These tests provide a basis for evaluation of TRACG's ability to predict the performance of specific BWR components. The tests include: (1) jet pump data for forward and reverse flow; (2) steam separator data for phase separation and pressure drop; (3) data for emergency core cooling (ECC) injection and distribution in a BWR upper plenum; and (4) core spray distribution data. Section 4 contains a detailed description of TRACG qualification against component performance tests.

- *Integral system effects tests.* These tests consist of scaled simulations of a BWR. The primary purpose of these tests is to evaluate the integral system performance and the interaction between the various components in the system. These tests include LOCA simulations for jet pump BWRs in the TLTA, FIST, SSTF and ROSA test facilities, for a non-jet pump external pump plant in the FIX facility and for the ESBWR in the GIST facility. Section 5 contains a detailed description of TRACG qualification against integral system effects tests.

- *Standard BWR nodalization.* Based on the nodalization used for TRACG qualification against separate effects, component performance and integral system effects tests, guidelines were developed for nodalization of the various BWR components and regions. These guidelines were used to develop a standard BWR nodalization that is consistent with the nodalization used to evaluate individual models and phenomena. This nodalization is then used for all full-scale BWR simulations. Section 6.0 contains a description of the standard BWR nodalization for both LOCA and transient applications.

- *BWR plant tests.* This category includes transient and stability tests for BWR plants. Section 7.0 contains a detailed description of TRACG qualification against BWR plant tests.

Table 2-1 summarizes the test facilities and experimental data used for TRACG qualification.

Table 2.1-1 TRACG Qualification Data Base

Separate Effects Tests	
Void Fraction	Rod bundle data (FRIGG [2-1], Toshiba [2-2 and 2-3]) Simple geometry data (Christensen [2-4], Wilson [2-5], Bartolomei [2-6], CISE [2-7]). Large D_H data (EBWR [2-8 and 2-9], OHT [2-10 to 2-12]). Level swell data (GE) (PSTF [2-13])
Heat Transfer	THTF (ORNL) [2-14 and 2-15]. CSHT (GE) [2-16 to 2-21]
Counter-Current Flow Limiting (CCFL)	CSHT (GE) [2-22, 2-23]
Critical Flow	Marviken [2-24, 2-25]. PSTF (GE) [2-13] Edwards blowdown [2-26]
Pressure Drop	Full-scale bundle data (GE) [2-27 and 2-28]
Critical Power	ATLAS (GE) [2-29]
Stability / Natural Circulation	FRIGG [2-30]
Kinetics	SPERT [2-31]. Boron reactivity model vs. reactor physics models [2-32]
Component Performance Tests	
Jet Pump	INEL 1/6th scale [2-33]. Full-scale jet pump performance data (Cooper [2-34], LaSalle) [2-35])
Separator	Full-scale separator performance data (GE) [2-36 through 2-39]
Upper Plenum Mixing (ECCS)	SSTF (GE) [2-40 through 2-42]
Upper Plenum Spray Distribution	SSTF (GE) [2-43]
Boron mixing	Vallecitos 1/6th-scale facility [2-44]
Integral System Effects Tests	
Single bundle/full height	TLTA: Boil-off; large break LOCAs (GE) [2-45] FIST: Large break LOCA; small break LOCA; LPCI break (GE) [2-46 through 2-48]. FIX-II: Large and intermediate break LOCAs [2-49 through 2-51]
Multiple bundle/parallel channel	SSTF: Parallel channel effects; refill/reflood (GE) [2-52 through 2-54]. ROSA-III: Large and small break LOCAs [2-55 and 2-56]
ESBWR	GIST: GDCS performance (GE) [2-57 and 2-58]
Plant Data	
Pressurization events	Peach Bottom: Turbine trip tests [2-59] Hatch 2: MSIV closure test
Flow transients	Hatch 2: Two-pump trip test NMP-2: Pump upshift test
Level transients	Leibstadt: Loss of feedwater test
Reactor stability	LaSalle: Core-wide oscillations Leibstadt: Regional oscillations NMP-2: Core-wide oscillations Peach Bottom: Low-flow stability tests [2-59]

2.2 REFERENCES

[2-1] O. Nylund, R. Eklund and R Rydalm, OF–64b. Results of Void Measurements, FRIGG PM-105, June 1970.

[2-2] S. Morooka, T. Ishizuka, M. Iizuka and K. Yoshimura, Experimental Study on Void Fraction in a Simulated BWR Assembly (Evaluation of Cross-Sectional Averaged Void Fraction), Nuclear Engineering and Design 114, pp. 91-98 (1989).

[2-3] T. Mitsutake, S. Morooka, K. Suzuki, S. Tsonoyama and K. Yoshimura, *Void Fraction Estimation within Rod Bundles Based on Three-Fluid Model and Comparison with X-Ray CT Void Data*, Nuclear Engineering and Design **120**, pp. 203-212 (1990).

[2-4] H. Christensen, *Power-to-Void Transfer Function*, ANL6385, July 1961.

[2-5] J. F. Wilson, R. J. Grenda and J. F. Patterson, *Steam Volume Fraction in a Bubbling Two-Phase Mixture*, Trans. Am. Nucl. Soc. 4(2), p 356-357, 1961.

[2-6] G. G. Bartolomei, V. A. Suvorov and S. A. Tevlin, *Hydrodynamics of Steam Generation a Two–Circuit Nuclear Power Plant*, Teploenergetika 10(1), p 52-57, 1963.

[2-7] G. Agostini, A. Era and A. Premoli, Density Measurements of Steam-Water Mixtures Flowing in a Tubular Channel Under Adiabatic and Heated Conditions, CISE-R-291, December 1969.

[2-8] J. F. Matousek, Modification of the EBWR for Higher Power Operation, ANL-6552, April 1962.

[2-9] M. Petrick and E. A. Spleha, Thermal Hydraulic Performance Characteristics of EBWR, ANL 6693, May 1963.

[2-10] H.A. Hasanein, A.M.C. Chan, M. Kawaji and Y. Yoshioka, Steam-Water Two-phase Flow in Large diameter Vertical Piping at High Pressures and Temperatures, 4th JSME/ASME Joint International Conference on Nuclear Engineering, New Orleans, USA, March 1996.

[2-11] A.M.C. Chan, Void Fraction Measurements in Large Diameter Pipes with Thick Metal Walls or Complex Internal Geometries, Proceedings of the National Heat Transfer Conference, 1992, American Nuclear Society, pp. 236-244.

[2-12] A.M.C. Chan and D. Bzovey, Measurement of Mass Flux in High Temperature High Pressure Steam-Water Two-Phase Flow using a Combination of Pitot Tubes and a Gamma Densitometer, Journal of Nuclear Engineering and Design, 1990, Vol. 122, pp. 95-104.

[2-13] J. A. Findlay, BWR Refill-Reflood Program Task 4.8 - Model Qualification Task Plan, General Electric Company, GEAP-24898, August 1981.

[2-14] D. K. Felde, et al., Facility Description-THTF MOD 3 ORNL PWR BDHT Separate-Effects Program, NUREG/CR-2640 (ORNL/TM-7842), September 1982.

[2-15] D. G. Morris, et al., An Analysis of Transient Film Boiling of High Pressure Water in a Rod Bundle, NUREG/CR-2469 (ORNL/NUREG-85), March 1982.

[2-16] J. G. M. Andersen, H. Abel–Larsen and P. Hansen, *CORECOOL – Part IV Verification–Test Run 110*, SHH-12-77, June 1977.

[2-17] J. G. M. Andersen, H. Abel–Larsen and P. Hansen, *CORECOOL – Part IV Verification–Test Run 111*, SHH-10-77, June 1977.

[2-18] J. G. M. Andersen, H. Abel–Larsen and P. Hansen, *CORECOOL – Part IV Verification–Test Run 112*, SHH-11-77, June 1977.

[2-19] J. G. M. Andersen, H. Abel–Larsen and P. Hansen, *CORECOOL – Part IV Verification–Test Run 113*, SHH-21-77, August 1977.

[2-20] J. G. M. Andersen, H. Abel–Larsen and P. Hansen, *CORECOOL – Part IV Verification–Test Run 120*, SHH-13-77, June 1977.

[2-21] J. G. M. Andersen, H. Abel–Larsen and P. Hansen, CORECOOL – Part IV Verification–Test Run 121, SHH-14-77, June 1977.

[2-22] D. D. Jones, Subcooled Counter Current Flow Limiting Characteristic of the Upper Region of a BWR Fuel Bundle, NEDG-23549, July 1977.

[2-23] D. D. Jones and S. S. Dua, General Electric Company Analytical Model for Loss-of-Coolant Analysis in Accordance with 10CFR50 Appendix K; Amendment No. 4 – Saturated Countercurrent Flow Characteristics of a BWR Upper Tieplate, NEDE-20566-4-P, July 1978.

[2-24] The Marviken Full-Scale Critical Flow Test - Third Series, Results from Test 15, MXC-215, Marviken Power Station, Sweden, September 1979.

[2-25] The Marviken Full-Scale Critical Flow Test - Third Series, Results from Test 24, MXC-224, Marviken Power Station, Sweden, September 1979.

[2-26] R. Edwards and T. P. O'Brien, *Studies of Phenomena Connected with the Depressurization of Water Reactors*, Journal of the British Nuclear Energy Society, V. 9, pp 125-135, April 1970.

[2-27] Matzner and D. A. Wilhelmson, Critical Power and Pressure Drop Tests – Step II Fuel Design Standardization Program for BWR/2–5 Reload Fuel, NEDC-31499P, 1987.

[2-28] Critical Power and Pressure Drop Tests of Simulated 10X10 Bundle Designs Applicable to GE14, NEDC-32874P, March 2000.

[2-29] TASC-03A – A Computer Program for Transient Analysis of a Single Channel, NEDC-32084P-A, Rev. 2, July 2002.

[2-30] O. Nylund, et al., Hydrodynamic and Heat Transfer Measurements on a Full-Scale Simulated 36 Rod BHWR Fuel Element with Non-Uniform Axial and Radial Heat Flux Distribution, FRIGG-4, ASEA-ATOM, December 1970.

[2-31] R. K. McCardell, D. I. Herborn and J. E. Houghtailing, Reactivity Accident Test Results and Analyses for the SPERT III E-Core – A Small, Oxide-Fueled,

Pressurized Water Reactor, IDO-17281, AEC Research and Development Report, March 1969.

[2-32] J. G. M. Andersen et al., TRACG Model Description, NEDE-32176P, Rev. 3, April 2006.

[2-33] H. S. Crapo, *One-Sixth Scale Model BWR Jet Pump Test*, Idaho National Engineering Laboratory LTR 20–105, November 1979.

[2-34] G. W. Fitzsimmons, Hydraulic Performance Tests of the Cooper Production Jet Pump, NEDE–13155, February 1971.

[2-35] H. M. Ondang, Hydraulic Performance Test of the LaSalle Production Jet Pump, NEDE–20981, August 1975.

[2-36] Kudirka, Performance of Improved and Original 1965 Product Line Steam Separators, NEDE-13026, July 1969.

[2-37] Kudirka and C. L. Swan, Performance of Production Steam Separators for the 1967 Product Line, NEDE-13060, December 1969.

[2-38] Kudirka and C. L. Swan, Quality Control Tests of Two 1967 Product Line Steam Separators, NEDE-13063, January 1970.

[2-39] H. Choe, Performance of AS-2B Production Steam Separator for BWR/6, NEDE-21242, June 1978.

[2-40] D. G. Schumacher et al., BWR Refill-Reflood Program Task 4.4 – CCFL/Refill System Effects Tests (30° Sector) SSTF System Response Test Results, General Electric Company, (GEAP-22046, NUREG/CR-2568, EPRI NP-2374), March 1982.

[2-41] J. A. Findlay, BWR Refill-Reflood Program Task 4.4 – CCFL/Refill System Effects Tests (30° Sector) Evaluation of ECCS Mixing Phenomena, General Electric Company, (GEAP-22150, NUREG/CR-2786, EPRI NP–2542), December 1982.

[2-42] J. A. Findlay, BWR Refill-Reflood Program Task 4.4 – CCFL/Refill System Effects Tests (30° Sector) Evaluation of Parallel Channel Phenomena, General Electric Company, (GEAP-22044, NUREG/CR-2566, EPRI NP-2373), March 1982.

[2-43] S. A. Sandoz et al., Core Spray Design Methodology Confirmation Tests, NEDO-24712-A, March 1983.

[2-44] Fitch, J. R., et al., TRACG Qualification for SBWR, NEDC-32725P, Rev. 1 August 2002.

[2-45] L. S. Lee, G. L. Sozzi and S. A. Allison, *BWR Large Break Simulation Tests – BWR Blowdown/Emergency Core Cooling Program*, Volumes 1 & 2, General Electric Company, (GEAP–24962-1, NUREG/CR–2229, EPRI NP–1783), March 1981.

[2-46] W. S. Hwang, Md. Alamgir and W. A. Sutherland, *BWR Full Integral Simulation Test (FIST) Phase I Test Results*, (GEAP-30496, NUREG/CR-3711, EPRI NP-3602), November 1983.

[2-47] W. A. Sutherland et al., BWR Full Integral Simulation Test (FIST) Phase II Test Results and TRAC-BWR Model Qualification, (GEAP-30876, NUREG/CR-4128, EPRI NP-3988), October 1985.

[2-48] W. A. Sutherland and W. S. Hwang, BWR FIST Test and Analysis, Proceedings of the USNRC 12th Water Reactor Safety Research Information Meeting (NUREG/CP-0058, Vol. 1), October 22-26, 1984, Gaithersburg, Maryland.

[2-49] L. Nilsson and PA Gustafson, *FIX-II – LOCA Blowdown and Pump Trip Heat Transfer Experiments*, Summary Report for Phase 2: Part 1, Studsvik Technical Report NR-83/238, February 1983.

[2-50] L. Nilsson et al., FIX-II – LOCA Blowdown and Pump Trip Heat Transfer Experiments; Experimental Results from LOCA Test No. 5052, Studsvik Technical Report NR-83/323, March 1984.

[2-51] O. Sandervag and D. Wennerberg, , FIX-II Experimental Results of Test 3025 (ISP-15), Studsvik Technical Report NR-83/283, July 1983.

[2-52] D. G. Schumacher, T. Eckert and J. A. Findlay, BWR Refill–Reflood Program Task 4.4 – CCFL/Refill System Effects Tests (30° Sector) SSTF System Response Test Results, (GEAP–22046, NUREG/CR–2568, EPRI NP-2374), March 1982.

[2-53] J. A. Findlay, BWR Refill-Reflood Program Task 4.4 – CCFL/Refill System Effects Test (30° Sector) Evaluation of ECCS Mixing Phenomena, (GEAP-22150, NUREG/CR-2786, EPRI NP-2542), December 1982.

[2-54] J. A. Findlay, BWR Refill-Reflood Program Task 4.4 – CCFL/Refill System Effects Test (30° Sector) Evaluation of Parallel Channel Phenomena, (GEAP-22044, NUREG/CR-2566, EPRI NP-2373), December 1982.

[2-55] H. Nakamura et al., ROSA-III 200% Double-Ended Break Integral Test Run 926 (HPCS Failure), JAERI-M 84-008, February 1984.

[2-56] Y. Anoda et al., Experiment Data of ROSA-III Integral Test Run 912 (5% Split Break Test without HPCS Actuation), JAERI-M 82-010, February 1982.

[2-57] J.M. Mross, Final Test Report: Testing of the Gravity-Driven Cooling System for the Simplified Boiling Water Reactor, GE Nuclear Energy, NEDO-31680, July 1989.

[2-58] P.F. Billig, Simplified Boiling Water Reactor (SBWR) Program Gravity-Driven Cooling System (GDCS) Integrated Systems Test - Final Report, GE Nuclear Energy, GEFR-00850, October 1989.

[2-59] Transient and Stability Tests at Peach Bottom Atomic Power Station Unit 2 at End of Cycle 2, EPRI NP-564, June 1978.

3.0 SEPARATE EFFECTS TESTS

In this section of the document, the adequacy of the basic TRACG thermal hydraulic models will be assessed using data from a large number of separate effects tests. Test cases were chosen to cover the most important basic models and correlations in TRACG. The test cases include data for void fraction, heat transfer, counter-current flow limitation (CCFL), critical flow, channel pressure drop, channel critical power, thermal hydraulic instability and reactor kinetics. The following is a brief summary of how each of these models is assessed:

- Modeling of interfacial shear is assessed by examining the capability of TRACG to predict void fraction data. The data include single tube data, rod bundle data and data for large hydraulic diameters. The test conditions cover both adiabatic tests, where there is no effect of heat transfer on the void fraction, and heated tests. The tests also cover a wide range of flow conditions, where pressure, flow rate and inlet subcooling have been varied to ensure that all the major flow regimes are covered. The void fraction comparisons are contained in Section 3.1.

- Modeling of wall friction is assessed through pressure drop comparisons. These comparisons, which use data from the ATLAS test facility, include a wide range of flow conditions that cover the major flow regimes. The ATLAS pressure drop comparisons are described in Section 3.5. In addition, the natural circulation tests performed in the FRIGG facility provide an evaluation of the wall friction model in TRACG. The FRIGG natural circulation tests are described in Section 3.7.

- Interfacial heat transfer is difficult to measure directly but the modeling of interfacial heat transfer can be assessed indirectly through its effect on flashing and condensation rates and on thermal non-equilibrium for the gas and liquid phases. Subcooled boiling has been assessed through the void fraction comparisons described in Section 3.1. Flashing occurs in the PSTF level swell tests, which are described in Section 3.1.5, and in the critical flow tests, which are described in Section 3.4. Interfacial condensation heat transfer is important in the CCFL tests described in Section 3.3 and in the upper plenum tests described in Section 4.3. Thermal non-equilibrium conditions occur in these tests as well as in the THTF tests described in Section 3.2. Taken together, these tests cover a wide range of thermodynamic conditions and the major flow regimes which are important for TRACG predictions.

- Modeling of wall heat transfer is assessed on the basis of a large number of tests. It is present in all the heated void fraction tests described in Section 3.1 and in the pressure drop tests described in Section 3.5. Special heat transfer tests are described in Section 3.2. The THTF tests included film boiling heat transfer and the core spray heat transfer (CSHT) tests included thermal radiation heat transfer. In addition, all the LOCA integral system effects tests described in Section 5 provide extensive information on the wall heat transfer models. Boiling transition is assessed in the THTF heat transfer tests described in Section 3.2.1, in the comparisons to ATLAS critical power data described in Section 3.6 and in the LOCA integral system effects tests.

- Flow limitation effects include CCFL and critical flow. Modeling of CCFL and subcooled CCFL breakdown is assessed in Section 3.3 using CSHT CCFL test data; critical flow modeling is assessed in Sections 3.4 and 3.1.5. Flow limitation effects are also present in all the LOCA integral systems tests described in Section 5.

- The capability of TRACG to predict thermal hydraulic instability and the propagation of kinematic void fraction waves is assessed in Section 3.7 through comparisons with data from the FRIGG stability tests.

- The kinetics model is assessed through a comparison to data from the SPERT reactivity insertion test in Section 3.8.

The manner in which TRACG is applied for simulation of the tests described above is an important consideration in assessing the adequacy of the basic thermal hydraulic models. Input modeling strategies have been developed over time and it has been found that it is neither practical nor necessary to perform detailed sensitivity studies for nodalization or time step for each case. Instead, nodalization studies will be shown for key phenomena. For example, fluid region nodalization studies are shown for the level swell and depressurization tests. Effects of heat slabs and nodalization near the break are examined for critical flow tests. Nodalization effects on void fraction are evaluated for the heated channel tests. Time step and convergence criteria are discussed generically and their effects are evaluated by sensitivity studies for representative calculations.

Specific guidelines for nodalization are based on judgment and experience. For void fraction and critical power calculations in a fuel channel and similar geometries, a cell length on the order of a few hydraulic diameters - about 15 cm for a BWR fuel channel - is appropriate. This cell size is used in most of the void distribution and channel heat transfer studies presented in this section. For the PSTF, a larger cell size is used in accordance with the larger hydraulic diameter. A finer nodalization is used for the Marviken critical flow tests to resolve the temperature profile upstream of the break. Special care is taken with cell size for the stability calculations to minimize numerical diffusion. For stability calculations, an explicit numerical scheme is employed with the time step controlled by setting the limiting Courant number to 1.0. Sensitivity studies on cell size and time step for the stability analyses are documented in Section 3.7. Nodalization for integral systems tests makes use of major regional boundaries as demarcations for noding. A range of nodalizations has been used for the test facility regions that correspond to the lower plenum and downcomer depending on geometric details, the locations of injection lines and the locations of test instrumentation. Noding within fuel channels depends on the nature of the transient to be simulated.

Experience gained from TRACG simulations of separate effects tests, component tests and integral systems tests has led to fixed nodalization schemes for several BWR components. These nodalizations are discussed in the context of qualification studies presented in Section 4. These qualification studies have in turn led to specific nodalization guidelines for modeling BWRs. Section 6 presents a comprehensive discussion of the standard BWR nodalization and includes sensitivity studies that serve to confirm the overall nodalization strategy.

In contrast to spatial nodalization, which is largely under the control of the TRACG user operating with a set of guidelines, time step is largely beyond the user's control. The problem time span can be divided into segments and the user can specify a minimum and maximum time step in each time segment but TRACG determines the actual time step on the basis of algorithms

that are designed to maximize the accuracy of the calculation while minimizing the computation time. Two criteria, specified by input, are used for this purpose:

- Convergence – The iterations to obtain a solution to the thermal-hydraulic equations are required to converge within a prescribed convergence criterion. If convergence is obtained with a low iteration count, the time step is allowed to increase up to the user-specified maximum. If a high iteration count is required, the time step is reduced. If the time step is reduced below the user-specified minimum, the problem will stop.

- Rate-of-Change – TRACG examines the rate of change of the primary dependent variables. These include the pressure, non-condensable gas partial pressure, liquid and vapor temperatures and the void fraction. In addition, TRACG checks the rate of change of the temperature of structures, such as fuel rods and heat slabs, and of the nodal power for cases where the three-dimensional (3D) kinetics model is applied. If the rate-of-change is small, the time step is allowed to increase up to the user-specified maximum. If the rate-of-change is large, the time step is reduced and the calculation terminated if the reduction takes it below the specified minimum time step.

In addition to the above factors, a TRACG option allows the time step to be controlled by the material Courant number. A detailed discussion of time step control can be found in Section 8.2.4 of the TRACG Model Description Report [3-1]. The sensitivity of the TRACG calculations to the time step control inputs will be shown as part of the PSTF comparisons in this section. The impact of time step size is evaluated for typical BWR transient and LOCA simulations in Section 6.

3.1 VOID FRACTION

In the following subsections, the adequacy of TRACG for predicting void fraction is evaluated by comparison to void fraction data. The heated channel tests include data from a full-size simulated BWR fuel bundle (FRIGG OF-64 [3-2]) and a single tube (Christensen [3-3]). The adiabatic tests include data from large hydraulic diameter test facilities (Wilson [3-4], Bartolomei [3-5] and EBWR [3-6 and 3-7]). The heated channel tests cover typical conditions in a BWR core while the adiabatic tests cover typical conditions for the BWR upper plenum and the ESBWR chimney. Depressurization and level swell data from the PSTF facility [3-8] provide qualification data for the assessment of the level tracking model in TRACG and support the evaluation of the TRACG critical flow model (Section 3.4). The Toshiba 16-rod bundle tests [3-9, 3-10] extend the database used for TRACG qualification of interfacial shear models (void fraction data) to lower pressures. Void data obtained in a large diameter vertical pipe under high temperature and high pressure using the pump test facility of Ontario Hydro Technologies (OHT) in Canada [3-11 through 3-13] support the application of TRACG for void fraction calculations in a chimney geometry such as that employed in the ESBWR. The CISE tests [3-14] provide adiabatic single-tube data at a hydraulic diameter characteristic of GE BWR 10x10 fuel.

3.1.1 Frigg Of–64 Tests

3.1.1.1 Test Description

This section presents and discusses comparisons between TRACG calculations and void fraction data from the FRIGG OF-64 tests. The FRIGG OF–64 tests simulated a full-scale 64-rod boiling water reactor (BWR) fuel bundle. OF-64 was the second test section used in the FRIGG test program. It was designed as a full-scale simulation of an Oskarshamn-I fuel assembly. It consisted of 64 heated rods placed in an 8x8 array. A slightly conservative [[   ]] BWR heat flux distribution was simulated. A description of the experiment including details of the test section geometry and instrumentation is given in Reference 3-2. The void fraction distribution measurements were performed using a gamma ray attenuation technique. The standard deviation of the measurement error for the average void fraction was 2.0% and the systematic mean error was -0.4%. The parameter ranges for the FRIGG-OF-64 tests are shown in Table 3.1-1 and the test conditions are given in Tables 3.1-2 and 3.1-3.

Table 3.1-1
FRIGG OF-64 Test Parameter Ranges

[[	
	]]

Table 3.1-2
Test Conditions (4.8 MPa)

[[			
			]]

SEPARATE EFFECTS TESTS

Table 3.1-3
Test Condition (6.8 MPa)

[[			
			]]

3.1.1.2 TRACG Model

The TRACG nodalization used for modeling the OF-64 bundle is shown in Figure 3.1-1. The components used for the simulation include:

- A CHAN component containing 24 cells of length [[   ]]

- A FILL component specifying the inlet temperature and flow.

- A BREK component specifying the outlet pressure.

- A FILL component at the channel leakage path specifying zero flow (i.e., no leakage).

3.1.1.3 Results of TRACG vs. Test Data Comparisons

[[

]]

Table 3.1-4
Mean and Standard Deviations for TRACG Model

[[		
		]]

SEPARATE EFFECTS TESTS

Channel Outlet   BREK   Specify system pressure

CHAN
(24 cells)

                         FILL

                  Leakage Path
                  (zero flow)

Channel Inlet
                  FILL   Specify inlet flow and enthalpy
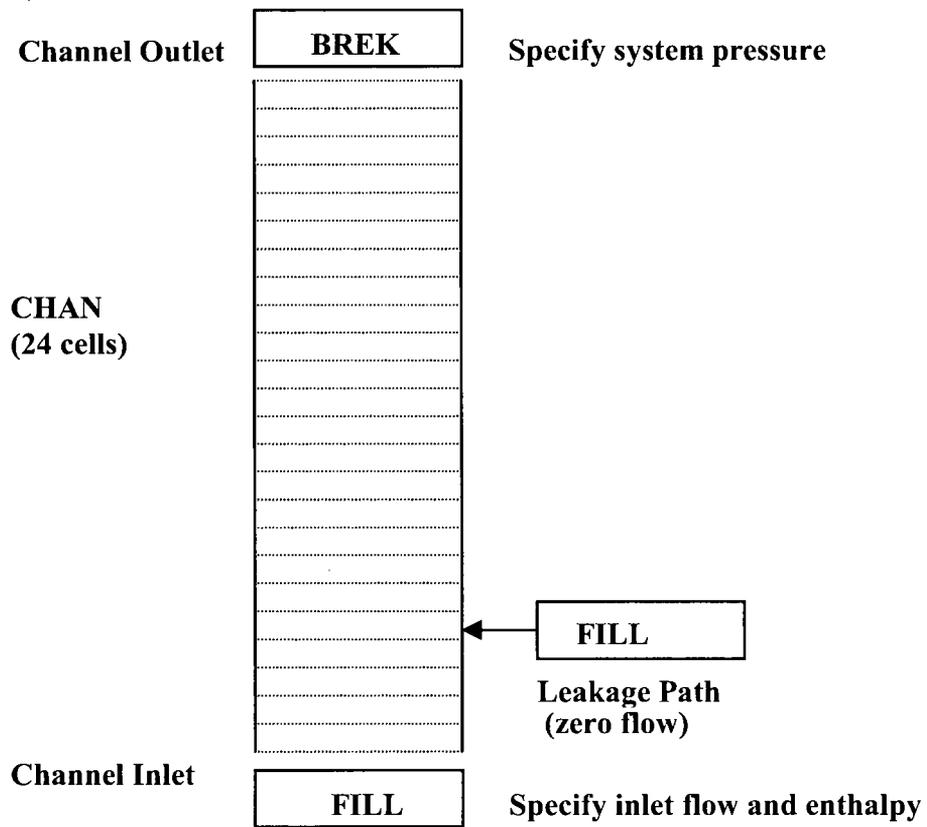
Figure 3.1-1. TRACG Nodalization for the FRIGG Channel

[[

]]

Figure 3.1-2. TRACG Deviation from FRIGG Void Fraction at a Pressure of 4.8 MPa

[[

]]

Figure 3.1-3. TRACG Deviation from FRIGG Void Fraction at a Pressure of 6.8 MPa

[[

]]

Figure 3.1-4. TRACG vs. FRIGG Void Fraction at a Pressure of 4.8 MPa

[[

]]

Figure 3.1-5. TRACG vs. FRIGG Void Fraction at a Pressure of 6.8 MPa

3.1.1.4 Sensitivity Study on the Effect of Nodalization on Fuel Channel Void Fraction

[[

]]

[[

]]

Figure 3.1-6. Void Fraction Nodalization Sensitivity for FRIGG OF-64 Fuel Channel

SEPARATE EFFECTS TESTS

3.1.2 Christensen Subcooled Boiling Tests

3.1.2.1 Test Description

In the Christensen subcooled boiling tests [3-3], subcooled single-phase liquid flowed into a heated tube with a length of 1.27 m and a 4.44 x 1.11 cm rectangular cross section. The test section was induction heated by passing an AC current through the test section wall. The void fraction was measured at various axial locations along the test section using the gamma ray attenuation technique. A gamma source within a lead collimator with a 0.8 mm slit was traversed across the test section at 16 elevations above the inlet. The measured void profile was integrated to determine the average void fraction at each elevation. The total composite error for the void fraction measurements was estimated to be ±0.025 (±2.5 %). The test conditions for the two tests chosen for comparison with TRACG calculations are summarized in Table 3.1-5.

3.1.2.2 TRACG Model

The TRACG model used to simulate the test facility included FILL, PIPE and BREK components (Figure 3.1-7). The PIPE component was divided into 20 equal-length cells.

3.1.2.3 Comparison of TRACG Calculations and Christensen Test Data

[[

]]

Table 3.1-5
Christensen Test Conditions

	Test 1	Test 2
Hydraulic Diameter	0.01788 m	0.01788 m
Pressure	5.514 MPa	6.893 MPa
Inlet Mass Flux	881.6 kg/m^2-s	873.3 kg/m^2-s
Inlet Equilibrium Quality	- 0.04 to 0.06	- 0.04 to 0.06
Heat Flux	495.3 kW/m^2	493.5 kW/m^2
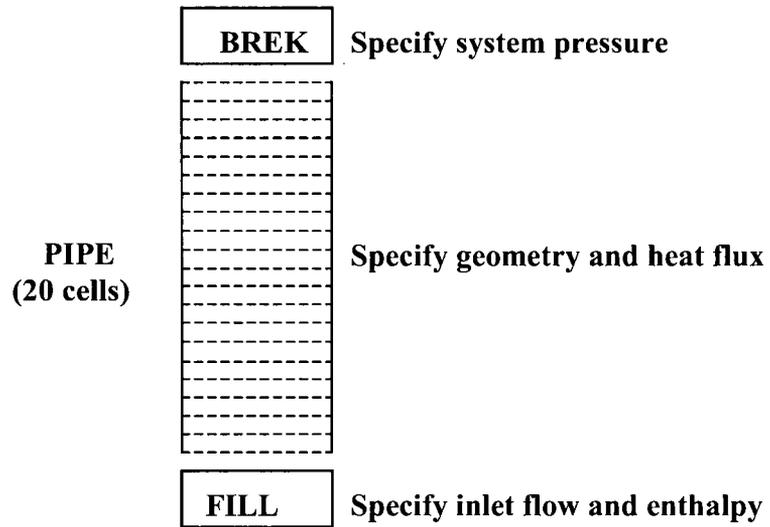
Figure 3.1-7. TRACG Model for Christensen Test

SEPARATE EFFECTS TESTS

[[

]]

Figure 3.1-8. Comparison of TRACG with Christensen Test at 5.5 MPa

[[

]]

Figure 3.1-9. Comparison of TRACG with Christensen Test at 6.9 MPa

3.1.3 Wilson and Bartolomei Bubble Rise Tests

3.1.3.1 Test Description

The Wilson and Bartolomei bubble rise tests were conducted by bubbling steam through stagnant liquid in an adiabatic test section. The test conditions and parameter ranges for the tests are given in Table 3.1-6. In Wilson's experiment [3-4], steam was bubbled through saturated water in a 3.66 m vertical pressure vessel with a diameter of 0.48 m. Steam entered the water through a perforated plate at the bottom of the vessel. The void fraction was determined from a manometer pressure difference measurement (Figure 3.1-12). Reference 3-4 does not provide an estimate of the measurement error.

The Bartolomei tests [3-5] were performed in a thick-walled 5 m vertical pressure vessel with a diameter of 1.22 m (Figure 3.1-10). Water was heated by high pressure hot water coils inside the vessel. The void fraction was measured at different levels within the vessel with a pair of diametrically opposed gamma ray detectors. The gamma radiation was provided by Co^{60} sources mounted in small diameter tubes. The detectors were mounted in a carriage that could be located at any of five discrete positions in the horizontal direction between the vessel center and the wall and then moved continuously in the vertical direction. The void fraction was measured at selected radial locations at twelve elevations within the vessel. Measurement uncertainty was not discussed in Reference 3-5 but, based on discussion in the Christensen paper [3-3], it is estimated that the measurement error did not exceed ±0.025 (±2.5%).

Table 3.1-6
Wilson and Bartolomei Test Conditions

	Wilson	Bartolomei
Pressure	2.2 MPa	4.6 MPa
Hydraulic Diameter	0.48 m	1.22 m
Vapor Flux	0.2 - 0.8 m/s	0.04 - 0.1 m/s
Void Fraction	30 - 47 %	12 - 20 %

The same TRACG model (Figure 3.1-11) was used to simulate both the Wilson and Bartolomei test facilities. The basic element of the model is a four-cell PIPE component. The inlet of the PIPE is connected to a FILL component that sets the inlet conditions and flow. The exit of the PIPE is connected to a BREK component that maintains the pressure.

[[

]]

SEPARATE EFFECTS TESTS
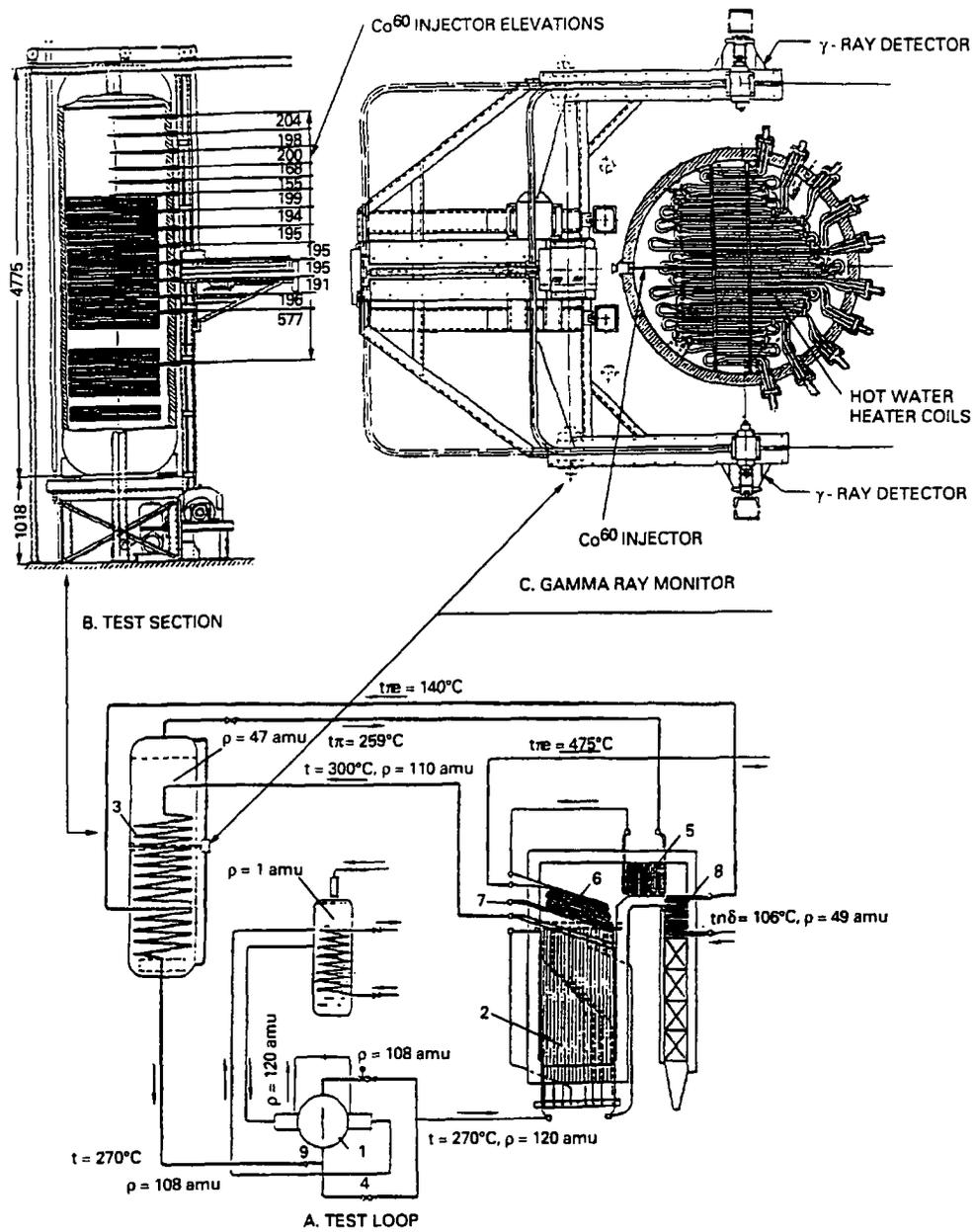
Figure 3.1-10. Schematic of Bartolomei Test Facility [3-4]

┌──────────┐
│   BREK   │ Specify system pressure
└──────────┘

PIPE   Specify geometry and heat flux
(4 cells)

┌──────────┐
│   FILL   │ Specify inlet flow and quality
└──────────┘
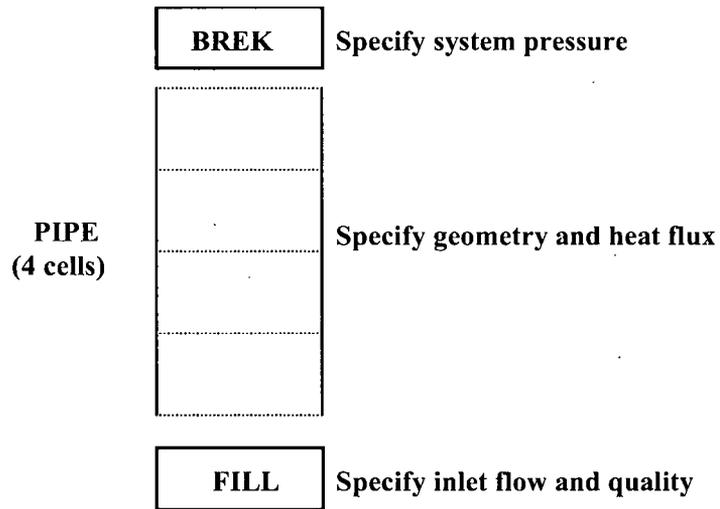
Figure 3.1-11. TRACG Model for Wilson and Bartolomei Tests

[[

]]

Figure 3.1-12. Comparison of TRACG with Wilson Test Data

[[

]]

Figure 3.1-13. Comparison of TRACG with Bartolomei Test Data

[[

3.1.4   EBWR Tests

Tests were conducted in the Experimental Boiling Water Reactor (EBWR) in which the chimney void fraction was measured for various flow rates and qualities [3-6, 3-7]. The EBWR pressure vessel is about 7 m high and the chimney is a straight riser section over the core about 1 m in height (Figure 3.1-15). The chimney void fraction was determined from static pressure difference measurements at the chimney center and near the wall over the height indicated in the sketch (Probes A and B). The specially designed probes were water cooled to prevent flashing in the sensing lines (Figure 3.1-16). The test conditions and parameter ranges for the EBWR tests are given in Table 3.1-7. The data were taken at powers ranging from 15 to 100 MW that produced a range of two-phase mixture levels in the chimney. For each test, the total core flow rate and inlet subcooling were measured and the inlet quality for the chimney section was determined from a mass and energy balance. As shown by the data in Figure 3.1-15, the void fraction was larger in the center of the chimney than near the chimney wall. There was no discussion of measurement error in Reference 3-7. However, the scatter in the data about their mean suggests the test data uncertainty is on the order of ±2.0%.

Table 3.1-7
EBWR Test Conditions

Chimney Diameter	1.17 m
Chimney Height	1.22 m
Inlet Diameter	1.58 m
Inlet Section Height	0.48 m
System Pressure	4.241 MPa
Mass Flux	$705 - 815 \text{ kg/m}^2\text{-s}$
Void Fraction	12 – 58 %

[[

]]
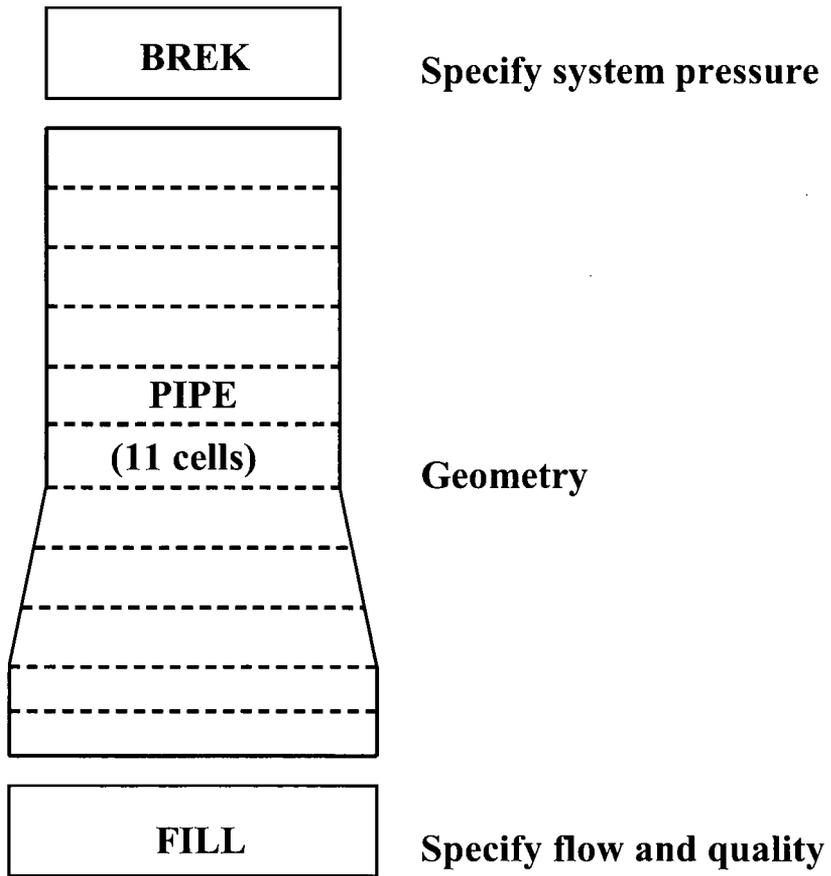
Figure 3.1-14. TRACG Model for EBWR Tests

[[

]]
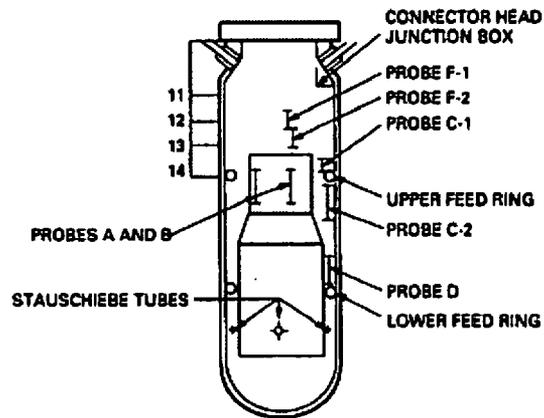
EBWR Test Facility

Figure 3.1-15. Comparison of TRACG with EBWR Tests
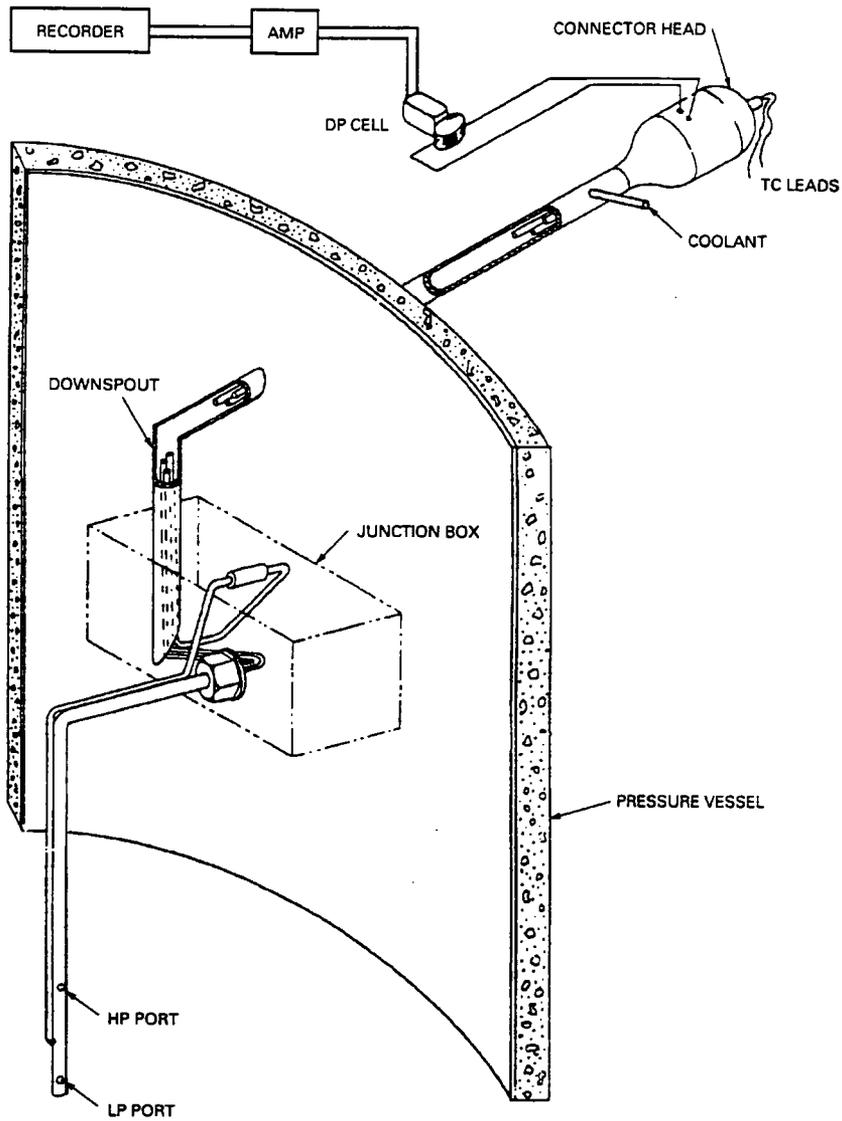
Figure 3.1-16. Schematic of EBWR ΔP Probe and Read-Out Instrumentation [3-7]

3.1.5 PSTF Level Swell Tests

The PSTF level swell tests provide information on liquid flashing during depressurization and the subsequent swell of the liquid level. In this section, PSTF test data are used to assess the level tracking model in TRACG. The PSTF tests also provide useful data for evaluation of the TRACG critical flow model as described in Section 3.4.

3.1.5.1 PSTF Test Facility

The PSTF facility [3-8] consists of a 4.2 m tall vessel with an internal diameter of 1.19 m (Figure 3.1-17). A blowdown pipe, connected to the bottom of the vessel at an elevation of 0.76 m, could be fitted with nozzles of various diameters ranging from 0.054 m to 0.092 m. In some of the tests, the blowdown pipe included a vertical standpipe inside the vessel with a diameter of 0.25 m (referred to as a "dip tube" - Figure 3.1-17). The inlet to the standpipe was in the upper part of the vessel at an elevation of 3.2 m. In other tests, the standpipe section was removed and the inlet to the blowdown pipe was at the 0.76 m elevation in the vessel.

In the level-swell tests, the vessel was filled with water to an elevation ranging from 1.67 m to 2.90 m. The system was heated and pressurized to a pressure of approximately 7.2 MPa. A rupture disk at the end of the blowdown pipe was then broken and the system depressurized through the blowdown pipe. For the tests where the blowdown pipe included the vertical standpipe ("top" break), the break flow was primarily steam and the system depressurized more or less quickly, depending on the size of the nozzle. In these tests, the liquid in the vessel flashed, causing the liquid level to rise initially and then subside toward the end of the depressurization. For the tests where the standpipe was removed ("bottom" break), the blowdown was primarily liquid and two-phase flow and the system initially depressurized slowly with a correspondingly slow decrease in the level. When the level dropped below the entrance to the blowdown pipe, the depressurization rate increased. The increased depressurization rate during caused increased flashing of the liquid and the level drop subsided.

Measurement uncertainties for the PSTF level-swell tests are summarized in Table 3.1-8:

Table 3.1-8
Measurement Uncertainties in the PSTF Tests

Pressure	±70kPa (±10 psia)
Void Fraction	±0.05 (±5.0%)
Blowdown Flow Rate	±2.3 kg/s (±5lbm/s)
Two-Phase Level (Test 5801-13)	±0.115 m (±4.9 in)
Two-Phase Level (Test 5801-15)	±0.150 m (±5.9 in)
Two-Phase Level (Test 5801-19)	±0.080 m (±3.1 in)

SEPARATE EFFECTS TESTS
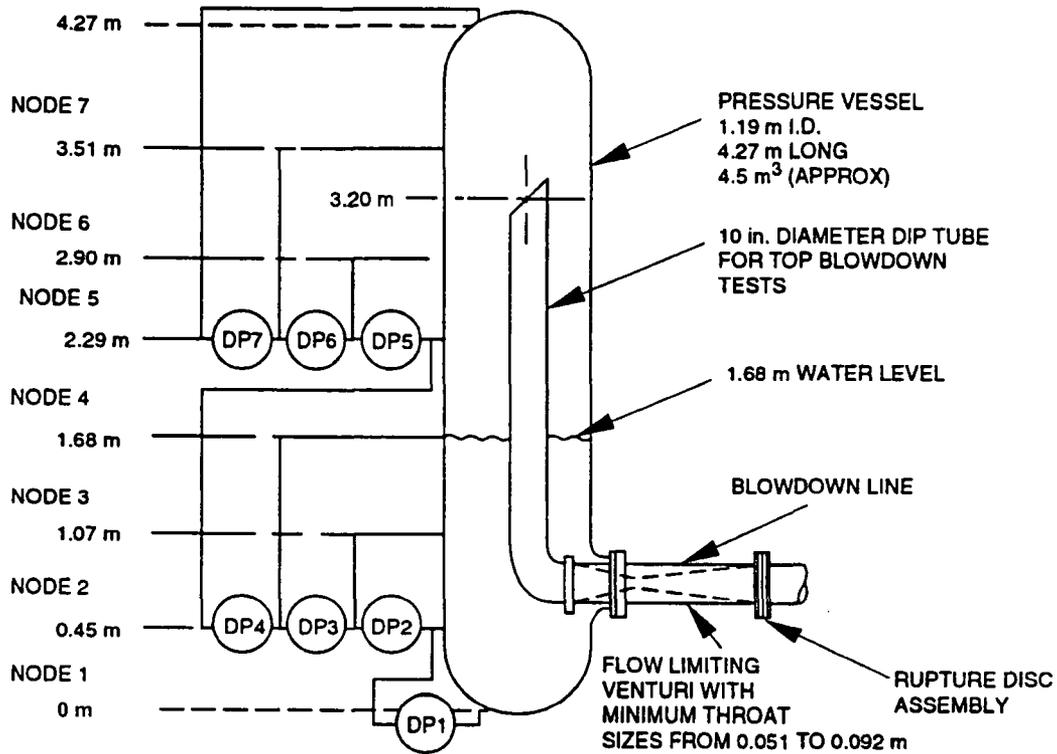
Figure 3.1-17. PSTF Test Facility

3.1.5.2 TRACG Model of PSTF Facility

The PSTF vessel was simulated with the TRACG VSSL component using 15 axial levels and one radial ring. Using a single radial ring at each level is equivalent to a one-dimensional simulation of the PSTF vessel. The blowdown pipe was simulated with a PIPE component using seven cells when the vertical standpipe was included and one cell when the vertical standpipe was removed. The TRACG nodalization is indicated in Figure 3.1-18.
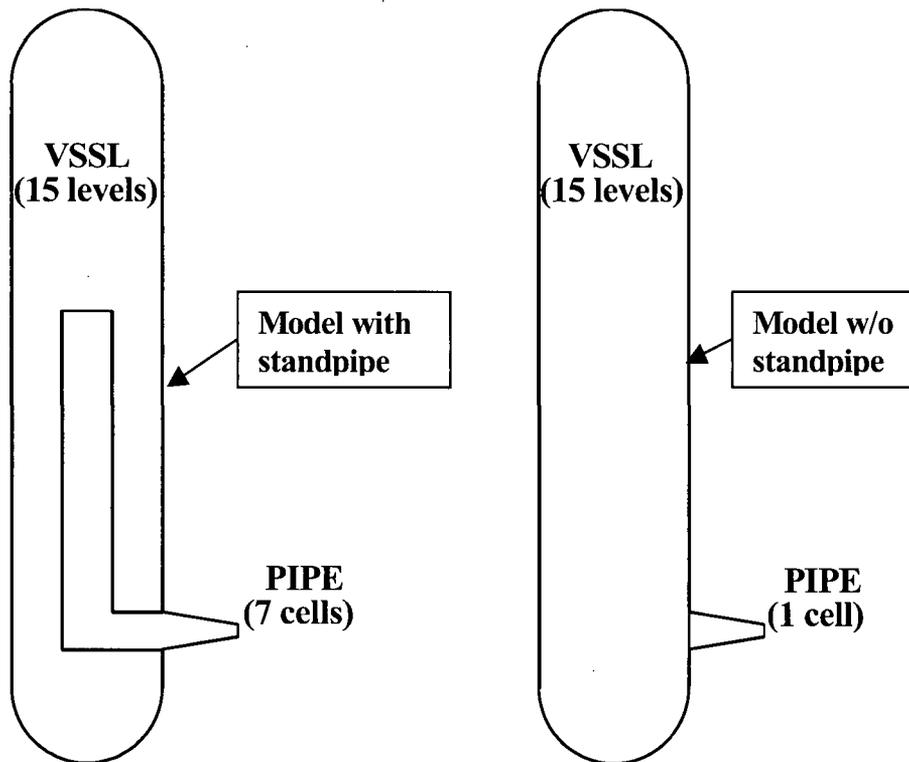
Figure 3.1-18. TRACG Models for PSTF

3.1.5.3 Results

TRACG predictions were compared to six tests from the PSTF test facility. The test conditions for these six tests are described in Table 3.1-9. There were four top-break and two bottom break tests. Level data for two top-break tests (Tests 5801-13 and 15) and two bottom break tests (5803-01 and 02) are used for comparison to TRACG in this section. Tests 5801-15, 5803-01 and 5803-02 are used along with Tests 5801-19 and 5702-16 for the critical flow comparisons described in Section 3.4.2.

Table 3.1-9
PSTF Test Conditions for TRACG Qualification

Test	Nozzle Dia.	Break Type	Initial Pressure	Initial Level
5801–13	0.0540 m	Top	7.3 MPa	1.67 m
5801–15	0.0635 m	Top	7.3 MPa	1.67 m
5801–19	0.0762 m	Top	7.3 MPa	1.67 m
5702–16	0.0921 m	Top	7.3 MPa	1.67 m
5803–01	0.0540 m	Bottom	7.2 MPa	2.90 m
5803–02	0.0762 m	Bottom	7.2 MPa	2.90 m

[[

]]

SEPARATE EFFECTS TESTS

[[

]]

Figure 3.1-19. Pressure Comparison for PSTF Test 5801-13

[[

]]

Figure 3.1-20. Level Comparison for PSTF Test 5801-13

[[

]]

Figure 3.1-21. Pressure Comparison for PSTF Test 5801-15

[[

]]

Figure 3.1-22. Level Comparison for PSTF Test 5801-15

[[

]]

Figure 3.1-23. Pressure Comparison for PSTF Test 5803-01

[[

]]

Figure 3.1-24. Level Comparison for PSTF Test 5803-01

[[

]]

Figure 3.1-25. Pressure Comparison for PSTF Test 5803-02

[[

]]

Figure 3.1-26. Level Comparison for PSTF Test 5803-02

3.1.5.4 PSTF Sensitivity Studies

[[

]]

[[

]]

Figure 3.1-27. Pressure Sensitivity to Nodalization for PSTF Test 5801-15

[[

]]

Figure 3.1-28. Level Sensitivity to Nodalization for PSTF Test 5801-15

[[

]]

Figure 3.1-29. Pressure Sensitivity to Convergence Criterion for PSTF Test 5801-15

[[

]]

Figure 3.1-30. Level Sensitivity to Convergence Criterion for PSTF Test 5801-15

[[

]]

Figure 3.1-31. Pressure Sensitivity to Maximum Time Step for PSTF Test 5801-15

[[

]]

Figure 3.1-32. Level Sensitivity to Maximum Time Step for PSTF Test 5801-15

SEPARATE EFFECTS TESTS

3.1.6   Toshiba Low-Pressure Void Fraction Tests

The separate effects database used for TRACG qualification of interfacial shear models (void fraction data) is mostly at high pressure. The Toshiba tests [3-9, 3-10] were added to extend the qualification basis to lower pressures. The Toshiba void fraction data are for a 16-rod bundle at 0.50 and 1.00 MPa.

3.1.6.1   Test Facility and Test Matrix

[[

]]

Table 3.1-10
Estimated Measurement Accuracies for Toshiba Void Fraction Tests

[[	
	]]

[[

]]

3.1.6.2   TRACG Model

The TRACG model simulates the rod bundle and the measurement section with a CHAN component. The CHAN component simulates a 4x4 array of heated rods together with an unheated channel wall. There was no heat transfer from the channel wall to the outside. In the test, the vessel wall was well insulated and the stagnant water in the annular bypass region heated up to saturation temperature before the void fraction measurements were made. Thus, there was negligible heat loss through the channel wall. A constant inlet flow rate is specified through a FILL component. The test section exit pressure is set with a BREK component. The leakage flow from the channel to the bypass region was not present in the test, and the leakage flow was set to zero through a zero velocity FILL. [[

]]

The initial temperature in all TRACG cells was set to the measured inlet temperature. The power and exit pressure (BREK) were set to the measured value. The inlet velocity was calculated based on the measured flow, density at the inlet temperature and bundle cross-sectional flow area. This value was specified with the inlet FILL. An initial long calculation was made to obtain converged values for the heater rod temperatures. (The heater rod temperatures are not relevant to the final results, as these are steady-state tests. However, a good estimate for the steady-state temperatures shortens the time needed for the fluid conditions to reach steady-state for the individual cases.) TRACG calculations were run for 60 seconds for the individual cases. Longer calculations were made to spot check and confirm that the fluid conditions had reached steady-state values.

3.1.6.3   Results and Discussion

[[

]]

3.1.6.4 Conclusion

[[

]]

Table 3.1-11
Range of Parameters for Toshiba Tests

Parameter	Toshiba Tests
Lattice Size	4 x 4
Rod Bundle D_h (m)	0.01
Rod Bundle L/ D_h	374
Mass Flux (kg/m^2 -s)	833, 1390
Pressure (MPa)	0.5, 1.0
Void Fraction	0.47 - 0.88
Flow regimes	Bubbly-Churn, Transition, Annular

Table 3.1-12
Comparison of Toshiba Void Data with TRACG Calculations
Test CT01 300 Series: Nominal Pressure 1.00 MPa; Nominal Mass Flux 1390 kg/m^2-s

[[

]]

Test CT01 400 Series: Nominal Pressure 1.00 MPa; Nominal Mass Flux 833 kg/m2-s

[[

]]

Test CT01 110 Series: Nominal Pressure 0.50 MPa; Nominal Mass Flux 1390 kg/m2-s

[[

]]

* Defined as : $(h - h_{f,sat})/h_{fg}$

Overall statistics: [[   ]]

[[

]]

Figure 3.1-33. Test Bundle Cross-Section
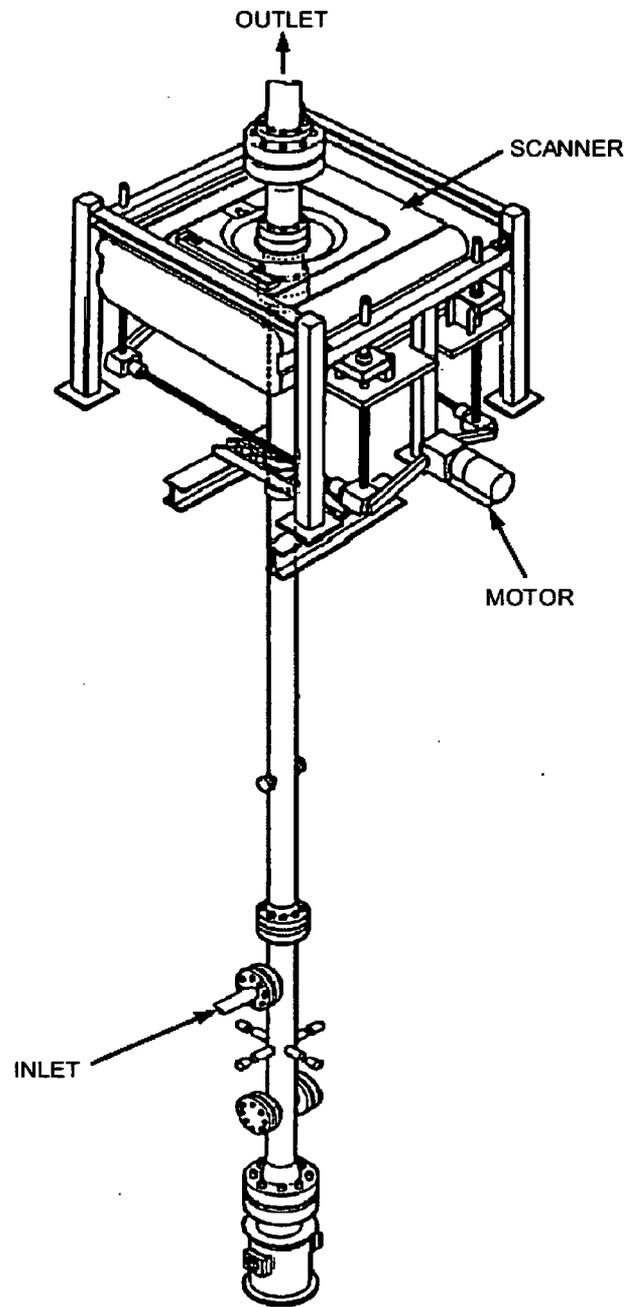
Figure 3.1-34. External View of Test Section

SEPARATE EFFECTS TESTS

CHANNEL BOX

VESSEL

UNHEATED ROD

Be

Al

VOID MEAS.
POINT

45 MM

END OF HEATED
LENGTH

(a)

Be

Al

(b)
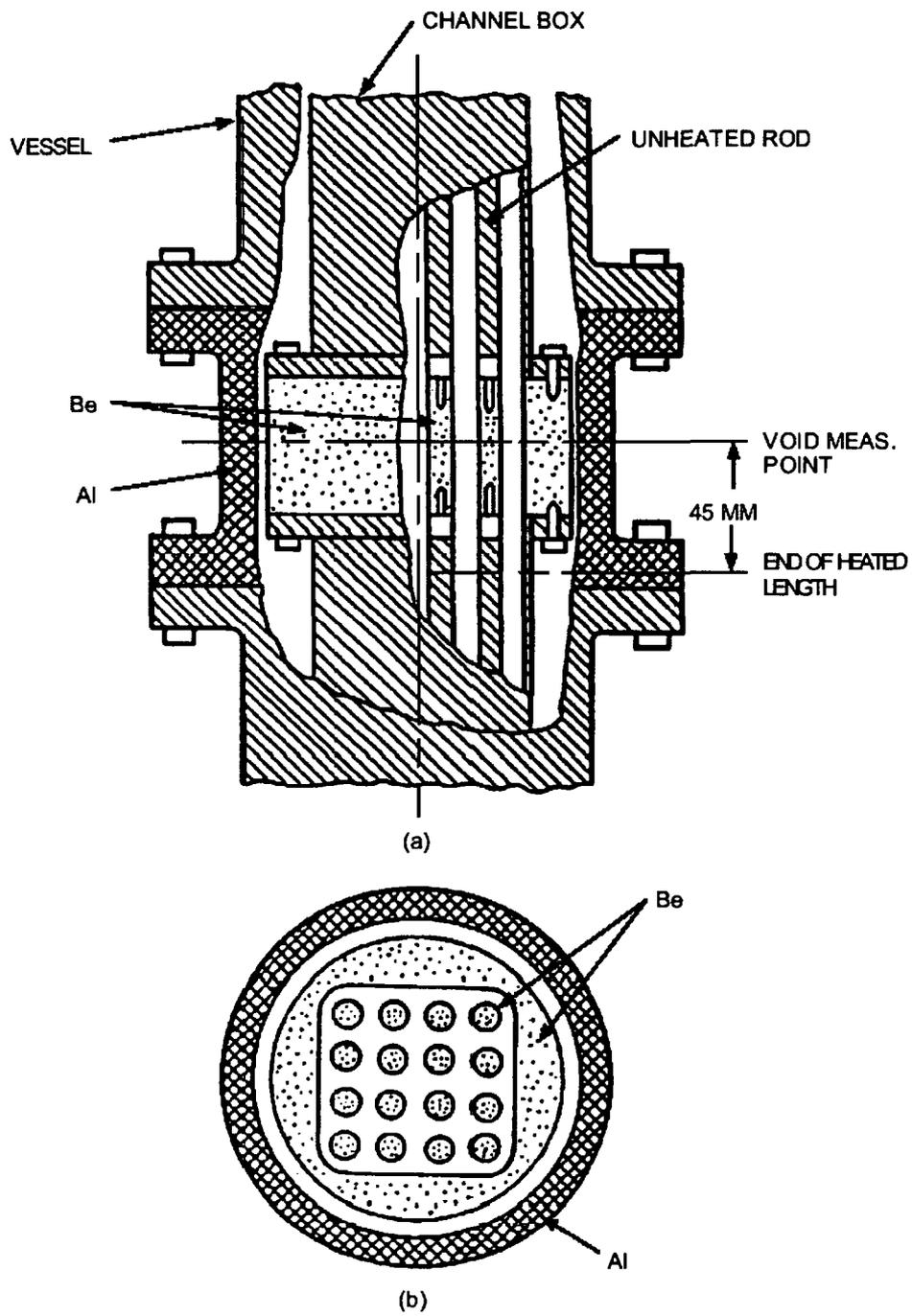
Figure 3.1-35. Void Measurement Section
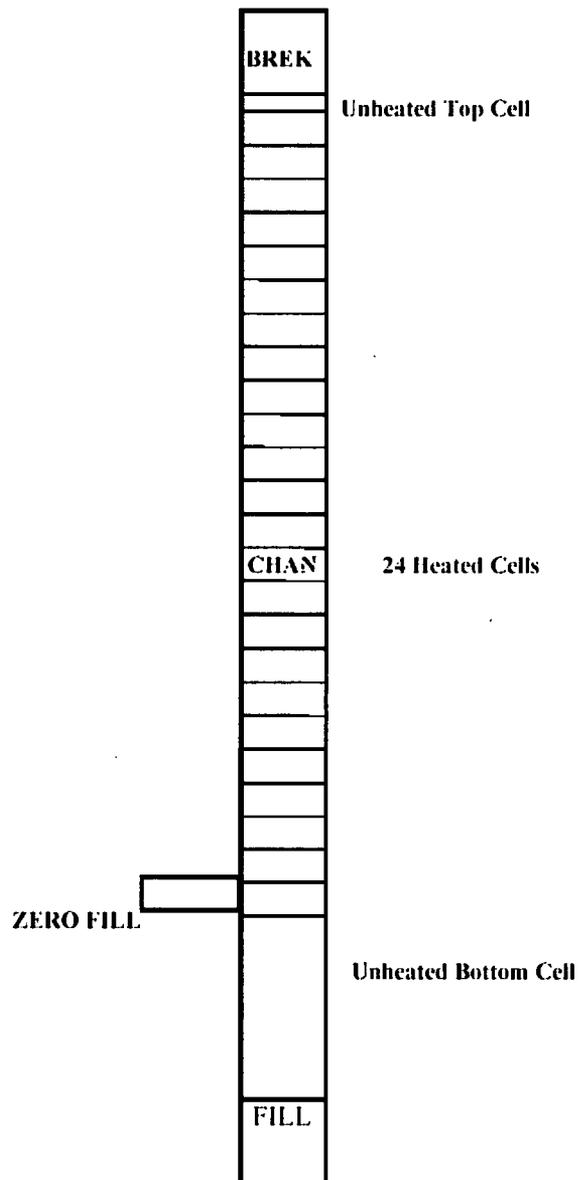
Figure 3.1-36. TRACG Model for Toshiba Test

SEPARATE EFFECTS TESTS

[[

]]

Figure 3.1-37. TRACG vs. Toshiba CT Void Data at 1.0 MPa and 1390 Kg/m2-s

[[

]]

Figure 3.1-38. TRACG vs. Toshiba CT Void Data at 1.0 MPa and 833 Kg/m2-s

SEPARATE EFFECTS TESTS

[[

]]

Figure 3.1-39. TRACG vs. Toshiba CT Void Data at 0.5 MPa and 1390 Kg/m2-s

3.1.7 Ontario Hydro Void Fraction Tests

During 1994, void data in a 24 in. (61-cm O.D.) vertical pipe under high temperature and high pressure were obtained using the pump test facility of Ontario Hydro Technologies (OHT) in Canada [3-11]. This section describes the TRACG simulation of the OHT void fraction tests.

3.1.7.1 Test Facility

The OHT Pump Test Loop with a full-scale CANDU reactor pump was used to perform the void fraction test. The pump is a vertical, single suction and double volute centrifugal pump. The configuration of the OHT Test Loop is shown schematically in Figure 3.1-40. The loop has three parallel, vertical inverted-U branches, connecting the suction and discharge headers. Each branch features a flow control valve and a venturi flow-meter. The loop branches were fabricated using 24 in. (61.0 cm O.D., 51.8 cm I.D.) carbon steel pipes and the suction and discharge headers were made out of 36 in. (91.4 cm O.D.) carbon steel pipes. The height of all the branches was about 12 m, which represents a length-to-diameter ratio of about 24. The loop is designed for operation up to 9.4 MPa and 280°C in pressure and temperature, respectively.

The test section was the riser of the branch closest to the pump. Figure 3.1-41 shows a schematic of the test section and the instruments involved. The suction and discharge headers were closed and the other two inverted-U branches were valved off during the void tests. The test section is a 12.4 m long, 24 in. (51.8 cm I.D.) carbon steel pipe. The riser features a perforated stainless steel plate type flow straightener located inside the pipe at about 2.0 m from its inlet above the discharge header and a venturi-meter near the top of the pipe. The flow through the test section could be controlled using a flow control valve located at the downcomer of the branch. A specially designed multi-detector gamma densitometer and a five-tap Pitotmeter for local void fraction and velocity head measurements were located at about 7.2 m from the riser inlet. Pressure and differential pressure transducers were also installed to measure the pressure drop along the length of the test section.

The gamma densitometer was specially designed to measure void fraction and phase distributions in large diameter, thick-walled steel pipes. A Cesium-137 gamma source with a principal photon energy of 0.662 MeV was used. Lead collimators with four internal partitions were provided on both sides on the pipe to define the beam cross-section and to divide the pipe into five sections for chordal-average void fraction measurements. The void fraction was determined from the attenuated gamma intensities using the following expression:

$$\alpha_j = \frac{\ln[N(\alpha_j)/N(0)]}{\ln[N(1)/N(0)]}$$

(3.1-1)

where:

$N(\alpha_j)$ = attenuated gamma intensity for a given void fraction α_j in the test pipe

$N(0)$ = attenuated gamma intensity when the test pipe is filled with liquid only

$N(1)$ = attenuated gamma intensity when the test pipe is filled with vapor only

Five chordal-average void fraction measurements (α_j, where j=1 to 5) were thus obtained using Equation 3.1-1.

The OHT multi-detector gamma densitometer was calibrated statically using a piece of pipe identical to the test pipe and air/water at room temperature. In the calibration, the pipe was closed at the bottom and "simulators" of different shapes and sizes were used to simulate the different void and flow patterns. Details of the static calibration were described in Reference 3-12. It was found that the measured void fractions compared very well with the actual void fractions in the test pipe with a maximum deviation of about 5% void. The ability of the multi-detector gamma densitometer to identify phase distributions for different cross-section average void fractions was also demonstrated in Reference 3-12.

Five Celesco differential pressure transducers (Model DP 30) were connected to the stainless steel tubes to measure the velocity heads for the five Pitot tubes (Figure 3.1-41). The transducers had a range of 0 to 34 kPa and were bled regularly to ensure that the connecting lines were free from vapor bubbles.

The dynamic head in two-phase flows is given by:

$$\Delta P = \frac{1}{2}[\alpha \rho_s u_s^2 + J(1-\alpha)\rho_f u_f^2] \tag{3.1-2}$$

where:

α = Local void fraction

ρ_s = Steam density

ρ_f = Water density

u_s = Local steam velocity

u_f = Local water velocity

J = A momentum exchange factor ranging in value from 1 to 2 and being a strong function of the void fraction.

In the void data analysis, J was assumed to have a constant value of 1.0. The local dynamic pressure heads as measured by the Pitotmeter can thus be written as:

$$\Delta P_j = \frac{1}{2}[\alpha_j \rho_s u_{s,j}^2 + J(1-\alpha_j)\rho_f u_{f,j}^2], \tag{3.1-3}$$

where j takes the values from 1 to 5.

Assuming no slip between the two phases (i.e., $u_f = u_g$), the local mass flux can be given by:

$$G_j = \sqrt{2\Delta P_j[\alpha_j \rho_s + (1-\alpha_j)\rho_f]} \tag{3.1-4}$$

where ΔP_j and α_j are measured using the Pitotmeter and multi-detector gamma densitometer, respectively. The total mass flux is obtained from the local mass fluxes using the following expressions:

$$G_r = \frac{\sum_{j=1}^{5} G_j A_j}{A_r} \tag{3.1-5}$$

and

SEPARATE EFFECTS TESTS

$$A_r = \sum_{j=1}^{5} A_j,$$ (3.1-6)

where A_r is the total flow area of the test pipe, and A_j is the cross-section area of the local pipe segment associated with measuring volume j.

The methodology used to measure two-phase mass fluxes was verified both in vertical and horizontal two-phase flows using 4 in. Sch. 80 pipes. Detailed descriptions of the calibration loops can be found in Reference 3-13. In both loop configurations, reasonable agreement (within 15%) between the measured and actual total two-phase mass fluxes was obtained.

Two Celesco differential pressure transducers (Model DP 30) were used to measure the pressure drop along the length of the test section above the Pitotmeter, as shown in Figure 3.1-41. The transducers had the same range as those used in the annubar (i.e., 0-34 kPa). The axial pressure drop measurements were also used to deduce the average void fraction in the test section, assuming the axial acceleration and friction pressure drops were negligible. The average void fraction, $\alpha_{\Delta h}$, can thus be expressed as:

$$\overline{\alpha_{\Delta h}} = \frac{\rho_f}{\rho_f - \rho_s} - \frac{\Delta P_t}{(\rho_f - \rho_s)gh}$$ (3.1-7)

where:

ΔP_t = Pressure drop along the length of the test section

g   = Gravitational acceleration

h   = The distance over which the pressure drop was measured

The average void fraction as obtained from Equation 3.1-7 can be compared with the average void fraction measured directly by the multi-detector gamma densitometer using the following expression:

$$\overline{\alpha_{rD}} = \frac{\sum_{j=1}^{5} \alpha_j A_j}{A_r}$$ (3.1-8)

where α_{rD} is the average void fraction obtained from the gamma densitometer measurements.

The nominal operating conditions in the test loop were controlled by heat addition from the pump and heat removal by an air-cooled heat exchanger. The test loop temperature was controlled using a bypass flow to a 6 MW water-to-air heat exchanger. The bypass flow was taken at a location between the universal venturi tube and the flow control valve. During the heatup phase in preparation for the tests, the bypass flow to the heat exchanger was valved off so that the test loop could be heated up from room temperature to 280°C in about two and one-half hours. After the test loop attained the desired temperature, a bypass flow through the heat exchanger was established to maintain the loop temperature constant. The bypass flow through the heat exchanger was adjusted continually during the test as the pump motor power dropped off under two-phase flow operation. Typically, the loop temperature could be held to within 5°C of the target value.

Two-phase flow and void fraction in the test loop were created by draining water from the loop into a storage tank. The void fraction in the test section was monitored by the gamma densitometer during the tests. Draining was interrupted several times to maintain a constant void fraction in the test section. The flow through the test section could then be varied by adjusting the flow control valve in the test section slowly and in steps. Three test section void fractions at 25%, 50% and 75% were attempted during the tests to study the effect of varying mass flow rates on two-phase flow behavior in the test pipe. The two-phase mass flux in the test section was varied from about 600 to 2200 kg/m²s during the tests.

During the test, the two-phase flow conditions in the test loop and the test section were varied slowly, and the loop temperature was held to within 5°C of the target value. It may be assumed that quasi-steady-state conditions prevailed during the test and useful two-phase flow test data could also be obtained while the loop was being drained.

The test procedure also provided in-situ calibration for the gamma densitometer in each test. At the beginning of the test, full pipe conditions with water at the test temperature were obtained for all the five detectors. Empty pipe conditions with steam at the same test temperature were obtained at the end of the test. Uncertainties in void fraction measurements could thus be reduced significantly.

The measured void distributions across the diameter of the test pipe were plotted at different times during the transient and shown in Figure 3.1-42. The measured void distribution in the pipe is symmetrical with respect to the pipe center and is relatively flat in profile for all void fractions.

Axial pressure drops at two locations along the test section were measured downstream of the Pitotmeter and gamma densitometer (Figure 3.1-41). The two measurements behaved essentially the same, as expected. Since the frictional and acceleration pressure drops are negligible in the present tests, these axial pressure drops can be used to calculate the average void fraction in the test section. Figure 3.1-43 shows the comparison of the average void fractions in the test section calculated from the axial pressure drop measurements (using Equation 3.1-7) with the corresponding values obtained using the gamma densitometer (using Equation 3.1-8). In general, the average void fractions based on pressure drop measurements were found to be in good agreement with, but slightly lower than the gamma densitometer measurements. This is due to the fact that the acceleration and frictional pressure drops were not included in the hydrostatic head calculations. This comparison also supports the use of the cross-sectional average of the void measurements for comparison with TRACG results. Furthermore, this comparison also suggests that the axial void distribution along the test section during the transient could be relatively uniform.

Since the test results for different tests at the same nominal temperature were found to be very similar, only two tests, one at each temperature, were analyzed and discussed in Reference 3-8. These tests were run at nominal temperatures of 280°C (6.4 MPa) and 230°C (2.8 MPa). For the low-pressure test (230°C), oscillations with large amplitudes in the axial ΔP and void fraction were observed at the intermediate void fraction. By studying the ΔP-cell and pump head measurements through Fast Fourier Transform in the frequency domain, it was determined that the oscillations observed during the low-pressure test were caused by the dynamic behavior of the pump under two-phase flow conditions and its interaction with the piping system. These oscillations are not a fundamental property of the two-phase flow in the vertical test section. Therefore, the low-pressure data are not included for the TRACG qualification.

3.1.7.2 TRACG Model

A TRACG model was set up to simulate the OHT test section. Figure 3.1-44 shows the TRACG nodalization used in this simulation. The components used in the simulation include a TEE component, two FILL components and a BREK component. The main branch of the TEE component contains 13 cells. Cells 1 to 3 simulate part of the 36 in (91.4-cm O.D.) discharge header (Figure 3.1-40, horizontal piping, 0.9144 m O.D, 0.7763 m I.D.) in the test loop. Cells 4 through 13 simulate the vertical test section (Figure 3.1-41, 0.518 m I.D.). The cell center elevation at Cell 9 matches the measurement location for the system pressure and void fraction. The TRACG calculated pressure and void fraction at this cell are compared to the respective test data. The one-dimensional model (TEE component) is used to simulate the test section (10 vertical cells) in this comparison.

The BREK component connected to the top of the simulated test section is used to specify the outlet pressure. The two FILL components connected to the bottom of the TEE component are used to specify the inlet mass flows and temperature, one FILL component for the steam mass flow and the other FILL component for the liquid mass flow.

Separate liquid and vapor mass fluxes were estimated from the measured total mass flux and measured void fraction, assuming no slip between the two phases. These mass fluxes were then converted into the liquid and vapor flow rates. These flow rates are used in the FILL components connected to the bottom of the TEE component as boundary condition for the simulation.

[[

]]

The actual heat addition from the pump, heat losses in the test section, and heat removal by the heat exchanger were not measured during the tests. However, the loop temperature was held relatively constant to within 5°C of the target value. Therefore, as a first approximation, the test section was modeled with no heat loss. No heat addition from the pump and heat removal by the heat exchanger were included in the simulation.

3.1.7.3 Results and Conclusion

[[

SEPARATE EFFECTS TESTS

]]

SEPARATE EFFECTS TESTS

Table 3.1-13
Comparison of TRACG/OHT Void Fraction During the Time Periods of Varying Mass
Flow Rate (280°C/6.4 MPa)

[[				
				]]
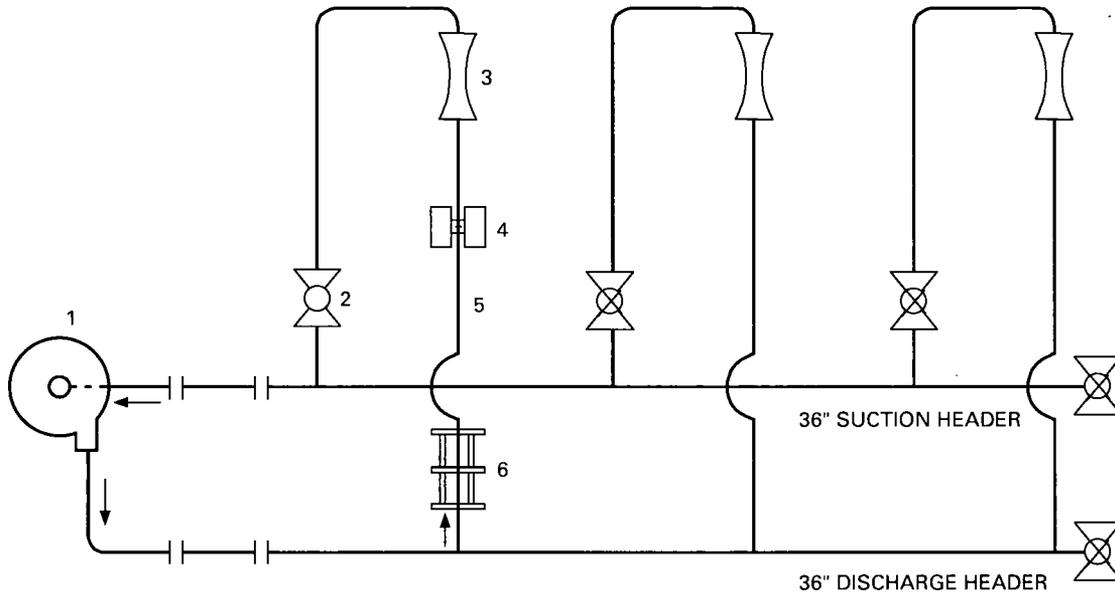
1-PUMP (BRUCE NGS 'A' PUMP)

2-FLOW CONTROL VALVE

3-UNIVERSAL VENTURI TUBE

4-GAMMA DENSITOMETER AND FIVE TAP PITOMETER

5-24" CARBON STEEL PIPE (12m IN LENGTH)

6-PERFORATED S.S. PLATE TYPE FLOW STRAIGHTENING VANE

Figure 3.1-40. Schematic Diagram of the Test Facility
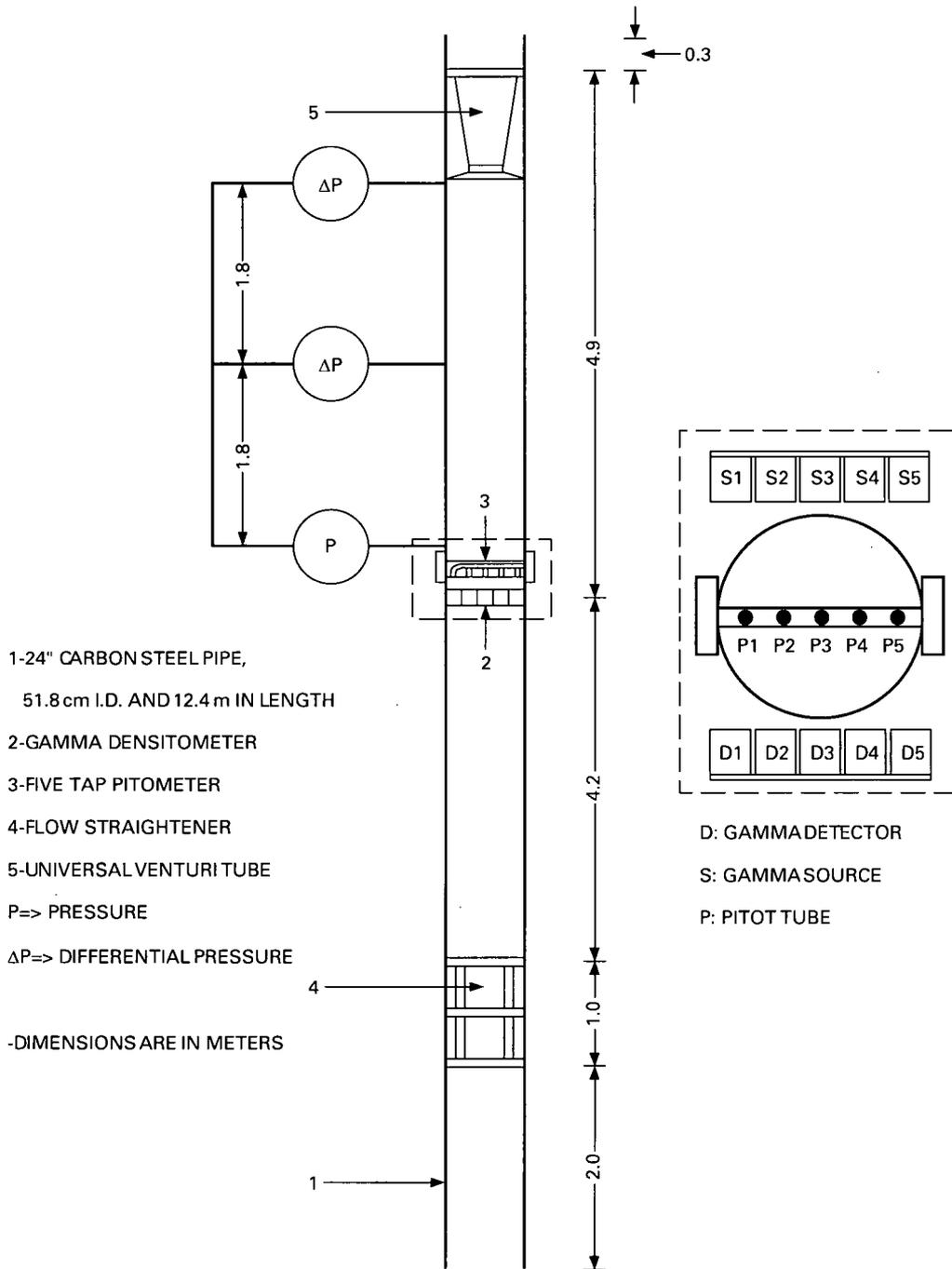
Figure 3.1-41. Schematic Diagram of the Test Section

1-24" CARBON STEEL PIPE,

  51.8 cm I.D. AND 12.4 m IN LENGTH

2-GAMMA DENSITOMETER

3-FIVE TAP PITOMETER

4-FLOW STRAIGHTENER

5-UNIVERSAL VENTURI TUBE

P=> PRESSURE

ΔP=> DIFFERENTIAL PRESSURE

-DIMENSIONS ARE IN METERS

D: GAMMA DETECTOR

S: GAMMA SOURCE

P: PITOT TUBE
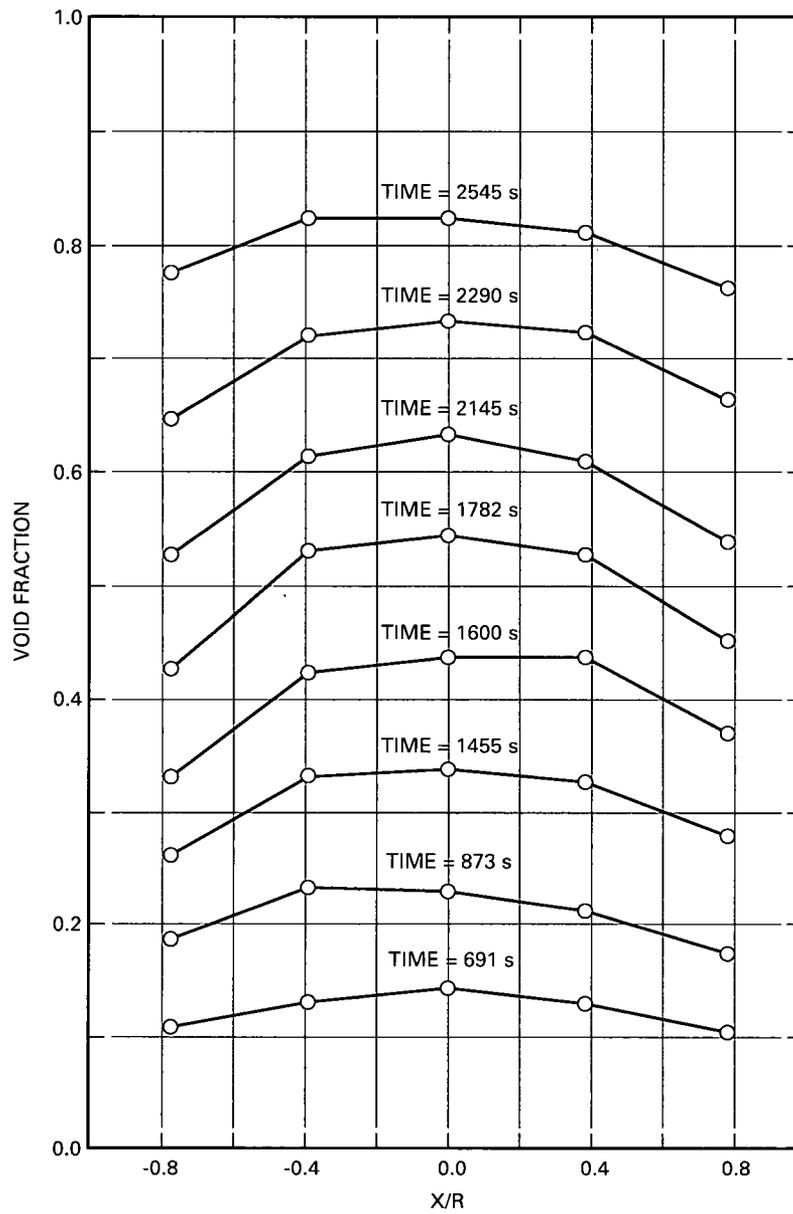
NOTE: TIME-AVERAGED DATA WAS USED FOR PLOTTING THIS GRAPH.
ORIGINAL DATA WAS AVERAGED OVER 36 SECONDS.

Figure 3.1-42. Radial Void Fraction Distribution at Nominal Temperature of 280°C

Figure 3.1-43. Average Void Fractions from the Gamma Densitometer Measurements vs. those Obtained using the Axial Pressure Drop Measurements at 280°C

SEPARATE EFFECTS TESTS
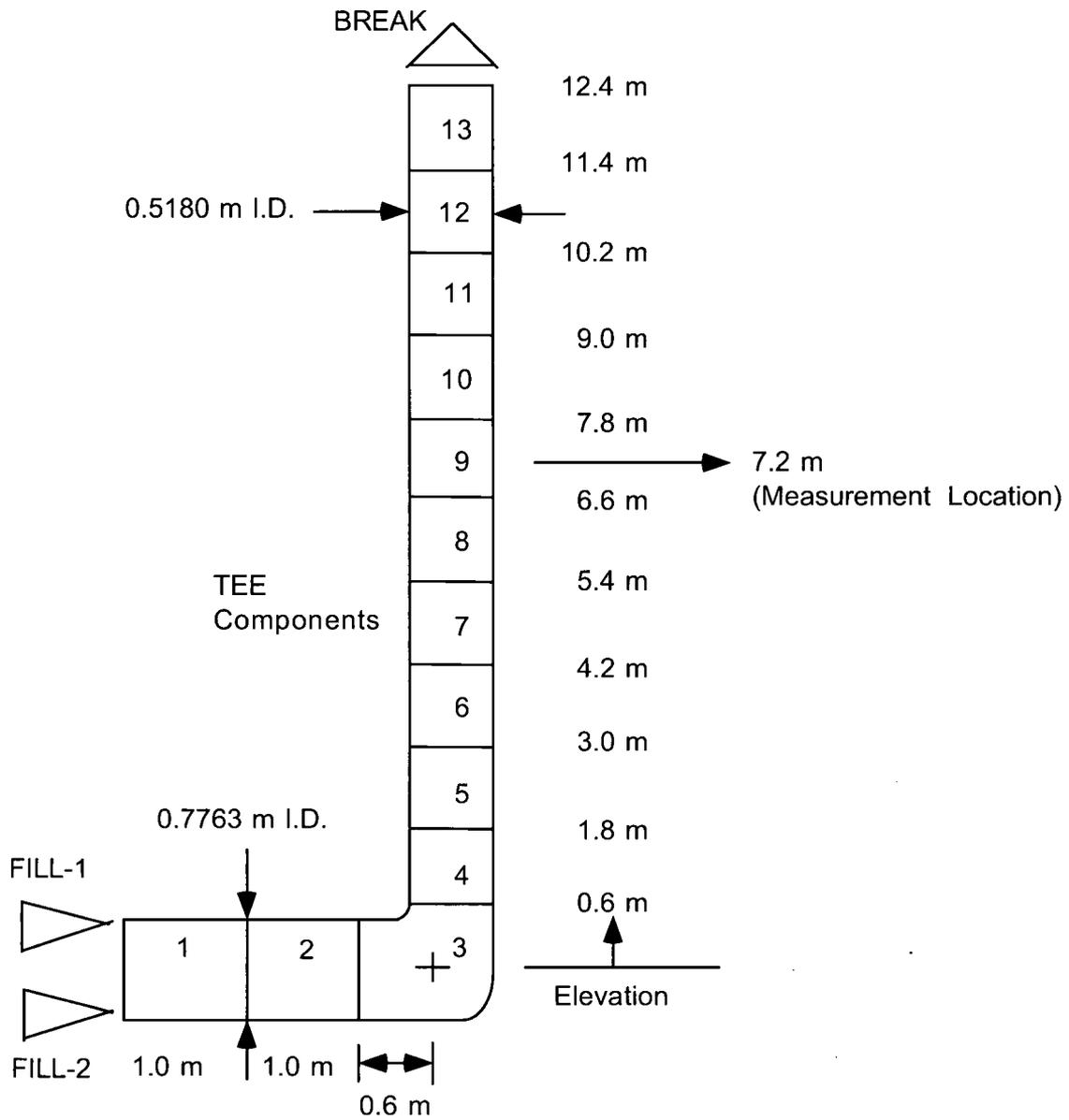
Figure 3.1-44. TRACG Model Description of OHT Test

[[

]]

Figure 3.1-45. Local Void Fluctuations at ~2000 s at Nominal Temperature of 280° C

[[

]]

Figure 3.1-46. Local Void Fluctuations at ~2500 s at Nominal Temperature of 280° C

[[

]]

Figure 3.1-47. Comparison of TRACG and Time-Averaged Data for Average Void Fraction at Nominal Temperature of 280°C

3.1.8 CISE Density Measurement Tests

Tests were performed at the CISE (Centro Informazioni Studi Esperienze) IETI-1 facility in Italy to measure the density of high quality steam-water mixtures flowing upward in a heated channel at high pressure [3-14].

3.1.8.1 Test Facility and Measurement Procedure

The CISE test facility consisted of a vertical stainless steel tubular test section with a 0.91 cm inside diameter and a length of 414 cm situated in an open-circuit flow loop that discharged to the atmosphere through a pressure control valve. In addition to the test section and the pressure control valve, the loop components included a pump and two preheaters upstream of the test section and a downstream condenser. The condenser decreased the temperature of the primary fluid below 100 °C before it entered the pressure control valve. Capability was provided for both adiabatic tests, in which the required fluid enthalpy in the test section was obtained by using the two preheaters in series, and tests with direct current heating of the test section. For the adiabatic tests, the first preheater raised the liquid to saturation and the second preheater produced the desired inlet quality. Tests were conducted over a range of pressures and inlet mass fluxes.

Figure 3.1-48 shows a schematic of the test section and two fast-operating valves that were located close to the test section inlet and outlet. The tests were conducted by simultaneously closing the fast-operating valves after steady-state conditions were established. The fluid between the two valves was drained, condensed and weighed. Appropriate corrections were introduced to account for the difference between the actual mass in the test section before valve closure and the mass collected and weighed. These corrections accounted for: (1) the difference between the locations of the valves and the inlet and exit of the test section; (2) mass lost in the draining and condensation process; and (3) mass remaining in the test section after draining. In addition, a bounding estimate of the error introduced by any imbalance between the inlet and outlet flow rates during the closure of the valves was made. The facility and the experimental procedure were designed to minimize the magnitude of these corrections. [[

]]

3.1.8.2 TRACG Model

The TRACG model of the CISE test facility consisted of a 1-D PIPE component connected to a FILL component at the inlet and a BREK component at the exit (Figure 3.1-49). The BREK component is used to maintain the test section exit pressure and the FILL component provides homogeneous flow with the desired inlet mass flux and quality. The first cell of the PIPE component allows for transition to nonhomogeneous conditions with slip between the liquid and vapor phases. The remaining four cells of the PIPE simulate the CISE test section. An iterative procedure was used to determine a BREK pressure that would make the average pressure in Cells 3 and 4 of the PIPE component match the CISE test section pressure.

3.1.8.3 Results and Discussion

[[

]]

3.1.8.4   Conclusion

The mean and standard deviations of TRACG predictions of void data from the CISE density measurement tests are consistent with those determined from other void qualification studies (see, e.g., Sections 3.1.1 and 3.1.6). As such, they provide further support for the conclusion that the interfacial shear models in TRACG are adequate for the prediction of void fraction over a wide range of BWR plant conditions.
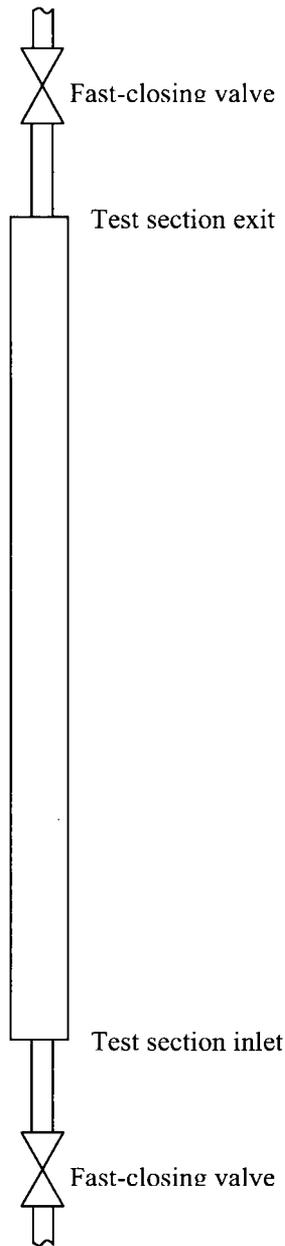
Figure 3.1-48. CISE Test Section with Fast-Closing Valves

SEPARATE EFFECTS TESTS

BREK   Prescribed Pressure

PIPE

FILL   Prescribed Flow and Quality
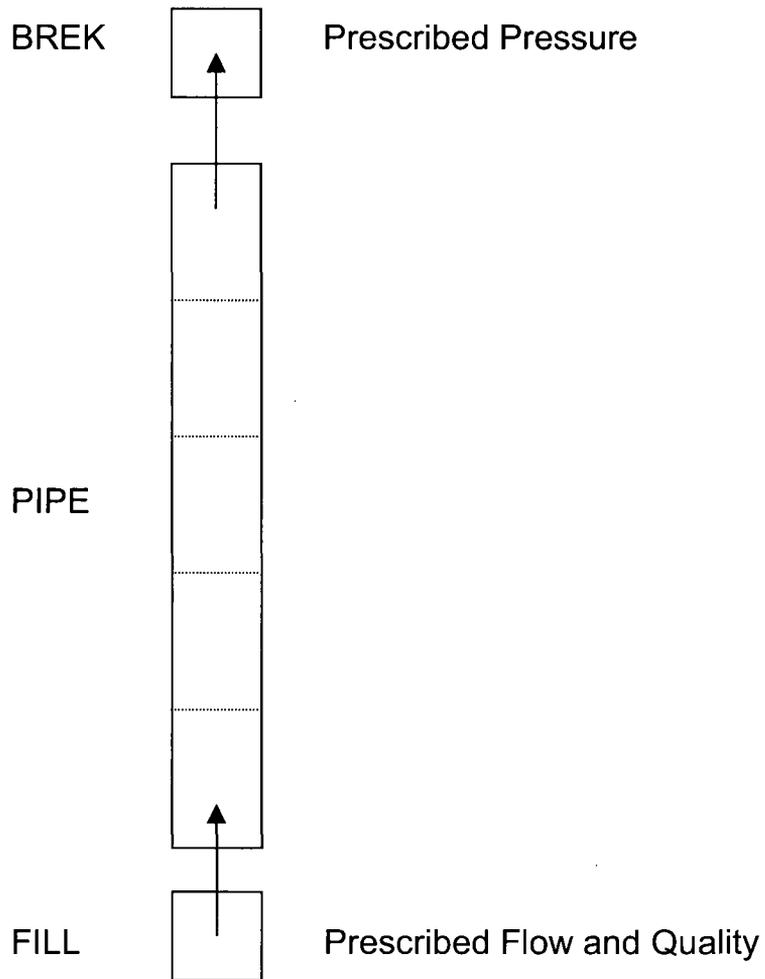
Figure 3.1-49. TRACG Model of CISE Test Facility

[[

]]

Figure 3.1-50. Comparison of TRACG and CISE Void Data at 4.9 MPa and 388 kg/m2-s

[[

]]

Figure 3.1-51. Comparison of TRACG and CISE Void Data at 4.9 MPa and 1081 kg/m2-s

[[

]]

Figure 3.1-52. Correlation of TRACG Predictions with CISE Void Data at 4.9 MPa

3.2 HEAT TRANSFER

This section addresses the adequacy of the TRACG models and correlations for film boiling, post-dryout and core spray heat transfer by comparisons to test data from the Oak Ridge National Laboratory (ORNL) Thermal Hydraulic Test Facility (THTF) and the General Electric Core Spray Heat Transfer (CSHT) test facility. The data comparisons also address interfacial heat transfer, which can be important in film boiling where the temperatures of the liquid and vapor phases differ. (In other two-phase regimes, interfacial heat transfer does not contribute significantly to the overall thermal resistance.) Wall heat transfer at the onset of boiling is of primary interest for void prediction and post-dryout heat transfer is of primary interest for the prediction of fuel temperatures. Other TRACG heat transfer regimes described in the TRACG model description report [3-1] are of lesser importance for transient and safety calculations and are based on well established correlations that do not require further independent qualification.

3.2.1 THTF Film Boiling Tests

3.2.1.1 Test Facility and Test Description

The Thermal Hydraulic Test Facility (THTF) [3-15] was an experimental test loop at Oak Ridge National Laboratory designed to represent typical pressurized water reactor (PWR) fuel bundles. The facility had a wide range of capabilities for thermal-hydraulic testing using electrical resistance heaters in a well-instrumented multirod geometry. The rod bundle, which included 60 heated and 4 unheated rods, was 3.66 m in height and was mounted in a vertical test section. It was cooled by demineralized water with normal steady-state flow upward through the bundle. Each of the 60 heated rods was instrumented with one centerline and three sheath thermocouples at each of four elevations. The temperature measurement uncertainty was ±11 K.

The test loop included a pump, pressurizer and heat exchanger and volumes representing the downcomer and upper and lower plenum regions. In addition to the rod thermocouples, the THTF instrumentation included measurements of channel inlet flow, system pressure and a large array of measurements of channel vapor temperatures. Although the upper end of the pressure range for the THTF tests was significantly above the range of interest for a BWR, the test section depressurized to levels that are characteristic of BWR transients. Of primary importance for TRACG qualification is the inclusion in the tests of sustained periods of forced convection film boiling heat transfer over a wide range of conditions.

Tests 3.06.6B and 3.08.6C [3-16] were chosen for the TRACG qualification studies. The steady-state conditions prior to the initiation of the transient for these two tests are shown in Table 3.2-1. The transients were initiated by breaking the test section outlet rupture disk assembly. The bundle power was then ramped up over a short time interval. For Test 3.06.6B, the bundle power was maintained at 2.3 MW for the first 8 s, raised to 7.8 MW over a period of 2 s, slowly reduced to 3.2 MW at 16 s and tripped off at 17.6 seconds. The pump was tripped at transient initiation. Film boiling occurred from 10 to 25 s as the pressure decreased from 15 to 5.8 MPa. For Test 3.08.6C, the bundle power was maintained at 2.4 MW for the first 7 s, raised to 7.8 MW over a period of 2 s, held at that level until 27.5 s and then reduced to 3.2 MW at 32 s. The pump was left on for approximately the first 20 s of the test. Film boiling occurred from 10 to 35 s as the pressure dropped from 12.9 MPa to 6.6 MPa. The lower ends of the pressure ranges for both tests are typical of BWR transients.

SEPARATE EFFECTS TESTS

3.2.1.2 TRACG Model

The THTF test section was simulated by a TRACG CHAN component with 34 cells, 22 of which were heated. FILL and BREK components were used to prescribe the measured bundle inlet flow and exit pressure. [[

]]

3.2.1.3 Results and Discussion

[[

]]

Film boiling heat transfer in TRACG is calculated with a modified form of the Bromley correlation at low void fraction and with the SGT correlation at high void fraction. Comparisons between TRACG calculations and the THTF separate effects tests represent one element of the validation of the TRACG film boiling heat transfer models. The modified Bromley and SGT correlations are discussed in detail and compared to additional data in the TRACG Model Description Report [3-1]. Also, in Section 5.0 of this report, comparisons of TRACG calculations and test measurements are shown for the TLTA and FIST integral systems effects tests. A significant feature of these tests is film boiling in BWR fuel bundle geometries at pressures less then one MPa.

3.2.1.4 Conclusions

[[

]]

Table 3.2-1
Steady-State Conditions Prior to Transient Initiation

Quantity	Test 3.06.6B	Test 3.08.6C
Inlet flow (m³/s)	0.0079	0.0082
Inlet temperature (K)	547	538
Outlet temperature (K)	610	598
Bundle power (MW)	2.3	2.4
Outlet pressure (MPa)	14.8	12.8
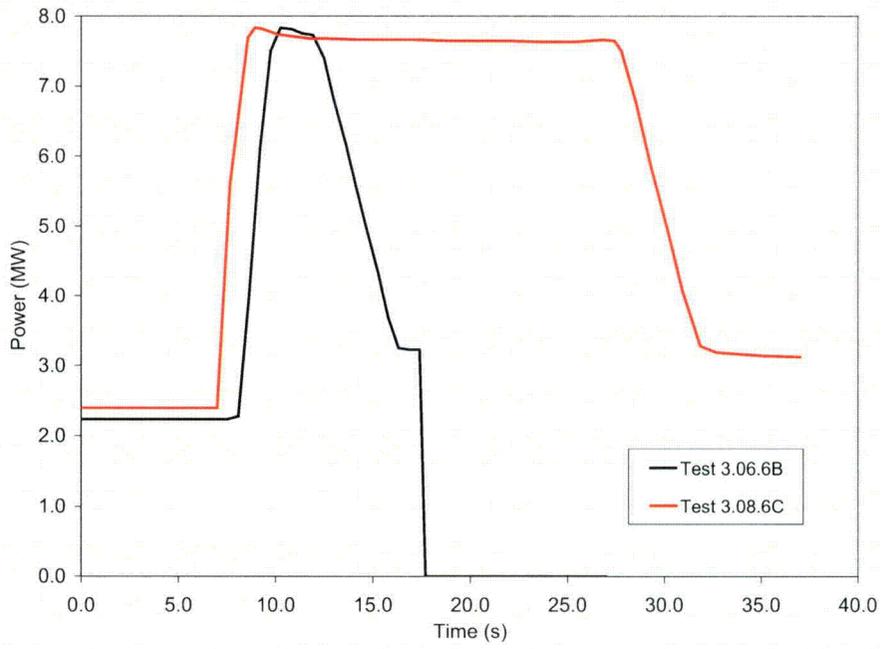
Figure 3.2-1. Bundle Power Histories for THTF Film Boiling Tests

[[

]]

[[

]]

Figure 3.2-2. TRACG Rod Grouping for THTF Test Simulation

[[

]]

Figure 3.2-3. Rod Temperature Comparison for THTF Test 3.06.6B at 2.4 m

[[

]]

Figure 3.2-4. Rod Temperature Comparison for THTF Test 3.06.6B at 3.6 m

SEPARATE EFFECTS TESTS

[[

]]

Figure 3.2-5. Rod Temperature Comparison for THTF Test 3.08.6C at 2.4 m

[[

]]

Figure 3.2-6. Rod Temperature Comparison for THTF Test 3.08.6C at 3.6 m

3.2.2 Core Spray Heat Transfer

In this section, the adequacy of TRACG for prediction of core spray heat transfer is evaluated by comparison with test data from a simulated BWR fuel bundle in the General Electric Core Spray Heat Transfer (CSHT) test facility [3-18]. The heat transfer modes that play a significant role in these tests include convective heat transfer under dispersed flow conditions, radiation and axial conduction-controlled quenching. Comparisons between TRACG predictions and test measurements are made for three high-temperature steady-state radiation tests (no spray) and a series of six transient spray tests.

3.2.2.1 Test Facility

A schematic of the test section of the General Electric Core Spray Heat Transfer facility is shown in Figure 3.2-7. The central feature of the facility is a full-scale simulation of an 8x8 fuel bundle with 63 electrically heated (fuel) rods and one unheated (water) rod. [[

]] The average relative powers to each of the rod groups, which varied from test to test, are shown in the table in Figure 3.2-8. The relative axial power distribution in the heated rods is shown in Figure 3.2-9. For the transient spray tests, liquid is injected through a spray nozzle at the top of the fuel bundle, which is open to the atmosphere. Clad temperatures were measured at five axial locations on the water rod and at three axial locations on all other rods. The rod temperature measurement uncertainty is ±4 K. Key test facility geometric parameters are listed in Table 3.2-2.

Table 3.2-2
Key Geometric Parameters for the CSHT Facility

Bundle Heated Length	3.98 m
Bundle Flow Area	0.01 m^2
Rod Diameter	0.00626 m

3.2.2.2 Test Description

Three steady-state radiation tests and six transient spray tests were included in the CSHT qualification study. For the steady-state tests, no liquid was injected at the top of the fuel bundle and the bundle contained only stagnant air. Under these conditions, the convective heat transfer is minimized and radiation heat transfer is the dominant mode. A constant power of 25 kW was applied to the bundle, while the outside of the channel box was cooled by water at a temperature of 311 K. The tests were conducted until equilibrium conditions were obtained.

The test conditions for the six transient spray tests are shown in Table 3.2-3. The parameters varied for the individual tests were the power, spray flow rate and the peak rod temperature at which the spray flow was initiated. To start the test, the power was held constant with no spray until the average rod temperature at some instrumented elevation in one of the rod groups reached the value shown under PCT$_{init.}$. Spray was then initiated and the bundle power was decreased to simulate decay heat (Figure 3.2-10). Run 120 was essentially a repeat of Run 113.

Table 3.2-3
Test Conditions for CSHT Transient Spray Tests

Run No.	P (kPa)	PCT$_{init.}$ (K)	Q$_{init.}$ (kW)	W$_{spray}$ (kg/s)	T$_{spray}$ (K)
110	101	930	250	0.19	311
111	101	1062	248	0.19	311
112	101	1156	249	0.19	309
113	101	933	300	0.29	311
120	101	936	300	0.28	313
121	101	942	300	0.51	314

3.2.2.3 TRACG Model

Figure 3.2-11 shows a schematic of the TRACG nodalization. The rod bundle is modeled with a CHAN component containing 24 heated cells. (There is some variation in the lengths of the cells that is not reflected in the nodalization diagram.) A TEE component represents the unheated region below the rod bundle. The atmospheric pressure boundary condition is imposed by a BREK component and the spray liquid is injected by a FILL component via a TEE component at the top of the bundle. Liquid that reaches the bottom of the bundle is drained to a FILL component but no steam is allowed to leave at the bottom. A loss coefficient, established on the basis of exit steam flow measurements taken during CCFL testing in the same facility (Section 3.3), was imposed at the interface between the test section and the BREK component. The exit loss causes the bundle to operate at a pressure that exceeds atmospheric pressure by an amount that depends on the exit steam flow. A convective boundary condition on the outside of the channel wall simulates the cooling associated with spray to the bypass.

As discussed above, the 64 rods in the simulated 8x8 bundle are divided into [[ ]]groups to account for the radial power distribution within the bundle as shown in Figure 3.2-8. The axial power distribution shown in Figure 3.2-9 is the same for each rod group. In addition to the rod grouping, input data are supplied that enable TRACG to locate each rod within the bundle and calculate the properties of the radiation heat sink available to that rod. For the CSHT tests, the channel wall, which is quenched from the outside, was the dominant heat sink and was more accessible to the peripheral rods than to the interior rods.

The TRACG CHAN component is one-dimensional in the sense that it admits only a single temperature for each phase and a single void fraction, liquid velocity and vapor velocity within a given axial cell. Two TRACG features address the potential effects of radial variations in the properties of the fluid surrounding the rods. The first of these selectively applies a multiplier to the Sun-Gonzalez-Tien (SGT) heat transfer coefficient that governs convective rod heat transfer under dispersed flow conditions. [[The SGT heat transfer coefficient is reduced by 20% for the interior rods (the shaded region in Figure 3.2-8) to account for the expectation that the vapor temperature will be higher in the interior of the bundle than on the periphery. The basis for the 20% reduction is explained in Reference 3-17.]]

[[

]]

3.2.2.4 Results for Steady-State Test

[[

Figure 3.2-12

Figure 3.2-8

]]

3.2.2.5 Results for Transient Tests

[[

Figure 3.2-13   Figure 3.2-18

Figure 3.2-13   Figure 3.2-18

]]

3.2.2.6 Summary and Conclusions

TRACG was used to simulate three steady-state radiation-only tests and six transient core spray tests performed in the General Electric Core Spray Heat Transfer (CSHT) test facility. The tests were performed on a full-scale electrically heated 8x8 fuel bundle. The results of the comparisons of TRACG calculations with measured data support the following conclusions:

[[

Table 3.2-4 Statistical Summary for CSHT Qualifiaction Cases

[[

]]
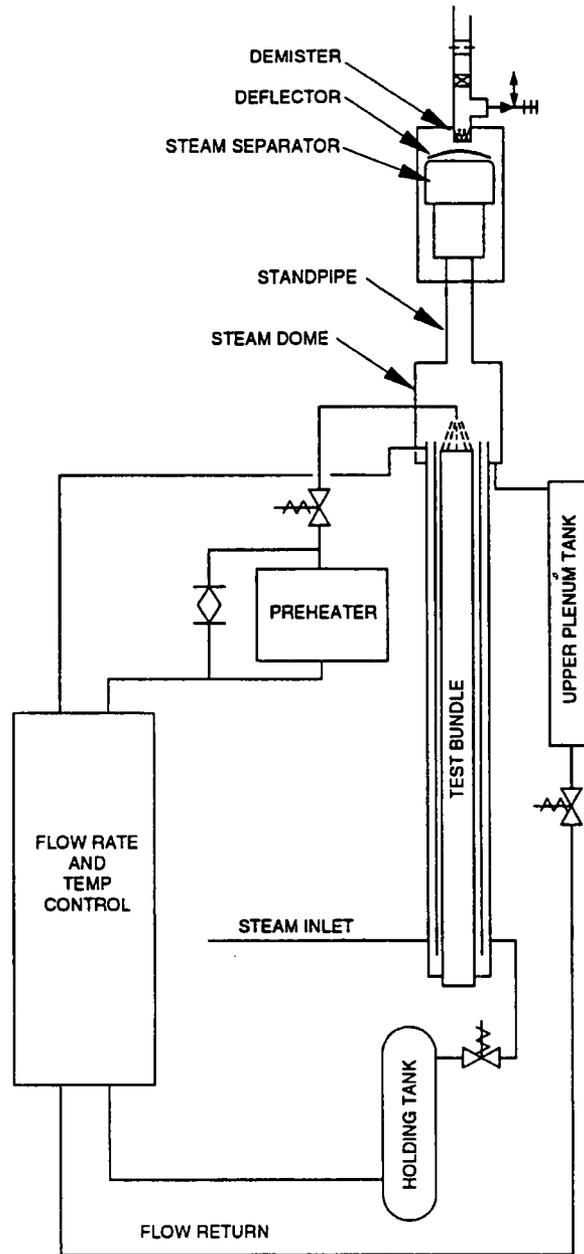
Figure 3.2-7. CSHT Facility Test Loop Schematic

SEPARATE EFFECTS TESTS

[[

]]

[[

]]

Figure 3.2-8. CSHT Facility Rod Groups
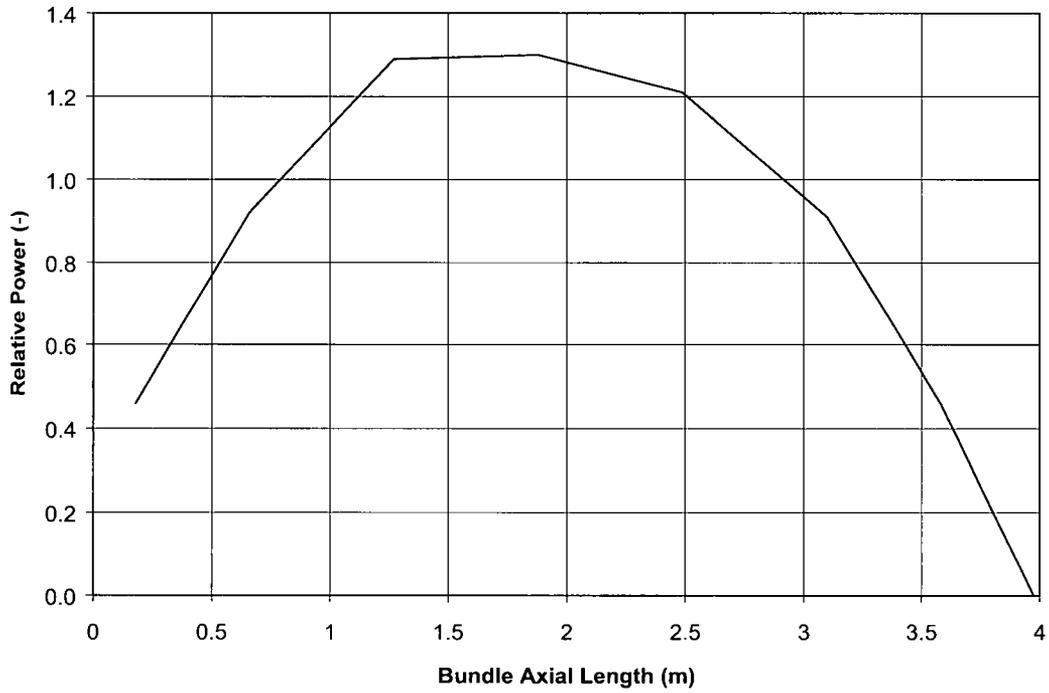
Figure 3.2-9. CSHT Facility Relative Axial Power Distribution
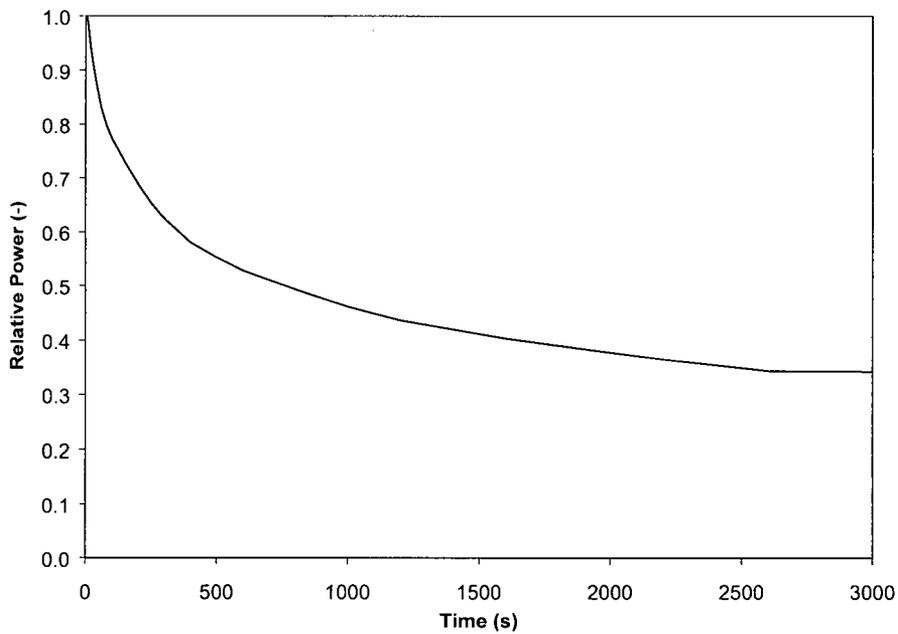
Figure 3.2-10. CSHT Normalized Bundle Power vs. Time
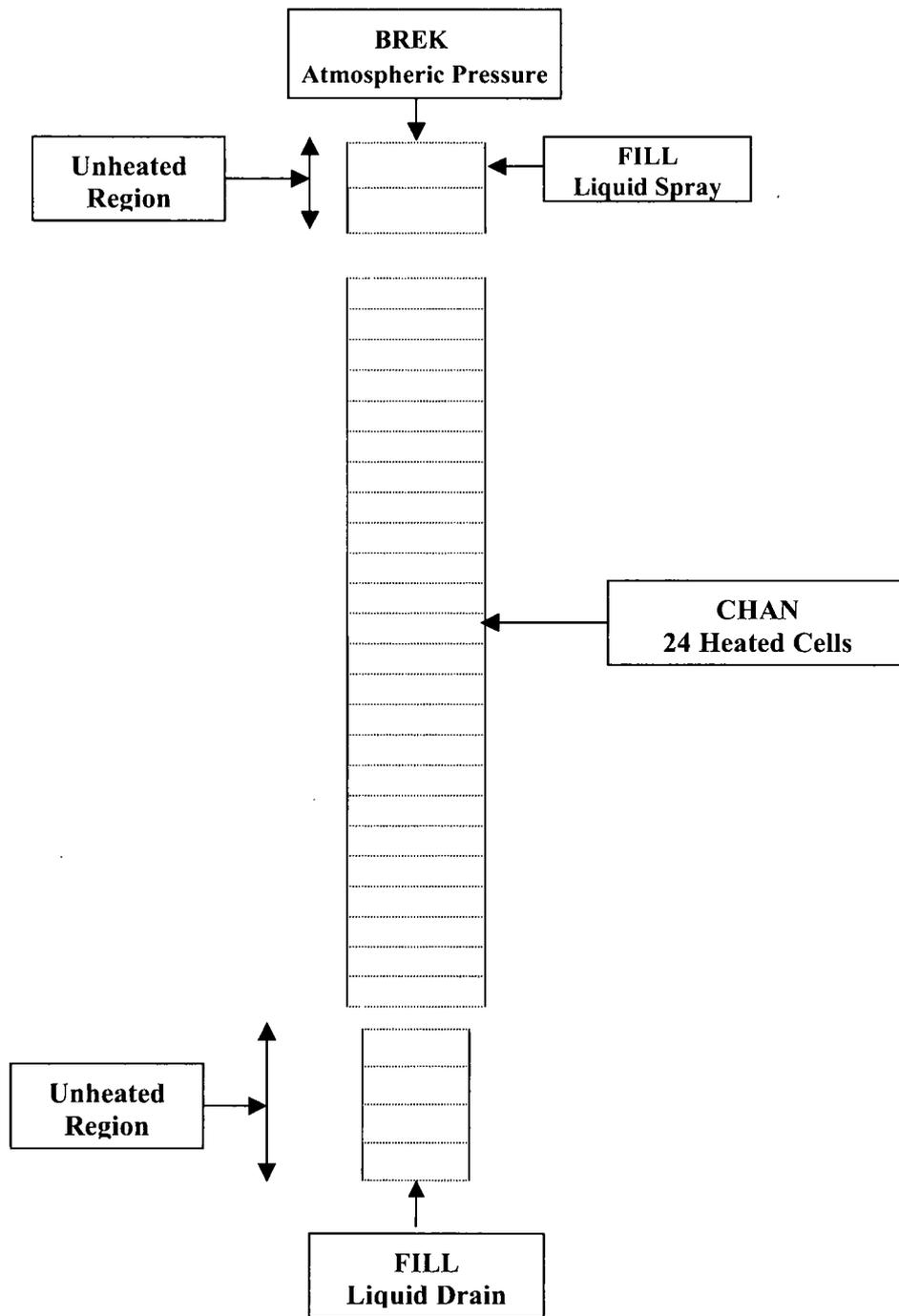
Figure 3.2-11. TRACG Nodalization of the CSHT Facility Bundle

[[

]]

Figure 3.2-12. CSHT Steady-State Radiation Test Temperature Profile

[[

]]

Figure 3.2-13. CSHT Run 110 Temperature Comparison

[[

]]

Figure 3.2-14. CSHT Run 111 Temperature Comparison

[[

]]

Figure 3.2-15. CSHT Run 112 Temperature Comparison

SEPARATE EFFECTS TESTS

[[

]]

Figure 3.2-16. CSHT Run 113 Temperature Comparison

[[

]]

Figure 3.2-17. CSHT Run 120 Temperature Comparison

[[

]]

Figure 3.2-18. CSHT Run 121 Temperature Comparison

3.3 COUNTER-CURRENT FLOW LIMITATION

Emergency core cooling systems (ECCS) are activated during a hypothetical loss-of-coolant accident (LOCA) in a boiling water reactor (BWR) to maintain the temperature of the fuel cladding below a given limit. Although the reactor is shut down during the LOCA, the core retains its sensible heat from full power operation and it continues to generate power in the form of decay heat. Thus, steam will be generated from the ECCS water as it contacts the core region. This steam will flow upward through the core and into the upper plenum region. The action of steam flowing upward while coolant water flows downward can lead to a condition termed "counter-current flow limiting" (CCFL) that restricts the water downflow. For the application of TRACG to LOCA calculations, CCFL correlations derived from separate effects test data are implemented at locations where CCFL may occur - for example, the upper tieplate (UTP) and side entry orifice (SEO). The code ensures that the liquid downflow for a given steam upflow at each of these locations is no larger than that permitted by the CCFL correlation. In this section, CCFL data covering a range of liquid subcoolings from tests performed in the CSHT facility [3-18] are first presented to illustrate various aspects of CCFL behavior. Calculations using a TRACG model of the CSHT test facility are then compared with the data set used to obtain the design CCFL correlation at the UTP [3-26].

3.3.1 Description of the Experiment

[[

]]

3.3.2 CCFL Tests with Variable Liquid Subcooling

[[

]]

Table 3.3-1
CSHT CCFL Tests with Variable Liquid Subcooling

[[		
		]]

Figure 3.3-2 shows the liquid drain flow plotted against the injected steam flow with the subcooling of the injected liquid as a parameter. The following observations can be made with reference to the experimental results shown in Figure 3.3-2:

- When the steam flow is less than the condensation capacity of the subcooled liquid downflow, all of the steam is condensed below the UTP and the drain flow is the sum of the injected liquid flow and the condensed steam. This condition, called "subcooled CCFL breakdown", can be described as follows:

$$\text{If} \quad W_g < W_{cond} = \frac{W_{\ell 0} c_{p\ell} \Delta T_\ell}{h_{fg}} \quad \text{then} \quad W_\ell = W_{\ell 0} + W_g \tag{3.3-1}$$

where $W_{\ell 0}$ and W_ℓ denote, respectively, the injected liquid flow and the drain flow.

- When the steam flow exceeds the condensation capacity of the injected liquid flow, a pool of saturated liquid forms above the UTP and the system behavior becomes the same as for saturated liquid injection. The drain flow is limited by CCFL and the data can be correlated in terms of the liquid and vapor volumetric fluxes by a Kutateladze relationship of the form [3-26]:

$$\sqrt{K_g} + m\sqrt{-K_\ell} = \sqrt{K} \tag{3.3-2}$$

[[

]]

3.3.3 Test to Establish Design CCFL Correlation at UTP

[[

]]

3.3.4 TRACG Model for Comparison with UTP CCFL Design Correlation

[[

]]

3.3.5 Results and Conclusion

[[

]]

[[

]]
Figure 3.3-1. CSHT Facility Test Bundle for CCFL Tests

SEPARATE EFFECTS TESTS

[[

]]
Figure 3.3-2. Upper Tie Plate CCFL Test Data with Subcooled Spray Flow

[[

]]
Figure 3.3-3. TRACG Compared with UTP CCFL Design Correlation

3.4 CRITICAL FLOW

This section evaluates the capability of TRACG to predict critical flow. Critical flow is important for the calculation of the break flow in a BWR LOCA simulation and for the calculation of flow through valves, such as bypass and safety/relief valves, in simulations of BWR transients. Data from the Marviken Critical Flow Tests [3-27], PSTF test facility [3-8] and the Edwards test [3-28] are used for evaluating the critical flow model in TRACG. The Edwards test and the PSTF tests are small-scale tests and the Marviken tests are large-scale tests.

3.4.1 Marviken Critical Flow Tests

The critical flow data from the Marviken facility are for break configurations of large diameter and relatively short lengths with subcooled and low quality stagnation conditions. Marviken Tests 15 and 24 were selected for the TRACG assessment. The break nozzle in each experiment had a diameter of 0.5 m and length-to-diameter (L/D) ratios of 3.6 and 0.33 for Tests 15 and 24, respectively.

3.4.1.1 Marviken Facility

The Marviken test facility [3-27] was originally intended to be a heavy water moderated power reactor. The facility consists of a pressure vessel, a discharge pipe, a test nozzle and a rupture disc assembly. The vessel (Figure 3.4-1) was the actual power reactor pressure vessel. Most of the original internal components were removed when it was converted to a test facility. The internal structures that remained were the peripheral part of the core superstructure and the cylindrical wall and bottom of the moderator tank. Gratings were installed at three elevations in the lower vessel regions to preclude the formation of vortices.

The discharge pipe (Figure 3.4-2) consisted of seven components: an axisymmetric inlet section, a connection piece, two pipe spools, two instrumentation rings and an isolation ball valve. The discharge pipe, penetrating and welded to the bottom of the vessel, allowed fluid from the vessel to enter the discharge pipe at an elevation 0.740 m above the vessel bottom. The pertinent dimensions of the discharge pipe component are shown in Figure 3.4-2.

The test nozzle was connected at the lower end of the discharge pipe as shown in Figure 3.4-2. The diameter and length of the test nozzle were the primary variables in the Marviken critical flow test program. The nozzles used for Tests 15 and 24 are shown in Figure 3.4-3. The nozzle used in Test 15 had a diameter of 0.500 m and a length of 1.809 m, yielding an L/D ratio of 3.6. The nozzle used for Test 24 had a diameter of 0.500 m and a length of 0.166 m, yielding in an L/D ratio of 0.33. The diameter was constant downstream of the convergent section of the test nozzle.

The downstream end of the test nozzles was built as a rupture disc assembly with two identical rupture discs. The critical flow transients were initiated by overpressurizing the space between the two discs, inducing failure of the downstream disc. As a result, the upstream disc also failed, breaching the primary system. The rupture discs were designed to fail along their entire periphery so as to be completely removed from the nozzle exit region.

3.4.1.2 Test Description

Prior to an experiment, the vessel was completely filled with deionized water and the integrity of the rupture discs was checked. The water level was then drained to about the 16.4 m elevation with respect to the bottom of the vessel. The water was heated by drawing cool water from the bottom of the vessel and circulating it through an electric boiler. The heated water was then reintroduced into the steam dome region of the vessel. To obtain the desired axial fluid temperature profile, additional unheated water was reintroduced to the vessel through a spray ring in the upper vessel region. During the warmup process, the vessel was periodically vented to purge air from the system. Detailed information concerning the heatup procedures can be found in Reference 3-27.

The warmup process produced an axial temperature profile in the vessel with saturated conditions in the steam dome at 5.04 and 4.96 MPa for Tests 15 and 24, respectively. The axial temperature profiles are shown in Figure 3.4-5. Both tests had a region in which nearly constant saturated temperature conditions existed near the top of the vessel and, further down, a nearly constant temperature region in which 31 and 33 K subcooling existed in Tests 15 and 24, respectively. The initial fluid temperature in the test nozzle was 450 and 453 K in Tests 15 and 24, respectively, with a linear axial temperature gradient between the nozzle and the vessel due to heat losses prior to the start of the experiment. The flow measurement uncertainty for the Marviken tests was ±135 kg/s.

3.4.1.3 TRACG Nodalization

[[

]]

3.4.1.4 Boundary and Initial Conditions

The initial conditions used for the TRACG calculations for Tests 15 and 24 are presented in Table 3.4-1. As stated earlier, the fluid temperature profiles at the initiation of each test are shown in Figure 3.4-5. The containment portion of the facility consisted of a series of interconnected rooms that were vented to the atmosphere. To eliminate the need to explicitly model the containment, a pressure curve for the volume into which the discharge occurred (taken from the experimental results in References 3-29 and 3-30) was supplied for each test by means of the BREK component described above. The containment pressure curves are shown in Figure 3.4-6.

3.4.1.5 Results

[[

]]

Table 3.4-1
Initial Conditions for Marviken Critical Flow Tests

Parameter	Test 15	Test 24
Steam dome pressure	5.04 MPa	4.96 MPa
Lower vessel subcooling[a]	31 K	33 K
Initial vessel liquid level	19.93 m	19.89 m
Initial system mass	327 Mg	328 Mg
Atmosphere pressure	100.0 kPa	101.5 kPa
Initial elevation of subcooled region[b]	15.5 m	17 m
Initial fluid temperature in the discharge pipe	450 K to 506 K	453 K to 503 K
Initial fluid temperature in the vessel	See Figure 3.4-5	See Figure 3.4-5

[a] Subcooling values are referenced to T_{sat} in the steam dome.

[b] Elevations are with respect to the bottom of the vessel.

Table 3.4-2
Comparison of Blowdown Flow Ratios for Marviken Tests 15 and 24

[[			
			]]
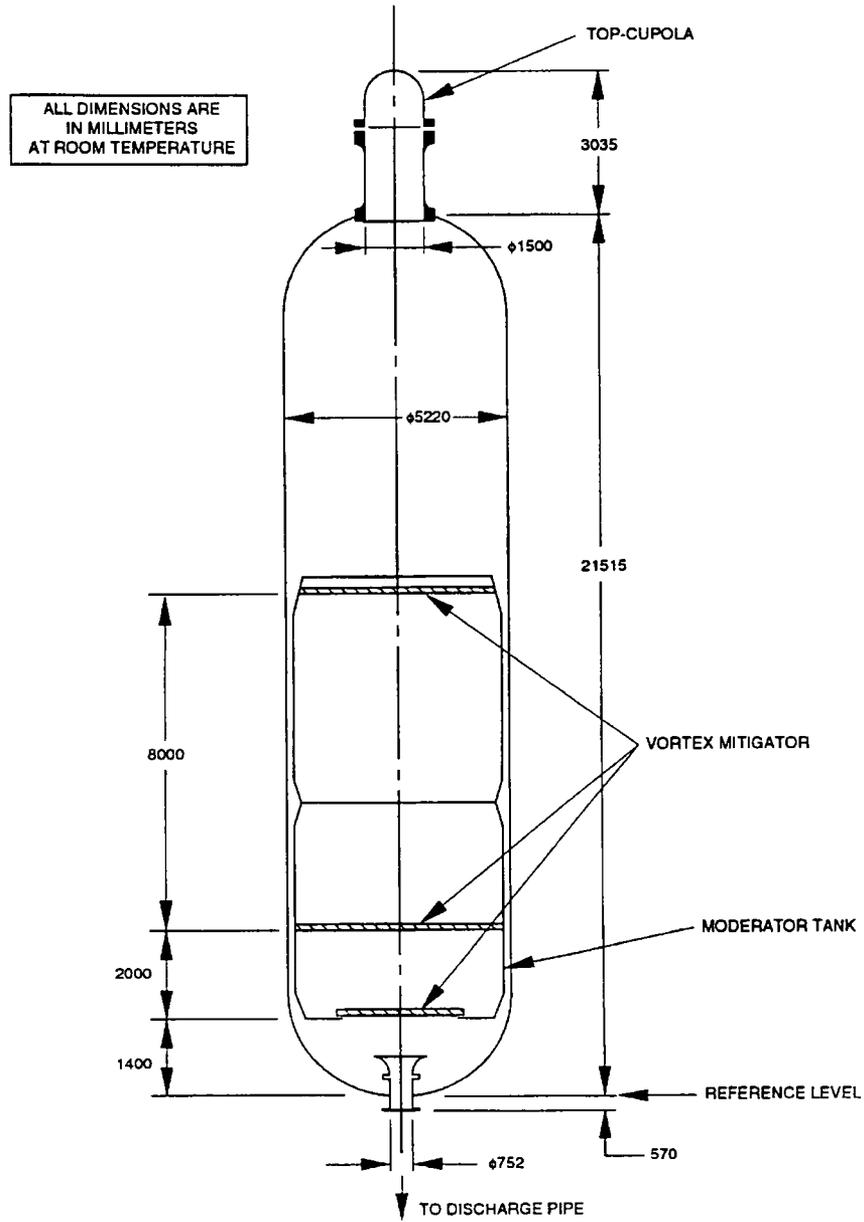
Figure 3.4-1. Marviken Pressure Vessel
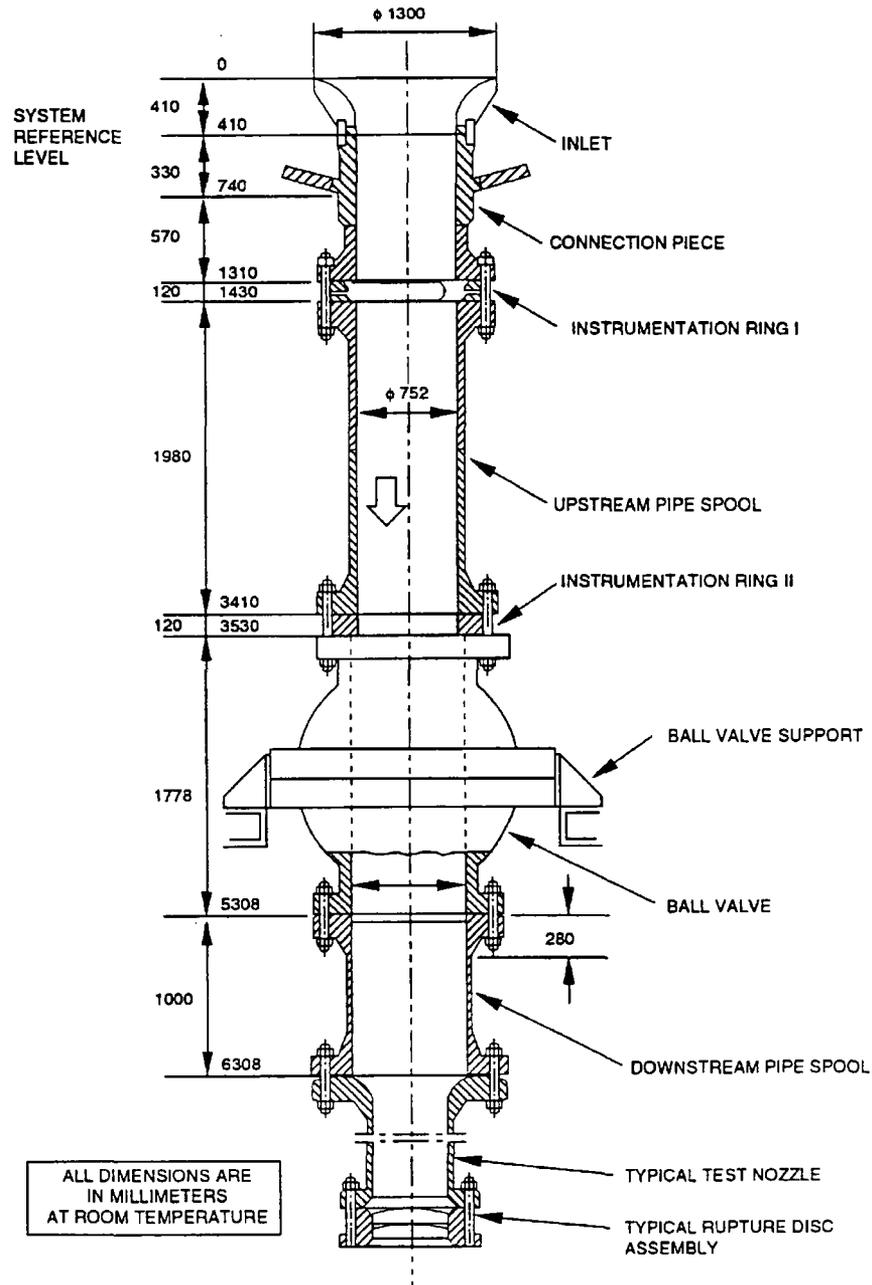
Figure 3.4-2. Discharge Pipe, Test Nozzle, and Rupture Disk in the Marviken Facility
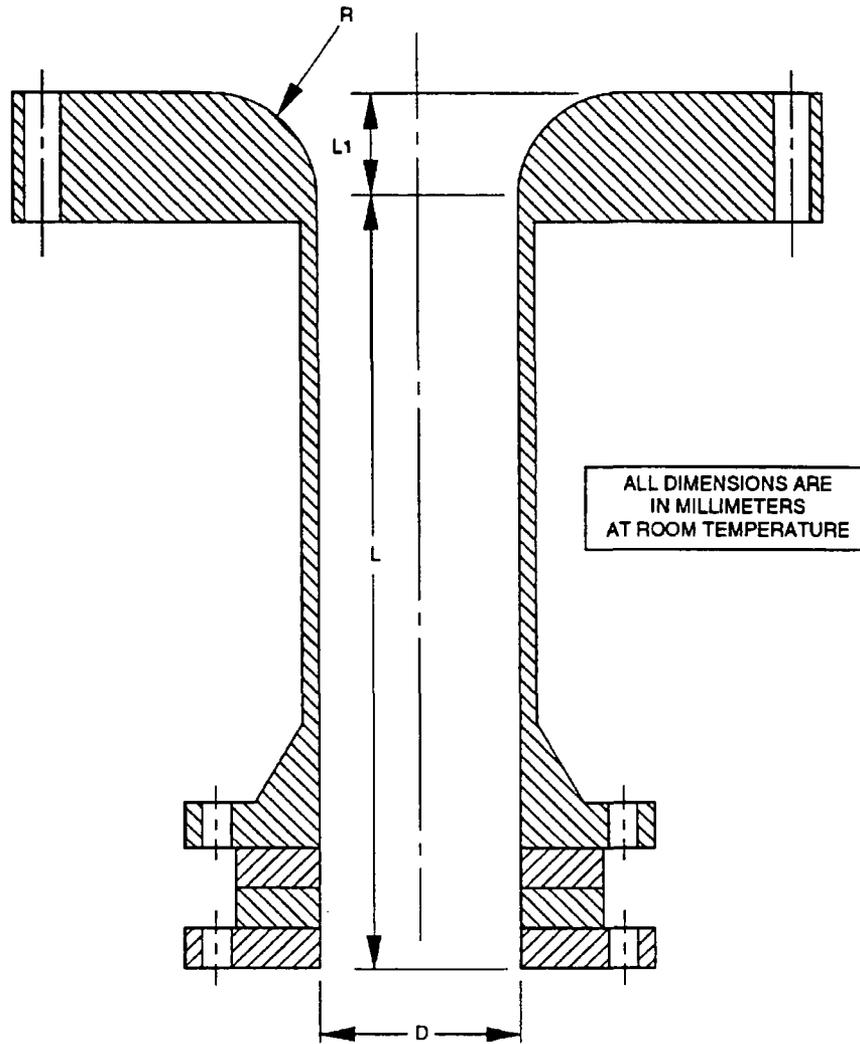
D	L/D	L	L1	R
500	3.6	1809	156	250
500	0.3	166	225	250

Figure 3.4-3. Dimensions of the Test Nozzles for Tests 15 and 24

[[

]]

Figure 3.4-4. TRACG Model for Marviken

SEPARATE EFFECTS TESTS
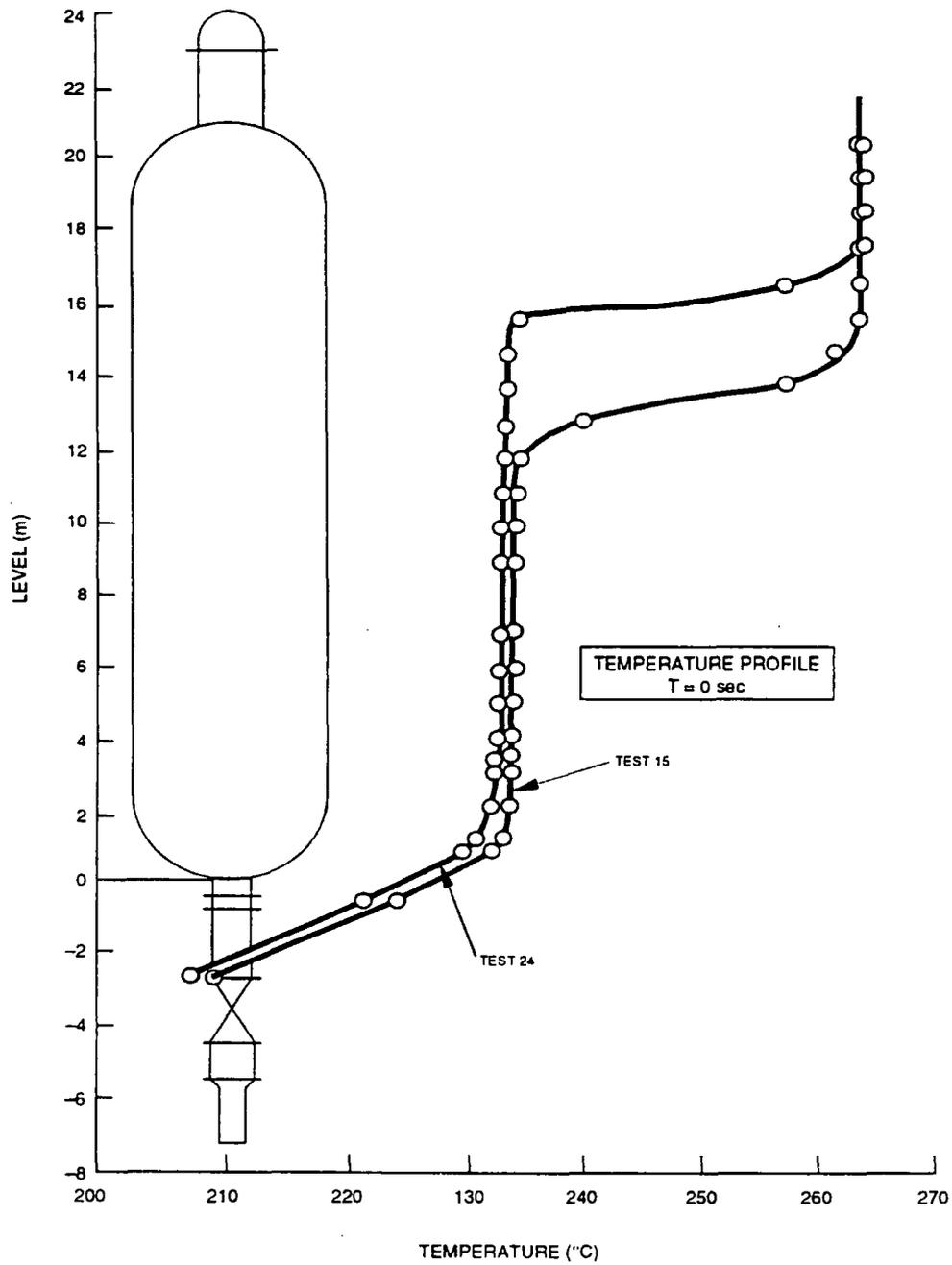
Figure 3.4-5. Axial Fluid Temperature Profiles for Marviken Tests 15 and 24
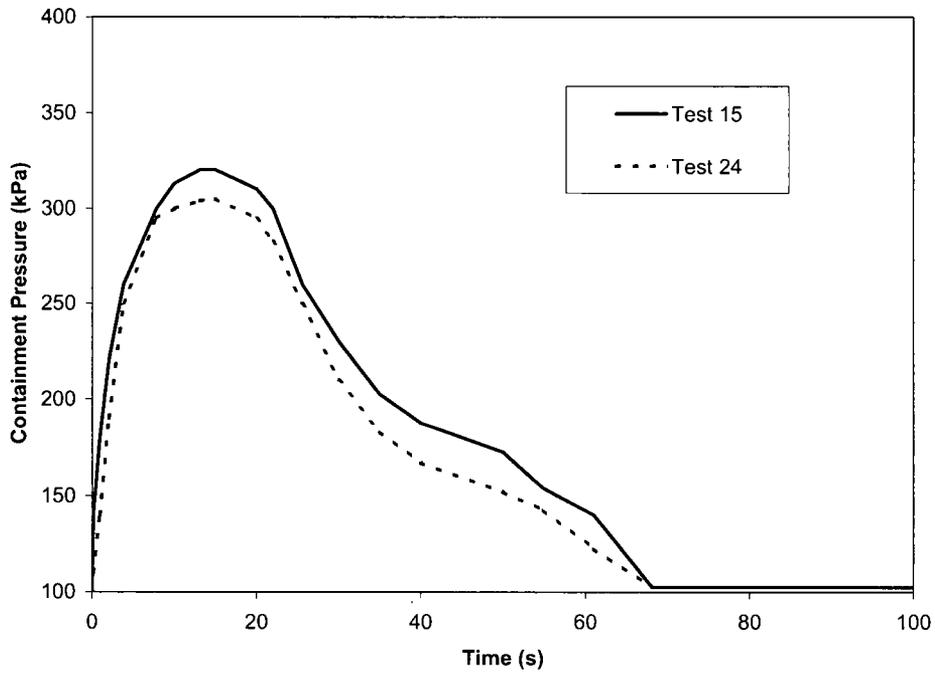
Figure 3.4-6. Containment Pressure for Marviken Tests 15 and 24

[[

]]

Figure 3.4-7. Comparison of Break Flow for Marviken Test 15

[[

]]

Figure 3.4-8. Comparison of Break Flow for Marviken Test 24

3.4.1.6   Sensitivity Studies on Marviken

[[

[[

]]

]]

Figure 3.4-9. Effect of Wall Heat Transfer on Break Flow, Marviken Test 15

SEPARATE EFFECTS TESTS

[[

]]

Figure 3.4-10. Effect of Nodalization on Break Flow, Marviken Test 15

3.4.2 PSTF Critical Flow Tests

Level-swell data from the PSTF tests [3-8] were previously used for the qualification of TRACG for the calculation of void fraction (Section 3.1.5). These tests also provide useful data for qualification of TRACG for the calculation of critical flow. The PSTF test facility and test conditions and the TRACG model for the facility are described in Section 3.1.5. This section contains comparisons between the test data and TRACG calculations relevant to the TRACG critical flow model. The flow measurement uncertainty in the PSTF facility is 2.25 kg/s and the measurement uncertainty for pressure is ±70 kPa.

[[

]]

[[

]]

Figure 3.4-11. PSTF Test 5801–15, Break Flow

[[

]]

Figure 3.4-12. PSTF Test 5803–01, Break Flow

SEPARATE EFFECTS TESTS

[[

]]

Figure 3.4-13. PSTF Test 5803–02, Break Flow

[[

]]

Figure 3.4-14. PSTF Test 5801–19, Pressure

[[

]]

Figure 3.4-15. PSTF Test 5702–16, Pressure

3.4.3   Edwards Blowdown

Edwards [3-28] performed blowdown tests that are used as a standard for evaluating critical flow models for rapid depressurization. The test section for the experiment consisted of a 4.096 m-long horizontal pipe with an inner diameter of 0.073 m. The pipe was filled with liquid that was heated and pressurized to 7.0 MPa. The saturation pressure corresponding to the initial liquid temperature was approximately 2.4 MPa. To initiate the experiment, a glass plate covering the end of the pipe was broken and the pipe depressurized in approximately 0.6 seconds. The pressure measurement uncertainty for the test was ±14 kPa and the void fraction measurement uncertainty was ±3%.

[[

]]·

[[

]]

Figure 3.4-16. Edwards Blowdown, Pressure

SEPARATE EFFECTS TESTS

[[

]]

Figure 3.4-17. Edwards Blowdown, Void Fraction

3.5 FUEL BUNDLE PRESSURE DROP

The pressure losses through the fuel bundles, steam separators and jet pumps are the most important from the standpoint of TRACG qualification for the calculation of RPV pressure drop. This section compares TRACG fuel bundle pressure drop calculations with experimental data obtained from two General Electric fuel designs tested in the ATLAS thermal-hydraulic test facility. In Section 4, TRACG comparisons to jet pump (Section 4.1) and steam separator (Section 4.2) flow and pressure drop data are presented. The TRACG fuel bundle pressure drop calculations use inputs derived from separate effects testing to obtain the irreversible loss coefficients for the bundle spacers and tieplates. The losses through the spacers and tieplates are the major contributors to the bundle pressure drop measured in the ATLAS tests. The flow range for the ATLAS tests does not cover LOCA conditions. The LOCA flow range is covered by the TLTA and FIST data comparisons presented in Section 5 of this report.

The core bypass - the region inside the core shroud but outside the active fuel channels – is also an important reactor flow path. During normal operation and most transients, the bypass flow is largely single-phase and is dominated by elevation head except at the bypass inlet. GE has performed separate effects tests to determine the losses at the bypass inlet. Under LOCA conditions, where the bypass may not be single-phase or may not be full, the TLTA and FIST tests provide qualification pressure drop data. The downcomer and the upper plenum are also part of the recirculation loop flow path. In these regions, the pressure drop under normal operating conditions and during transients is primarily elevation head and is calculated in a straightforward manner by TRACG. Under LOCA conditions, the TLTA and FIST integral tests again provide the necessary pressure drop qualification data.

3.5.1 ATLAS Thermal-Hydraulic Test Facility

The ATLAS test facility was a single-bundle test loop capable of simulating BWR operating conditions. The ATLAS bundle pressure drop tests included in this qualification study were performed with simulated GE9 and GE14 BWR fuel [3-31 and 3-32]. The ATLAS test bundles were electrically heated full-scale replicas of the actual fuel bundles. Figures 3.5-1 and 3.5-2, respectively, are schematics of the GE9 and GE14 ATLAS fuel bundles. Table 3.5-1 lists the significant characteristics for each of these fuel bundle geometries. Measurement uncertainties of the ATLAS test facility are summarized in Table 3.5-2. The pressure drop across the bundle was measured with differential pressure transducers at the elevations shown in Figures 3.5-1 and Figure 3.5-2.

]]

3.5.2 TRACG Model

The TRACG model for the GE9 fuel bundle uses a CHAN component with 30 cells and the model for the GE14 fuel bundle uses a CHAN component with 25 cells (Figure 3.5-3). The reason for the difference in the number of cells for the two fuel models is historical in nature and is not significant from the standpoint of TRACG predictive capability. In both models, the inlet mass flux is set by a FILL component at the bundle inlet and the system pressure is set by a BREK component at the bundle exit.

3.5.3 Results

[[

]]

Table 3.5-1
ATLAS GE9 and GE14 Test Bundle Characteristics

Lattice	GE9 (8x8)	GE14 (10x10)
Number of full- length heated rods	60	78
Number of part- length heated rods	N/A	14
Number of water rods	1	2
Diameter of heated rods	[[	
Diameter of water rods		
Channel width (inside)		
Heated length of full-length rods		
Heated region of part-length rods		
Shoulder length of part-length rods		
Axial heat flux profile		
Peak to average heat flux (axial)		]]
Number of spacers	7 (Figure 3.5-1)	8 (Figure 3.5-2)
Spacer type	Ferrule	Ferrule

Table 3.5-2
ATLAS Test Facility Measurement Uncertainties

[[	
	]]

[[

]]

Figure 3.5-1. GE9 ATLAS Test Bundle Schematic

[[

]]

Figure 3.5-2. GE14 ATLAS Test Bundle Schematic

Outlet

CHAN
(GE9: 30 cells)
(GE14: 25 cells)

Inlet

BREK — Specify system pressure

Specify geometry and heat flux

FILL — Specify inlet flow and subcooling
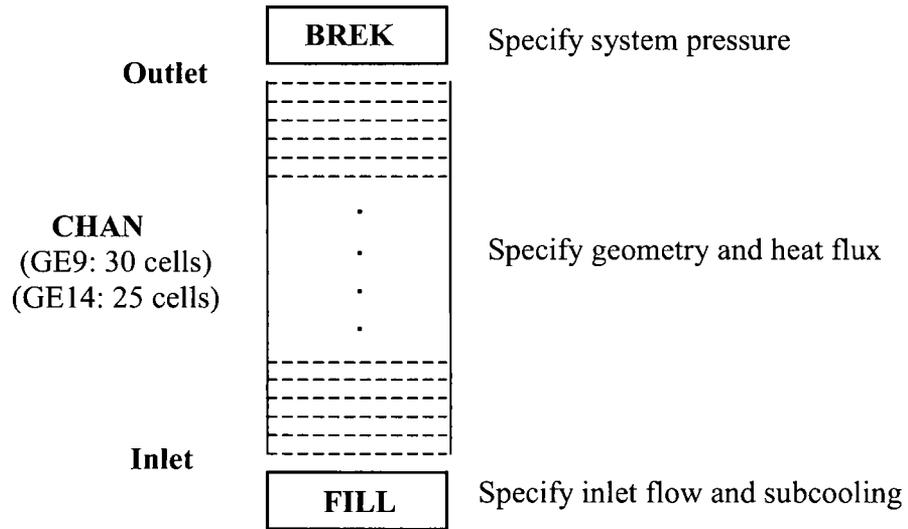
Figure 3.5-3. ATLAS Fuel Bundle TRACG Nodalizations

[[

]]

Figure 3.5-4. GE9 ATLAS Bundle Pressure Drop Comparison

[[

]]

Figure 3.5-5. GE14 ATLAS Bundle Pressure Drop Comparison

[[

]]

Figure 3.5-6. GE9 ATLAS Bundle Pressure Drop Comparison

[[

]]
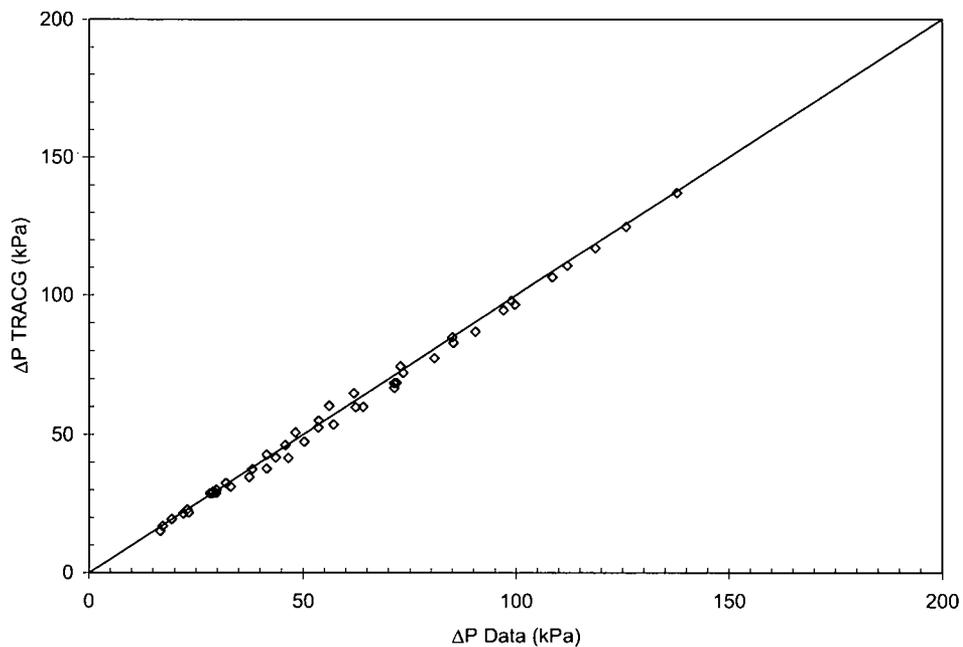
Figure 3.5-7. GE9 ATLAS Bundle Pressure Drop Summary Comparison

[[

]]

Figure 3.5-8. Relative Error in GE9 ATLAS Bundle Pressure Drop

[[

]]

Figure 3.5-9. Relative Error in GE14 ATLAS Bundle Pressure Drop

3.6 CRITICAL POWER

This section compares TRACG transient critical power calculations with experimental data obtained from General Electric fuel designs tested in the ATLAS thermal-hydraulic test facility. As described in Section 3.5, ATLAS was a single-bundle test loop capable of simulating BWR operating conditions. The ATLAS test bundles were electrically heated full-scale replicas of the actual fuel bundles. Extensive testing in ATLAS provided the steady-state critical power database for the GEXL correlation that is employed in TRACG to predict the onset of boiling transition (BT). ATLAS testing also included transient critical power tests that are used to demonstrate satisfactory performance of the GEXL correlation under conditions of varying power, pressure and flow. Flow oscillation tests at constant power and pressure are used to demonstrate GEXL performance under conditions where density wave oscillations are likely to occur. Section 3.6.1 describes comparisons of TRACG-GEXL predictions to experimental data for flow oscillation tests of a simulated GE11 fuel bundle. Transient testing in ATLAS testing also included pressurization-event tests that simulated a load rejection (or turbine trip) without bypass and with or without an accompanying recirculation pump trip and an ABWR all-pumps trip test. Section 3.6.2 describes comparisons of TRACG-GEXL predictions to experimental data for pressurization-event tests of GE9, GE11 and GE14 fuel bundles and an ABWR all-pumps trip test of the GE14 bundle.

3.6.1 Flow Oscillation Tests

[[

]]

3.6.1.1   *TRACG Input Model for Simulation of Flow Oscillation Tests*

[[

]]

3.6.1.2   *Results and Discussion*

[[

]]

3.6.2 Pressurization-Event and ABWR All-Pumps Trip Tests

3.6.2.1 Test Description

[[

]]

3.6.2.2 Sample Test Results

[[

]]

3.6.2.3 TRACG Model

[[

]]

3.6.2.4 Results and Discussion

[[

]]

3.6.3 Conclusions

[[

]]

Table 3.6-1
ATLAS GE11 Test Bundle Characteristics

[[	
	]]

Table 3.6-2
ATLAS Pressurization Event and All-Pumps Trip Tests with Boiling Transition

[[				
				]]

SEPARATE EFFECTS TESTS

[[

]]

Figure 3.6-1. GE11 ATLAS Test Bundle Schematic

[[

]]

Figure 3.6-2. ATLAS GE11 Fuel Bundle with TRACG Rod Grouping

SEPARATE EFFECTS TESTS

[[

]]

**Figure 3.6-3. ATLAS and TRACG Inlet Mass Fluxes
for Flow Oscillation Test (Run 209)**

[[

]]

Figure 3.6-4. Rod Temperature Comparison for ATLAS Run 205 at 4.8 MW

[[

]]

Figure 3.6-5. Rod Temperature Comparison for ATLAS Run 206 at 4.9 MW

[[

]]

Figure 3.6-6. Rod Temperature Comparison for ATLAS Run 209 at 5.2 MW

[[

]]

Figure 3.6-7. GE14 Pressurization Event without Recirculation Pump Trip (Run 1412)

[[

]]

Figure 3.6-8. GE14 Pressurization Event with Recirculation Pump Trip (Run 1418)

[[

]]

Figure 3.6-9. GE14 ABWR All-Pumps Trip Test (Run 1314)

[[

]]

Figure 3.6-10. Comparison of ΔCPR/ICPR for Pressurization-Event and ABWR All-Pumps Trip Tests

3.7 NATURAL CIRCULATION AND STABILITY

Thermal-hydraulic instability caused by density waves in a channel can occur in boiling two-phase flow when the power exceeds a threshold that depends on flow, pressure and inlet subcooling. Traditionally, this instability has been analyzed using frequency domain methods. The frequency domain method consists of a first order perturbation at a given frequency to the steady-state solution. Neglecting second order terms, a linear system of equations is formed and solved to determine the rate of growth or decay of the oscillation produced by the perturbation as a function of frequency. The maximum growth rate characterizes the thermal-hydraulic stability of the channel. Frequency domain methods generally predict the onset of instability well. However, because they are based on a linearized model, they cannot predict what will happen after the system becomes unstable. To capture the nonlinear effects of an unstable system, time domain methods are required. The purpose of this section is to evaluate the adequacy of TRACG for the prediction of thermal-hydraulic instability by comparison to experimental data from the FRIGG facility [3-34]. Two types of tests were run in the FRIGG facility. One test series used a pseudo-random signal imposed on the system to determine the system response as a function of frequency. A second test series provided a more deterministic measurement of the onset of unstable behavior. In these tests, which started from steady-state natural circulation operation, the system power was slowly increased until the onset of unsteady behavior was observed. This second series of tests was simulated with TRACG. Comparisons of TRACG predictions of the channel power for the onset of limit cycle oscillations to the power measured in the tests is considered the best assessment of the code's ability to predict the onset of unstable operation.

3.7.1 Facility and Test Description

A schematic of the FRIGG test loop is shown in Figure 3.7-1. The FRIGG test loop employed a circular channel containing 36 electrically heated rods with one large unheated rod in the center (Figure 3.7-2). The FT-36C (FRIGG-4) series of natural circulation tests were used for the TRACG qualification study described herein. These experiments were performed with a cosine axial power distribution as shown in Figure 3.7-3. During natural circulation operation, subcooling at the inlet to the channel was controlled via a feedwater supply located at the top of the downcomer. Pressure was maintained constant in the steam separator by controlling the coolant flow rate to the condenser. Test series were performed over a pressure range from 2 to 5 MPa. Most of these test series were performed with an inlet subcooling of approximately 5 K but one test series was performed with a system pressure of 5 MPa and an inlet subcooling of approximately 15 K. No information was provided about the measurement uncertainty in these natural circulation tests. The test runs used for TRACG qualification are summarized in Table 3.7-1.

Table 3.7-1
FT-36C (FRIGG-4) Tests used for TRACG Qualification

Pressure	Subcooling	Run Number
2 MPa	5 K	601206 - 601210
3 MPa	5 K	601199, 601201 - 601204
4 MPa	5 K	601195 - 601198
5 MPa	5 K	601179 - 601181
5 MPa	15 K	601137, 601141, 601144 - 601146

3.7.2   System Model and Input Generation

[[

]]

3.7.3   Test and Simulation Procedures

[[

•   ]]

3.7.4   Steady-State Calculations

[[

]]

3.7.5 Onset of Instability and Sensitivity Studies

[[

]]

3.7.6 Conclusions

The applicability of TRACG to time domain stability analysis has been assessed by comparison with stability data from the FRIGG test facility. On the basis of these comparisons, it can be concluded that:

[[

•

]]

Table 3.7-2
TRACG–Data Steady–State Comparison

Pressure (MPa)	Power (kW)	Flow Rate (kg/s)		
		Data	TRACG	Error (%)
2.07	1480	12.28	12.15	-1.09
2.07	1980	11.74	11.36	-3.20
2.07	2480	10.74	10.44	-2.76
2.07	2980	9.75	9.49	-2.74
2.07	3233	9.22	9.02	-2.19
3.05	1980	11.74	11.90	1.33
3.06	3485	10.00	10.02	0.25
3.07	3997	9.55	9.43	-1.23
3.07	4340	9.01	9.03	0.22
4.06	5040	9.28	9.49	2.30
4.07	5461	8.79	9.08	3.29
5.03	6566	8.94	8.96	0.24
4.99	2480	11.30	11.55	2.27
5.00	4516	10.65	10.91	2.41
5.00	6088	9.57	9.72	1.58
5.00	6379	9.35	9.48	1.41
5.00	6577	9.08	9.31	2.56
			Mean	0.27
			StDev	2.12
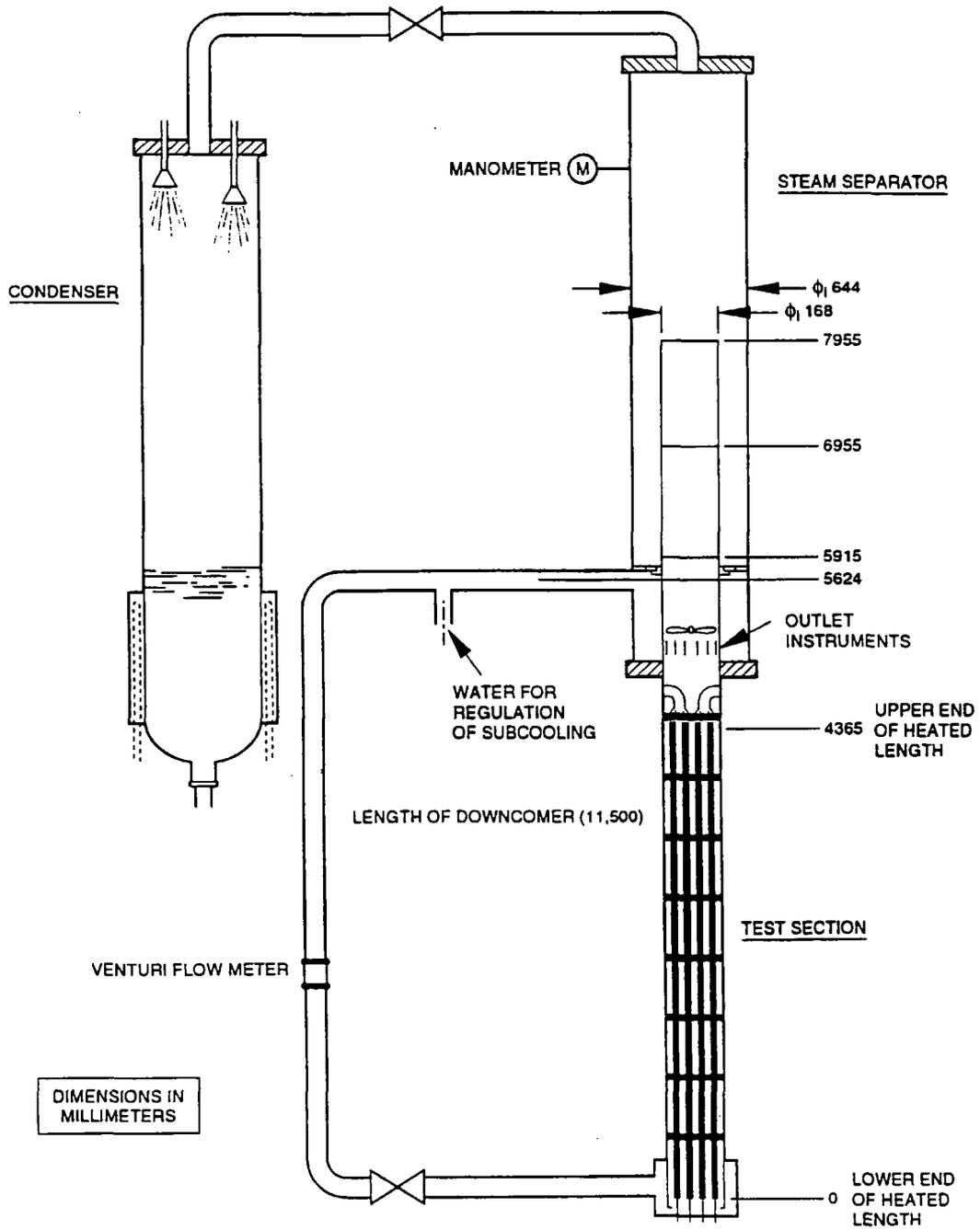
Figure 3.7-1. FRIGG Test Loop

SEPARATE EFFECTS TESTS
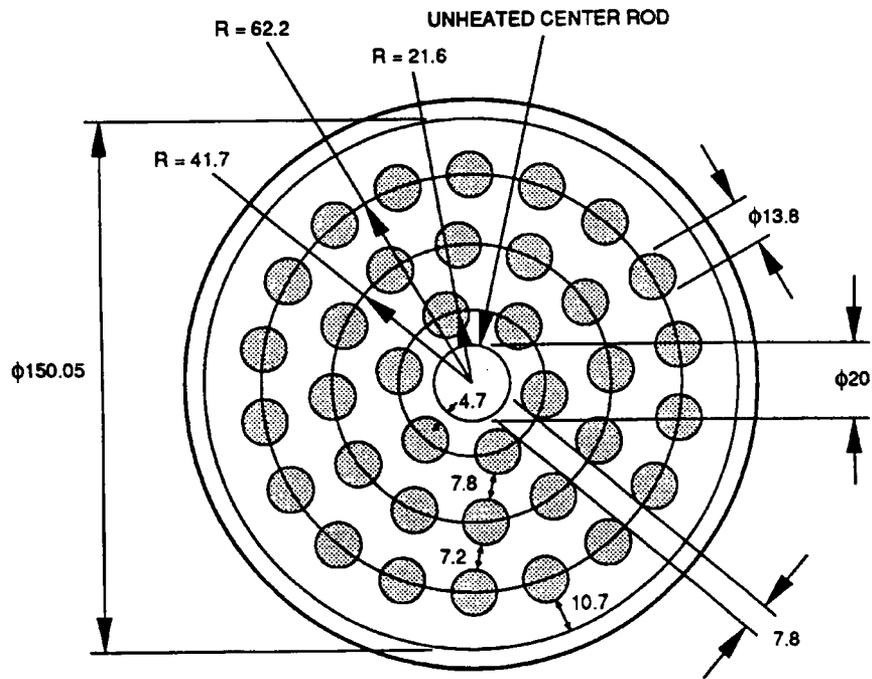
Figure 3.7-2. FRIGG Heated Channel Cross Section
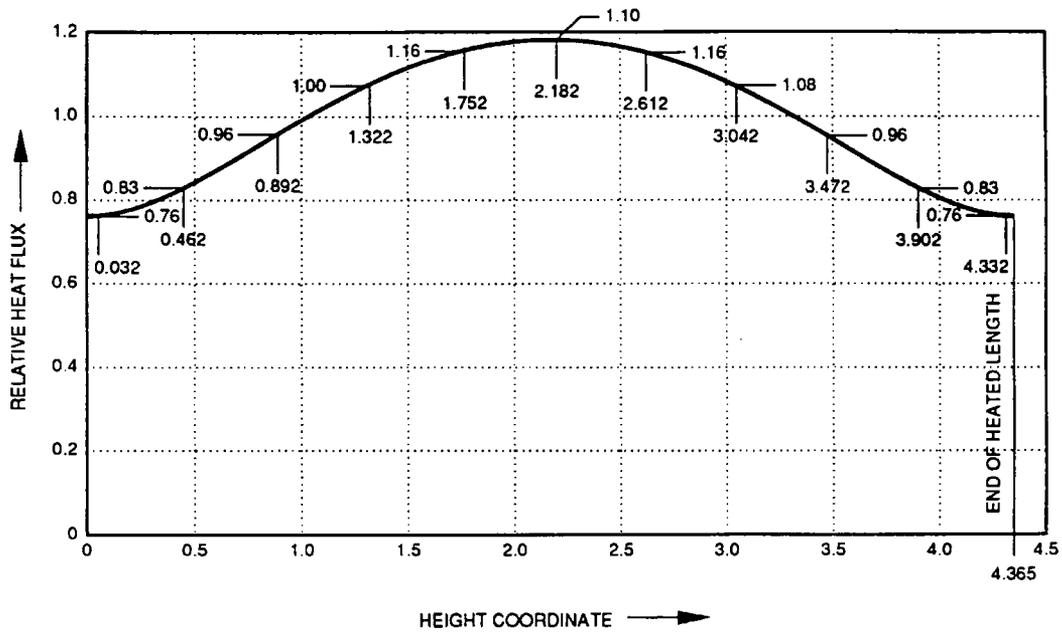
Figure 3.7-3. FRIGG Axial Heat Flux Distribution

[[

]]

Figure 3.7-4. TRACG FRIGG Loop Nodalization

SEPARATE EFFECTS TESTS

[[

[[

]]

Figure 3.7-5. Distribution of Loss Coefficients

[[

]]

Figure 3.7-6. FRIGG Data Comparison, P = 2 MPa, ΔT = 5 K

[[

]]

Figure 3.7-7. FRIGG Data Comparison, P = 3 MPa, ΔT = 5 K

[[

]]

Figure 3.7-8. FRIGG Data Comparison, P = 5 MPa, ΔT = 15 K
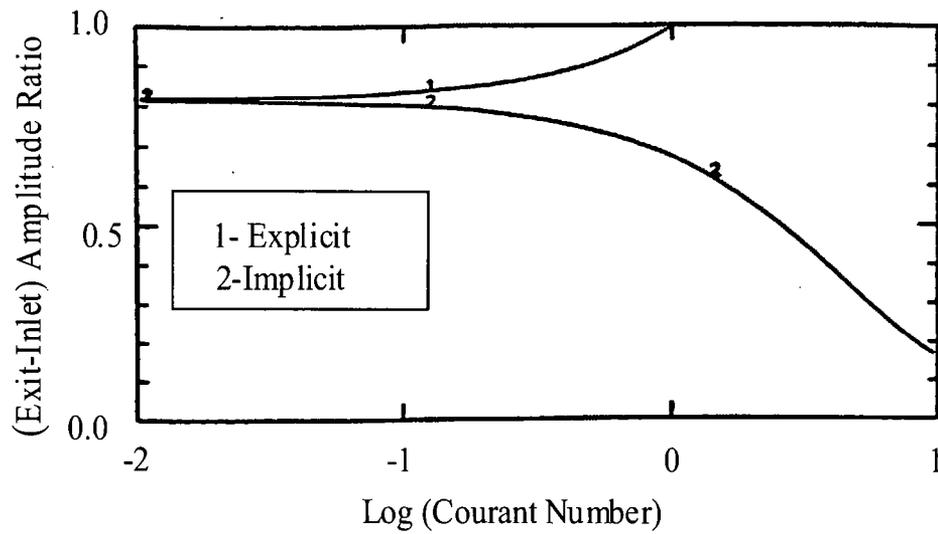
Figure 3.7-9. FRIGG Damping Trends

[[

]]

Figure 3.7-10. FRIGG Sensitivity to Courant Number

[[

]]

Figure 3.7-11. FRIGG Nodalization Sensitivity Studies

[[

]]

Figure 3.7-12. FRIGG Decay Ratio Comparisons for 20, 24, 32, 40 and 80 Nodes

[[

]]

Figure 3.7-13. FRIGG Sensitivity to Number of Nodes

[[

]]

Figure 3.7-14. FRIGG Decay Ratio Comparison at 2 MPa and 5 K Subcooling

[[

]]

Figure 3.7-15. FRIGG Decay Ratio Comparison at 3 MPa and 5 K Subcooling

[[

]]

Figure 3.7-16. FRIGG Decay Ratio Comparison at 4 MPa and 5 K Subcooling

[[

]]

Figure 3.7-17. FRIGG Decay Ratio Comparison at 5 MPa and 5 K Subcooling

SEPARATE EFFECTS TESTS

[[

]]

Figure 3.7-18. FRIGG Decay Ratio Comparison at 5 MPa and 15 K Subcooling

[[

]]

Figure 3.7-19. FRIGG Comparisons of Oscillation Onset Power

3.8 SPERT REACTIVITY INSERTION TEST

TRACG has been used to calculate an experimental rod drop transient performed at the SPERT III facility [3-37]. The test simulated was a $1.21 reactivity insertion from a cold startup condition. This section describes the SPERT III facility, initial test conditions, TRACG modeling and results of TRACG comparisons with the test data.

3.8.1 SPERT-III Test Facility and Test Description

The SPERT III facility was designed as a small-scale pressurized water reactor. The fuel was sintered UO_2 (10.5 g/cm^3) enriched to 4.8%. The fuel rods were 11.8 mm (0.466 in.) in diameter and were configured in 4x4 and 5x5 boiling water reactor (BWR) type fuel bundles. The spacing between the centers of the fuel bundles was 7.62 cm. The control rods, which were made of borated steel, were of two types: (1) a single cruciform transient rod and (2) eight box shim rods. The transient rod was located in the center of the core and was inserted into the core from the bottom. The shim rods were in the second and third fuel rings and were inserted from the top of the core. Each shim rod had a fuel leader that consisted of a 16-rod fuel bundle. The placement of the fuel and control components in the SPERT III core is shown on Figure 3.8-1. Each core quadrant contained two coupled shim rods. Table 3.8-1 summarizes the primary design characteristics of the SPERT III core. SPERT III Test No. 43, a cold reactivity insertion transient, was initiated from a temperature of 294 K (70°F) without coolant flow. The reactivity insertion at cold startup conditions was $1.21 ± 0.05.

3.8.2 TRACG Model and Test Simulation

[[

]]

3.8.3 Results

[[

]]

3.8.4 Conclusion

A TRACG rod drop calculation was performed for comparison with SPERT III Test 43, a cold reactivity insertion transient. On the basis of the results described in Section 3.8.3 above, it can be concluded that TRACG adequately models the phenomena that govern the response to a control rod drop accident at cold conditions.

SEPARATE EFFECTS TESTS

3-145

Table 3.8-1
Design Characteristics of the SPERT III Core

Component	Specification
VESSEL AND PRIMARY SYSTEM	
Vessel Type	All welded multi–layer vessel
Vessel Composition	304L Stainless Steel
Vessel Size	1.3 m inside diameter by 7.24 m high
Design Pressure	16.8 MPa
Design Temperature	955 K
Flow Characteristics	1260 kg/s upward through the core
Heat Removal Capabilities	Up to 60 MW for ½ hour duration
CORE	
Configuration	Approximately cylindrical, 0.66 m diameter
Number and Type of Fuel Assemblies	48 25-rod assemblies and 12 16-rod assemblies
Moderator – Reflector	Light water
Non–Moderator to Moderator Ratio	1.03
FUEL	
Type	UO_2 pellets
Length of Fuel Rods	1.04 m
Active Length	973 mm
Pitch	Square, 14.9 mm
Fuel Rod OD	11.8 mm
Clad Thickness	0.5 mm
Enrichment	4.8%
UO_2 Density	10.5 g/cm^3
Mass of UO_2 per Fuel Rod	913.5g
Mass of U238 per Fuel Rod	766.4 g
Mass of U235 per Fuel Rod	38.5 g
Cladding	Type 348 stainless steel
CONTROL RODS	
Number and Type	8 total, in units of 2 per quadrant
Composition	Fuel follower and Type 18-8 stainless steel with 1.35 wt% B–10
Dimension of Poison Section	63.4 mm square by 1.17 m high
Dimension of Fuel Follower	63.4 mm square by 1.16 m high
TRANSIENT RODS	
Type	Cruciform shape
Composition	Upper Section: 18-8 stainless steel. Poison Section: 1.35 wt% B–10 stainless steel
Length	Poison Section: 970 mm

16 Rod Bundle

Shim Control Bundle

Standard 25 Rod Bundle
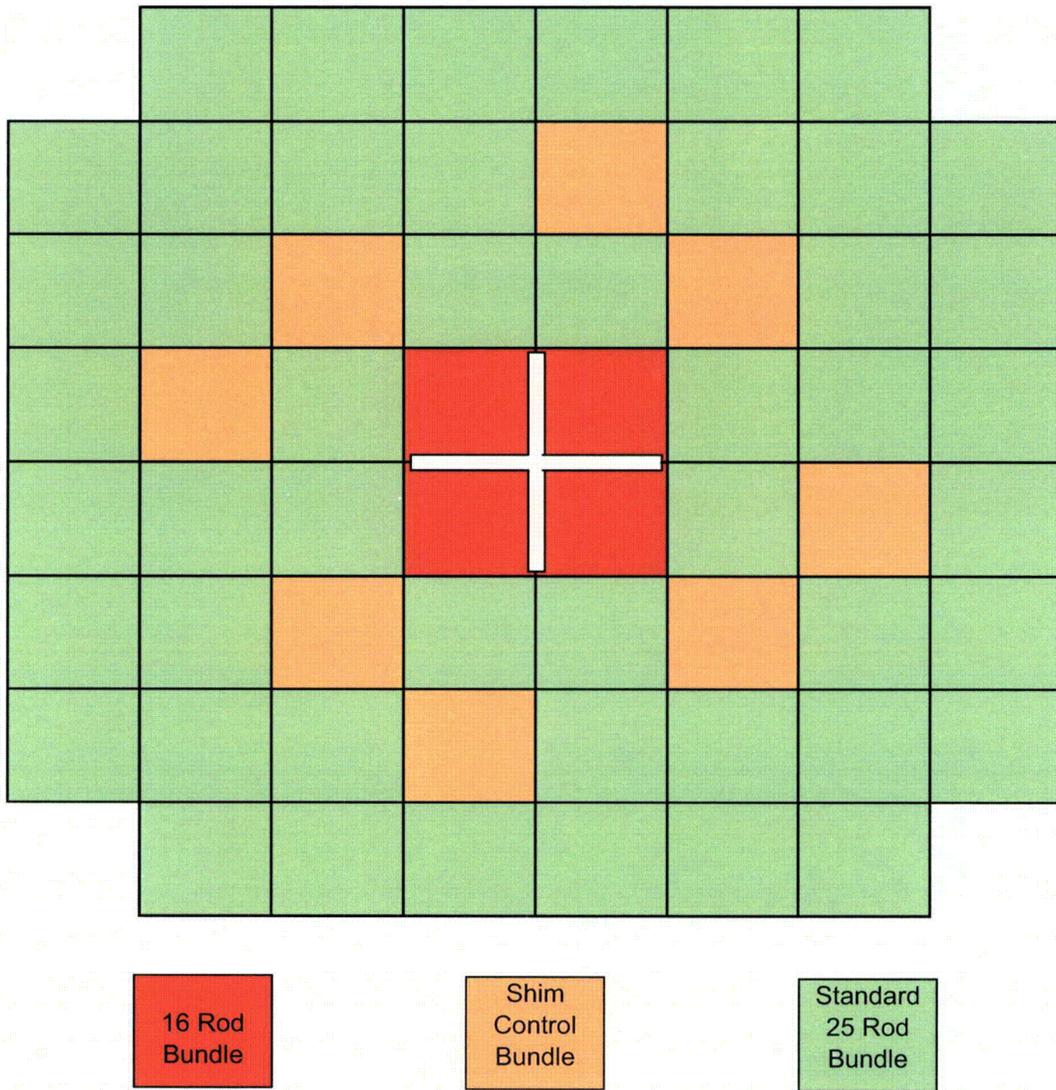
Figure 3.8-1. SPERT Core Configuration

[[

]]
Figure 3.8-2. Power vs. Time – SPERT III (Test 43) $1.21 ± $0.05 Rod Drop

[[

]]
Figure 3.8-3. Energy Release – SPERT III (Test 43) $1.21 ± $0.05 Rod Drop

3.9 REFERENCES

[3-1] J. G. M. Andersen et al., TRACG Model Description, NEDE-32176P, Rev. 3, April 2006.

[3-2] O. Nylund, R. Eklund and R Rydalm, OF–64b. Results of Void Measurements, FRIGG PM-105, June 1970.

[3-3] H. Christensen, Power-to-Void Transfer Function, ANL6385, July 1961.

[3-4] J. F. Wilson, R. J. Grenda and J. F. Patterson, Steam Volume Fraction in a Bubbling Two-Phase Mixture, Trans. Am. Nucl. Soc. 4(2), p 356-357, 1961.

[3-5] G. G. Bartolomei, V. A. Suvorov and S. A. Tevlin, Hydrodynamics of Steam Generation in a Two–Circuit Nuclear Power Plant, Teploenergetika 10(1), p 52-57, 1963.

[3-6] J. F. Matousek, Modification of the EBWR for Higher Power Operation, ANL-6552, April 1962.

[3-7] M. Petrick and E. A. Spleha, Thermal Hydraulic Performance Characteristics of EBWR, ANL 6693, May 1963.

[3-8] J. A. Findlay, BWR Refill-Reflood Program Task 4.8 - Model Qualification Task Plan, General Electric Company, GEAP-24898, August 1981.

[3-9] S. Morooka, T. Ishizuka, M. Iizuka and K. Yoshimura, Experimental Study on Void Fraction in a Simulated BWR Assembly (Evaluation of Cross-Sectional Averaged Void Fraction), Nuclear Engineering and Design 114, pp. 91-98 (1989).

[3-10] T. Mitsutake, S. Morooka, K. Suzuki, S. Tsonoyama and K. Yoshimura, Void Fraction Estimation within Rod Bundles Based on Three-Fluid Model and Comparison with X-Ray CT Void Data, Nuclear Engineering and Design 120, pp. 203-212 (1990).

[3-11] H.A. Hasanein, A.M.C. Chan, M. Kawaji and Y. Yoshioka, Steam-Water Two-phase Flow in Large diameter Vertical Piping at High Pressures and Temperatures, 4th JSME/ASME Joint International Conference on Nuclear Engineering, New Orleans, USA, March 1996.

[3-12] A.M.C. Chan, Void Fraction Measurements in Large Diameter Pipes with Thick Metal Walls or Complex Internal Geometries, Proceedings of the National Heat Transfer Conference, 1992, American Nuclear Society, pp. 236-244.

[3-13] A.M.C. Chan and D. Bzovey, Measurement of Mass Flux in High Temperature High Pressure Steam-Water Two-Phase Flow using a Combination of Pitot Tubes and a Gamma Densitometer, Journal of Nuclear Engineering and Design, 1990, Vol. 122, pp. 95-104.

[3-14] G. Agostini, A. Era and A. Premoli, Density Measurements of Steam-Water Mixtures Flowing in a Tubular Channel Under Adiabatic and Heated Conditions, CISE-R-291, December 1969.

[3-15] D. K. Felde, et al., Facility Description-THTF MOD 3 ORNL PWR BDHT Separate-Effects Program, NUREG/CR-2640 (ORNL/TM-7842), September 1982.

[3-16] D. G. Morris, et al., An Analysis of Transient Film Boiling of High Pressure Water in a Rod Bundle, NUREG/CR-2469 (ORNL/NUREG-85), March 1982.

[3-17] B. S. Shiralkar et al., TRACG Application for Emergency Core Cooling Systems/Loss-of-Coolant-Accident Analysis, NEDE-33005P, (to be issued).

[3-18] D. D. Jones, Subcooled Counter Current Flow Limiting Characteristic of the Upper Region of a BWR Fuel Bundle, NEDG-23549, July 1977.

[3-19] J. G. M. Andersen, CORECOOL : A Model for the Temperature Distribution and Two-Phase Flow in a Fuel Element Under LOCA Conditions, NEDO-21325, July 1976.

[3-20] J. G. M. Andersen, H. Abel–Larsen and P. Hansen, CORECOOL – Part IV Verification–Test Run 110, SHH-12-77, June 1977.

[3-21] J. G. M. Andersen, H. Abel–Larsen and P. Hansen, CORECOOL – Part IV Verification–Test Run 111, SHH-10-77, June 1977.

[3-22] J. G. M. Andersen, H. Abel–Larsen and P. Hansen, CORECOOL – Part IV Verification–Test Run 112, SHH-11-77, June 1977.

[3-23] J. G. M. Andersen, H. Abel–Larsen and P. Hansen, CORECOOL – Part IV Verification–Test Run 113, SHH-21-77, August 1977.

[3-24] J. G. M. Andersen, H. Abel–Larsen and P. Hansen, CORECOOL – Part IV Verification–Test Run 120, SHH-13-77, June 1977.

[3-25] J. G. M. Andersen, H. Abel–Larsen and P. Hansen, CORECOOL – Part IV Verification–Test Run 121, SHH-14-77, June 1977.

[3-26] D. D. Jones and S. S. Dua, General Electric Company Analytical Model for Loss-of-Coolant Analysis in Accordance with 10CFR50 Appendix K; Amendment No. 4 – Saturated Countercurrent Flow Characteristics of a BWR Upper Tieplate, NEDE-20566-4-P, July 1978.

[3-27] The Marviken Full–Scale Critical Flow Tests-Interim Report Description of the Test Facility, MXC-101, Marviken Power Station", Sweden, October 1979.

[3-28] A. R. Edwards and T. P. O'Brien, Studies of Phenomena Connected with the Depressurization of Water Reactors, Journal of the British Nuclear Energy Society, V. 9, pp 125-135, April 1970.

[3-29] The Marviken Full-Scale Critical Flow Test - Third Series, Results from Test 15, MXC-215, Marviken Power Station, Sweden, September 1979.

[3-30] The Marviken Full-Scale Critical Flow Test - Third Series, Results from Test 24, MXC-224, Marviken Power Station, Sweden, September 1979.

[3-31] B. Matzner and D. A. Wilhelmson, Critical Power and Pressure Drop Tests – Step II Fuel Design Standardization Program for BWR/2-5 Reload Fuel, NEDC-31499P, 1987.

[3-32] Critical Power and Pressure Drop Tests of Simulated 10X10 Bundle Designs Applicable to GE14, NEDC-32874P, March 2000.

[3-33] TASC-03A – A Computer Program for Transient Analysis of a Single Channel, NEDC-32084P-A, Rev. 2, July 2002.

[3-34] O. Nylund, et al., Hydrodynamic and Heat Transfer Measurements on a Full-Scale Simulated 36 Rod BHWR Fuel Element with Non-Uniform Axial and Radial Heat Flux Distribution, FRIGG-4, ASEA-ATOM, December 1970.

[3-35] J. G. M. Andersen et al., Time Domain Analysis of Thermal Hydraulic Stability with TRACG – Sensitivity to Numerical Methods and Qualification to Data, BWR Stability Symposium, Idaho, 1989.

[3-36] T. Mitsutake, Channel Stability Experiments in 14 MW Heat Transfer Loop (HTL), Toshiba Corporation, Nuclear Energy Group, May 1986.

[3-37] R. K. McCardell, D. I. Herborn and J. E. Houghtailing, Reactivity Accident Test Results and Analyses for the SPERT III E-Core – A Small, Oxide-Fueled, Pressurized Water Reactor, IDO-17281, AEC Research and Development Report, March 1969.

4.0   COMPONENT PERFORMANCE TESTS

In this section the TRACG component models are assessed by comparison of model predictions with BWR component test data. The following data are included in these comparisons:

- *Jet Pump Data.* This set of data includes test data from a 1/6-scale jet pump covering all possible flow regimes of jet pump operation and data for normal operating conditions from single- and five-nozzle full-scale prototypical jet pumps. Only the 1/6-scale jet pump data were used in the development of the jet pump model. The full-scale jet pump data were used strictly for qualification. The qualification against jet pump data is described in Section 4.1.

- *Steam Separator Data.* These tests include data for full-scale prototypical two-stage and three-stage steam separators. The data consist of measurements of the carryunder quality, the carryover liquid mass fraction and the steam separator pressure drop. The qualification against steam separator data is described in Section 4.2.

- *Upper Plenum Mixing Data.* In these tests, the effects of injection of ECC core spray into the upper plenum are evaluated. The focus is on ECC penetration into the upper plenum and the amount of subcooling at the upper tie plate. The upper plenum data were taken in the SSTF test facility. The qualification against the SSTF upper plenum data is described in Section 4.3.

- *Spray Distribution Data.* The SSTF core spray distribution tests provided separate effects data on the behavior of highly subcooled spray injected into a steam environment with steam updraft. Data from these tests are used for evaluation of the TRACG spray model as described in Section 4.4.

4.1   JET PUMP PERFORMANCE

Jet pumps from various test facilities have been used for the qualification of the TRACG jet pump model. Detailed data covering both forward and backward flow were taken for a 1/6-scale jet pump at Idaho National Engineering Laboratory (INEL). Data for full-scale jet pumps were taken for the normal flow mode for a one-nozzle jet pump from a BWR/4 and a five-nozzle jet pump from a BWR/5.

4.1.1   INEL 1/6 Scale Jet Pump Data

The 1/6-scale jet pump used in the INEL test [4-1] was a scaled version of a one-nozzle jet pump. The jet pump was mounted in a test vessel that was equipped with three pipe connections allowing the drive pressure and suction and drive flows to be controlled separately. The fluid temperature and pressure and the differential pressures across the jet pump components were measured in the test. Measurement uncertainty was not available for the INEL test data. Steady-state tests were conducted for six values of the drive flow. Three of these were positive drive flows (1.4, 2.8 and 4.2 ltr/sec) and three were negative drive flows (-1.4, -2.8 and -4.2 ltr/sec). The suction flow was varied to cover an M–ratio ranging from approximately -2 to 4.

[[

]]

The M-ratio is defined as:

$$M = \frac{W_{suction}}{W_{drive}}$$ (4-1)

A convenient way of reporting the jet pump pressure drop data is through the N-ratio, which is defined as:

$$N = \frac{P_{discharge} - P_{suction}}{P_{drive} - P_{discharge}}$$ (4-2)

When the jet pump N-ratio is plotted as a function of the M-ratio, the same performance curve is obtained for different values of the drive flow. The efficiency of the jet pump is defined as:

$$Eff = M * N$$ (4-3)

The TRACG model for the jet pump component (JETP) uses a fixed nodalization with two nodes for the drive line and four nodes for the mixing, diffuser and discharge sections (Figure 4.1-1). A FILL component is attached to the drive line to control the drive flow and BREK components are attached to the suction and discharge to control the jet pump system pressure and pressure drop. In the TRACG simulation of a given test, the drive flow is set via the FILL component, the system pressure is set via the BREK component at the discharge and the BREK component at the suction is used to vary the suction pressure to obtain the desired suction flow rates.
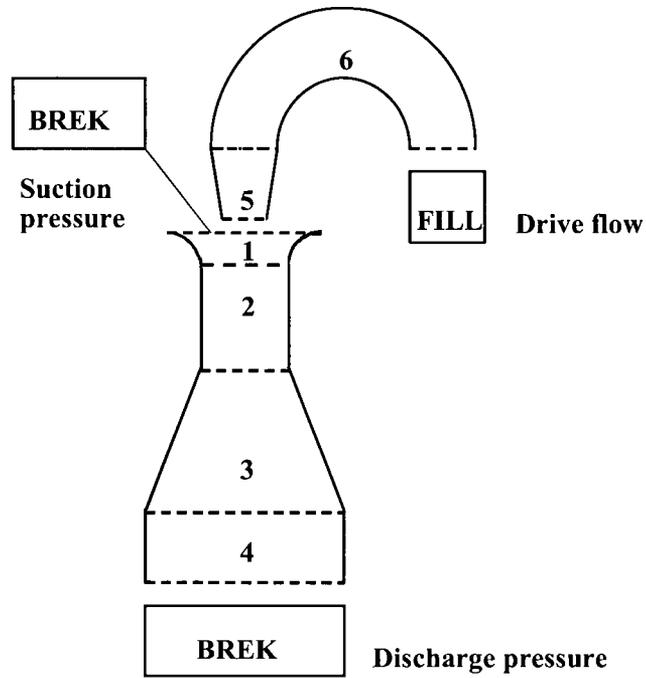
Figure 4.1-1. TRACG Jet Pump Model

[[

]]

[[

]]

Figure 4.1-2. Comparison to INEL 1/6 Scale Jet Pump Data

4.1.2   BWR/4 Full-Scale One-Nozzle Jet Pump Data

Jet pump performance data were taken for a full-scale prototype of a BWR/4 jet pump [4-2]. The BWR/4 jet pump is a one-nozzle jet pump similar to the INEL jet pump. The test setup was similar to that used for the INEL jet pump with the exception that data were only taken for normal operation of the jet pump (i.e., positive drive and suction flows). Measurement uncertainties for the full-scale BWR/4 and 5 jet pump data are summarized in Table 4.1-1.

Table 4.1-1
Measurement Uncertainties for Jet Pump Performance Tests

[[	
	]]

The TRACG model for the BWR/4 jet pump used the same nodalization as for the INEL jet pump (Figure 4.1-1). Comparisons were made to five of the tests conducted for the BWR/4 jet pump. The test conditions for these tests are given in Table 4.1-2.

Table 4.1-2
Test Conditions for the BWR/4 Jet Pump Comparisons

[[			
			]]

[[

]]

[[

]]

Figure 4.1-3. Comparison to BWR/4 Jet Pump Tests 1-4 and 500
(Note that Tests 2 through 4 and 500 have been displaced in N-Ratio)

[[

]]

Figure 4.1-4. TRACG N-Ratio Deviations for BWR/4 Jet Pump Tests

4.1.3   BWR/5 Full-Scale Five-Nozzle Jet Pump Data

Jet pump performance data were taken for a full-scale prototype of a BWR/5 jet pump [4-3]. The BWR/5 jet pump is a five-nozzle jet pump. The test setup was similar to that used for the INEL jet pump, except that data were only taken for normal operation of the jet pump (i.e., positive drive and suction flows). The TRACG model for the BWR/5 jet pump used the same nodalization as for the INEL jet pump. [[

]]

COMPONENT PERFORMANCE TESTS

[[

]]

Figure 4.1-5. Comparison to BWR/5 Jet Pump Data

4.1.4 Conclusions

TRACG calculations were compared to 1/6-scale jet pump test data covering normal and abnormal operating conditions and to full-scale (one-nozzle and five-nozzle) jet pump data for normal operating conditions. Based on these comparisons, it can be concluded that: (1) TRACG accurately describes the jet pump performance for all modes of operation; and (2) there is no bias due to scale.

4.2 STEAM SEPARATOR

The TRACG steam separator model has been qualified against test data for full-scale prototypical two-stage and three-stage steam separators. The parameters that define separator performance (and were measured in these tests) are the carryover (the fraction of liquid in the separator exit steam flow), the carryunder (the fraction of steam in the separator exit liquid flow) and the separator pressure drop. Both carryover and carryunder are given as mass flow ratios in %. The steam separator is designed to have its best performance under normal operating conditions, i.e., in the range of 10 to 12% inlet quality for two-stage separators (BWR/2 through 5) and 12 to 14% inlet quality for three-stage separators (BWR/6). Both carryunder and carryover are at their minimum values near the normal operating conditions for the two-stage and three-stage separators.

[[

]]This is important for LOCA modeling where high separator inlet quality is predicted to occur early in the blowdown for a main steam line break (MSLB). Under other LOCA conditions, where the level has dropped below the separator skirt or has risen above the top of the separator, the calculations are insensitive to the separator model because both separator exit paths connect to the mixing region above the shroud.

Separator performance, particularly the carryunder, is also important in predicting the correct response of the BWR during anticipated operating occurrences (AOOs). In particular, during those transients where there is a loss of feedwater, loss of feedwater heating or loss of forced recirculation flow, separator carryunder will affect the core inlet enthalpy and, therefore, the core power. For accurate simulation of these cases as well as the LOCA cases discussed above, accurate modeling of separator carryunder is important.

4.2.1 Steam Separator Data

Extensive qualification of the separator model has been performed on the basis of test data presented in References 4-4 through 4-7. In addition, full-scale performance test data for two-stage and three-stage BWR steam separators have been reported in the open literature [4-8 through 4-10]. [[

]]

4.2.2 TRACG Steam Separator Model

[[

]]

COMPONENT PERFORMANCE TESTS

4.2.3   Results and Discussion

[[

]]

4.2.4 Conclusions

The following conclusions can be made on the basis of the results and discussion presented in Section 4.2-3:

[[

•

]]

Table 4.2-1
Measurement Uncertainties for Steam Separator Performance Tests [4-5]

[[	
	]]

Table 4.2-2
Statistical Properties of TRACG Predictions of Separator Test Data

[[				
				]]
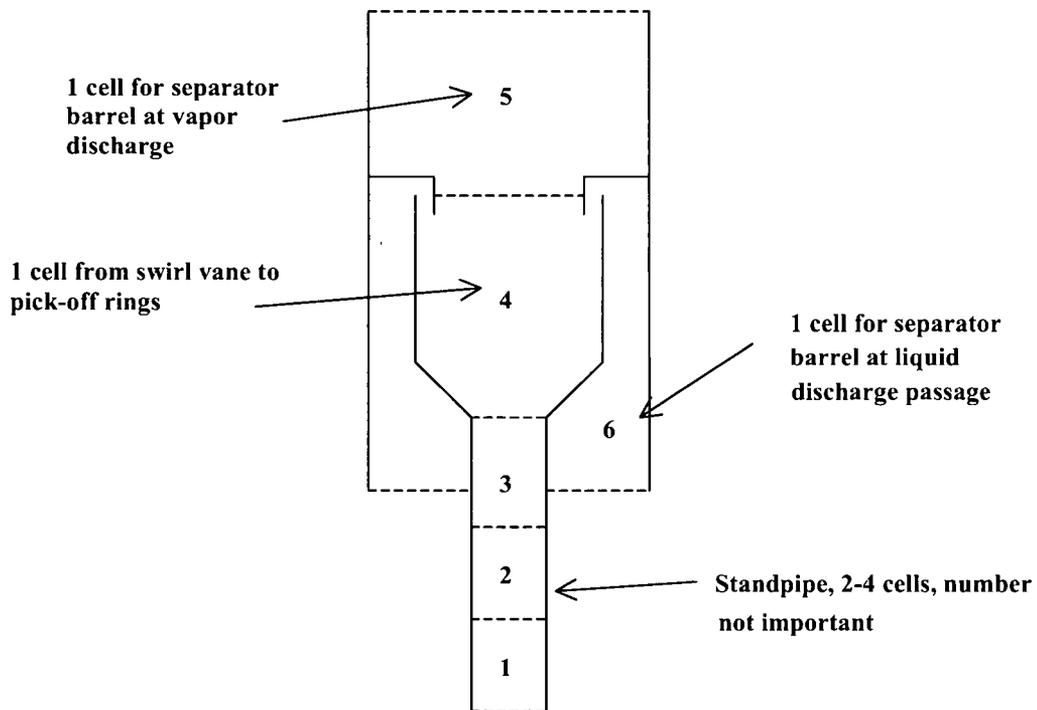
Figure 4.2-1. TRACG Steam Separator Model

[[

]]

**Figure 4.2-2. Comparison of Carryunder vs. Inlet Flow for BWR/2&3 2-Stage
Separator; Separator Skirt Submergence – 0.559 m (22 inches)**

[[

]]

**Figure 4.2-3. Comparison of Carryover vs. Inlet Flow for BWR/2&3 2-Stage
Separator; Separator Skirt Submergence – 0.559 m (22 inches)**

[[

]]

Figure 4.2-4. Comparison of Carryunder vs. Inlet Flow for BWR/4&5 2-Stage Separator; Separator Skirt Submergence – 0.635 m (25 inches)

[[

]]

Figure 4.2-5. Comparison of Carryover vs. Inlet Flow for BWR/4&5 2-Stage Separator; Separator Skirt Submergence – 0.635 m (25 inches)

[[

]]

Figure 4.2-6. Comparison of Carryunder vs. Submergence for BWR/4&5 2-Stage Separator; Inlet Flow = 61.1 kg/s (485,000 lbm/hr)

[[

]]

Figure 4.2-7. Comparison of Carryover vs. Submergence for BWR/4&5 2-Stage Separator; Inlet Flow = 61.1 kg/s (485,000 lbm/hr)

[[

]]

Figure 4.2-8. Comparison of Carryunder vs. Inlet Flow for BWR/6 3-Stage Separator; Separator Skirt Submergence – 0.254 m (10 inches)

[[

]]

Figure 4.2-9. Comparison of Carryover vs. Inlet Flow for BWR/6 3-Stage Separator; Separator Skirt Submergence – 0.254 m (10 inches)

COMPONENT PERFORMANCE TESTS

[[

]]

Figure 4.2-10. Comparison of Carryunder vs. Inlet Flow for BWR/6 3-Stage Separator; Separator Skirt Submergence – 1.016 m (40 inches)

[[

]]

Figure 4.2-11. Comparison of Carryover vs. Inlet Flow for BWR/6 3-Stage Separator; Separator Skirt Submergence – 1.016 m (40 inches)

[[

]]

**Figure 4.2-12. 2-Stage Separator Pressure Drop with
Inlet Flow = 61.1 kg/s (485,000 lbm/hr)**

4.3 UPPER PLENUM EFFECTS

The upper plenum mixing experiment in the SSTF provides separate effects data on the interactions produced by highly subcooled ECC injection into a two–phase mixture with steam updraft. The multidimensional mixing in the upper plenum creates a subcooling distribution that varies both radially and axially. The injected ECC fluid drained mostly through the peripheral region bundles and, accordingly, the highest subcooling was observed near the peripheral region of the upper plenum.

TRACG simulation of the SSTF mixing experiment demonstrates the ability of the code to capture the observed multidimensional mixing phenomena in the upper plenum. The upper plenum modeling used in these calculations is the same as that used in the BWR LOCA models. Prediction of the distribution of mass and subcooling in the upper plenum is an important part of the TRACG qualification for LOCA simulation.

4.3.1 Features of the SSTF Facility

The Steam Sector Test Facility (SSTF), shown schematically in Figure 4.3-1, was a relatively large-scale representation of a BWR. The facility was designed to evaluate the system behavior and controlling phenomena during the refill and reflood phases of a BWR LOCA [4-12]. The effects simulated are also of interest for inadvertent HPCS injection. The main features of the SSTF were:

- Full scale 30° sector representation of a BWR/6-218 (i.e., 1/12 volume scaling).

- Fifty-eight simulated bundles with BWR production hardware for the upper tie plates and the side entry orifice regions; bundle steam injection to simulate vapor generation due to rod heat transfer.

- Full-height upper plenum with prototypical representations of the High Pressure Core Spray (HPCS) and the Low Pressure Core Spray (LPCS) Systems.

- Simulated bypass region with mockup control rods and a prototypical representation of the Low Pressure Coolant Injection (LPCI) system.

- Simulated lower plenum and guide tubes with steam injection capability to represent vapor generation from stored energy release to the fluid during a blowdown and for simulating flashing when running constant pressure separate effects tests.

- Volume scaled annulus region with mockup of the recirculation line break.

The test facility was instrumented in detail. Differential pressure transducers were located throughout the system. Parallel strings of ΔP transducers were placed in the lower plenum, bypass and upper plenum. These instruments aided in evaluating the radial variation of the pressure and regional mass inventory. Six of the 58 bundles were instrumented with two ΔP transducers each. Thermocouples were located just below the upper tie plate for each of the 58 bundles. Thermocouples were also placed at key locations in the vessel to measure the fluid temperature. A large number of conductivity elements were placed in the lower plenum, bundles, bypass, annulus and the upper plenum. These conductivity probe measurements are used to estimate local void fractions and/or mixture densities. Uncertainties in the SSTF test data that are used for the TRACG comparisons are summarized below.

Table 4.3-1
Measurement Uncertainties for the SSTF Tests

Directly Measured	Subcooling	± 0.5 K
Derived	Collapsed Level	± 22 mm of water

A series of separate effects and system response tests were conducted in the SSTF facility [4-13, 4-14 and 4-15]. The separate effects tests were typically run at constant pressure to address such phenomena as ECC mixing and parallel channel behavior. The system response test involved depressurization from 1.03 MPa (150 psia) with a primary focus on the system behavior and interaction of controlling phenomena during the refill/reflood phase of a BWR LOCA.

The SSTF Upper Plenum Mixing Test (SE3-1A) was a separate effects test. During the experiment, the system pressure was maintained at a nearly constant value of 0.214 MPa (31 psia). The total steam injection rate into the bundles was about 5.04 kg/s (40,000 lbm/hr) and the subcooled HPCS injection rate into the upper plenum was 0.0282 m^3/s (448 gpm). The subcooling of the ECC fluid was 87 K (156°F). Steam was also injected into the steam dome at a rate of 1.36 kg/s (10,800 lbm/hr) to maintain system pressure and to prevent air from entering the system during steam condensation in the upper plenum.

Initially, a shallow pool of two-phase mixture existed in the upper plenum with a collapsed level of about 0.2 m (8 in). The bypass and the lower plenum were initially filled with saturated water and remained full throughout the test. The water level in the bundle region was maintained above the level of the lower tie plates to prevent steam communication through the bundle entry regions. The upper plenum liquid inventory increased slowly following the onset of HPCS injection. Most of the HPCS fluid drained through the bundles in the peripheral region of the simulated core as indicated by the response of the bundle conductivity elements. The liquid downflow through the bundles in the middle and central core regions was small in consequence of counter-current flow limitation (CCFL) at the upper tie plates. The fluid subcooling above the upper tie plates was about 4 K (7°F) near the peripheral region and near zero in the center of the upper plenum. The maximum upper plenum inventory corresponded to a collapsed level of approximately 0.5 m (20 in) in comparison to a total upper plenum height of 1.8 m (71 in).

4.3.2 TRACG Input Models and Nodalization

The primary consideration in the TRACG nodalization scheme used for the SSTF is that it be consistent with that used for the BWR LOCA models. To achieve this objective, a number of modifications were made to the TRACG model that was used for the prediction of the SSTF tests in Reference 4-16. The upper plenum is modeled in detail to capture effects produced by the interactions between the ECC flows and steam exiting from the simulated fuel bundles. As in the test, steam communication between the bundles through the lower plenum in the TRACG model is prevented by filling the lower plenum and bypass with sufficient water to cover the side-entry inlet orifices.

The earlier TRACG model for simulation of Test SE3-1A [4-16] used a VSSL component with eight axial levels, six radial rings and two azimuthal sectors to model the test facility pressure vessel. The 30° sector was modeled by one azimuthal sector and the second (330°) azimuthal sector was effectively isolated from the model by setting its volumes and flow areas to zero. For the current predictions, the revised nodalization shown in Figure 4.3-2 was adopted. (The same nodalization is used in Section 5.3 for prediction of the SSTF system response test.) A

major difference between the revised model and the earlier model is the use of more axial levels to represent the lower plenum and bypass. (It may be noted, however, that these regions are relatively inactive in the upper plenum mixing tests.) Another change is the reduction in the number of radial rings from six to four, consistent with the modeling used for the BWR. The core region can be adequately represented by three rings because, apart from the center and peripheral regions, the large open areas in the lower plenum, bypass and upper plenum have nearly uniform flow and vapor fraction distributions. The representation of the core region by three radial rings is an important BWR modeling feature that is supported, in part, by this simulation of the SSTF tests. Finally, one VSSL azimuthal sector is used with appropriate adjustments in the cell volumes and z-direction flow areas to represent the 30°-sector test facility.

The bottom five levels of the VSSL component represent the lower plenum and Levels 6 through 9 represent the bypass. As stated above, these regions are relatively inactive during Test SE3-1A and this modeling detail is of primary importance for prediction of phenomena (e.g., mixing in the lower plenum) for the system response tests (Section 5.5). Levels 10 through 13, consisting of 11 active cells, are used to represent the upper plenum. The steam dome is located in Level 14 at the top of Ring 4. The lower levels of Ring 4 are used to model the downcomer.

The axial level locations for the upper plenum are chosen to align the cell centers with instrument tap locations. The fluid volume subtended by each pair of axial levels is preserved. The high-pressure spray system (HPCS) is connected to the peripheral ring (Ring 3) at Level 11. Three groups of HPCS nozzles are modeled. The TRACG Upper Plenum Model is not used in these calculations so detailed information about the spray nozzles is not needed as part of the input description. Consistent with the TRACG BWR model, the spray is distributed proportionately, i.e., on the basis of the z-direction flow areas, to the two outer rings at the top of the core with no spray going to the central ring. An evaluation of the TRACG Upper Plenum Model on the basis of spray distribution test data from the SSTF is presented in Section 4.4.

In the earlier SSTF model, the 58 simulated fuel bundles were modeled by five TRACG CHAN/TEE component combinations. A CHAN/TEE combination is required to represent both the side entry orifice and steam injection flow paths. One CHAN/TEE component represented the bundles in the region encompassed by each of the five inner rings in the original six-ring VSSL component. For the current predictions of the upper plenum mixing tests, the detail provided by these same five CHAN/TEE components was judged sufficient to capture the relevant system response characteristics. In the framework of the revised VSSL model with three inner rings, the eight bundles in Ring 1 (central) and Ring 3 (peripheral) were modeled with one CHAN/TEE component in each ring. The remaining three CHAN/TEE components represent, respectively, 8, 18 and 16 bundles grouped by their radial position in Ring 2 (Figure 4.3-3).

In the TRACG BWR model, a larger number of CHAN components are used to accurately represent the core power distribution and the limiting bundles in the center and middle rings of the core. This BWR modeling feature motivated the development of a second TRACG model with a more refined representation of the SSTF bundles. This more detailed model, consisting of 13 CHAN/TEE components, permitted an improved representation of the power distribution simulated in the SSTF. As noted earlier, steam was injected into the fuel bundles to simulate decay heat and variations in the bundle steam injection rate simulated variations in bundle power. The core layout at the top of Figure 4.3-3 shows the normalized steam flow fractions for each of the 58 bundles. The model with 13-CHAN/TEE components groups bundles with similar steam flows together.

As for the five-CHAN/TEE model, the 13-CHAN/TEE model represents the eight bundles in the peripheral ring (Ring 3) with one CHAN/TEE component. These peripheral bundles have smaller side entry orifices that provide more hydraulic resistance to liquid downflow than the side entry orifices in the other bundles. The peripheral bundles also have a lower power, which was simulated in the test facility by injecting less steam into those bundles. The highest power bundles in the SSTF were located at about mid-radius in the core (Bundles 36 & 37). To further maintain consistency with the TRACG BWR model in which limiting bundles are segregated as individual CHAN components, Bundle 37 was represented by a separate CHAN/TEE component and was connected to the center ring of the VSSL component so that it would receive no spray.

Figure 4.3-4 shows a schematic of the bundle nodalization. As stated above, each bundle is modeled with the combination of a CHAN component and a TEE component. The CHAN component with eight cells models the lower part of the bundle, including the side entry orifice and the leakage path. The TEE component, with three cells in its primary branch and one cell in its secondary branch, models the upper part of the bundle, including the upper tie plate and the bundle steam injection. The number of cells used in the CHAN and TEE components was decided by making cell boundaries coincide with flow area changes (e.g., tie plates, spacers, upper rodded section, etc.) and cell centers correspond with measurement tap and bundle steam injection locations. The nodalization of the bundle so obtained is judged to be adequate for capturing the thermal-hydraulic response.

The standpipes that connect the steam dome with the upper plenum are grouped into three 2-cell PIPE components, one for each radial ring. The steam dome is modeled in Level 14 of Ring 4 (Figure 4.3-2). The standpipes and the steam dome are not nodalized in detail because it is expected that finer nodalization of these regions would have little impact on the upper plenum mixing response. To maintain the nearly constant system pressure of 0.214 MPa (31 psia) for Test SE3-1A, a BREK component is connected to the steam dome. A second BREK component is attached to the lower plenum to remove liquid build-up from HPCS operation.

The initial conditions for the input model are derived from the test data. Of primary importance are the conditions in the upper plenum and bundles prior to the ECCS initiation. Steady-state differential pressure and conductivity probe readings are utilized to obtain the magnitude and distribution of initial upper plenum and bundle inventories.

As discussed above, an important constraint on the input model for simulation of the SSTF tests was consistency with the standard TRACG BWR plant model. The TRACG BWR plant model (discussed in Section 6 of this report) serves as a guideline for selecting components and component nodalizations for the qualification studies. In turn, the qualification studies can suggest modifications in the plant model to improve the representation of the phenomena governing BWR transient system behavior. [[

]] The tests showed that the region of greatest upper plenum subcooling and most importance for ECC spray mixing was over the peripheral bundles. The tests further demonstrated that during the reflood/refill transient, there could be up to three different fuel bundle flow regimes operating in parallel. Additional nodalization studies [4-17] showed that the parallel channel behavior and upper plenum distributions observed in the SSTF data could be simulated with a 3-ring model. As a result, the

[[

                                                                ]]

4.3.3 Calculation Results

[[

4.3.4 Conclusions

A TRACG simulation of SSTF Upper Plenum Mixing Test SE3-1A was made for the purpose of assessing the performance of the code for upper plenum mixing. The following conclusions are drawn from comparisons of the TRACG prediction with the experimental data:

[[

•

]]

VENT

LPCS
WATER

LPCI
WATER

BLOWDOWN

HPCS
WATER

CORE
STEAM

RECIRCULATING
WATER

LOWER
PLENUM
STEAM

BYPASS
GUIDE TUBE
STEAM

WATER

WATER DISCHARGE
TO PO301 PUMP

WATER DRAIN
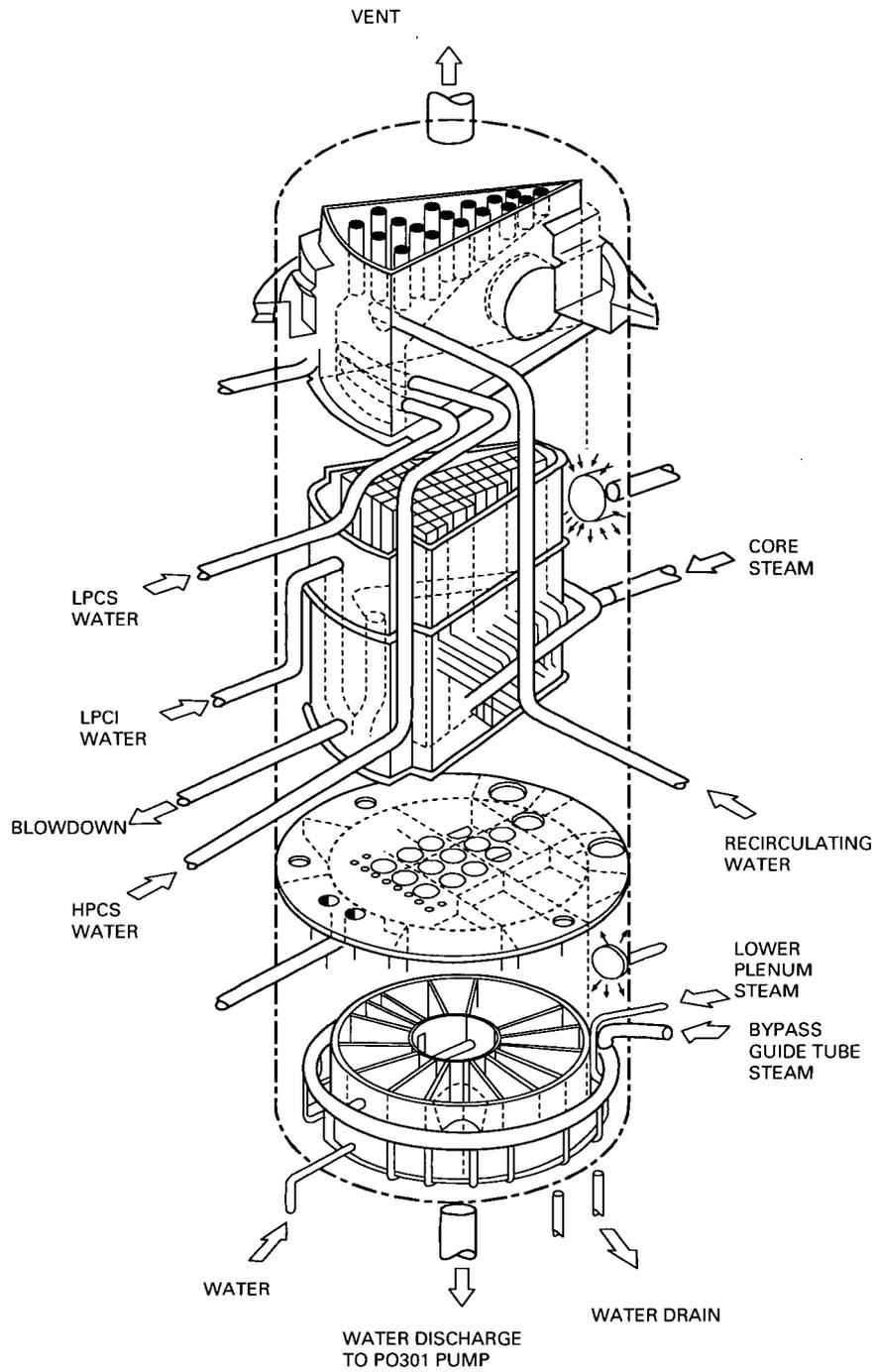
Figure 4.3-1. 30° Steam Sector Test Facility
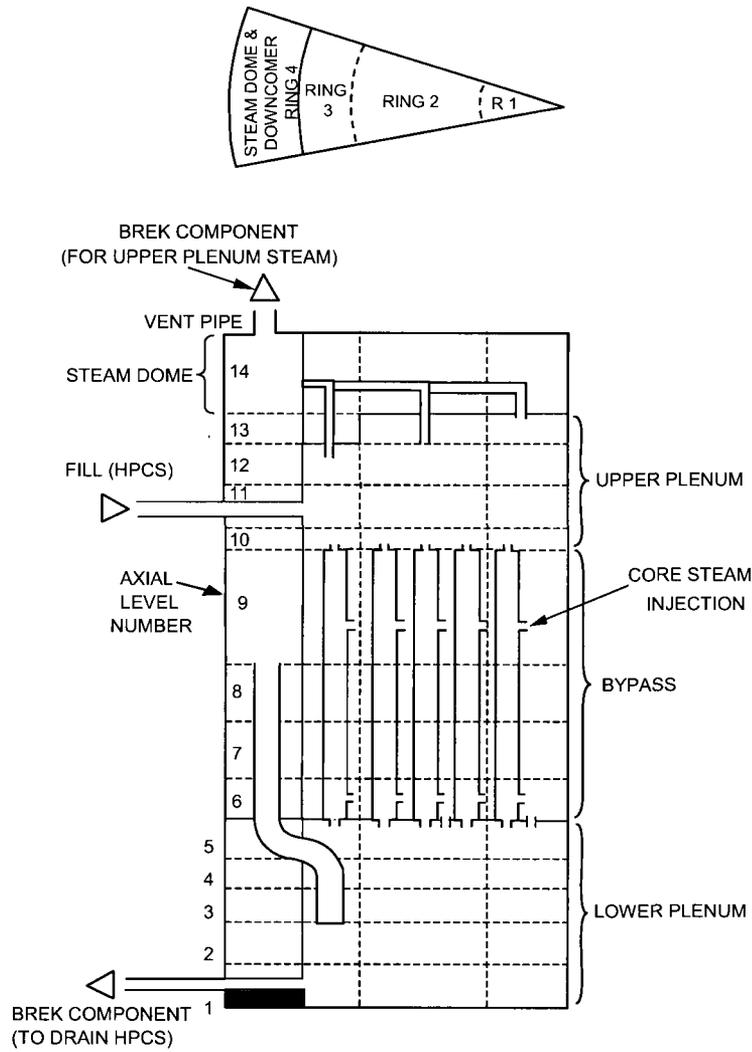
Figure 4.3-2. Input Model for the SSTF Upper Plenum Mixing Test with Five Channel Groups
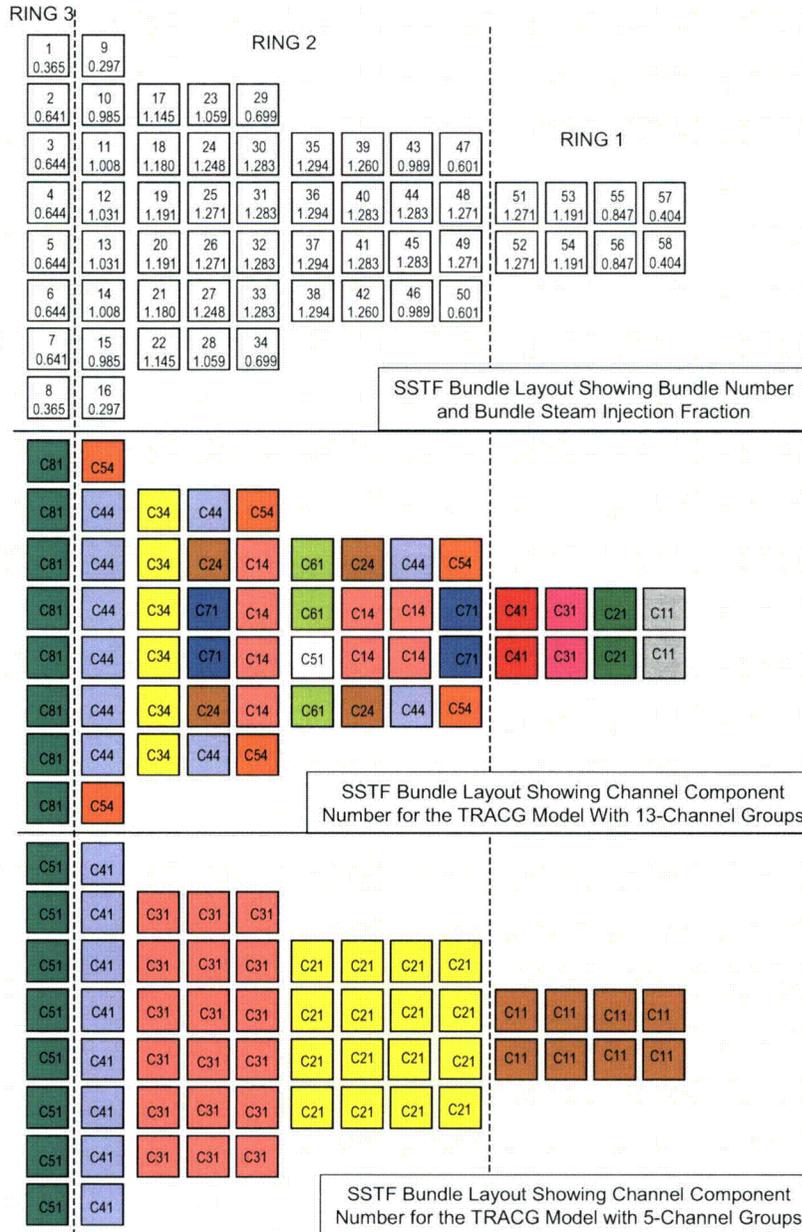
Figure 4.3-3. Channel Groupings for the Five-Channel and 13-Channel Input Models for the SSTF Upper Plenum Mixing Test

COMPONENT PERFORMANCE TESTS

UPPER TIE-PLATE

TEE COMPONENT

CORE STEAM

CHAN COMPONENT

BUNDLE-BYPASS
LEAKAGE PATH

SIDE ENTRY ORIFICE
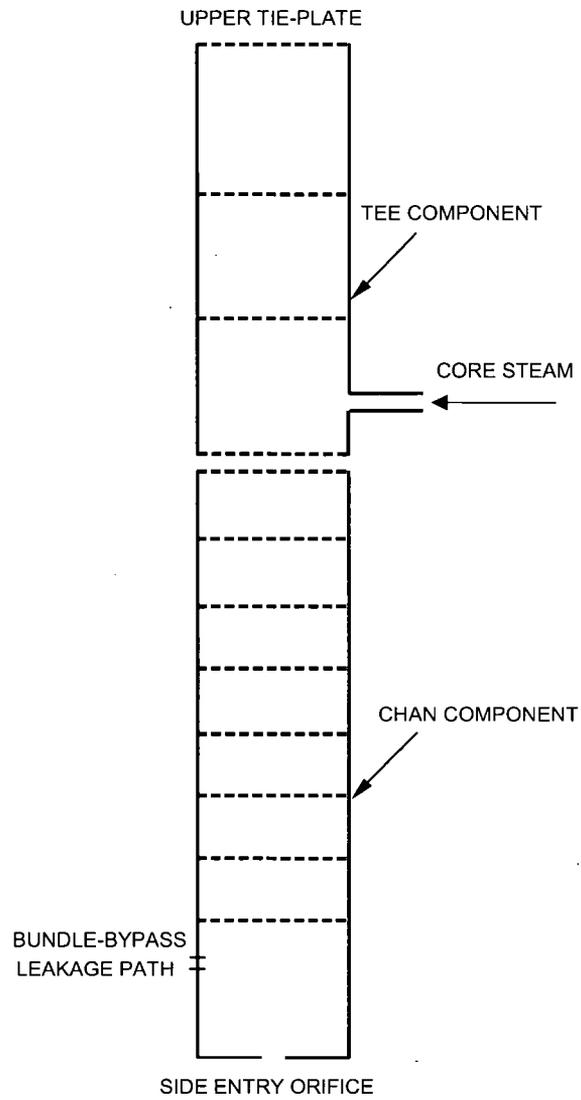
Figure 4.3-4. Nodalization of the SSTF Bundle Using CHAN and TEE Components

[[

]]

Figure 4.3-5. Comparison of Upper Plenum Pressure Drops for SSTF Test SE3-1A

[[

]]

**Figure 4.3-6. Upper Tie Plate Flows for Five-Channel TRACG Model
(SSTF Test SE3-1A)**

[[

]]

**Figure 4.3-7. Comparison of Peripheral Subcooling Above the Upper Tie Plate
(SSTF Test SE3-1A)**
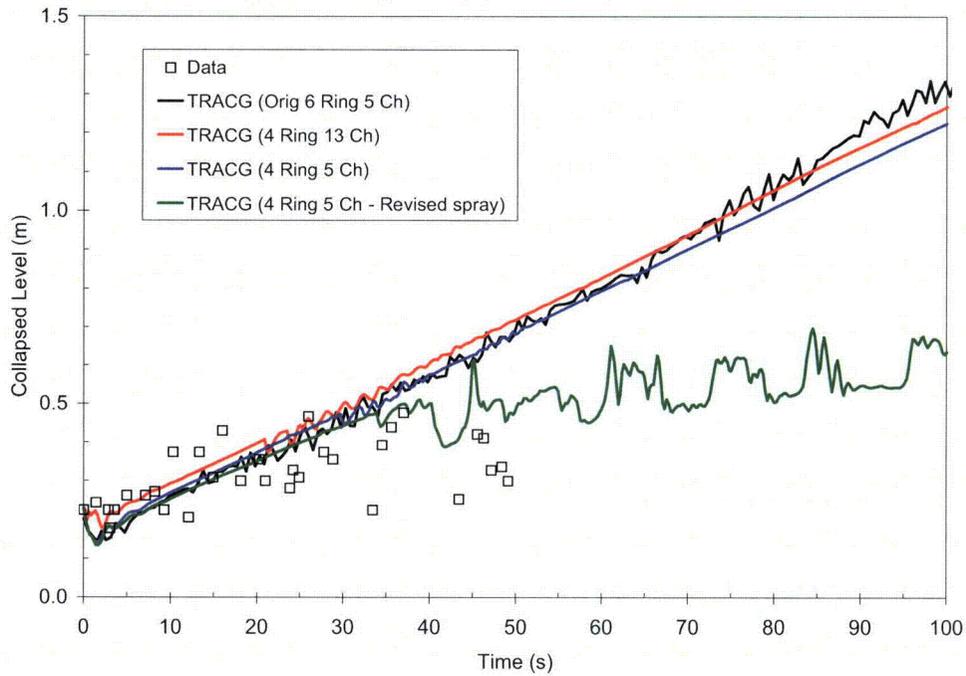
**Figure 4.3-8. Comparison of Upper Plenum Pressure Drops with Revised Spray
Distribution**

4.4   CORE SPRAY DISTRIBUTION

TRACG includes a model for calculating the radial position at which the spray emanating from a prescribed source will reach the elevation corresponding to the upper end of the fuel bundles in the reactor core (or the simulated reactor core in a test facility). The model bases its calculation on input data describing the radial and axial coordinates of the spray source, the velocity of the source at the end of the nozzle, the angle of inclination of the nozzle to the horizontal and the cone angle of the spray. The SSTF core spray distribution test provided separate effects data on the behavior of highly subcooled spray injected into a steam environment with steam updraft that can be used for the qualification of the TRACG spray model.

4.4.1   SSTF Core Spray Test Facility

The Steam Sector Test Facility (SSTF) was described in Section 4.3. Information on the configuration and instrumentation of the SSTF facility for the core spray tests is provided in Reference 4-18. The ECCS systems of interest for the spray distribution tests are the High Pressure Core Spray (HPCS) and the Low Pressure Core Spray (LPCS). Figure 4.4-1 shows the radial and azimuthal locations of the spray nozzles in relation to the 58 simulated fuel bundles. The nozzle designations starting with "U" are on the upper (HPCS) sparger and those starting with "L" are on the lower (LPCS) sparger. The upper and lower core spray spargers are full-scale mockups of 30° sectors of the reference HPCS and LPCS spargers in size, curvature and nozzle location. The abbreviation O.E. stands for "open elbow" and the terms "Street", "regular", etc. further identify the specific nozzle designs.

In addition to the standard SSTF instrumentation, the spray distribution tests had weir flow elements in each of the simulated fuel bundles. The weir measurements relate the spray flow to the bundle to the liquid level sustained in the weir tube. There was no independent measurement of spray flow to the bypass region. The nominal spray flow rate to each of the spargers in operation for a given test was 0.0331 m^3/s (525 gpm).

The core spray distribution tests were run as steady-state tests at constant system pressure with prescribed steam upflow through the simulated fuel bundles. (The bypass region had no steam upflow.) The total bundle steam flow was an independent test parameter and the steam flow distribution among the bundles was fixed in accordance with the bundle radial power factors in the reference (BWR/6-218) plant. The steam flow was individually set for each bundle by orifices in the steam manifold. The total steam upflow was limited to approximately one-half of the condensation capacity of the subcooled spray flow. This was done so that none of the spray flows to the individual bundles was limited by CCFL (Section 3.3). This ensured that the tests provided true separate effects data on the spray distribution. The system pressure was maintained by supplying steam to the steam dome that was admitted to the upper plenum through the simulated steam separators. The jet pump flow path that would otherwise allow steam to flow from the core back through the jet pumps and annulus to the upper plenum was closed off by raising the water level in the lower plenum to cover the jet pump exit.

The portion of the SSTF spray distribution test matrix selected for TRACG qualification is shown in Table 4.4-1.

Table 4.4-1
SSTF Spray Distribution Tests for TRACG Qualification

Test No.	Spray System	Pressure (kPa)	Total Steam Flow (kg/s)	Spray Temperature (K)
CS-3.1	LPCS	203	1.764	336
CS-3.2	HPCS	203	1.764	336
CS-27	HPCS	203	2.520	336
CS-29	HPCS	203	2.835	336
CS-30	HPCS	304	2.268	336
CS-41	HPCS	507	2.268	336

4.4.2   TRACG Input Model

The TRACG nodalization used for the simulation of the SSTF spray distribution tests (Figure 4.4-2) is similar to the model described in Section 5.3 for simulation of the system response tests. The radial and axial nodalizations of the VSSL component are identical and the fuel bundles are represented by the same CHAN and TEE component combination that was also used for simulation of the SSTF upper plenum mixing test (Figure 4.3-4). The model used for simulation of the spray distribution tests used five CHAN components to represent the 58 simulated fuel bundles. The placement of the CHAN components in the three inner rings of the VSSL component and the number of bundles represented by each CHAN are shown in Figure 4.4-2. A second difference was the addition of a BREK component at the entrance of each CHAN. The purpose of these components is to, in effect, accumulate the spray flow to the CHAN. By setting the BREK pressure equal to the system pressure, augmented by the initial head of water in the CHAN, the flow to the BREK becomes the sum of the spray flow entering the top of the associated TEE component plus any steam condensation within the TEE. In this way the BREK components function as direct counterparts to the weir flow meters in the test facility. One additional BREK component (not shown) was attached to Level 7 of Ring 2 of the VSSL to accumulate the spray flow to the bypass in a similar manner. (This component had no counterpart in the test facility.)

As shown on Figure 4.4-1 and Table 4.4-2, there are nine nozzles representing three distinct types on each of the two spargers. Each nozzle of a given type has the same (downward) inclination from the horizontal. Accordingly, three TRACG spray sources were used to represent the nozzles on each sparger. These spray sources were positioned on the outer face of Ring 3 in Level 11 of the VSSL component. The spray flows for each of the TRACG spray sources were compiled from the data in Table 5-1 of Reference 4-18. The nozzle diameters were set equal to the diameters of the header orifices given in Table 3-1 of same reference. The nozzle elevations relative to the top of the simulated fuel bundles were taken from the figure on p. 3-9 of Reference 4-13. The cone angles for the spray sources were derived from data in References 4-13, 4-19 and 4-20. The cone angle for the Spraco 2935M nozzle was taken to be the same as that given on p. 3-9 of Reference 4-13 for a nozzle identified as Spraco 3101. References 4-19 and 4-20 present spray distribution test data for one-inch and ¾ inch open elbow nozzles in a steam environment over a range of pressure and spray subcooling. The tests with 338 K spray subcooling were used to derive the cone angles. The tests showed relatively little sensitivity to pressure and, consequently, the data were averaged over the pressure range tested (101 to 507 kPa). The data are presented in terms of the radius of a circle that contains a given fraction of the

COMPONENT PERFORMANCE TESTS

spray flow at a specified distance from the nozzle. For the purpose of this analysis, the cone angle was defined such that it includes 95.5% of the spray. The cone angle for the one-inch open elbow nozzle was multiplied by 0.56 to obtain the cone angle for the one-inch open elbow nozzle with the nipple. A summary of the input data for the six TRACG spray sources is given in Table 4.4-2.

Table 4.4-2
SSTF Nozzle Spray Source Data

Spray Source	Nozzle Type	No.	Elevation* (m)	Incl. Angle (rad)	Diameter (m)	Flow Rate (m³/s)	Cone Angle (rad)
HPCS-1	Spraco 2935M	3	0.686	-0.646	0.0254	0.01155	1.134
HPCS-2	1 inch O.E. (Street)	2	0.686	-0.140	0.01905	0.00836	0.340
HPCS-3	1 inch O.E. (w/nipple)	4	0.686	-1.117	0.01575	0.01237	0.194
LPCS-1	Spraco 2935M	3	0.406	-0.436	0.0254	0.01201	1.134
LPCS-2	1 inch O.E. (Street)	2	0.406	-0.0524	0.01905	0.00809	0.340
LPCS-3	¾ inch O.E. (Regular)	4	0.406	-0.873	0.01575	0.01229	0.411

* Relative to top of simulated fuel bundles

4.4.3 Calculated Results vs. Test Data

The measured and calculated spray distributions were compared on the basis of the cumulative spray flows to the bundles in each of the three rings in the TRACG model and the spray flow to the bypass. Referring to Figures 4.4-1 and 4.4-2, the measured spray flows to the three rings were computed by summing the individual flows to the eight bundles in Ring 1, the 42 bundles in Ring 2 and the eight bundles in Ring 3. The spray flow to the bypass was evaluated by subtracting the sum of the measured flows to the 58 bundles from the sum of the total spray flow and the condensation capacity of the spray. The condensation capacity of the spray, expressed as mass per unit time, was computed from

$$w_c = \frac{c_p w_s \left(T_{sat} - T_s\right)}{h_{fg}}$$

w_s = spray mass flow rate

T_s = spray temperature

T_{sat} = saturation temperature

h_{fg} = latent heat of vaporization

c_p = specific heat at constant pressure

This process indicated that approximately one-third of the total spray flow went to the bypass. There was some uncertainty in this process because some of the bundle weir flow meters were over ranged for each of the tests selected for the qualification study. In fact, this was true for all but three of the tests (CS-2A, CS-2B and CS-2F) in the full test matrix. The spray flows to the bypass were computed for each of these three tests and the results again indicated that approximately one-third of the spray was going to the bypass. On this basis, it was concluded that the over ranged bundle flow meters (typically two or three of the flow meters in the outer ring) were not significant in terms of accounting for the total spray flow.

[[

]]

4.4.4 Summary and Conclusions

Six tests – one LPCS and five HPCS - from the SSTF core spray distribution test series were simulated with TRACG. The simulated set covered pressures from 203 kPa to 507 kPa and upward core steam flows from 1.76 to 2.27 kg/s. From the comparisons between the TRACG calculations and the measured spray distributions, the following conclusions may be drawn:

[[

]]
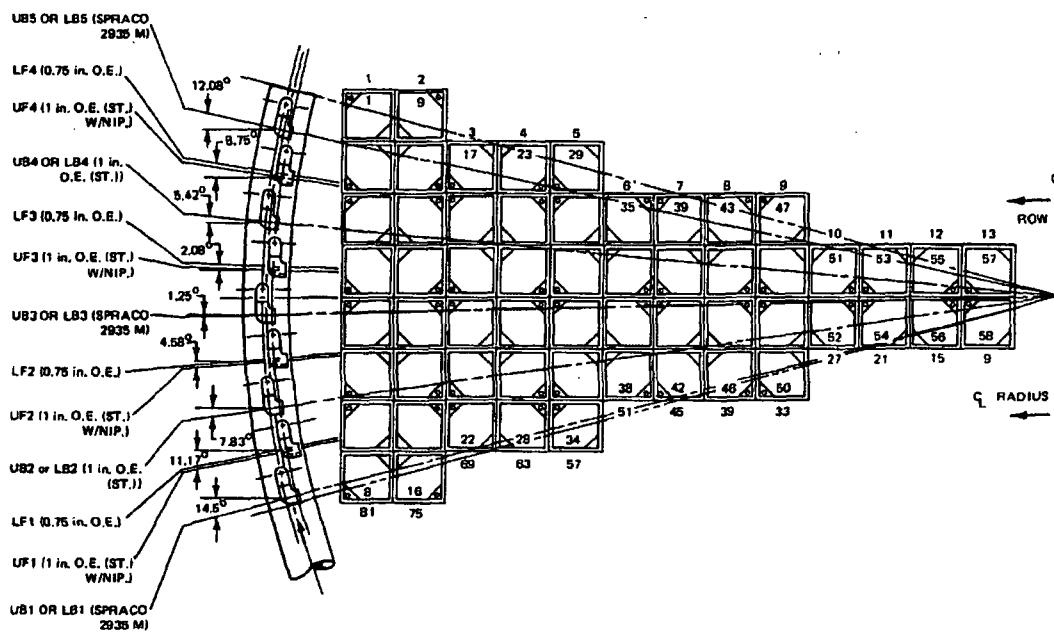
Figure 4.4-1. SSTF Spray Distribution Test Facility

COMPONENT PERFORMANCE TESTS
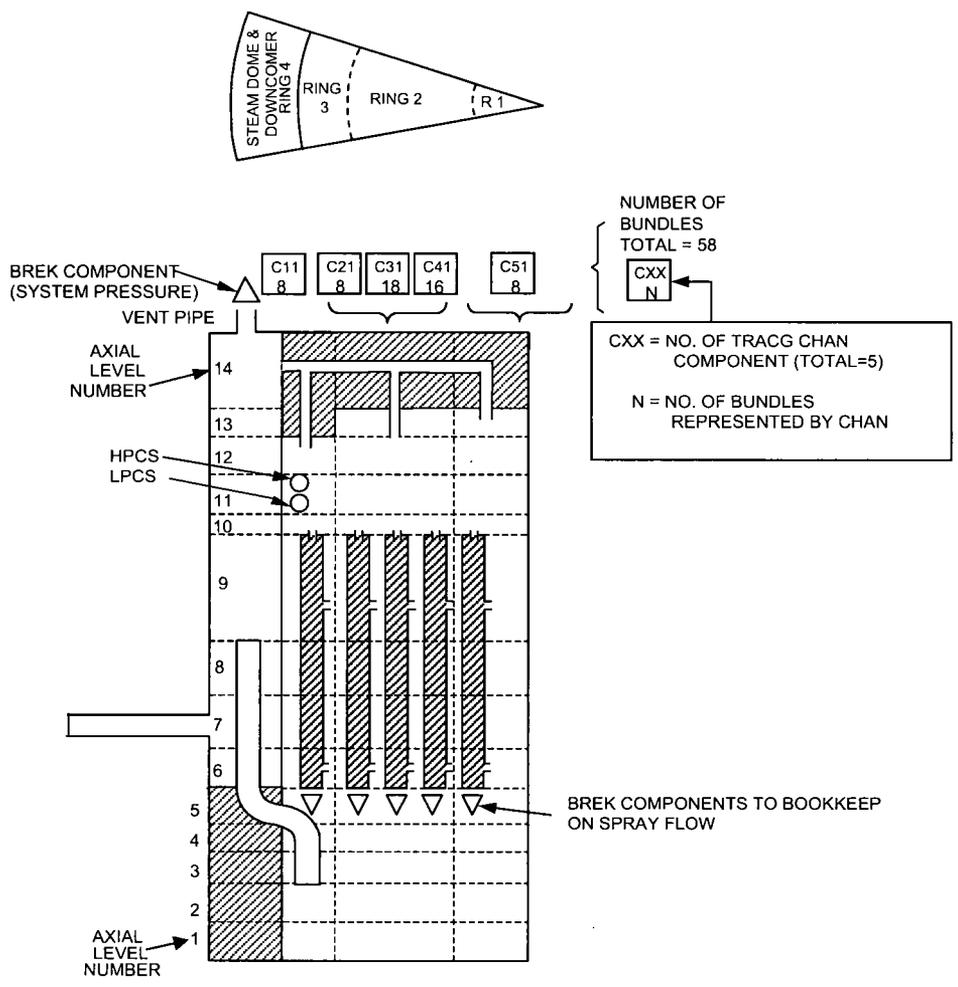
Figure 4.4-2. TRACG Model for SSTF Spray Distribution Tests

[[

]]

Figure 4.4-3. Spray Distribution Comparison for SSTF Test CS-3.1

[[

]]

Figure 4.4-4. Spray Distribution Comparison for SSTF Test CS-3.2

[[

]]

Figure 4.4-5. Spray Distribution Comparison for SSTF Test CS-27

[[

]]

Figure 4.4-5. Spray Distribution Comparison for SSTF Test CS-29

[[

]]

Figure 4.4-6. Spray Distribution Comparison for SSTF Test CS-30

[[

]]

Figure 4.4-7. Spray Distribution Comparison for SSTF Test CS-41

4.5 REFERENCES

[4-1] H. S. Crapo, *One-Sixth Scale Model BWR Jet Pump Test*, Idaho National Engineering Laboratory LTR 20–105, November 1979.

[4-2] G. W. Fitzsimmons, Hydraulic Performance Tests of the Cooper Production Jet Pump, NEDE–13155, February 1971.

[4-3] H. M. Ondang, Hydraulic Performance Test of the LaSalle Production Jet Pump, NEDE–20981, August 1975.

[4-4] A. A. Kudirka, Performance of Improved and Original 1965 Product Line Steam Separators, NEDE-13026, July 1969.

[4-5] A. A. Kudirka and C. L. Swan, Performance of Production Steam Separators for the 1967 Product Line, NEDE-13060, December 1969.

[4-6] A. A. Kudirka and C. L. Swan, Quality Control Tests of Two 1967 Product Line Steam Separators, NEDE-13063, January 1970.

[4-7] H. Choe, Performance of AS-2B Production Steam Separator for BWR/6, NEDE-21242, June 1978.

[4-8] R. H. Moen, et al., Advances in Boiling Water Reactor Steam Separator Systems, ASME 69–WA/NE–5, November 1969.

[4-9] E. L. Burley, Performance of Internal Steam Separator System in Boiling Water Reactors, ASME 69-WA/NE-24, November 1969.

[4-10] Wolf and R. H. Moen, Advances in Steam–Water Separators for Boiling Water Reactors, ASME 73-WA/PWR-4, November 1973.

[4-11] J. G. M. Andersen et al., TRACG Model Description, NEDE-32176P, Rev. 3, April 2006.

[4-12] J. E. Barton et al., BWR-Refill-Reflood Program, Task 4.4 – 30° SSTF Description Document, General Electric Company, (GEAP–24939, NUREG/CR–2133, EPRI NP–1584), June 1981.

[4-13] D. G. Schumacher et al., BWR Refill-Reflood Program Task 4.4 – CCFL/Refill System Effects Tests (30° Sector) SSTF System Response Test Results, General Electric Company, (GEAP-22046, NUREG/CR-2568, EPRI NP-2374), March 1982.

[4-14] J. A. Findlay, BWR Refill-Reflood Program Task 4.4 – CCFL/Refill System Effects Tests (30° Sector) Evaluation of ECCS Mixing Phenomena, General Electric Company, (GEAP-22150, NUREG/CR-2786, EPRI NP-2542), December 1982.

[4-15] J. A. Findlay, BWR Refill-Reflood Program Task 4.4 – CCFL/Refill System Effects Tests (30° Sector) Evaluation of Parallel Channel Phenomena, General Electric Company, (GEAP-22044, NUREG/CR-2566, EPRI NP-2373), March 1982.

[4-16] J. G. M. Andersen et al., TRACG Qualification, NEDO-32177, Rev. 2, January 2000.

[4-17] Md. Alamgir, BWR Refill-Reflood Program Task 4.8 – TRACG-BWR Model Qualification for BWR Safety Analysis Final Report, General Electric Company, (GEAP-22049, NUREG/CR-2471, EPRI NP-2377), July 1983.

[4-18] S. A. Sandoz et al., Core Spray Design Methodology Confirmation Tests, NEDO-24712-A, March 1983.

[4-19] S. K. Rhow and K. H. Sun, Analysis of One-Inch Open Elbow, VNC 12/14, VNC 14/16 Nozzles and the VNC Nozzle with Deflector Removed, NEDE-13454-0, February 1976.

[4-20] S. K. Rhow, Vertical Spray Test Results for ¾-Inch Open Elbow, One-Inch VNC 14/14 and VNC 9/16 Nozzles, NEDE-13454-1, July 1976.

COMPONENT PERFORMANCE TESTS

5.0   INTEGRAL SYSTEM EFFECTS TESTS

This section of the qualification report presents comparisons of TRACG calculations to data from integral system response tests. The TRACG predictions of experimental data from separate effects tests (Section 3) provide valuable information on the capabilities of specific analytical models in the code. These models were found to realistically represent: (1) flashing and void distribution; (2) two-phase level; (3) film boiling heat transfer; (4) upper plenum response; (5) CCFL; (6) pressure drop; (7) critical power; and (8) natural circulation. TRACG predictions of component performance tests (Section 4) demonstrate that the component models in the code realistically represent the observed behavior for the jet pump, steam separator, and upper plenum. A demonstration of TRACG's capability to predict upper plenum spray distribution was included for completeness but this model is not used for BWR LOCA analysis.

The integral systems tests consist mainly of loss-of-coolant accident (LOCA) simulations. The test facilities include the Two-Loop Test Apparatus (TLTA), the Full Integral Simulation Test (FIST), the 58-bundle Steam Sector Test Facility (SSTF), the ROSA-III test facility in Japan, the FIX-II facility in Sweden and the GE Gravity Drain Integral Systems Test (GIST). In general, the integral system effects tests are more complex than separate effects and component performance tests because the overall system responses depend not only on the performance of the individual analytical models in TRACG but also on the interaction between these models. Thus, a major purpose of the qualification studies based on integral system effects tests is to assess TRACG predictions of the phenomena and component interactions and how they affect the overall system response. A secondary purpose is to provide additional information for qualification of the individual models in TRACG.

Sections 5.1 and 5.2, respectively, present comparisons between TRACG calculations and test data from the TLTA and FIST facilities. These facilities are scaled representations of jet-pump BWRs. The tests include simulations of large and small break LOCAs that cover both the blowdown and the refill/reflood phases of the LOCA. Section 5.3 presents comparisons between TRACG calculations and test data from LOCA simulations performed in the SSTF facility, which also models a jet pump BWR. The SSTF simulations cover the refill/reflood phase of the LOCA. Section 5.4 presents comparisons between TRACG calculations and test data from LOCA simulations performed in the ROSA-III test facility. ROSA-III was a volumetrically scaled representation of the BWR/6-251 with an electrically heated core simulator. It was designed to study the response of the primary system, core and ECCS during a postulated LOCA. Section 5.5 presents comparisons between TRACG calculations and test data from LOCA simulations performed in the FIX-II test facility. The FIX-II facility was a scaled representation of the Swedish Oskarsham-2 external-pump BWR. Section 5.6 presents comparisons between TRACG calculations and test data from LOCA simulations performed in the GIST test facility. The objective of the GIST tests was to demonstrate the performance of the SBWR (now ESBWR) Gravity-Drain Cooling System (GDCS) for refill of the reactor vessel following a LOCA.

5.1   TLTA

This section describes four TLTA (Two-Loop Test Apparatus) tests and comparisons of TRACG simulations of these tests with the test data. The four tests are presented in Sections 5.1.1 through 5.1.4, respectively.

5.1.1 TLTA Boiloff Test 6441/6-1

TLTA Test 6441/6-1 provided thermal-hydraulic data for bundle uncovery in a natural circulation mode. The bundle power was 250 kW (scaled decay heat level) and the system pressure was maintained at approximately 2.76 MPa.

The objectives of the analysis are:

- To assess the code capability for predicting natural circulation hydraulics and void distribution through comparisons of calculated bundle void fractions with the data.

- To assess the effectiveness of the bundle heat transfer models through comparisons of the calculated and observed heater rod temperatures.

The key comparisons are between the measured and predicted bundle void fraction and rod temperatures. Direct comparisons to system flows are not possible because the system flows were not measured. The bundle in-flow was inferred from mass balances on the bypass and bundle using the boiloff rate determined from the bundle power.

5.1.1.1 Facility and Test Description

The TLTA had a single full-sized 8x8 electrically heated rod bundle. With a single bundle, the facility is a 1/624 volume-scaled representation of a BWR/6-218 Standard Plant. A detailed description of the TLTA can be found in the facility description report [5-1]. Experimental data for the Boiloff Test Series have been reported previously in Reference 5-2.

The facility configuration used for Test 6441/6-1 is shown in Figure 5.1-1. The ECCS and the recirculation systems were not used in this test. The feedwater system was activated in the latter part of the transient to refill the system. The single bundle core is simulated by 62 electrically heated rods and 2 water rods in an 8x8 lattice. Figure 5.1-2 shows a schematic of the bundle indicating the locations of thermocouples and pressure drop measurements along its length. Measurement and derived quantity uncertainties for this test are summarized in Table 5.1-1 Additional description of the TLTA facility is provided in Section 5.1.2 in the context of the analysis of the large break tests.

For Test 6441/6-1, the bundle power and system pressure were held constant at 250 ±2 kW and 2.758 ± 0.021 MPa, respectively. The initial mixture level was at the top of the bundle. The total system inventory decreased due to boiling in the bundle and steam flowing out through the steamline. The bundle was replenished with water from the downcomer and the bypass by natural circulation. With the decrease of water level in the downcomer and the bypass, the net pressure drop imposed on the bundle decreased. As a result, the bundle slowly uncovered, and the rods above the mixture level began to heat up. By 340 seconds, about one-third of the bundle was uncovered (mixture level at 2.54 m from the bottom of the heated length) and the peak clad temperature reached 712 K. At this time, the system was refilled by injecting cold water at a rate of approximately 68 liters/minute into the downcomer through the feedwater system. The bundle was refilled and all rods were quenched within 25 seconds.

5.1.1.2 System Input Definition and TRACG Nodalization

The TRACG nodalization scheme for the boiloff test is the same as that used for the analysis of the TLTA large break test (see details in Section 5.1.2), with the following exceptions:

- The recirculation loops are not modeled because they were isolated from the vessel for Test 6441/6-1.

- The jet pumps are modeled with PIPE components because the special features of the TRACG jet pump components are not needed for the simulation of Test 6441/6-1.

- The test facility systems that represent various elements of the BWR Emergency Core Cooling System (ECCS) are not modeled because they were not activated in Test 6441/6-1.

- A constant pressure (2.76 MPa) boundary condition is imposed on the system by means of a BREK component.

- A FILL component with prescribed flow and temperature is used to model refill by cold water injection to the downcomer from the simulated feedwater system in the test facility.

The heat loss from the vessel to the ambient is modeled using double-sided heat slabs. The outside heat transfer coefficient (5.6 W/m^2–K) for the heat slabs was determined from system heat-loss calibration tests. The measured system heat loss at a pressure of 2.76 MPa was about 35 kW [5-3].

5.1.1.3 Results and Discussion

Comparisons between the results calculated by TRACG and the corresponding test measurements for Test 6441/6-1 are presented in Figures 5.1-3 through 5.1-9. The calculation begins at test initiation and continues until 450 s at which time the rods were quenched to saturation and the bundle was reflooded.

Comparisons between calculated and measured bundle void fractions for various elevations spanning the boiloff and uncovery zones are shown in Figures 5.1-3 through 5.1-6. The test void fractions are derived from the pressure drop measurement locations DP28, DP29, DP30 and DP31 (Figure 5.1-2). In the boiloff tests, fluid velocities and accelerations in the bundle are very low and, consequently, the pressure drop measurements are essentially equal to the elevation head over the distance between the measurement locations. From the elevation head, an average density and the corresponding average void fraction between the measurement locations can be calculated. The transient void fractions derived in this manner have been smoothed to eliminate low amplitude fluctuations. This smoothing results in a small uncertainty in the derived void fractions that is estimated to be ±0.05 (Table 5.1-1). The TRACG nodalization of the bundle (Figure 5.1-14) shows that the TLTA pressure measurement spatial intervals include several TRACG cells. For example, measurement interval DP28 includes Cells 16 to 19. Thus, the void fraction inferred from the DP28 measurement is compared to a weighted average of the void fractions calculated for Cells 16 to 19 in the TRACG model (Figure 5.1-6).

[[

]]

5.1.1.4 Conclusions

The results presented in Section 5.1.1.3 comparing TRACG calculations and test measurements for the TLTA natural circulation boiloff test (Test 6441/6-1) support the following conclusions:

[[

•

]]

Table 5.1-1
Measurement Uncertainties for TLTA Test 6441/6-1

Directly Measured Quantities	Uncertainty
System Pressure	± 21 kPa
Fluid Temperature	± 3 K
Rod Temperature	± 3 K
Bundle ΔP	± 2% of reading ± 0.14 kPa
Bypass ΔP	± 2% of reading ± 0.14 kPa
Downcomer ΔP	± 2% of reading ± 0.14 kPa
Bundle Power	± 2 kW
Derived Quantities	**Uncertainty**
Bundle Inlet Flow	± 0.03 kg/s
Bundle Steam Flow	± 0.03 kg/s
Fluid Density	± 16 kg/m^3
Void Fraction	± 0.05
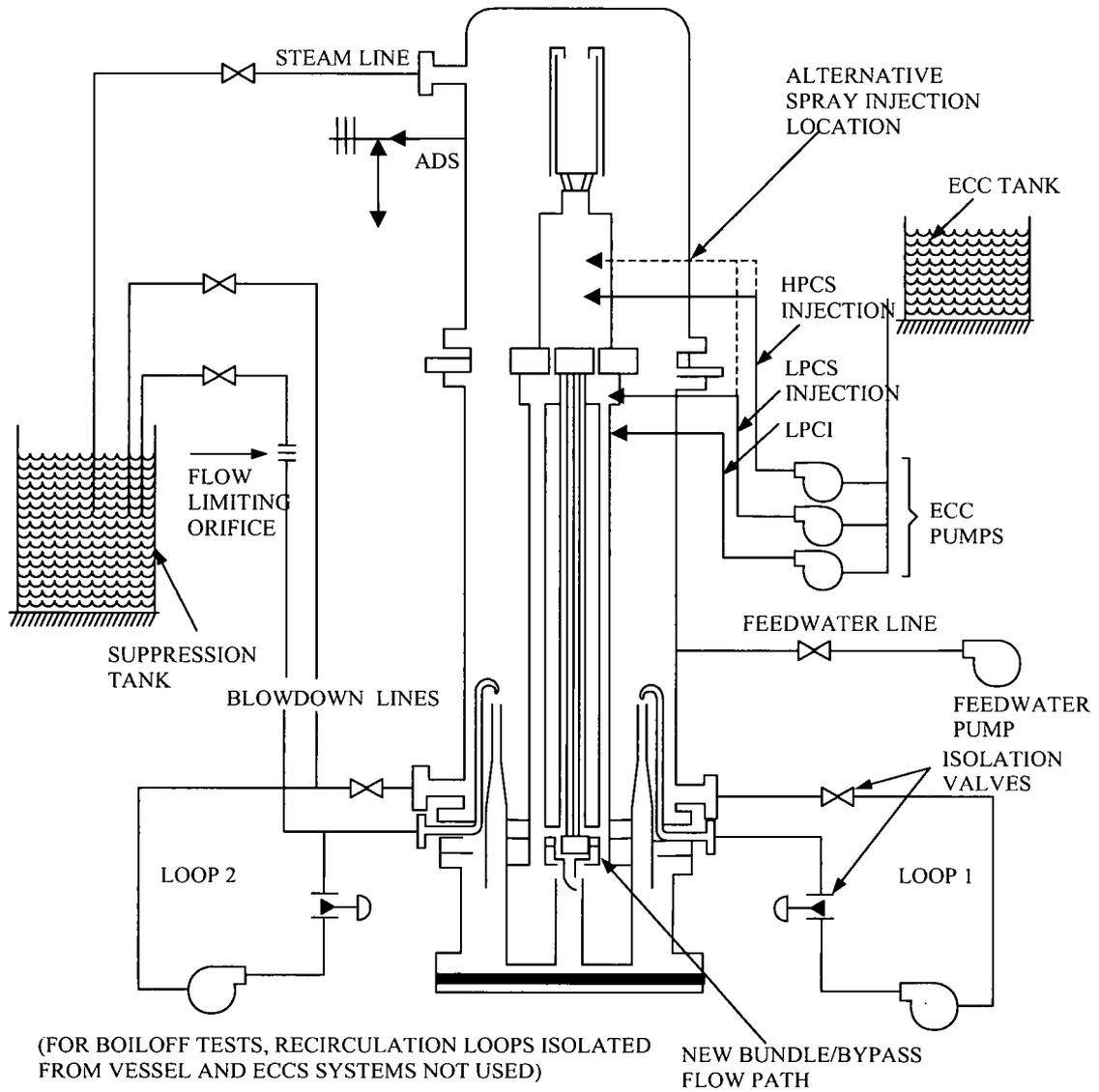
Figure 5.1-1. Two-Loop Test Apparatus (TLTA) Configuration

INTEGRAL SYSTEM EFFECTS TESTS
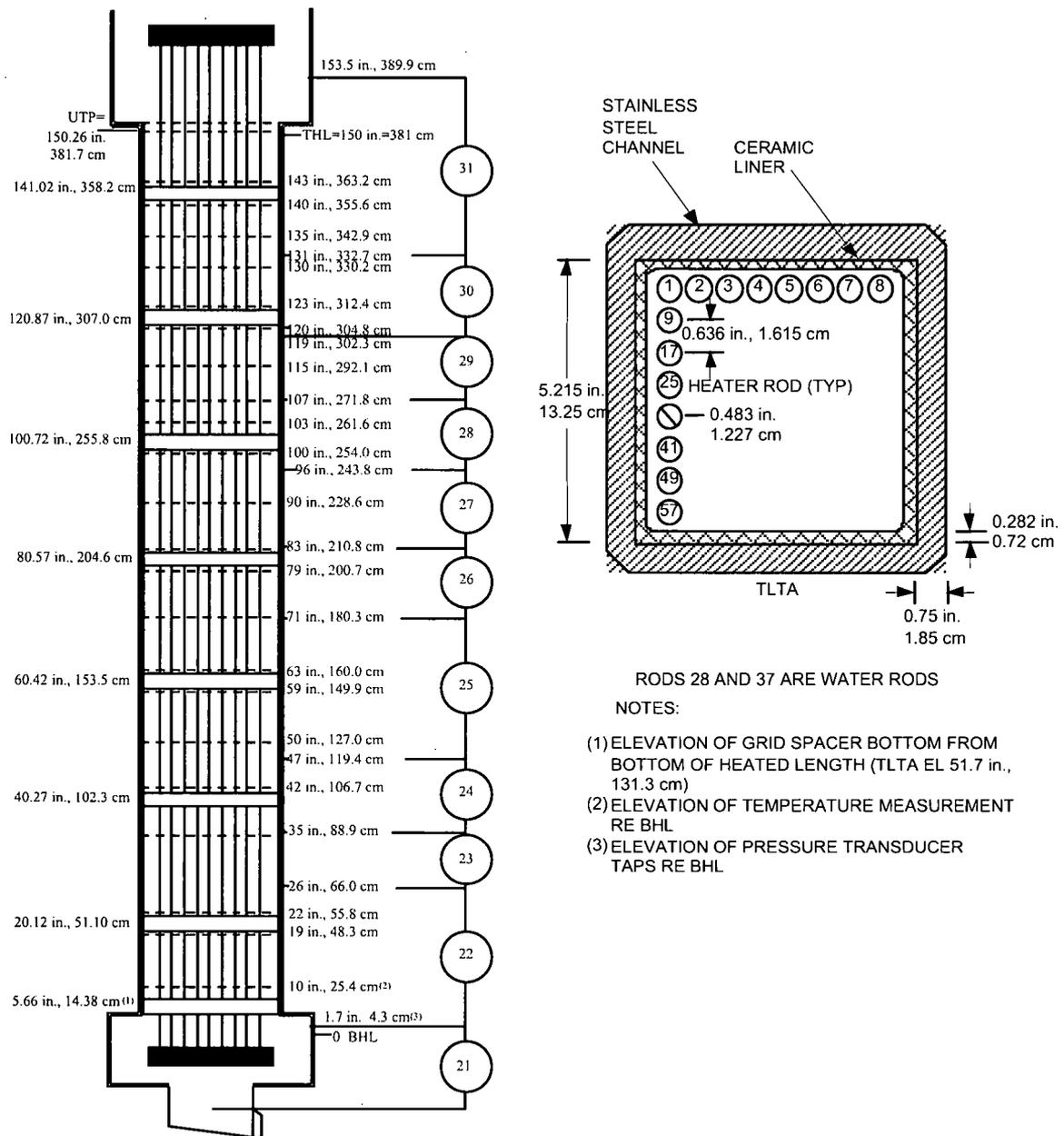
Figure 5.1-2. TLTA Bundle Temperature and Differential Pressure Measurements

[[

]]
Figure 5.1-3. Comparison of Void Fractions for Measurement DP31 for Test 6441/6-1
[[

]]
Figure 5.1-4. Comparison of Void Fractions for Measurement DP30 for Test 6441/6-1

[[

]]

Figure 5.1-5. Comparison of Void Fractions for Measurement DP29 for Test 6441/6-1

[[

]]

Figure 5.1-6. Comparison of Void Fractions for Measurement DP28 for Test 6441/6-1

[[

]]
Figure 5.1-7. Comparison of Rod Temperatures at 3.556 m Elevation for Test 6441/6-1

[[

]]
Figure 5.1-8. Comparison of Rod Temperatures at 3.3 m Elevation for Test 6441/6-1

[[

]]

Figure 5.1-9. Comparison of Rod Temperatures at 3.048 m Elevation for Test 6441/6-1

5.1.2 TLTA Large Break LOCA Test 6425/Run 2

The TLTA Large Break Test 6425/Run 2 provided integral system loss-of-coolant accident (LOCA) response data in a scaled BWR facility with a single full-sized 8x8 electrically heated bundle. The use of data from Test 6425/Run 2 for TRACG qualification provides assurance that TRACG can simulate complex transients involving system interaction effects and confirms TRACG capability for the prediction of specific LOCA-related phenomena including critical flow, counter-current flow limitation and boiling transition.

5.1.2.1 Facility and Test Description

A schematic diagram of the TLTA facility is shown in Figure 5.1-1. As described above, the facility is a scaled single-bundle representation of a BWR/6-218 Standard Plant including the lower plenum, core, bypass, upper plenum, steam separator, steam dome, downcomer, jet pumps and the two recirculation loops.

The TLTA LOCA depressurization tests were initiated by breaking rupture disks in the suction and drive lines of one of the recirculation loops. The operable ECC systems for Test 6425/Run 2 included High Pressure Core Spray (HPCS), Low Pressure Core Spray (LPCS) and one of the three Low Pressure Coolant Injection (LPCI) systems. Uncertainties for measurements from the three TLTA LOCA tests included in the TRACG qualification study are summarized in . The initial conditions for Test 6425/Run 2 are listed in Table 5.1-3. Figure 5.1-10 [5-3] shows the time-dependent boundary conditions and the performance of the ECC systems. The measured ECC flow rates are shown in more detail in Figure 5.1-11. The nominal ECC fluid temperature was 320 ± 8 K.

The early stage of the blowdown transient is characterized by rapid loss of inventory through the breaks, decrease in bundle power and coastdown of the recirculation pumps. Following the uncovery of the recirculation suction line, the system depressurized rapidly. The depressurization rate was slowed when bulk flashing started in the lower plenum. This sequence of events is illustrated by the behavior of key system response parameters in Figure 5.1-12. The liquid in the lower plenum, guide tubes and bypass began to flash at about 11 seconds from the start of the transient. This produced a two–phase flow surge through the bundle and jet pumps that redistributed liquid mass within the vessel.

As the transient proceeded, two-phase levels formed in the lower plenum, bundle, bypass and guide tube. Counter-current flow limitation (CCFL) was established at the side entry orifice (SEO), the upper tieplate (UTP), the top of the bypass and the junction between the bypass and guide tube. The bundle inventory decreased gradually in response to the combined effects of flashing, boiling and liquid downflow at the UTP and SEO. The bypass inventory also decreased due to flashing and flow from the bypass back into the bundle.

About 35 seconds from the start of the transient, the two-phase level in the lower plenum reached the jet pump exit plane. This allowed lower plenum steam to vent through the jet pumps in addition to the SEO. The decrease in SEO steam flow produced a substantial increase in the CCFL-controlled liquid downflow from the bundle to the lower plenum and bulk dryout of the bundle was initiated. The HPCS was started at 27 seconds and the first rewet of the rods was observed at 50 seconds. Other dryout locations continued to heat up at a decreasing rate as the

progressive rewet of the rods by top–down quenching proceeded in a more or less sporadic manner.

The LPCS and the LPCI flows began at 64 and 75 seconds, respectively. The LPCI flow, which is injected into the bypass, increased the bypass inventory and the leakage flow from the bypass to the bundle. This, in combination with the relatively strong CCFL at the SEO, allowed refill of the bundle to begin. At about 130 seconds, the bundle was reflooded with a two-phase mixture and all the rods were cooled to saturation temperature.

As the system depressurization rate decreased, less steam was produced in the lower plenum and the steam flow at the upper tieplate decreased accordingly. The combined effect of LPCS flow into the upper plenum and the reduced steam flow at the upper tieplate resulted in increased liquid downflow to the bundle. The peak rod temperature for the transient occurred just prior to this rewet. The CCFL at the top of the bypass broke down at about 95 seconds and the upper plenum inventory drained rapidly and filled the bypass. Shortly thereafter, the CCFL at the guide tube-to-bypass junction also broke down and the guide tube filled.

5.1.2.2 System Input Definition and TRACG Nodalization for TLTA Test 6425/Run 2

The TRACG nodalization used to model the TLTA is shown in Figure 5.1-13. Table 5.1-4 summarizes the TRACG components used for the model. The model has 111 cells with 32 cells in the VSSL component. The VSSL component has 16 axial levels, two radial rings and one azimuthal sector (Figure 5.1-13). Communication between VSSL cells is through open flow areas or one-dimensional (1D) components. The 1D components include the fuel bundle (CHAN component) connecting the lower and upper plenum, the guide tube (TEE component) connecting the bypass and lower plenum, and the jet pumps (JETP components). In addition, 1D PIPE components are used in combination with FILL components to represent the feedwater line, the HPCS line, the LPCS line, the LPCI line and the steamline. The stored heat in the vessel walls is modeled by lumped heat slabs. Two radial rings are shown in the VSSL component in Figure 5.1-13. The first ring is the boundary between the core and the downcomer region and the second ring is the outer boundary of the vessel.

Ten of the axial levels in the VSSL component correspond with either regional boundaries in the TLTA vessel (Levels 5, 10 and 12 through 16) or connection points for 1D components - jet pump/lower plenum (Level 2), lower plenum/rod bundle (Level 4), jet pump/downcomer (Level 7) and bundle mixing plenum (Level 10). The additional six levels provide more accurate representation of the regional thermal-hydraulic conditions and alignment with the instrumentation. The lower plenum region below the jet pump exit plane is represented by two axial levels (Levels 1 and 2) for calculation of the phase separation and void distribution during flashing. Comparisons with TLTA data have shown that two axial levels are sufficient. The boundaries of Levels 1 and 2 correspond with ΔP tap locations. The region between the jet pump exit and the side entry orifice is divided into two axial levels (Levels 3 and 4) to represent the bundle inlet fluid conditions. The boundary of Level 3 coincides with a lower plenum ΔP tap location. The region between the core support plate and the top of the jet pump is divided into two axial levels (Levels 6 and 7) for adequate representation of bypass fluid conditions near the leakage holes and the fluid conditions near the recirculation line inlet.

The vessel region between the top of the jet pump and the top of the core is subdivided into three axial levels (Levels 8, 9, and 10). Level 8 allows specification of the boundary between the

saturated and the subcooled regions in the downcomer prior to the initiation of blowdown. Level 9 is located close to the top of the bypass region to represent the thermal-hydraulic conditions near the bypass exit where CCFL is expected to limit bypass refill. The mixing plenum region is subdivided into two axial levels (Levels 11 and 12) for calculation of the pressure drop between two successive flow area restrictions (bundle/bypass exit area and the flow area restriction at the upper electrode plate at the bottom of the upper plenum). The center of level 11 corresponds to mixing plenum ΔP and thermocouple locations.

The rod bundle is modeled by a CHAN component with 26 cells (Figure 5.1-14). Cells 3 through 24 represent the heated length. The leakage path between the bundle and the bypass is in Cell 3. The cell boundaries coincide with spacer and tieplate locations and further subdivide the bundle to align the cells with measurement tap locations. The spacer and tieplate flow areas account for possible CCFL at these locations and the effect of local flow acceleration on the bundle void distribution. Experimental information has been used to establish the hydraulic loss coefficients for the bundle, bypass and bundle-to-bypass flow. The upper and lower tieplate and spacer loss coefficients are based on measurements for mass fluxes at or above 680 kg/m^2-s and pressures between 5.5 and 9.65 MPa. Loss coefficients for forward and backward flow to the bypass through the lower tie plate hole and the finger springs are based on measurements covering a temperature range from 339 K (150 °F) to 533 K (500 °F), pressures up to 6.9 MPa and flows up to 4000 kg/s. Correct specification of these flow path loss coefficients is required for TRACG to correctly calculate the bundle and bypass pressure drops that determine the flow and void fraction during the LOCA transient.

The heater rods are divided into eight TRACG rod groups in accordance with their lattice location and radial peaking factors (Figure 5.1-15). The chopped cosine axial power distribution for the heater rods is modeled using discrete values as shown in Figure 5.1-16. The model for an individual heater rod consists of seven radial nodes (Figure 5.1-17). Node 5 represents the approximate thermocouple location. The TRACG material property options provide for accurate representation of the rod heat capacity and thermal diffusivity.

5.1.2.3 Results and Discussion

[[

]]

INTEGRAL SYSTEM EFFECTS TESTS

5.1.2.4 Conclusions

The TRACG simulation of TLTA large break LOCA Test 6425/Run 2 shows satisfactory overall agreement with the test measurements. The calculation predicts the key events and the controlling phenomena (critical flow, CCFL/CCFL breakdown, boiling transition/rewet and regional inventory transients) with satisfactory accuracy. More specifically:

[[

]]

Table 5.1-2
Measurement Uncertainties for TLTA Tests 6425/Run 2, 6426/Run 1 & 6423/Run 3

Measured Quantities	
System Pressure	± 21 kPa
Fluid Temperature	± 3 K
Rod Temperature	± 3 K
Bundle ΔP	± 0.21 kPa
Bypass ΔP	± 0.21 kPa
Upper Plenum ΔP	± 0.21 kPa
Derived Quantities	
Bundle Inlet Flow	± 0.03 kg/s
Jet Pump Flow	± 0.5 kg/s
Break Flow	10% of Calculated Value
ECC Flows	± 0.05 to 0.1 kg/s(depending on ECC system)
Fluid Density	± 16 kg/m^3
Void Fraction	± 0.05
Mixture Level	± 0.15 m

Table 5.1-3
Initial Conditions for TLTA Test 6425/Run 2

Quantity	Initial Value [a]
Bundle Power [b]	5.05 ± 0.03 MW
Steam Dome Pressure	7198 ± 30 kPa
Lower Plenum Pressure	7384 ± 30 kPa
Lower Plenum Enthalpy	1228 ± 10 kJ/kg
Initial Water Level [c]	1.85 ± 0.2 m
Feedwater Enthalpy	95 ± 5 kJ/kg
Bundle Inlet to Outlet ΔP	117 ± 10 kPa
Steam Flow	2.7 ± 0.5 kg/s
Feedwater Flow	0.6 ± 0.1 kg/s
Drive Pump 1 Flow	4.1 ± 0.5 kg/s
Drive Pump 2 Flow	3.8 ± 0.5 kg/s
Jet Pump 1 Flow	10 ± 0.9 kg/s
Jet Pump 2 Flow	9 ± 0.9 kg/s
Bundle Inlet Flow	18 ± 2 kg/s

[a] Uncertainties are judged from the maximum of data fluctuations and/or absolute uncertainty of measurement.
[b] 5.05 MW is central core region average power; overall core average power is 4.60 MW.
[c] Relative to jet-pump support plate.

Table 5.1-4
TLTA Facility TRACG Components

TLTA Region	TRACG[a]
Break Lines	TEE 4, TEE 7 (secondary)
Broken Loop Suction Line	TEE 4, BREK 24
Broken Loop Drive Pump	PUMP 5
Broken Loop Drive Line Isolation Valve	VLVE 6
Broken Loop Drive Line	TEE 7, BREK 25, JETP 8 (secondary)
Broken Loop Jet Pump	JETP 8
Intact Loop Suction Line	PIPE 26
Intact Loop Suction Line Isolation Valve	VLVE 1
Intact Loop Drive Pump	PUMP 2
Intact Loop Drive Line Isolation Valve	VLVE 28
Intact Loop Drive Line	PUMP 2, JETP 3 (secondary)
Intact Loop Jet Pump	JETP 3
Heated Bundle	CHAN 20
Guide Tube	TEE 21, FILL 27
Feedwater Line	PIPE 11, FILL 10
Main Steamline	PIPE 18, FILL 19
HPCS Line	PIPE 17, FILL 16
LPCS Line	PIPE 15, FILL 14
LPCI Line	PIPE 13, FILL 12
Vessel and Internals	VSSL 9
Lower Plenum	VSSL Levels 1–5, Cell 1 and 2
Downcomer	VSSL Levels 6–14, Cell 2
Bypass Tubes	VSSL Levels 6–10, Cell 1
Mixing Plenum	VSSL Level 11, Cell 1
Upper Plenum	VSSL Levels 12–13, Cell 1
Standpipe and Steam Separator	VSSL Levels 14–15, Cell 1
Steam Dome	VSSL Level 16, Cells 1 and 2

[a] A TRACG component consists of one or more cells. The VSSL component is constructed with axial levels, radial rings and azimuthal sectors. A VSSL cell is defined by one sector in one ring of one level.
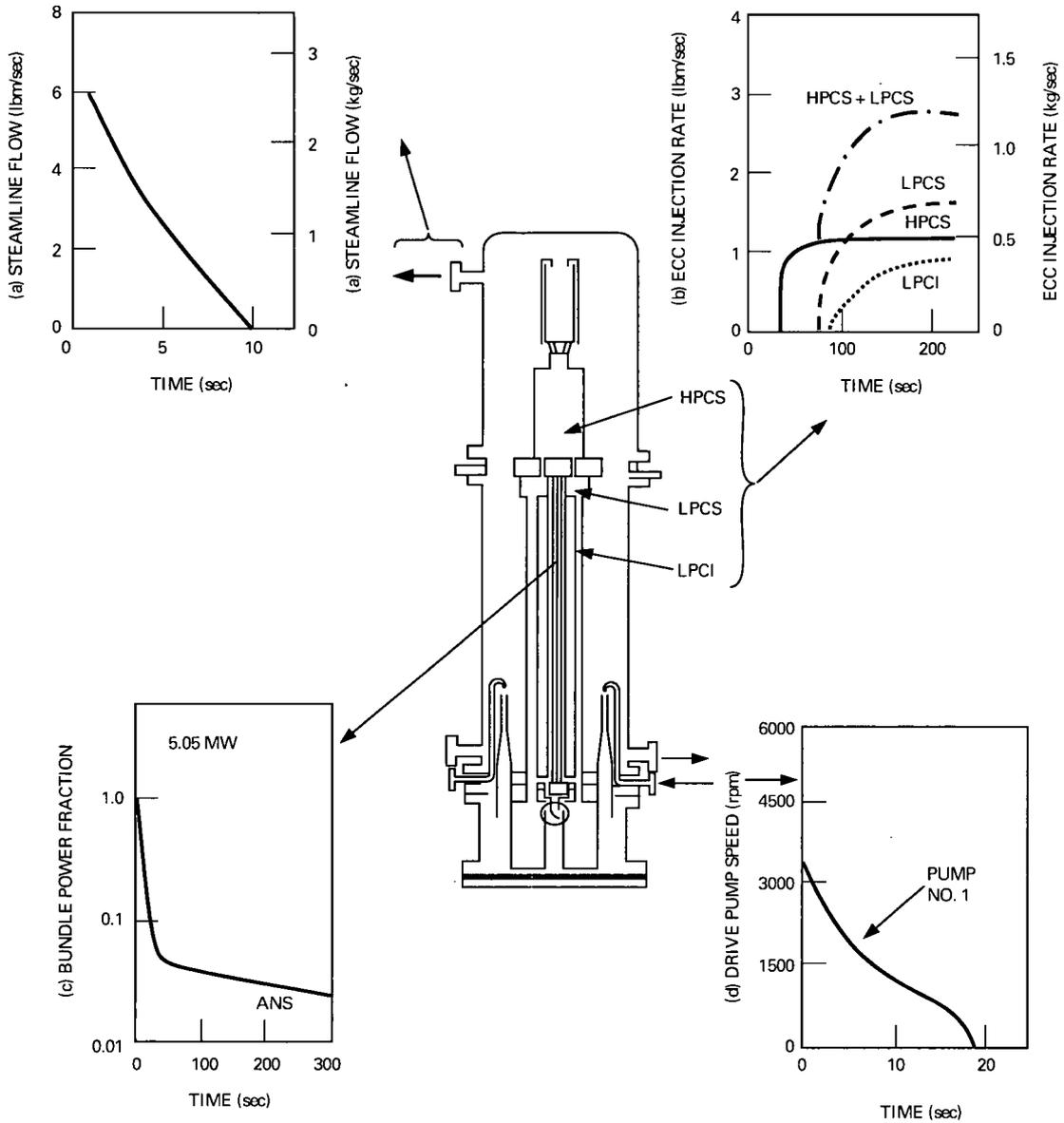
Figure 5.1-10. Controlled Boundary Conditions for TLTA Test 6425/Run 2
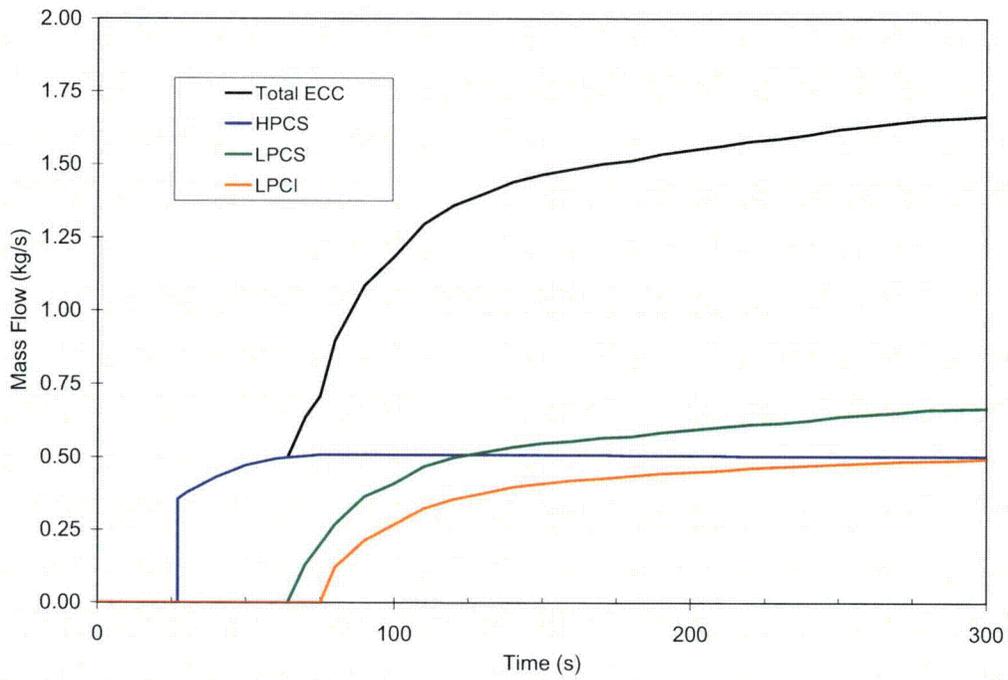
Figure 5.1-11. Measured ECC Mass Flows for TLTA Test 6425/Run 2
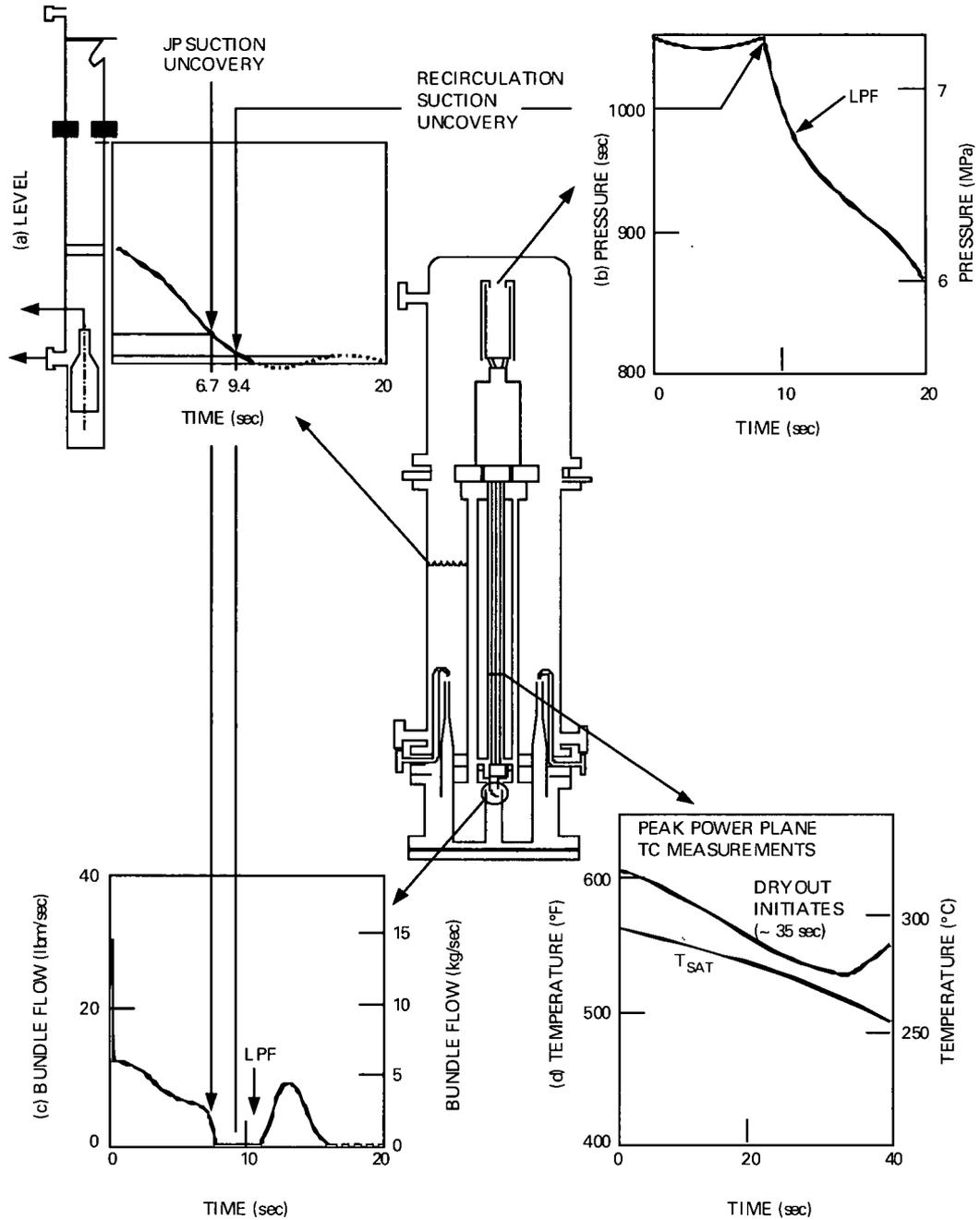
**Figure 5.1-12. Measured System Response in the Early Stage of the Blowdown
Transient for TLTA Test 6425/Run 2**
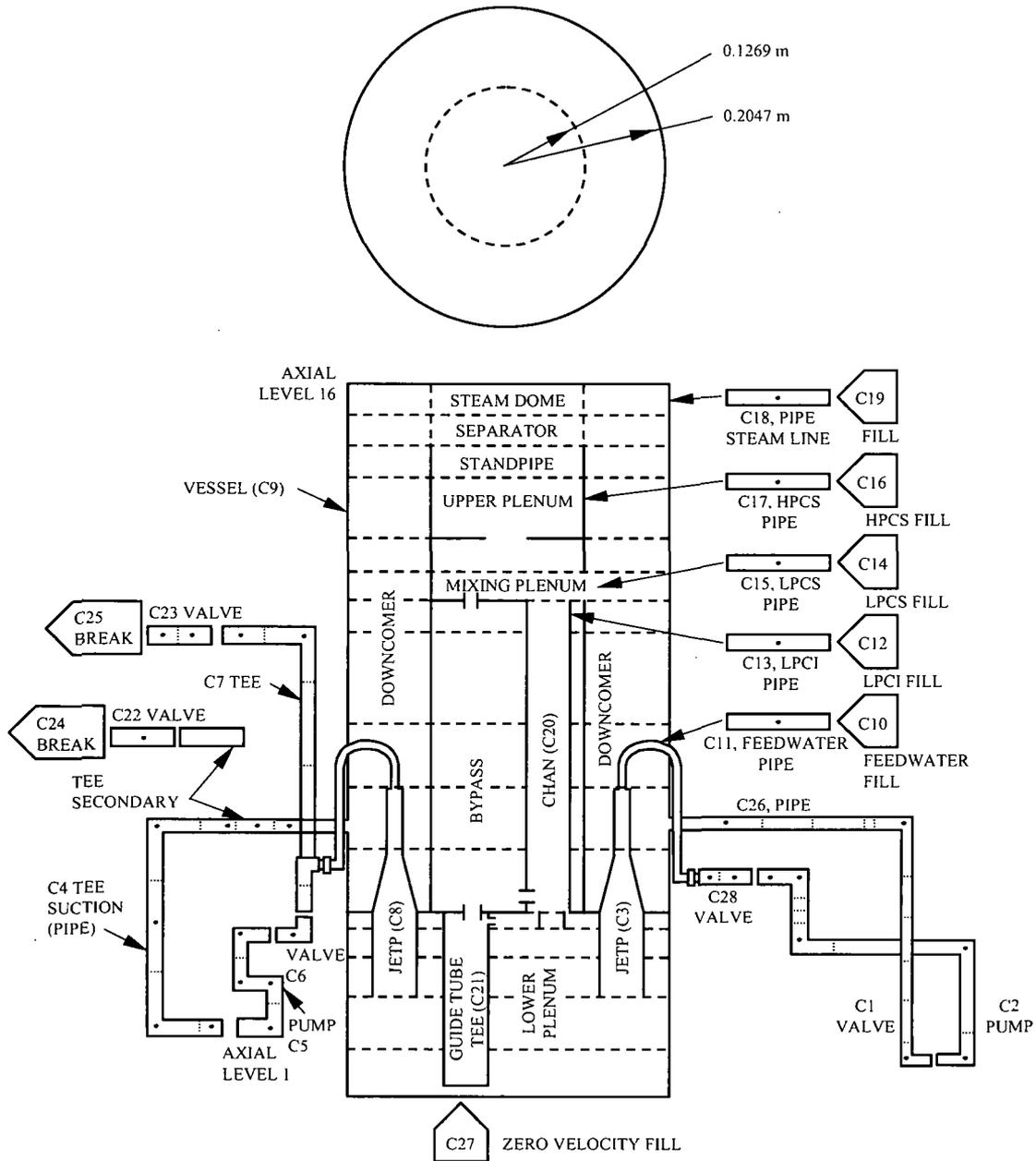
Figure 5.1-13. System Nodalization for TLTA Test 6425/Run 2
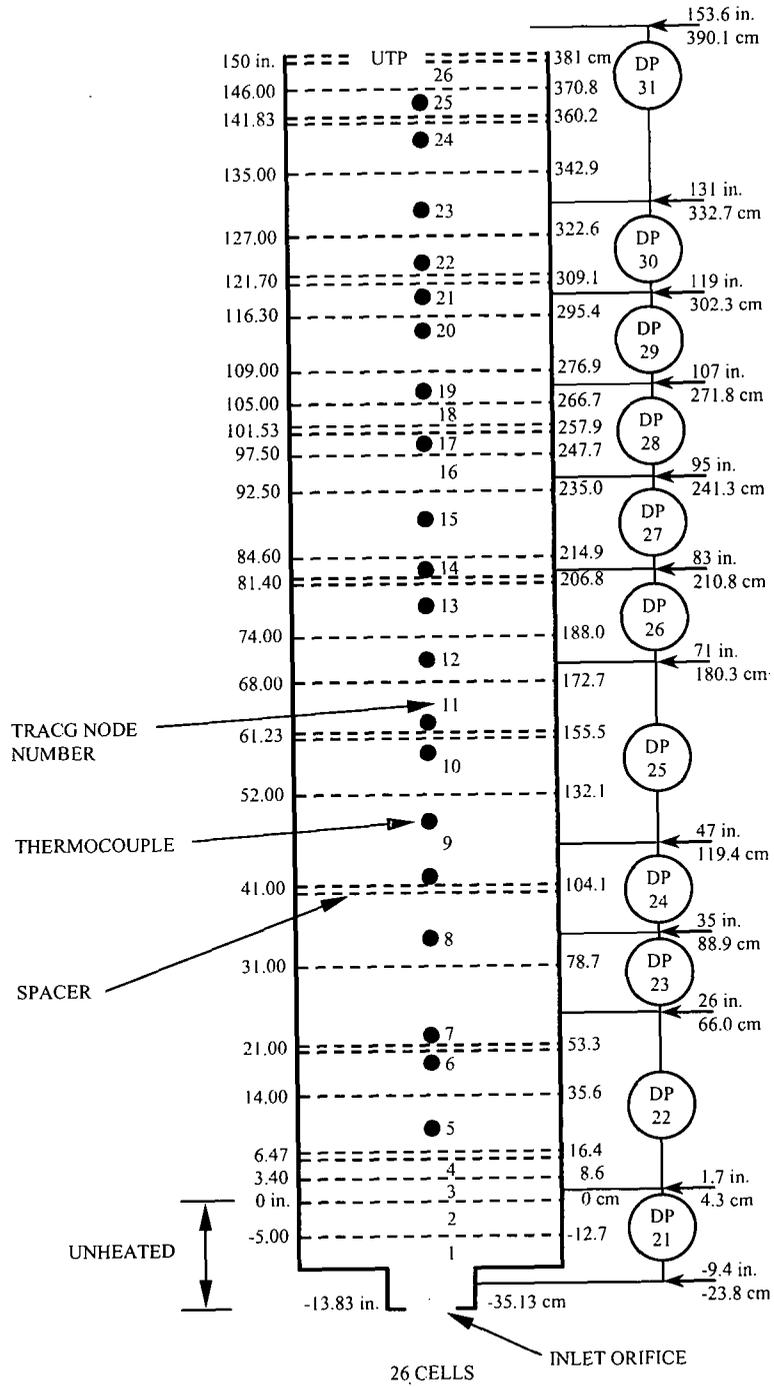
Figure 5.1-14. TLTA Bundle Nodalization

CHANNEL WALL

6 1.017	6 1.017	6 1.004	5 0.962	5 0.951	7 1.056	6 1.012	6 1.019
6 1.020	2 0.965	4 1.039	3 1.018	3 1.006	4 1.056	2 0.955	6 1.016
6 1.018	3 1.026	2 0.914	2 0.961	2 0.962	2 0.946	8 1.058	6 1.016
5 0.961	3 1.006	2 0.962	1 0.0	3 1.019	2 0.958	3 1.023	5 0.963
5 0.943	3 1.022	2 0.962	3 1.022	1 0.0	2 0.967	3 1.013	5 0.961
6 1.018	4 1.056	2 0.966	2 0.965	2 0.961	2 0.966	4 1.040	6 1.022
6 1.023	2 0.962	4 1.055	3 1.016	3 1.006	3 1.021	2 0.967	6 1.025
6 1.024	6 1.024	6 1.024	5 0.966	5 0.965	6 1.024	6 1.025	6 1.023

3 — ROD GROUP NUMBER
1.017 — LOCAL PEAKING FACTOR

Rod Group No.	No. Rods in Group	Average Peaking Factor
1	2	0.000
2	16	0.960
3	12	1.017
4	5	1.050
5	8	0.960
6	19	1.021
7	1	1.057
8	1	1.059

Figure 5.1-15. Rod Grouping for Simulation of TLTA Tests
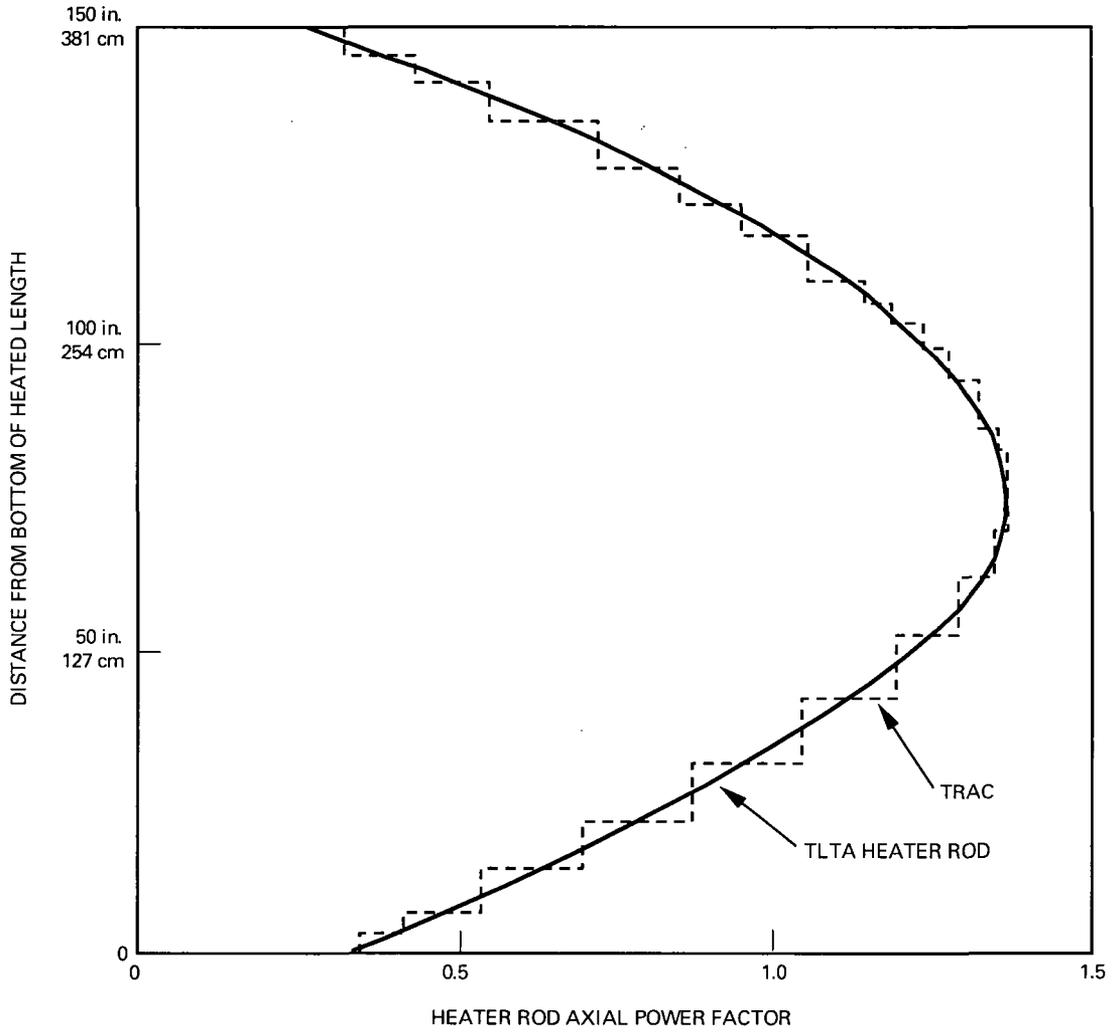
Figure 5.1-16. Axial Power Distribution for the TLTA Bundle

ACTUAL HEATER ROD

TRACG HEATER ROD NODALIZATION

$r_1 = 0.0$ in. (reference)
$r_2 = 0.0020$ in., 0.0051 cm
$r_3 = 0.1250$ in., 0.3175 cm
$r_4 = 0.1815$ in., 0.4610 cm
$r_5 = 0.2015$ in., 0.5118 cm
$r_6 = 0.2215$ in., 0.5626
$r_7 = 0.2315$ in., 0.5880 cm
$r_8 = 0.2415$ in., 0.6134 cm

MATERIAL

AIR GAP ③

INSULATOR ⑫

INCONEL 600 ⑩
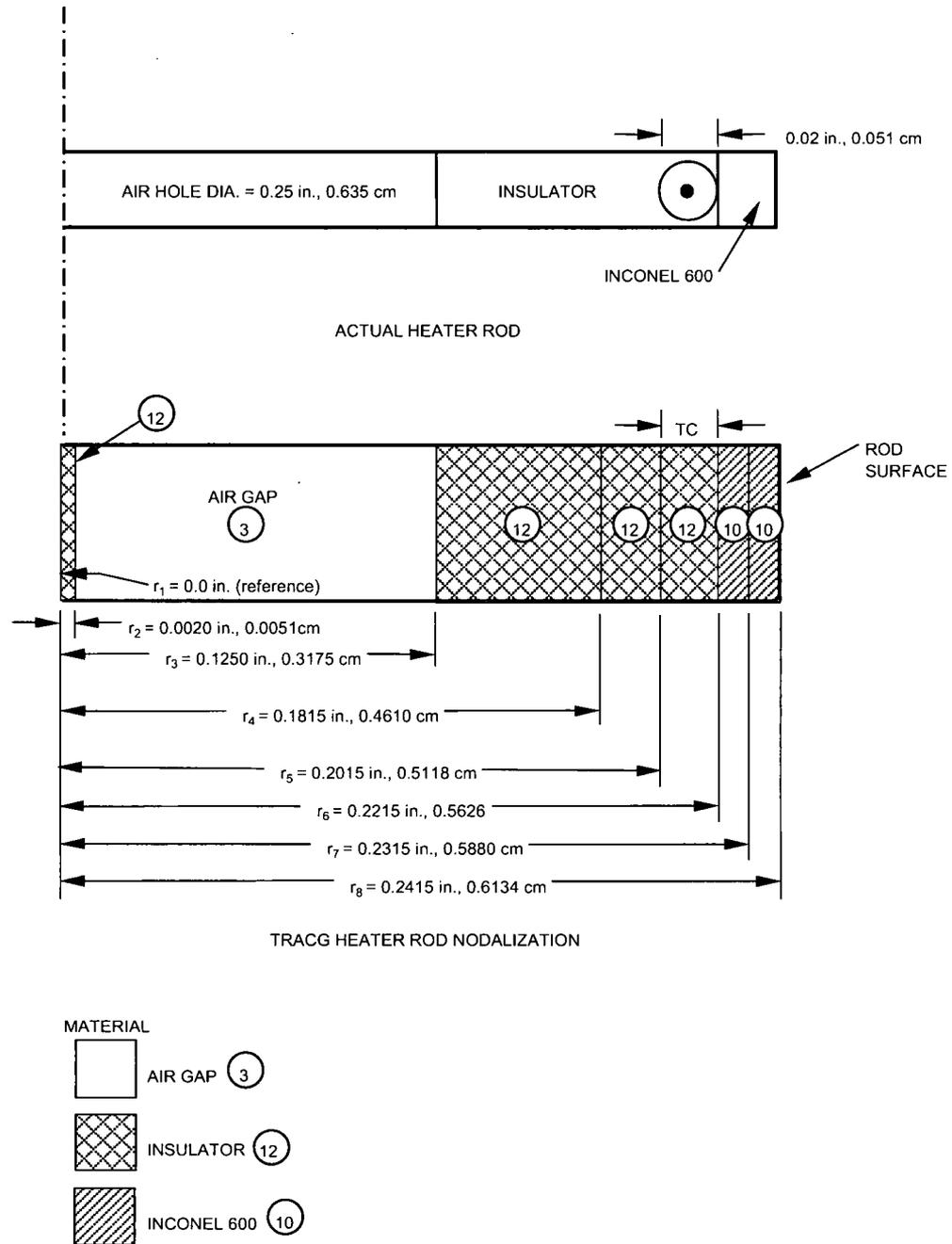
Figure 5.1-17. TLTA Heater Rod Model

[[

]]

Figure 5.1-18. Comparison of Steam Dome Pressures for Test 6425/Run 2

[[

]]

Figure 5.1-19. Comparison of Suction Line Break Flows for Test 6425/Run 2

[[

]]

Figure 5.1-20. Comparison of Drive Line Break Flows for Test 6425/Run 2

[[

]]

Figure 5.1-21. Comparison of Broken Loop Jet Pump Flows for Test 6425/Run 2

INTEGRAL SYSTEM EFFECTS TESTS

[[

]]

Figure 5.1-22. Comparison of Intact Loop Jet Pump Flows for Test 6425/Run 2

[[

]]

Figure 5.1-23. Comparison of Core Inlet Flows for Test 6425/Run 2

[[

]]

Figure 5.1-24. Comparison of Upper Plenum Pressure Drops for Test 6425/Run 2

[[

]]

Figure 5.1-25. Comparison of Bundle Pressure Drops for Test 6425/Run 2

[[

]]

Figure 5.1-26. Comparison of Rod Temperatures at 3.048 m Elevation for Test 6425/Run 2

[[

]]

Figure 5.1-27. Comparison of Rod Temperatures at 2 m Elevation for Test 6425/Run 2

[[

]]

Figure 5.1-28. Comparison of Rod Temperatures at 0.89 m Elevation for Test
6425/Run 2

5.1.3   TLTA Large Break LOCA with No-ECC, Test 6426/Run 1

TLTA Test 6426/Run 1 provides integral system response data for a large break LOCA with no active ECC systems. The initial and boundary conditions (other than the ECC flows) are identical to the TLTA large break LOCA Test 6425/Run 2 discussed in Section 5.1.2. Taken together, the TLTA ECC and No–ECC tests provide benchmark data for evaluating the effects of the ECC system on the BWR thermal-hydraulic response to a large break LOCA. The objective of the TRACG analysis of this test is to evaluate the ability of the code to predict the observed sequence of events and controlling phenomena. This evaluation is made by comparing the calculated and measured system responses for system pressure, regional pressure drops (inventories), flows and the thermal response of the heated rod bundle.

5.1.3.1   *Facility and Test Description*

The configuration of the TLTA facility and the initial and boundary conditions used in this experiment were similar to those of TLTA Test 6425/Run 2 (Section 5.1.2.1) with the principal difference that the ECC systems were not active. The initial conditions for Test 6426/Run 1 are shown in Table 5.1-5. During the first 25 seconds of the test, the broken loop recirculation line isolation valve failed to close. This produced a small bypass of the drive line break flow through the isolation valve [5-3]. Comparisons of the early system response between the TLTA ECC and No-ECC tests do not indicate any noticeable impact from the valve failure. Following blowdown, the system inventory depletes continuously. The downcomer, upper plenum, bypass, and rod bundle drain in succession and the rods heat up at a nearly linear rate.

5.1.3.2   *System Input Definition and TRACG Nodalization for TLTA Test 6426/Run 1*

The TRACG input model used for the simulation of Test 6426/Run1 is the same as for TLTA Test 6425/Run 2 (Section 5.1.2.2) with the difference that the ECC systems are not activated. The isolation valve failure is also not modeled because, as stated above, there was no noticeable impact of the valve failure in the test and the fractional flow area of the failed valve could not be ascertained from the test measurements. As will be seen, the total break flow prediction is quite close to the measured break flow during the valve failure period.

5.1.3.3   *Results and Discussion*

[[

INTEGRAL SYSTEM EFFECTS TESTS

]]

INTEGRAL SYSTEM EFFECTS TESTS

5.1.3.4 Conclusions

[[

•

:]]

Table 5.1-5
Initial Conditions for TLTA Test 6426/Run 1

Quantity	Initial Value [a]
Bundle Power [b]	5.05 ± 0.03 MW
Steam Dome Pressure	7198 ± 30 kPa
Lower Plenum Pressure	7363 ± 30 kPa
Lower Plenum Enthalpy	1223 ± 10 kJ/kg
Initial Water Level [c]	1.85 ± 0.2 m
Feedwater Enthalpy	154 ± 5 kJ/kg
Bundle Inlet to Outlet ΔP	103 ± 10 kPa
Steam Flow	2.7 ± 0.5 kg/s
Feedwater Flow	0.6 ± 0.1 kg/s
Drive Pump 1 Flow	3.7 ± 0.5 kg/s
Drive Pump 2 Flow	3.8 ± 0.5 kg/s
Jet Pump 1 Flow	7.3± 0.9 kg/s
Jet Pump 2 Flow	9.1 ± 0.9 kg/s
Bundle Inlet Flow	15 ± 2 kg/s

[a]) Uncertainties are judged from the maximum of data fluctuations and/or absolute uncertainty of measurement.
[b] 5.05 MW is central core region average power; overall core average power is 4.60 MW.
[c] Relative to jet-pump support plate.

[[

]]
Figure 5.1-29. Comparison of System Pressures for Test 6426/Run 1
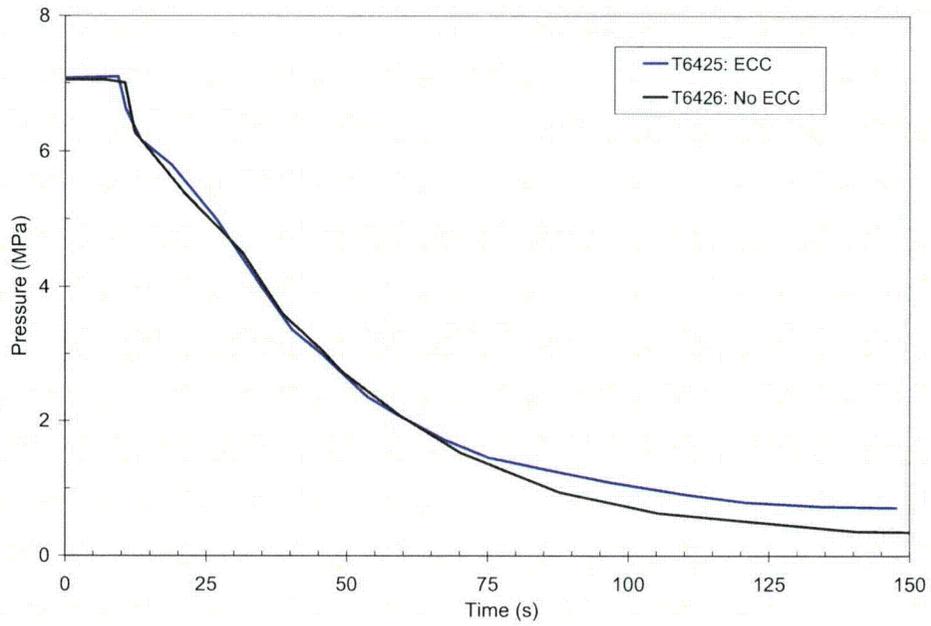
Figure 5.1-30. Comparison of Measured System Pressure Data (ECC and No-ECC)

[[

]]
Figure 5.1-31. Comparison of Calculated System Pressures (ECC and No ECC)

[[

]]
Figure 5.1-32. Comparison of Total Break Flow Rates for Test 6426/Run 1

[[

]]
Figure 5.1-33. Comparison of Upper Plenum Pressure Drops for Test 6426/Run 1

[[

]]
Figure 5.1-34. Comparison of Bypass Pressure Drops for Test 6426/Run 1

[[

]]
Figure 5.1-35. Comparison of Bundle Pressure Drops for Test 6426/Run 1

[[

]]
Figure 5.1-36. Comparison of Rod Temperatures 2.0 m Elevation for Test 6426/Run 1

[[

]]

Figure 5.1-37. Comparison of Rod Temperatures at 2.72 m Elevation for Test 6426/Run 1

5.1.4   TLTA Large Break, Peak Power LOCA Test 6423/Run 3

Test 6423/Run 3 was a large-break LOCA experiment from peak power. In addition to the high power, the total ECC flow rate was ~70% of the ECC flow rate in TLTA Test 6425/Run 2 (Section 5.1.1) and the ECC fluid temperature was about 55 K higher. Test 6423/Run 3 provided system response data that can be used to assess TRACG capability for prediction of BWR system response and, in particular, the rod bundle thermal-hydraulic response under high power and degraded core cooling conditions.

5.1.4.1   Facility and Test Description

The TLTA test facility [5-1] has been described in Sections 5.1.1.1 and 5.1.2.1. The initial (Table 5.1-6) and boundary conditions for Test 6423/Run 3 were similar to the TLTA average-power ECC Test 6425/Run 2 (Section 5.1.2) except for bundle power and ECC flow rate and temperature. The bundle power was 6.46 MW in contrast to 5.05 MW for the large break tests discussed in Sections 5.1.2 and 5.1.3. The HPCS and LPCS flow rates were about one-third of the nominal ECC case and the LPCI flow rate was about the same (Figure 5.1-38). As a result, the total ECC flow rate was about 70% of that for the nominal ECC TLTA test. The ECC fluid temperature was 366 ± 8 K or about 46 K higher than the nominal ECC case. The combined effect of reduction in ECC flow rate and increase in ECC fluid temperature was to significantly reduce the steam condensation capacity of the ECC injection.

The experimental data for TLTA Test 6423/Run 3 are reported in Reference [5-3]. Most of the system blowdown characteristics are similar to TLTA Test 6425 (Section 5.1.2). Because of the greatly reduced HPCS and LPCS flows, however, the conditions in the upper plenum and

bundle differed significantly from the earlier test. The upper plenum retains very little inventory in the long term and the rod temperatures are higher than for the tests with nominal ECC. From the initiation of bulk dryout until the end of the test, the bundle mid-plane (axial peak-power location) thermocouples do not indicate complete rewet of all the rods. Some rods quench sporadically while others are simultaneously heating up, reflecting wide variability in the planar fluid conditions in the highly voided bundle mid-plane region. The measured long-term void fractions in the midplane region (determined from ΔP measurements) are on the order of 95 to 99 percent. Higher and lower elevations show complete rewet and comparatively low void fractions. Even with the reduced cooling capacity of the ECC, the rod heatup rates are nearly a factor of two lower than for the test without ECC actuation (Section 5.1.3).

5.1.4.2 System Input Model Definition and TRACG Nodalization for Test 6423/Run 3

The TRACG input model used for simulation of TLTA Test 6423/Run 3 is the same as for Test 6425/Run 2 (Section 5.1.2). The measured power and ECC flows and temperatures are used as initial and boundary conditions for the calculation.

5.1.4.3 Results and Discussion

[[

]]

5.1.4.4 Conclusions

The comparison of test measurements and TRACG calculations for the TLTA integral system test with high bundle power and low ECC flow (Test 6423/Run 3), discussed in Section 5.1.4.3, supports the following conclusions:

[[

]]

Table 5.1-6
Initial Conditions for TLTA Test 6423/Run 3

Quantity	Initial Value [a]
Bundle Power	6.46 ± 0.03 MW
Steam Dome Pressure	7150 ± 30 kPa
Lower Plenum Pressure	7343 ± 30 kPa
Lower Plenum Enthalpy	1205 ± 10 kJ/kg
Initial Water Level [b]	1.85 ± 0.2 m
Feedwater Enthalpy	95 ± 5 kJ/kg
Bundle Inlet to Outlet ΔP	110 ± 10 kPa
Steam Flow	3.2 ± 0.5 kg/s
Feedwater Flow	0.5 ± 0.1 kg/s
Drive Pump 1 Flow	3.7 ± 0.5 kg/s
Drive Pump 2 Flow	3.8 ± 0.5 kg/s
Jet Pump 1 Flow	7.7 ± 0.9 kg/s
Jet Pump 2 Flow	8.6 ± 0.9 kg/s
Bundle Inlet Flow	15 ± 2 kg/s

[a] Uncertainties are judged from the maximum of data fluctuations and/or absolute uncertainty of measurement.
[b] Relative to jet-pump support plate.
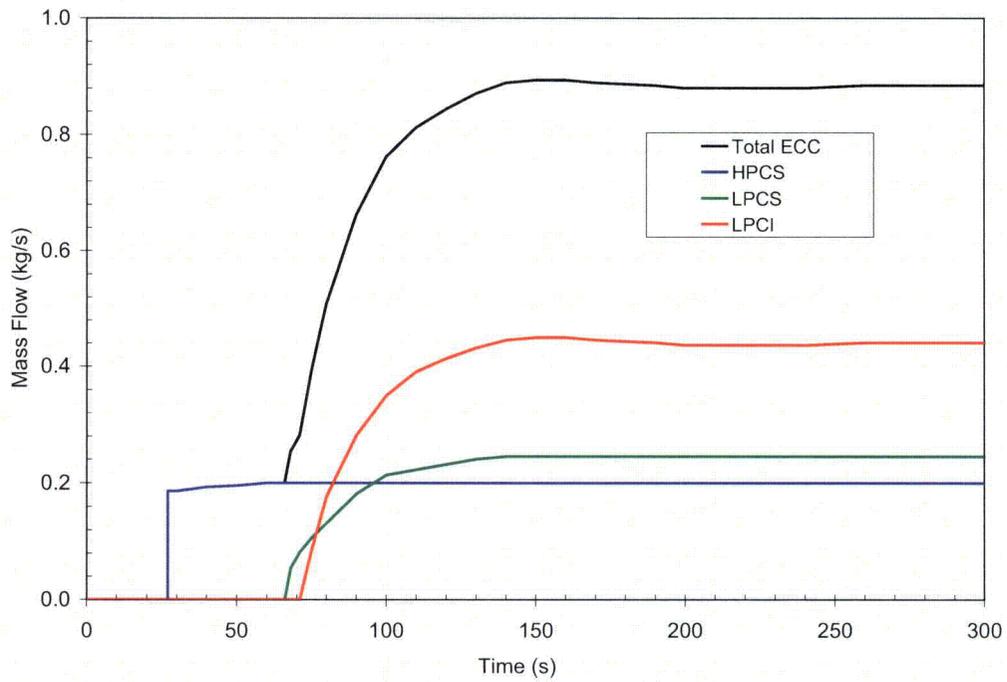
Figure 5.1-38. Measured ECC Mass Flow Rates for Test 6423/Run 3
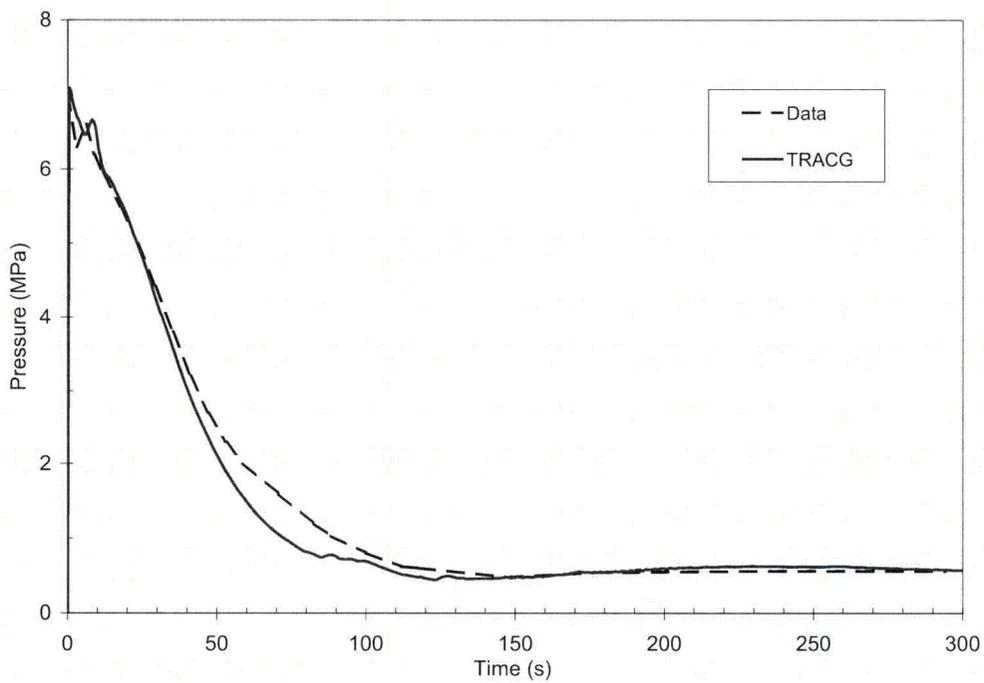
Figure 5.1-39. Comparison of System Pressures for Test 6423/Run 3
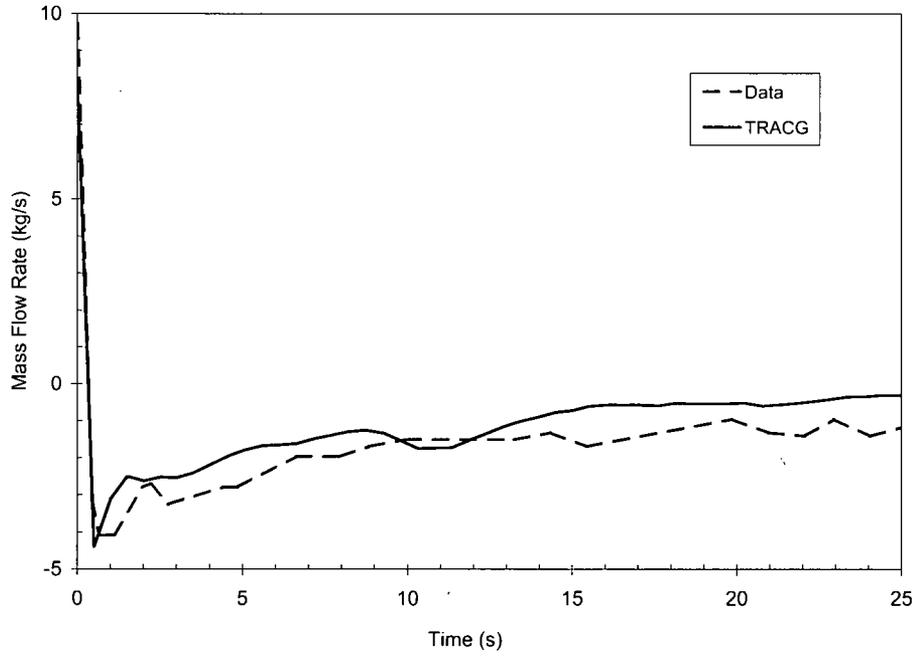
Figure 5.1-40. Comparison of Broken Loop Jet Pump Flows for Test 6423/Run 3

[[

]]

Figure 5.1-41. Comparison of Intact Loop Jet Pump Flows for Test 6423/Run 3

[[

]]

Figure 5.1-42. Comparison of Core Inlet Flows for Test 6423/Run 3

[[

]]

Figure 5.1-43. Comparison of Upper Plenum Pressure Drops for Test 6423/Run 3

[[

]]

Figure 5.1-44. Comparison of Bypass Pressure Drops for Test 6423/Run 3

[[

]]

Figure 5.1-45. Comparison of Bundle Pressure Drops for Test 6423/Run 3

[[

]]

Figure 5.1-46. Comparisons of Rod Temperatures at 3.048 m Elevation for Test 6423/Run 3 Showing Early Film Boiling,

[[

]]

Figure 5.1-47. Comparison of Rod Temperatures at 2.0 m Elevation for Test 6423/Run 3

[[

]]

**Figure 5.1-48. Comparison of Rod Temperatures at 0.89 m Elevation
for Test 6423/Run 3**

5.2 FIST

This section describes TRACG qualification studies performed on the basis of three FIST tests simulating large and small-break recirculation line LOCAs and an LPCI line LOCA.

5.2.1 The FIST Facility

The FIST facility (Figure 5.2-1) was an integral single-bundle system scaled from a BWR/6-218 Standard Plant [5-4]. It was capable of simulating full power steady-state operation and real-time LOCA and operational transients. Key features included a full-size, full-power electrically heated bundle with prototypical geometry, accurately scaled reactor regional volumes with full-scale heights and functional flow components such as jet pumps and a steam separator. The auxiliary systems included a heated feedwater system, two recirculation loops, a steamline system that provided system pressure control capability, automatic depressurization system (ADS), safety/relief valves (SRV) and automatic control system trip signals. A blowdown system simulated breaks in the various regions such as a recirculation line or ECC system line. The ECC systems consisted of the low pressure core spray (LPCS), the high pressure core spray (HPCS) and the low pressure coolant injection (LPCI) pumps. FIST tests were performed to simulate power transients, determine natural circulation flow characteristics and to simulate large and small recirculation line, steamline and LPCI line break LOCAs. Measurement uncertainties for the FIST LOCA tests described in this section are summarized in Table 5.2-1. Test results and data evaluations have been previously reported in References [5-5] through [5-7].

Table 5.2-1
Measurement Uncertainties for FIST LOCA Tests

Measured Quantities	
System Pressure	± 42 kPa
Fluid Temperature	± 2.3 K
Rod Temperature	± 0.8 % of reading (<±3 K)
Bundle ΔP	± 0.21 kPa
Bypass ΔP	± 0.21 kPa
Downcomer ΔP	± 0.21 kPa
Bundle Power	± 3 kW
Derived Quantities	
Bundle Inlet Flow	± 1.1 kg/s
Jet Pump Flow	± 0.5 kg/s
Break Flow	10 % of calculated value
ECC Flows	± 0.05 to 0.1 kg/s (depending on ECC system)
Fluid Density	± 32 kg/m^3
Void Fraction	± 0.05
Mixture Level	± 25 mm of water

5.2.2 Large Break Test 6DBA1B

5.2.2.1 Test Description

The large break LOCA test (6DBA1B) simulated a 0.207 m² guillotine break in one recirculation line followed by failure of two of the three LPCI pumps. Details of the test and data analysis are available in Reference [5-5]. The initial and boundary conditions for Test 6DBA1B are shown in Table 5.2-2. The facility was initially operating at steady-state, full-power conditions. The transient was initiated by opening the break and tripping power to the recirculation pumps (to simulate the simultaneous loss of off-site power). The recirculation pumps coasted down, feedwater flow was shut off and bundle power was controlled to simulate power decay following a scram. System pressure was maintained by the pressure control system until the falling water level in the downcomer reached the break location, allowing steam to escape through the break and depressurize the system. The high pressure ECC system (HPCS) was initiated at 27 s and began to refill the vessel. The HPCS refill was augmented by the low pressure ECC systems (LPCS, LPCI) after the system pressure fell below the shutoff head of these pumps.

System response following the break initiation was characterized by a sudden reversal of the broken loop jet pump flow and a corresponding decrease in core inlet flow. System pressure was maintained by the pressure control system for about eight seconds as the power decreased and the core flow decreased to a natural circulation rate. After the break uncovered, the rapid system depressurization caused flashing in the lower plenum and guide tube/bypass. This resulted in redistribution of the regional inventories. Following the flashing surge, CCFL was established at the bundle inlet and outlet and at the tops of the guide tube and the bypass.

The bundle inventory decreased from the combined effect of boiling, flashing and CCFL controlled liquid downflow through the side entry orifice (SEO). The lower plenum level dropped to the jet pump exit plane at about 40 seconds and lower plenum steam was vented through the jet pumps. That increased the CCFL controlled liquid drainage through the SEO, causing a reduction in bundle inventory and allowing bulk bundle dryout to occur. The HPCS flow controlled the early heatup rate and led to top-down rewet of some of the rods prior to the activation of the low pressure ECC systems. The LPCS and LPCI systems provided additional cooling to the bundle starting at 64 and 75 s, respectively. The entire bundle was quenched by bottom reflood at about 125 s. The measured rod temperatures showed wide variability in top-down rewet. Most of the rods showed little or no heatup. One thermocouple at the mid-plane location indicated a peak rod temperature of 642 K, which is also the PCT for the bundle.

Table 5.2-2
FIST Large Break Test 6DBA1B Initial and Boundary Conditions

Initial Conditions	
Pressure	7.19 MPa
Power	5.05 MW
Core Inlet Subcooling	9.85 K
Core Inlet Flow	18.55 kg/s
Feedwater Flow	2.45 kg/s
Feedwater Temperature	486 K
Steam Flow	2.63 kg/s
Water Level	14.15 m
Boundary Conditions	
Power Trip	0 s
Break Initiation	0 s
Recirculation Line Break Area	331.4 mm^2
ADS Flow Area	186.7 mm^2
ADS Trip	L1 + 105 s
Pump Trip	0 s
Feedwater Line Trip	0 s
MSIV Trip	Level at L1
HPCS Trip	35 s (a)
LPCS Trip	35 s [a]
LPCI Trip	35 s [b]
HPCS Temperature	322 K
LPCS Temperature	322 K
LPCI Temperature	322 K
Broken Loop Isolation	0 s
Intact Loop Isolation	13 s

[a] Shutoff pressure was 1.97 MPa
[b] Shutoff pressure was 1.68 MPa

5.2.2.2 System Input Model Definition and TRACG Nodalization

The FIST vessel is modeled in TRACG (Figure 5.2-2) with the VSSL component using two rings. As in the case of the TLTA model (Section 5.1), two radial cells are required to separate the region inside the shroud from the downcomer. The VSSL component is divided into 19 axial levels to provide adequate geometric definition of the principal regions in the system (lower plenum, core, bypass, etc.) including correspondence with measurement locations and flow path details, e.g., VSSL cell to component junction locations. Component models represent the rod

bundle, the steam separator, jet pumps, the guide tube, and the recirculation loops and pumps. Additional components are used to model the connecting pipes for the ECCS systems and the feedwater line. Selection of 1-D components and their nodalization is based on locating cell boundaries at instrument locations and providing adequate representation of flow conditions expected in the transient.

The rod bundle is modeled with a CHAN component with 21 cells. Cell boundaries are chosen to coincide with the spacer and the tieplate locations and to align the cells with measurement tap locations. The spacer and tieplate flow areas are accurately modeled to account for potential CCFL at these locations and to model the effect of local flow acceleration on the bundle void distribution. The 8x8 array of heater rods is subdivided into seven rod groups according to power peaking. Rod Group 7 consists of a single rod with a high radial peaking factor that is processed by the TRACG Hot Rod Model. A chopped cosine axial power distribution is used for the heater rods. Eight radial nodes are used to model the heater rods with one of the nodes corresponding to the thermocouple location. TRACG options for the selection of material properties enable the heat capacity and thermal diffusivity to closely match the actual heater rods.

Vessel wall heat capacity, stored energy and heat transfer characteristics are modeled with double-sided heat slab components coupling the principal regions of the vessel to its environment. The double-sided heat slabs are augmented by lumped capacity heat slabs to model heavy section flanges. In the calculation, the heat loss to the environment was specified using an outside heat transfer coefficient determined from system characterization tests that measured regional steady-state heat losses. System characterization tests at full power steady-state conditions also permitted the as-built single-phase flow loss coefficients throughout the system to be quantified. The selection of the rings and levels in the TRACG VSSL component that models the FIST pressure vessel is guided by:

- Regional boundaries in the test facility pressure vessel.

- Connecting points of various 1-D components within the vessel.

- The need for adequate representation of the regional thermal-hydraulic conditions.

- The desirability of consistency with the test measurement locations.

- Engineering judgment based on prior TRACG modeling experience.

Particular attention was given to the jet pump exit region, the vessel stored heat and the break location geometry. As observed in the test, the two-phase level in the lower plenum dropped to the jet pump exit plane. Detailed flow path modeling is necessary to capture the jet pump exit uncovery and the subsequent split in steam flow between the jet pump and core regions. The level tracking option, which allows determination of the two-phase level location within a VSSL cell, is particularly needed for the jet pump exit region and the break location in the lower downcomer. The vessel wall and flanges release energy to the fluid following a depressurization and thereby attenuate the system pressure decrease. Detailed heat slab modeling is needed to capture this effect.

5.2.2.3   Results and Discussion

[[

]]

5.2.2.4 Conclusions

[[

]]

SRV/ADS

MSIV

FEEDWATER
RCIC, HPCI

HPCS

LEVEL 1 —

Q(t)

FULL INTEGRAL SYSTEM TEST FACILITY

• FULL HEIGHT
• REGIONAL VOLUMES PROPORTIONAL
  TO CORE SIZE
• BWR COMPONENTS:
  - JET PUMP
  - STEAM SEPARATOR/DRYER
  - CHANNELED FUEL BUNDLE
• REACTOR CONTROL SYSTEM:
  - FEEDWATER/LEVEL
  - STEAM FLOW/PRESSURE
  - RECIRCULATION FLOW
  - POWER
  - SAFETY SYSTEM ACTIVATION
• ECC SYSTEMS:
  - HIGH PRESSURE CORE SPRAY
  - LOW PRESSURE CORE SPRAY
  - LOW PRESSURE COOLANT INJECTION

Figure 5.2-1. Schematic of the FIST Facility
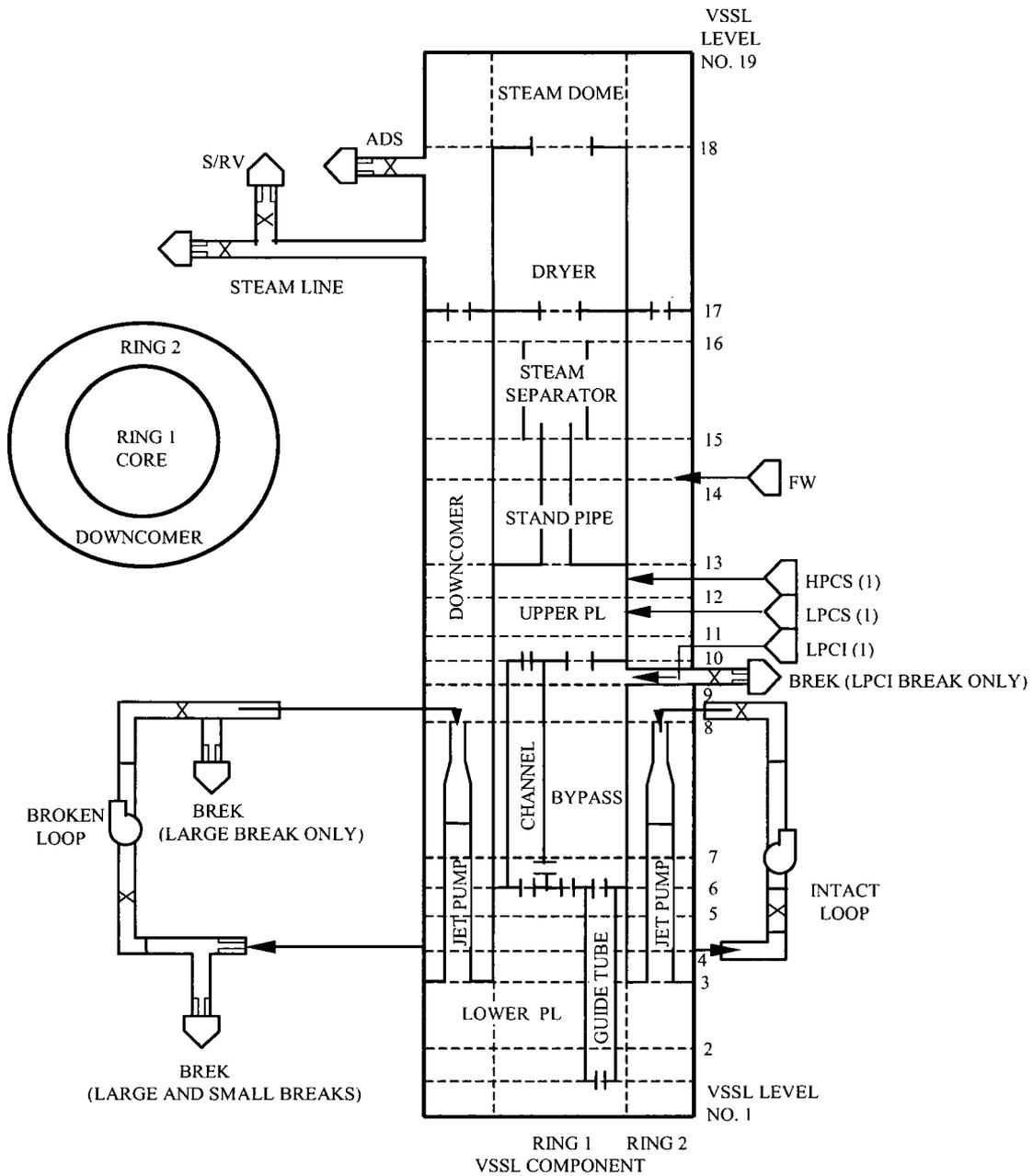
Figure 5.2-2. TRACG Input Model for the FIST Facility

[[

]]

Figure 5.2-3. Comparison of System Pressures for FIST Test 6DBA1B

[[

]]

Figure 5.2-4. Comparison of Broken Loop Jet Pump Flows for FIST Test 6DBA1B

INTEGRAL SYSTEM EFFECTS TESTS

[[

]]

Figure 5.2-5. Comparison of Intact Loop Jet Pump Flows for FIST Test 6DBA1B

[[

]]

Figure 5.2-6. Comparison of Bundle Pressure Drops for FIST Test 6DBA1B

[[

]]

Figure 5.2-7. Comparison of Bypass Pressure Drops for FIST Test 6DBA1B

[[

]]

Figure 5.2-8. Comparison of Downcomer Pressure Drops for FIST Test 6DBA1B

[[

]]

**Figure 5.2-9. Comparison of Rod Temperatures (Elevation 2.97 m)
for FIST Test 6DBA1B**

[[

]]

**Figure 5.2-10. Comparison of Rod Temperatures (Elevation 1.96 m)
for FIST Test 6DBA1B**

[[

]]

**Figure 5.2-11. Comparison of Rod Temperatures (Elevation 1.22 m)
for FIST Test 6DBA1B**

5.2.3 Small Break Test 6SB2C

5.2.3.1 Test Description

The small break LOCA Test 6SB2C simulated a 0.0046 m^2 break in the suction side of one of the recirculation pumps with the HPCS assumed to be unavailable. Details of the test and data analysis are available in Reference [5-5]. The initial and boundary conditions for the test are shown in Table 5.2-3. The LOCA transient was initiated from full power steady-state conditions. The recirculation pumps were tripped and feedwater flow was shut off. The bundle power was controlled to simulate the power decay transient following a scram. System pressure was maintained by the pressure control system until the falling downcomer water level reached the Level 1 setpoint, closing the main steam isolation valve (MSIV). The water level continued to fall until the Automatic Depressurization System (ADS) activated at 120 s after the Level 1 trip. This opened the safety/relief valve (SRV) and depressurized the system. The low pressure ECC injection began to refill the vessel when the system pressure decreased below the pump shutoff head. Rod heatup occurred due to bundle uncovery. The measured peak clad temperature (PCT) reached 769 K before the last of the rods was rewet by the ECC inflow.

5.2.3.2 System Definition TRACG Input Model

The TRACG input model utilized for the small break Test 6SB2C is similar to that used for the large break Test 6DBA1B (Section 5.2.2.2). The configuration of the broken recirculation loop is changed by closing off the BREK component in the discharge branch. The ECCS configuration was changed by making the HPCS unavailable.

5.2.3.3 Results and Discussion

[[

]]

5.2.3.4   Conclusions

[[

]]

Table 5.2-3
FIST Small Break Test 6SB2C Initial and Boundary Conditions

Initial Conditions	
Pressure	7.23 MPa
Power	5.05 MW
Core Inlet Subcooling	10.0 K
Core Inlet Flow	19.1 kg/s
Feedwater Flow	2.3 kg/s
Feedwater Temperature	478 K
Steam Flow	2.6 kg/s
Water Level	14.0 m
Boundary Conditions	
Power Trip	0 s
Break Initiation	0 s
Recirculation Line Break Area	7.44 mm^2
ADS Flow Area	186.7 mm^2
ADS Trip	L1 + 120 s
Pump Trip	0 s
Feedwater Line Trip	0 s
MSIV Trip	Level at L1
LPCS Trip[a]	35 s
LPCI Trip[b]	35 s
LPCS Temperature	322 K
LPCI Temperature	322 K
Broken Loop Isolation	20 s
Intact Loop Isolation	20 s

[a] Shutoff pressure was 1.97 MPa
[b] Shutoff pressure was 1.68 MPa

[[

]]

Figure 5.2-12. Comparison of System Pressures for FIST Test 6SB2C

[[

]]

Figure 5.2-13. Comparison of Steam Line Flows for FIST Test 6SB2C

[[

]]

Figure 5.2-14. Comparison of Integrated Break Flows for FIST Test 6SB2C

[[

]]

Figure 5.2-15. Comparison of ADS Flows for FIST Test 6SB2C

[[

]]

Figure 5.2-16. Comparison of Downcomer Pressure Drops for FIST Test 6SB2C

[[

]]

Figure 5.2-17. Comparison of Bypass Pressure Drops for FIST Test 6SB2C

[[

]]

Figure 5.2-18. Comparison of Bundle Pressure Drops for FIST Test 6SB2C

[[

]]

**Figure 5.2-19. Comparison of Rod Temperatures
(Elevation 2.97 m) for FIST Test 6SB2C**

[[

]]

**Figure 5.2-20. Comparison of Rod Temperatures
(Elevation 1.96 m) for FIST Test 6SB2C**

[[

]]

**Figure 5.2-21. Comparison of Rod Temperatures
(Elevation 1.22 m) for FIST Test 6SB2C**

INTEGRAL SYSTEM EFFECTS TESTS   5-71

5.2.4 LPCI Break Test 6LB1A

5.2.4.1 Test Description

FIST LOCA Test 6LB1A simulated a full-size 0.032 m^2 break in one of the LPCI lines in a BWR/6 plant. The HPCS was assumed to be unavailable. Details of the test and data analysis are available in Reference 5-6. The initial and boundary conditions for Test 6LB1A are shown in Table 5.2-4. The transient was initiated from full power steady-state condition and included a trip of the recirculation pumps and shutoff of the feedwater flow. The bundle power was controlled to simulate the power decay transient following a scram. System pressure was maintained by the pressure control system until the falling downcomer water level reached the Level 1 setpoint, closing the main steam isolation valve (MSIV). The water level continued to fall until the Automatic Depressurization System (ADS) was activated (at 120 s following the Level 1 trip) and opened the safety/relief valve (SRV) to depressurize the system. The low pressure ECC injection began to refill the vessel when the system pressure decreases below the pump shutoff head. Rod heatup occurred due to bundle uncovery and the measured peak clad temperature (PCT) reached 606 K before the last of the rods rewet.

5.2.4.2 System Definition TRACG Input Model

The input model used for the TRACG simulation of the FIST LPCI break test (Test 6LB1A) is similar to that described above for the large and small recirculation break tests (Figure 5.2-2). The difference is that the BREK components in the recirculation line were closed and a BREK component with a connection to Level 10 of the VSSL component was added to simulate the broken LPCI line.

5.2.4.3 Results and Discussion

[[

]]

5.2.4.4 Conclusions

[[

]]

5.2.5 Overall Conclusions for the FIST Comparisons

[[

]]

Table 5.2-4
FIST LPCI Break Test 6LB1A Initial and Boundary Conditions

Initial Conditions	
Pressure	7.18 MPa
Power	4.65 MW
Core Inlet Subcooling	8.9 K
Core Inlet Flow	18.0 kg/s
Feedwater Flow	2.3 kg/s
Feedwater Temperature	478 K
Steam Flow	2.5 kg/s
Water Level	14.1 m
Boundary Conditions	
Power Trip	0.3 s
Break Initiation	0 s
LPCI Line Break Area	50.6 mm^2
ADS Flow Area	185.8 mm^2
ADS Trip	L1 + 105 s
Pump Trip	0 s
Feedwater Line Trip	0 s
MSIV Trip	Level at L1 + 2 s
LPCS Trip	35 s [a]
LPCI Trip	35 s [b]
LPCS Temperature	322 K
LPCI Temperature	321 K
Broken Loop Isolation	20 s
Intact Loop Isolation	20 s

[a] Shutoff pressure was 1.97 MPa
[b] Shutoff pressure was 1.68 MPa

INTEGRAL SYSTEM EFFECTS TESTS

[[

]]

Figure 5.2-22. Comparison of System Pressures for FIST Test 6LB1A

[[

]]

Figure 5.2-23. Comparison of Jet Pump Flows for FIST Test 6LB1A

[[

]]

Figure 5.2-24. Comparison of Total Break Flows for FIST Test 6LB1A

[[

]]

Figure 5.2-25. Comparison of ADS Flows for FIST Test 6LB1A

[[

]]

Figure 5.2-26. Comparison of Downcomer Pressure Drops for FIST Test 6LB1A

[[

]]

Figure 5.2-27. Comparison of Bypass Pressure Drops for FIST Test 6LB1A

INTEGRAL SYSTEM EFFECTS TESTS

[[

]]

Figure 5.2-28. Comparison of Bundle Pressure Drops for FIST Test 6LB1A

[[

]]

**Figure 5.2-29. Comparison of Rod Temperatures
(Elevation 2.97 m) for FIST Test 6LB1A**

INTEGRAL SYSTEM EFFECTS TESTS

[[

]]

**Figure 5.2-30. Comparison of Rod Temperatures
(Elevation 1.96 m) for FIST Test 6LB1A**

[[

]]

**Figure 5.2-31. Comparison of Rod Temperatures
(Elevation 1.22 m) for FIST Test 6LB1A**

5.3 SSTF

The 58-bundle Steam Sector Test Facility (SSTF) [5-8] provided useful data on the thermal–hydraulic processes encountered during the refill-reflood phase of a multi-bundle system following a blowdown. SSTF Test SRT-3 (Run 26) and Test EA3-1 (Run 111) simulated the refill-reflood transient of a BWR following a large break LOCA. In Test SRT-3, the SSTF Emergency Core Cooling System (ECCS) was configured to simulate the refill-reflood transient for a BWR/6. The ECCS configuration for a BWR/4 was simulated in Test EA3-1. The experimental data indicate beneficial influences of multiple bundle interactions (parallel channel phenomena) in the prompt refill of the bypass, guide tubes and lower plenum and in the reflood of the core. Detailed discussion of the major aspects of the refill-reflood scenarios observed in the SSTF experiments were reported in References 5-9 through 5-11. These references include interpretation of the observed parallel channel flow regime transitions, the ECC mixing process, and the effect of boundary conditions (e.g., break size and ECC subcooling) on the refill-reflood response.

- The objectives of the SSTF TRACG qualification study are:

- To assess the capability of the code for predicting the integral system response (sequence of events and significant thermal-hydraulic phenomena) of a multi–bundle facility.

- To assess the code capability for realistic simulation of the parallel channel phenomena.

- To verify the compatibility among various analytical models in the code participating in the prediction of the complex multi–dimensional interactions.

5.3.1 Description of the Facility and the Test

The SSTF facility was described in Section 4.3. It is a 30° sector (58 full and partial bundles) representation of a BWR. The facility had provisions for steam injection in the lower plenum, bypass and guide tubes to simulate steam generation from vessel stored heat during a blowdown and to simulate flashing when running constant pressure separate effects tests. Steam could also be injected into each of the bundles to simulate steam generation from decay heat in a prototypical fuel bundle. The bundles had prototype BWR production hardware for the upper tie plate and the side entry orifice (SEO) regions. For the BWR/6 tests, ECC systems included the spargers and nozzles for the HPCS and LPCS to the upper plenum and for the LPCI into the bypass. ECC systems for the BWR/4 tests included a third sparger and set of nozzles (at an elevation in the upper plenum typical of a BWR/4) for the LPCS and LPCI that are directed into the jet pumps. The facility included arrangements for simulating recirculation line breaks and was designed for depressurization from 1.03 MPa, which corresponds to the onset of the refill-reflood phase of a typical BWR LOCA. The facility was instrumented in detail with pressure and differential pressure transducers, conductivity elements and thermocouples for measurement of fluid and wall temperatures. The locations of six bundles with detailed instrumentation are shown in Figure 5.3-1. Thermocouples were also placed in each of the 58 bundles, just below the upper tie plate. Instrumentation in the bundles for measuring pressure drop and mixture level is shown in Figure 5.3-2. Uncertainties for the SSTF measurements used for comparison with corresponding TRACG calculations are given in Table 5.3-1.

Table 5.3-1
Measurement Uncertainties for the SSTF Transient Tests

Measured Quantity	Measurement Uncertainty
System Pressure	± 66 kPa
Side Entry Orifice ΔP	± 0.21 kPa
Subcooling	± 0.5 K
Collapsed Level	± 25 mm of water

The initial conditions and steam injection rates for both of the tests considered here are shown in Figure 5.3-3. The initial conditions reflect the system conditions expected at the beginning of the refill-reflood phase following a large break LOCA for a reference BWR. The figure shows a different initial lower plenum mass for the two tests. The initial mass for the BWR/6 test was 50% full while the lower plenum was 40% full for the BWR/4 test. The initial steam injection rates in the lower plenum and the guide tube/bypass regions represent the combined effects of flashing and the vapor generation due to stored heat. With the onset of depressurization the steam injection rates are reduced and represent the vapor generation due to stored heat release only for the remainder of the transient.

The system depressurization is initiated by opening the break. The ECC systems (one HPCS, one LPCS, and one LPCI for the BWR/6 and one LPCS and two LPCIs for the BWR/4) are turned on simultaneously. As discussed in detail in References 5-9 and 5-11, the refill-reflood transient progresses as follows:

- Vapor generated in the lower plenum produces CCFL (see Section 3.3 for a discussion of TRACG qualification for CCFL) at the side entry orifice and at the upper tie plate in the bundles and, consequently, the core spray flows injected into the upper plenum initially drain into the bundles under CCFL conditions. In other words, during the early transient, flow to all the bundles is limited by counter-current flow. As the upper plenum peripheral region becomes subcooled, CCFL breakdown occurs at the upper tie plate of the peripheral bundles. This allows rapid refilling of these bundles. The peripheral bundles undergo transitions to a liquid downflow mode at about 10 seconds and contribute to draining of the upper plenum for the remainder of the transient.

- The injection of the LPCI into the peripheral regions of the bypass for the BWR/6 tests produces a rapid increase of the bypass inventory. The flow resistances in the radial direction contribute to a difference in the static head of the liquid between the peripheral and central regions of the bypass. The inventory in the counter-current flow limited bundles steadily increases due to a combination of in-leakage from the bypass through the lower tie plate holes and CCFL-controlled down flow at the upper tie plate. For the counter-current flow limited bundles, the leakage flow in the apex (central) region is lower than in the mid-radius regions due to the gradient of the static head in the bypass. Consequently, the mid-radius bundles (comprising the majority of the bundles in the simulated core) fill at a somewhat faster rate. The pressure drop for each bundle is the same (controlled by the overall core pressure drop). With increasing core pressure drop, at about 10 seconds into the transient, some of the apex bundles transition into a stable co-current upflow mode. Figure 5.3-4 shows a schematic of the multiple channel conditions prevailing at that time.

- The co-current upflow transition is marked by increased steam flow through the side entry orifice of the apex bundles, producing a larger pressure drop at the SEO due to frictional effects. A necessary condition for transition into co-current upflow is that the lower plenum level remains below the side entry orifices. Conductivity elements in the lower plenum indicate that this is the case in the test during the transition.

- The multi-dimensional phenomena leading to the flow regime transitions produce rapid refilling of the various regions. First, the increased steam flow through the SEO of the co-current upflow bundles reduces the pressure in these bundles near the leakage holes. Consequently, the post-transition leakage flows into the co-current upflow bundles are higher, producing a bundle flow of a dispersed two-phase mixture. Second, the diversion of some of the steam away from the counter-current flow limited bundles allows increased upper tie plate liquid downflow for these bundles, aiding their reflood. Third, the co-current up flow channels efficiently vent the lower plenum steam, increasing the jet pump head and allowing it to support a higher coolant level in the core.

- The lower plenum is refilled within about 80 seconds of the initiation of the test. The rising mixture level in the lower plenum covers the bundle side entry orifices and the co-current flow bundles switch back to the counter-current flow mode. Thus, within about 100 seconds of the initiation of the ECC system, the core is reflooded with a voided coolant mixture in the mid-radius and apex regions. The void fraction steadily decreases, increasing the liquid content of the bundles. The peripheral bundles fill very early in the transient and remain filled throughout.

- The major difference in the system response between the BWR/4 and BWR/6 tests is due to the effect of the BWR/4 LPCI flow into the jet pumps, which refills the lower plenum and covers the inlet orifices early in the reflood transient. Channel flooding from the bottom then becomes an important phenomenon. LPCI injection into the jet pumps condenses voids, insuring a single-phase head in the jet pumps and causing more liquid to be held in the core and upper plenum.

- The upper plenum shows a minor accumulation of ECC flow with a residual inventory corresponding to a collapsed level of 0.254 m. Conductivity element readings in the vicinity of the HPCS sparger indicate that the upper plenum two-phase level resides at the elevation of the HPCS nozzles. This behavior is expected. When the two-phase level is lower than the ECC injection elevation, there is sufficient steam available to rapidly saturate the injected ECC water. The overall liquid downflow in the bundles is then reduced to saturated CCFL flow. The upper plenum level and inventory increase until the two-phase mixture covers the nozzles. Then the ECC injection is in a submerged mode and the availability of steam is limited. Consequently, a greater fraction of the injected ECC water subcooling is retained and the liquid down-flow at the upper tie plate increases. This drops the two-phase level below the elevation of the nozzles and the cycle is repeated. In the BWR/4 tests, the LPCS sparger is positioned closer to the top of the channels than the HPCS and sufficient mass is held in the upper plenum to cover the spray header within several seconds of the start of the transient and to keep it covered.

5.3.2 TRACG Model and Nodalization

The nodalization for the TRACG model of the SSTF facility for the system response tests is shown in Figure 5.3-5. It is a relatively detailed input model that attempts to provide a realistic representation of the facility geometry. The facility region nodalization is similar to that used for the TRACG BWR LOCA model (Section 6). Particular attention has been paid to modeling flow-path loss characteristics for accurate pressure drop calculations. The nodalization is designed for direct one-to-one comparison of the calculated and measured values to demonstrate that key events and the complex multi–dimensional interactions observed in the test are captured by the code.

The SSTF vessel is modeled using the TRACG VSSL component with 14 axial levels, 4 radial rings and one azimuthal sector. Axial levels 1 through 5 represent the lower plenum. Levels 6 through 9 of Rings 1 through 3 represent the core bypass region. Levels 10 to 13 of Rings 1 to 3 model the upper plenum. Levels 6 through 13 of Ring 4 represent the annulus region. The steam dome is represented by level 14 of Ring 4. The rationale for the axial and radial nodalizations of the vessel with reference to the BWR is discussed in Section 4.3.

As in the TRACG BWR LOCA model, three radial rings represent the core region of the SSTF test facility. The rationale for the locations of the radial rings, the nodalization of the upper plenum and the nodalization of the bundles are described in Section 4.3 for the analysis of the SSTF Upper Plenum Mixing Test. Pairs of CHAN and TEE components are used to represent the fuel bundles. The TEE component, which is mounted on top of the CHAN component, provides a flow path for the steam injection that was used in the tests to simulate the effect of decay heat. To model the bundle-to-bundle variation in steam injection rate, a total of thirteen CHAN-TEE combinations are used in the TRACG model. Five CHAN and TEE components are used to model the bundles in the apex ring (Ring 1), seven CHAN and TEE components are used to represent the bundles in the large central ring (Ring 2) and one CHAN and TEE component pair is used to model the bundles in the peripheral ring (Ring 3). The number of bundles represented by each CHAN-TEE combination is shown in Figure 5.3-5. The core map in Figure 5.3-6 shows the locations of the bundles assigned to each of the CHAN-TEE components in the TRACG model. Note that, consistent with the BWR model that has a limiting bundle in the center ring, the highest power bundle (C51 in Figure 5.3-6) has been assigned to the center of the core (Ring 1) although its physical location is in Ring 2.

The 12 guide tubes in the facility are represented by two PIPE components, one each in Rings 1 and 2. The steam injection into the lower plenum and the guide tubes is accomplished using FILL components. The ECC systems are also modeled using FILL components. The blowdown line is modeled with a PIPE component. The two pipes representing the jet pumps, which connect the annulus to the lower plenum, are modeled with one PIPE component for the BWR/6 simulation. For the BWR/4 simulation, the PIPE is replaced by two TEE components, with the LPCI injection through the TEE side branch. For system initialization, a BREK component is connected to the vent pipe location in the steam dome. During the transient calculation, this vent pipe is isolated from the vessel.

For the prediction of the system response tests, the core spray option adopted for the BWR LOCA model is used. The spray is uniformly distributed between the central and peripheral rings (Rings 2 and 3), with no spray going into the apex ring (Ring 1). The ECC measured flow rates and temperatures are used directly as input to the calculation. The level-tracking model is used

for all vessel regions. Note that accurate calculation of the parallel channel interaction is dependent on correctly calculating the two-phase level in the various regions of the model.

5.3.3 Calculation Results for Test SRT-3

[[

]]

5.3.4 Calculation Results for Test EA3.1

[[

]]

5.3.5 Conclusions

TRACG calculations were made for two large break integral system tests performed in the multi-bundle SSTF facility and simulating two different ECCS arrangements. The calculations show good overall agreement with the data. The system depressurization is accurately calculated for both tests. In addition, TRACG successfully calculates the range of complex multi-dimensional phenomena observed in the tests. The following are specific conclusions:

- With the exceptions noted below, the calculations for both tests correctly predict the sequence of events and the governing multi-dimensional phenomena observed in the experiments.

- The observed parallel channel behavior (peripheral bundles in liquid downflow, middle bundles in counter-current flow and apex bundles in co-current upflow) in both tests is correctly calculated.

- The regional refills, inferred from pressure drop measurements in the bypass and the bundle in the BWR/6 test and the lower plenum in the BWR/4 test, show good agreement with the calculations.

- The upper plenum inventory is well predicted. Temporary decrease in the upper plenum level in the latter stage of the BWR/6 transient (both in the calculation and the data) is attributable to the guide tube CCFL breakdown.

[[

]]
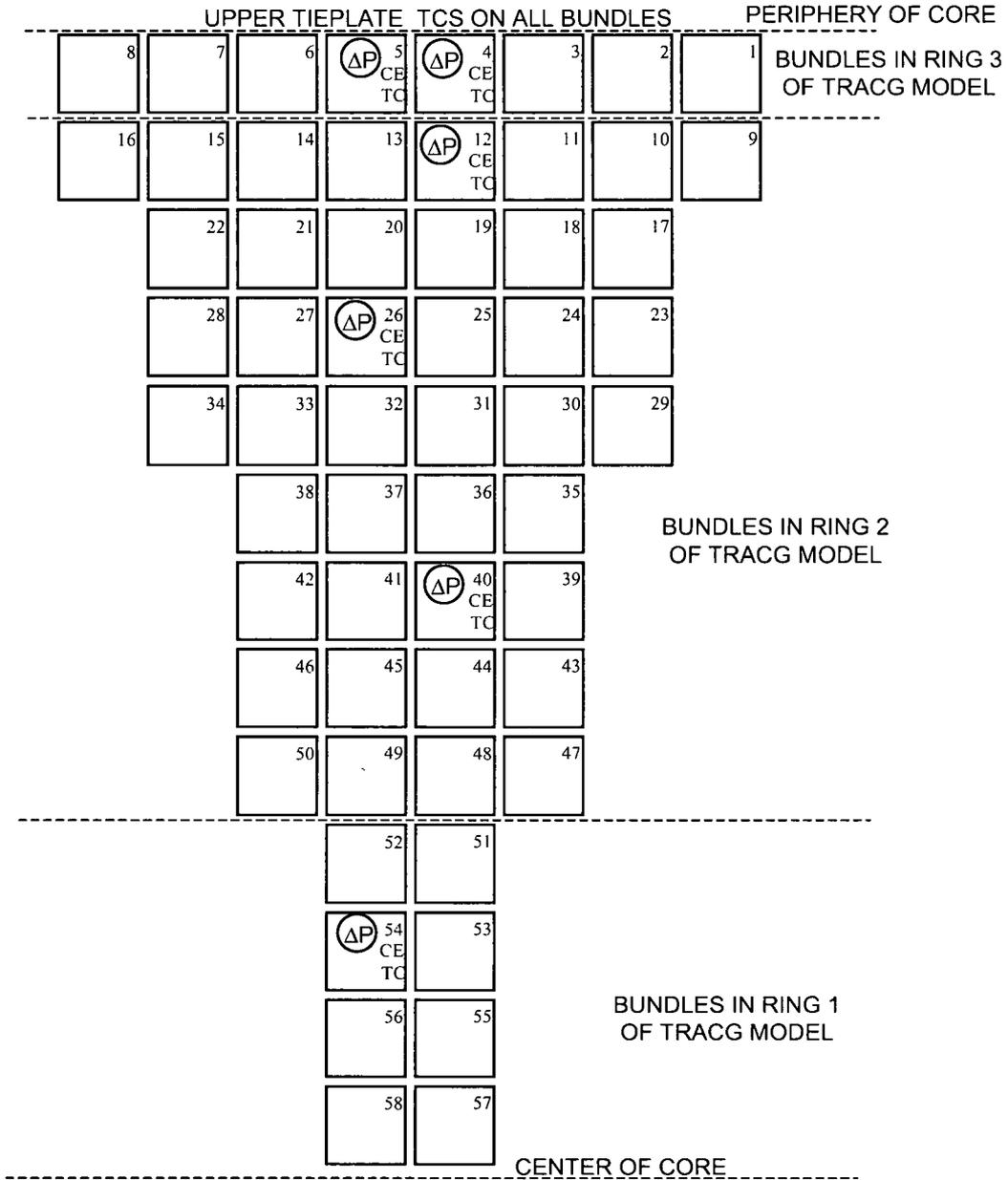
Figure 5.3-1. Location of Instrumented Bundles in the SSTF Facility
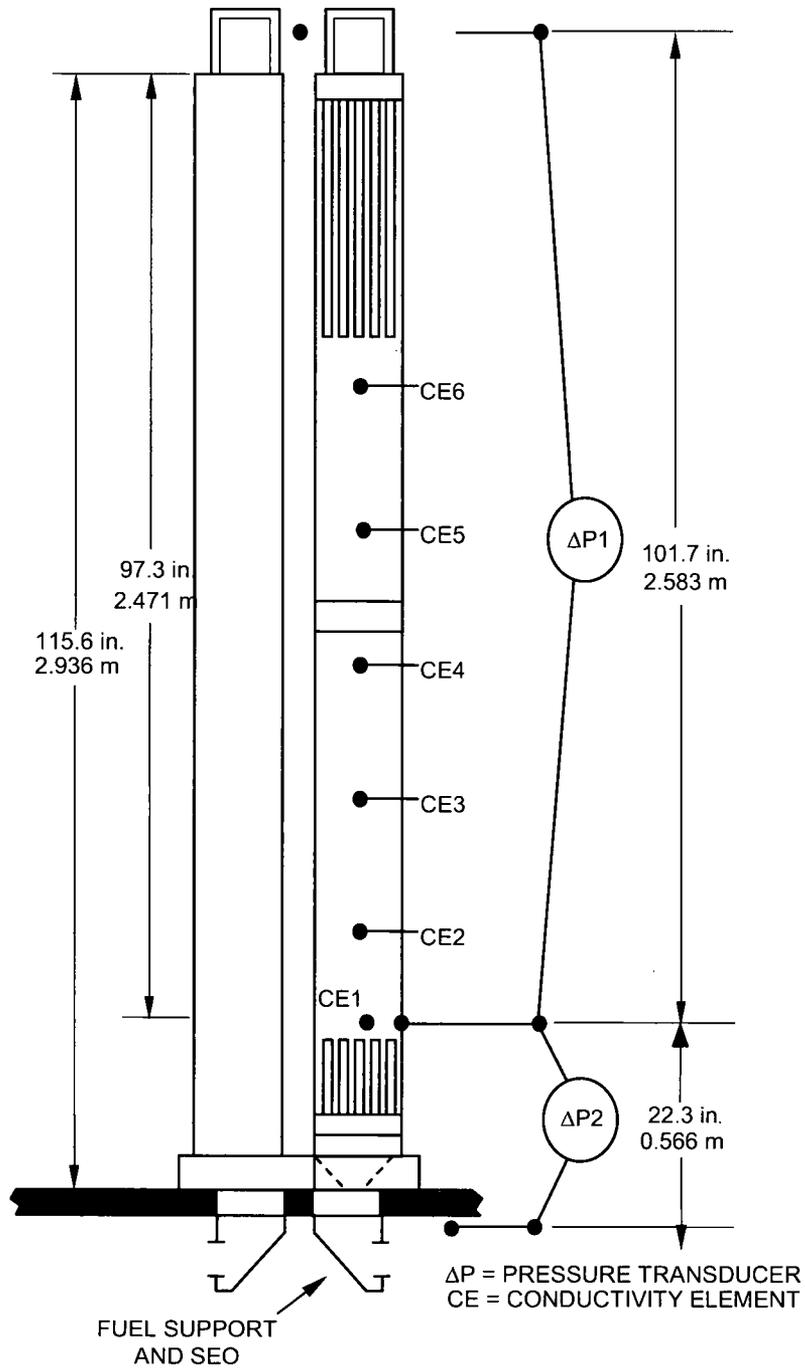
Figure 5.3-2. Channel Instrumentation
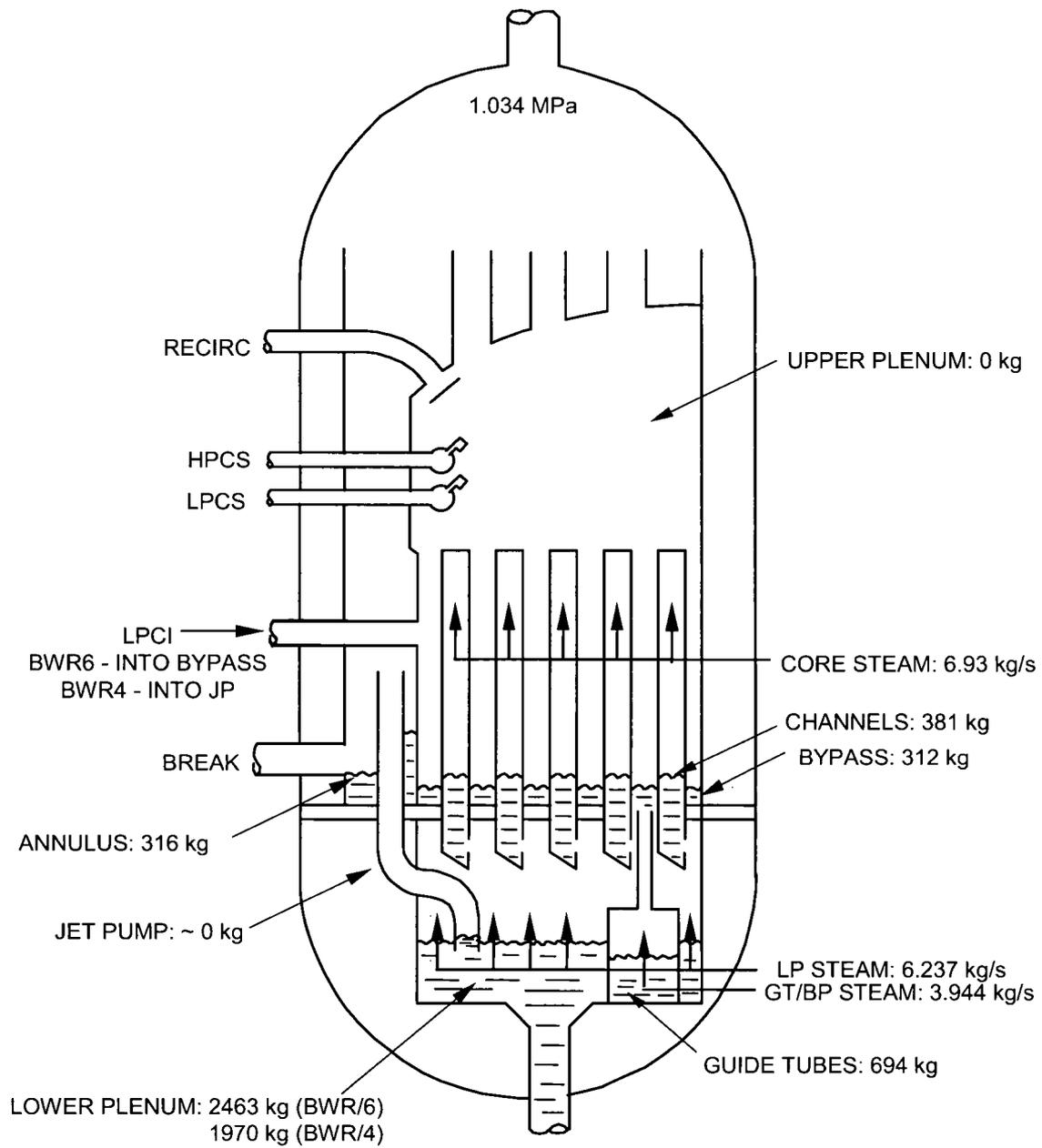
Figure 5.3-3. Initial Conditions for Reference System Response Test (SSTF SRT-3, Run 26 and EA3-1, Run 111)
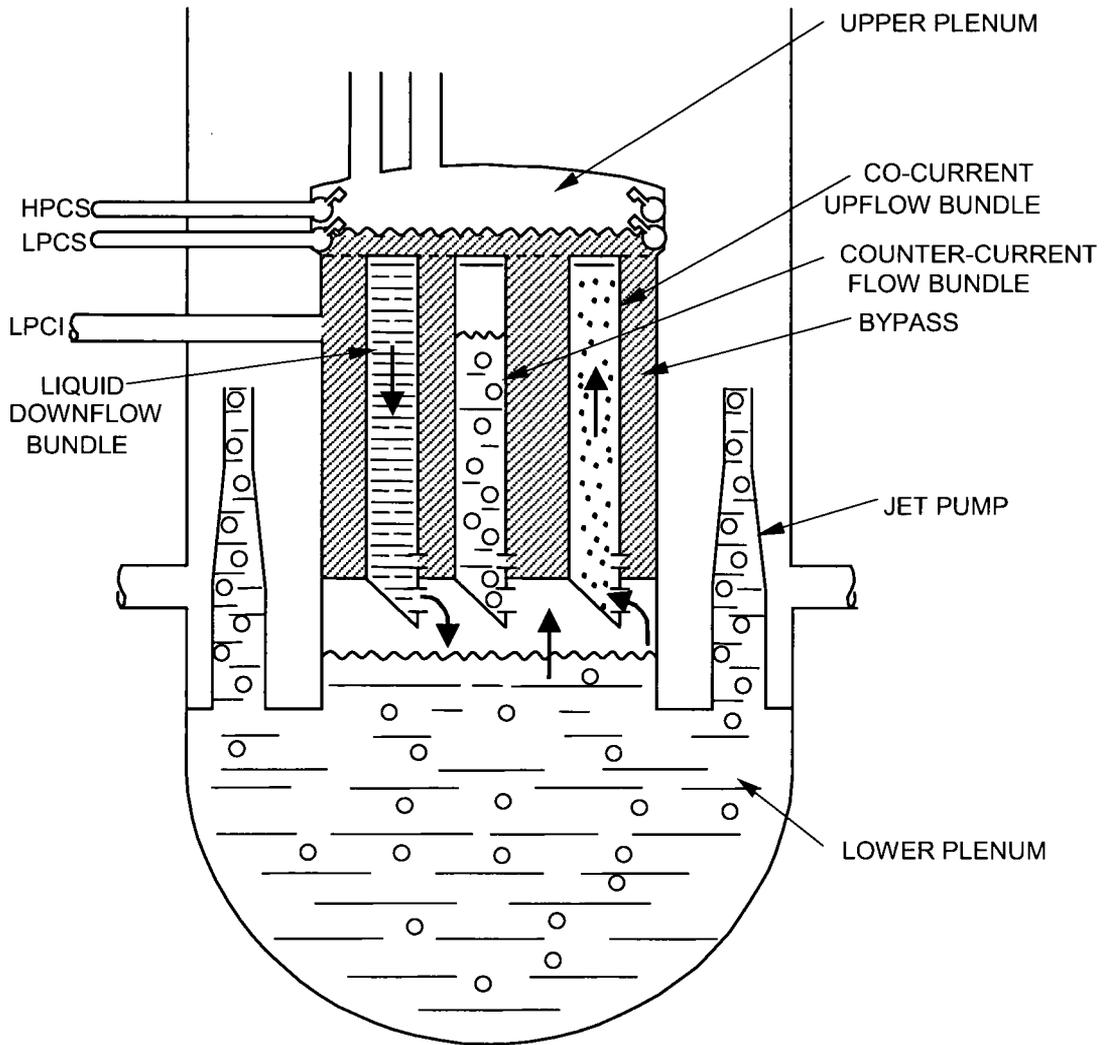
Figure 5.3-4. Multi-Channel Conditions for the BWR/6 at ~10 s
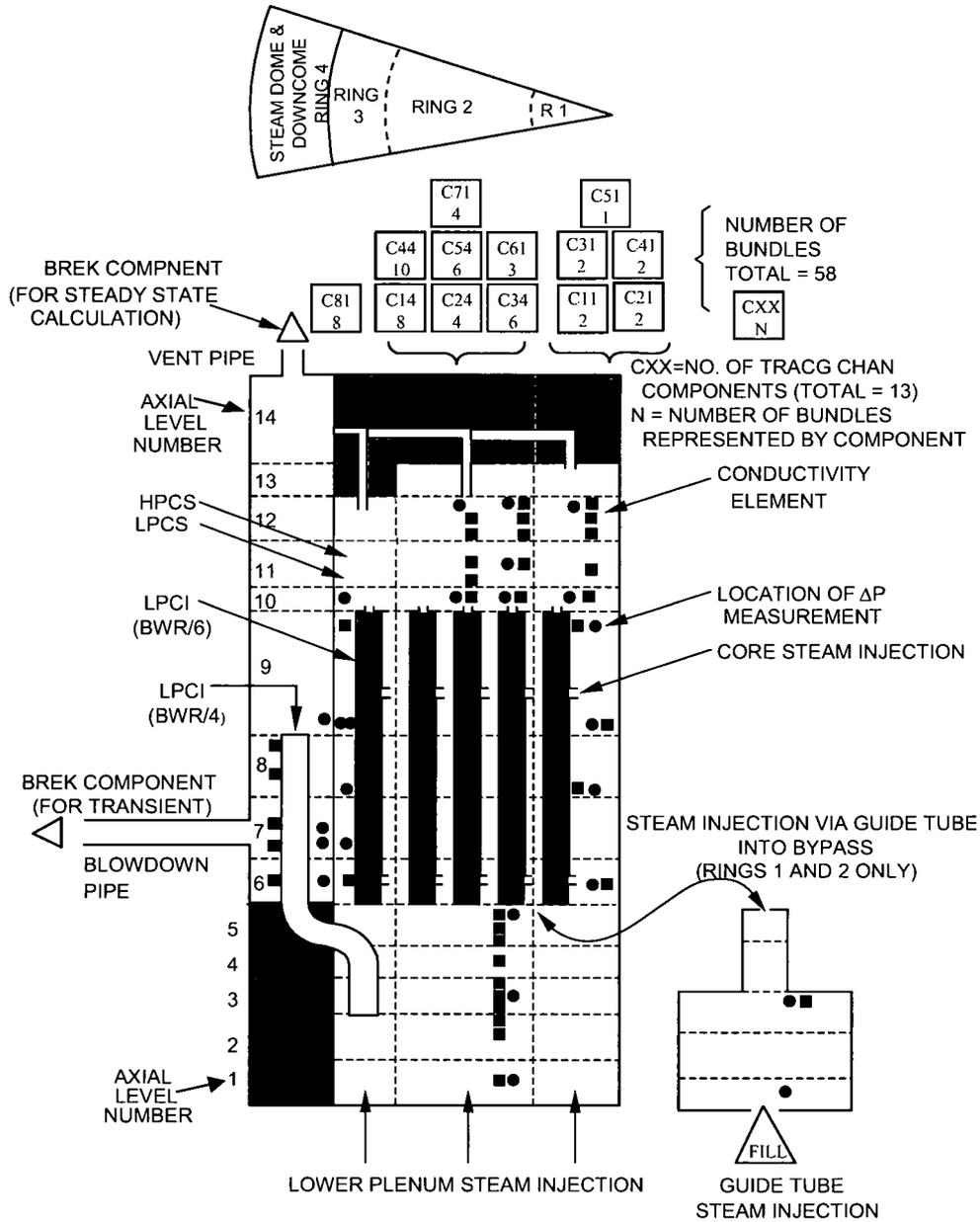
Figure 5.3-5. TRACG Nodalization for the SSTF System Response Tests
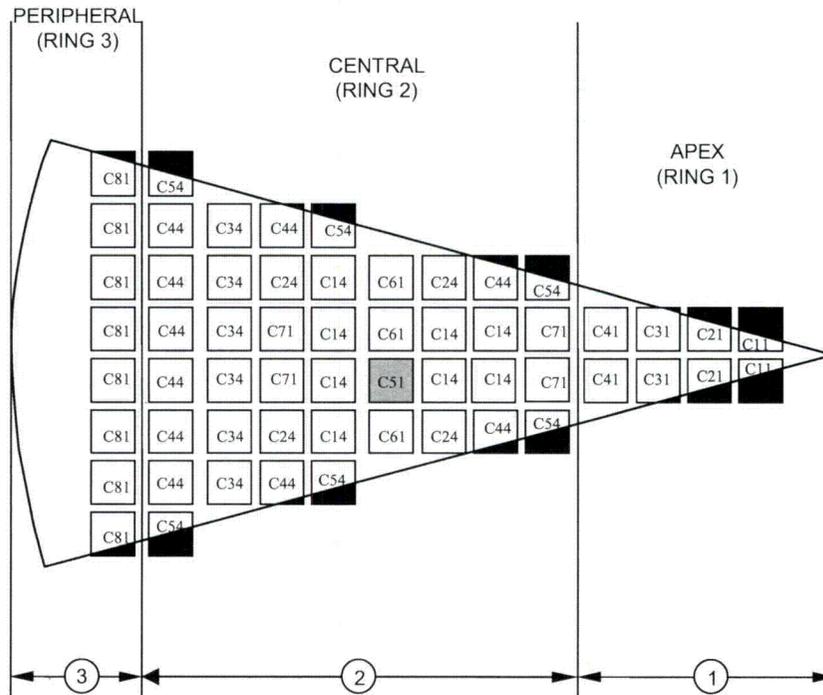
= MEASUREMENT BUNDLES

CXX = TRACG CHAN COMPONENT NUMBER

C51 = CHANNEL COMPONENT 51, HIGH POWER BUNDLE
(CONNECTED IN RING 1 IN TRACG MODEL)

Figure 5.3-6. TRACG CHAN Component Assignment for SSTF Core Region

[[

]]

Figure 5.3-7. Comparison of System Pressures (SSTF SRT-3, Run 26)

[[

]]

**Figure 5.3-8. TRACG Calculation of Lower Plenum Two-Phase Level
(SSTF SRT-3, Run 26)**

[[

]]

Figure 5.3-9. TRACG Calculation of SEO Vapor Velocities Showing Parallel Channel Transitions (SSTF SRT-3, Run 26)

[[

]]

Figure 5.3-10a. TRACG Calculation of Void Fraction in Four Lower Cells of a High Power Channel (CHAN51) (SSTF SRT-3, Run 26)

[[

]]

**Figure 5.3-11b. TRACG Calculation of Void Fraction in Four Lower Cells
of an Average Power Channel (CHAN14) (SSTF SRT-3, Run 26)**

[[

]]

**Figure 5.3-12c. TRACG Calculation of Void Fraction in Four Lower Cells
of the Peripheral Channel (CHAN81) (SSTF SRT-3, Run 26)**

[[

]]

**Figure 5.3-13. Comparison of the Side Entry Orifice Pressure Drop
for Co-Current Upflow Bundles (SSTF SRT-3, Run 26)**

[[

]]

**Figure 5.3-14. Comparison of Side Entry Orifice Pressure Drop
for Counter-Current Flow Bundles (SSTF SRT-3, Run 26)**

[[

]]

**Figure 5.3-15. Comparison of the Pressure Drop Across the Side Entry Orifice
of Peripheral Liquid Downflow Bundles (SSTF SRT-3, Run 26)**

[[

]]

Figure 5.3-16. Comparison of Bypass Pressure Drop (SSTF SRT-3, Run 26)

[[

]]

Figure 5.3-17. Comparison of Upper Plenum Pressure Drop (SSTF SRT-3, Run 26)

[[

]]

Figure 5.3-18. Comparison of Upper Plenum Subcooling (SSTF SRT-3, Run 26)

INTEGRAL SYSTEM EFFECTS TESTS

[[

]]

Figure 5.3-19. Comparison of Collapsed Level for the Counter-Current Flow Bundles (SSTF SRT-3, Run 26)

[[

]]

Figure 5.3-20. Comparison of System Pressure (SSTF EA3-1, Run 111)

[[

]]

Figure 5.3-21. Comparison of Lower Plenum Temperatures at the Periphery Near Bottom (SSTF EA3-1, Run 111)

[[

]]

Figure 5.3-22. Comparison of Lower Plenum Temperatures at the Periphery at Mid-Height (SSTF EA3-1, Run 111)

[[

]]

Figure 5.3-23. Comparison of Lower Plenum Temperatures on the Periphery Near the Top (SSTF EA3-1, Run 111)

[[

]]

Figure 5.3-24. TRACG Calculated Jet Pump (TEE67) LPCI Injection, Suction and Discharge Flows (SSTF EA3-1, Run 111)

[[

]]

Figure 5.3-25. TRACG Calculated Blowdown Flow (SSTF EA3-1, Run 111)

[[

]]

Figure 5.3-26. Comparison of Lower Plenum Void Fraction (SSTF EA3-1, Run 111)

[[

]]

Figure 5.3-27. Comparison of Lower Plenum Mass Fraction (SSTF EA3-1, Run 111)

5.4 ROSA-III

5.4.1 ROSA-III Test Facility and Test Matrix

The ROSA-III test facility [5-12] is a volumetrically scaled (1/424) BWR system with an electrically heated core simulator. It was designed to study the response of the primary system, core and ECCS during a postulated LOCA. The test facility consists of four subsystems: pressure vessel; steam and feedwater lines; recirculation loops; and ECCS. Figure 5.4-1 shows a schematic diagram of the ROSA-III facility and Figure 5.4-2 shows the internal details of the pressure vessel. Table 5.4-1 compares significant parameters of ROSA-III with the corresponding parameters of the BWR/6-251 system upon which it was based.

As shown in Figure 5.4-2, the ROSA-III pressure vessel includes the major components simulating the internal structure of the reference BWR. The vessel interior has simulations of the core, lower and upper plenums, downcomer annulus, steam separator, steam dome and steam dryer. The ROSA-III core consists of four half-length fuel assemblies and a simulated control rod. Each of the four assemblies has 62 electrically heated rods and two water rods in an 8x8 array. The fuel assembly is supported by lower and upper tieplates and four intermediate spacers. The effective heated length of the simulated fuel rods is 1.88 m and the axial power distribution follows the truncated cosine profile shown in Figure 5.4-3. The bundle radial power distribution is shown in Figure 5.4-4. The power supplied to Fuel Assembly A is 40% larger than the power supplied to each of Fuel Assemblies B, C and D. The heated rods within each assembly are further divided into three groups with relative powers of 1.1, 1.0 and 0.875, as shown at the bottom of Figure 5.4-4. Orifice plates are used to control the core inlet flow.

The steam line is connected to the steam dome of the pressure vessel and contains a control valve to maintain a steady-state system pressure prior to the initiation of the simulated LOCA transient. The steam line has a branch representing the Automatic Depressurization System (ADS). Feedwater is drawn from the feedwater tank through the feedwater line to a sparger located below the steam separator.

Each of the recirculation loops includes a recirculation pump and two jet pumps. The jet pumps were installed outside the pressure vessel to facilitate scaling of their volume and height relative to the core. One of the recirculation loops was equipped with two break simulators, each having a fast-opening blowdown valve and a nozzle or orifice to adjust the break size. This arrangement permitted the break type (double-ended or split), size and location to be varied. A fast-closing shutoff valve is used to block communication between the two sides of the break during the simulation of a double-ended rupture.

The ROSA-III facility includes the full complement of ECCS systems available in a BWR/6 plant - High-Pressure Core Spray (HPCS), Low-Pressure Core Spray (LPCS), Low Pressure Coolant Injection (LPCI) and ADS. The HPCS and LPCS provide coolant to the top of the core and the LPCI injects to the bypass. The ROSA-III simulation of each of these systems includes a supply tank, pump, piping and control system.

ROSA-III is equipped with an extensive instrumentation system to obtain relevant thermal-hydraulic data during a simulated LOCA. Measurements include system pressure, differential pressures, flow rates, fluid and metal temperatures, collapsed levels, two-phase mixture levels and fluid densities.

The ROSA-III break simulations were conducted by first establishing steady-state conditions at a system pressure of 7.4 MPa, lower plenum subcooling of 10 K, core inlet flow of 16 kg/s and core power of 3.97 MW. The core power was set by the capacity of the electric power supply and corresponds to 44% of the scaled (1/424) BWR/6 steady-state power. After steady-state conditions were established, the blowdown valves were opened and core power was reduced in accordance with a predetermined curve. To compensate for the limitation of the power supply, the core power was held constant for approximately 9 s after the break. The core power was then decreased to match the fuel rod surface heat transfer in the reference BWR. The ECCS actuated automatically and injected water into the pressure vessel when the downcomer level or system pressure setpoints were reached.

Two ROSA-III tests that simulated breaks in the recirculation line on the suction side of the recirculation pump were selected for TRACG qualification. Test 926 [5-12] simulated a 200% break (guillotine rupture) and Test 912 [5-13] simulated a 5% split-type break Both tests were conducted with the HPCS inactive. The ROSA-III test series established that failure of the HPCS was the most severe single failure for a recirculation line suction break for all break sizes. For Test 926, the steam line closed at 8.5 s and the LPCS and LPCI were initiated at 71 s and 93 s, respectively. For Test 912, the steam line closed at 24 s and the LPCS and LPCI were initiated at 318 s and 406 s, respectively.

5.4.2 TRACG Input Model for Simulation of ROSA-III Tests

The TRACG input model, configured for simulation of the double-ended break, is shown in Figure 5.4-5. The modification of the recirculation line model to represent the 5% split break is shown in Figure 5.4-6. The VSSL component has 13 axial levels and three radial rings. In the core region (Levels 5 to 7), Rings 1 and 2 represent the bypass regions for the high-power and average-power rod bundle components, respectively. Ring 3 represents the downcomer. Levels 1 and 2 and the two inner rings of Levels 3 and 4 represent the lower plenum. The two inner rings of Levels 8 and 9 represent the upper plenum. The exit plane of the steam separator coincides with the top of Level 12.

Other components shown in Figure 5.4-5 include the guide tubes for the rod bundle components and the jet pump, recirculation pump and associated piping for the intact and broken loops. TRACG FILL and PIPE components are used to represent the ECCS system, which includes LPCS injection to the central and peripheral regions of the upper plenum and LPCI injection to the central and peripheral regions of the bypass. The steam line in the model terminates in a FILL component. For steady-state operation, prior to the opening of the valves simulating the break, the FILL component was set to draw a steam flow equivalent to the core power (3.97 MW). When the break valves were opened, the steam line was closed by setting the FILL to zero flow.

The ROSA fuel assembly is represented by two TRACG CHAN components. Referring to Figure 5.4-4, CHAN01 represents Channel Box A, the channel with the highest radial peaking factor, and is located in Ring 1 of the VSSL component (Figure 5.4-5). CHAN02 represents Channel Boxes B, C and D and is located in Ring 2 of the VSSL component. The simulated fuel rods in each of the CHAN components are divided into four rod groups in accordance with the local peaking factors (1.1, 1.0, and 0.875) shown in the table at the bottom of Figure 5.4-4. A separate rod group is used for the two water rods in each of the CHAN components. Figure 5.4-7 shows the TRACG CHAN component axial nodalization. The length of the bundle is divided

into 14 cells with Cells 3 through 13 covering the heated section. The length of the cells ranges from 0.073 m to 0.235 m. The nodalization is primarily dictated by the objective of accurately representing the axial power distribution (Figure 5.4-3). Core inlet flow enters at the lower face of Cell 1 and the bundle-to-bypass leakage path is from Cell 2.

5.4.3 Results and Discussion

[[

]]

5.4.4 Conclusions

The following conclusions may be drawn from the comparison of TRACG predictions and measurements for ROSA-III Tests 926 (large double-ended break) and 912 (small split break).

The depressurization transients for both tests are satisfactorily predicted by TRACG.

[[

]]

Table 5.4-1
ROSA-III Compared to BWR/6

	BWR/6-251	ROSA-III	Ratio
No. of Recirculation Loops	2	2	1
No. of Jet Pumps	24	4	6
No. of Separators	251	1	251
No. of Fuel Assemblies	848	4	212
Active Fuel Length (m)	3.76	1.88	2
Total Volume (m^3)	621	1.42	437
Power (MW)	3800	4.40	864
Pressure (MPa)	7.23	7.23	1
Core Flow (kg/s)	1.54×10^4	36.4	424
Recirculation Flow (liters/s)	2970	7.01	424
Feedwater Flow (kg/s)	2060	4.86	424
Feedwater Temperature (K)	489	489	1

INTEGRAL SYSTEM EFFECTS TESTS
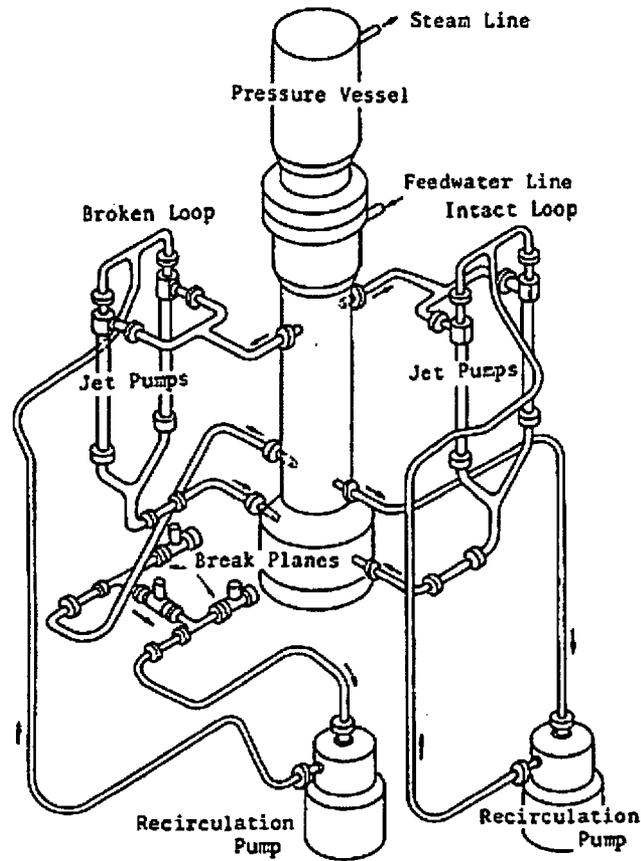
Figure 5.4-1. ROSA-III Test Facility
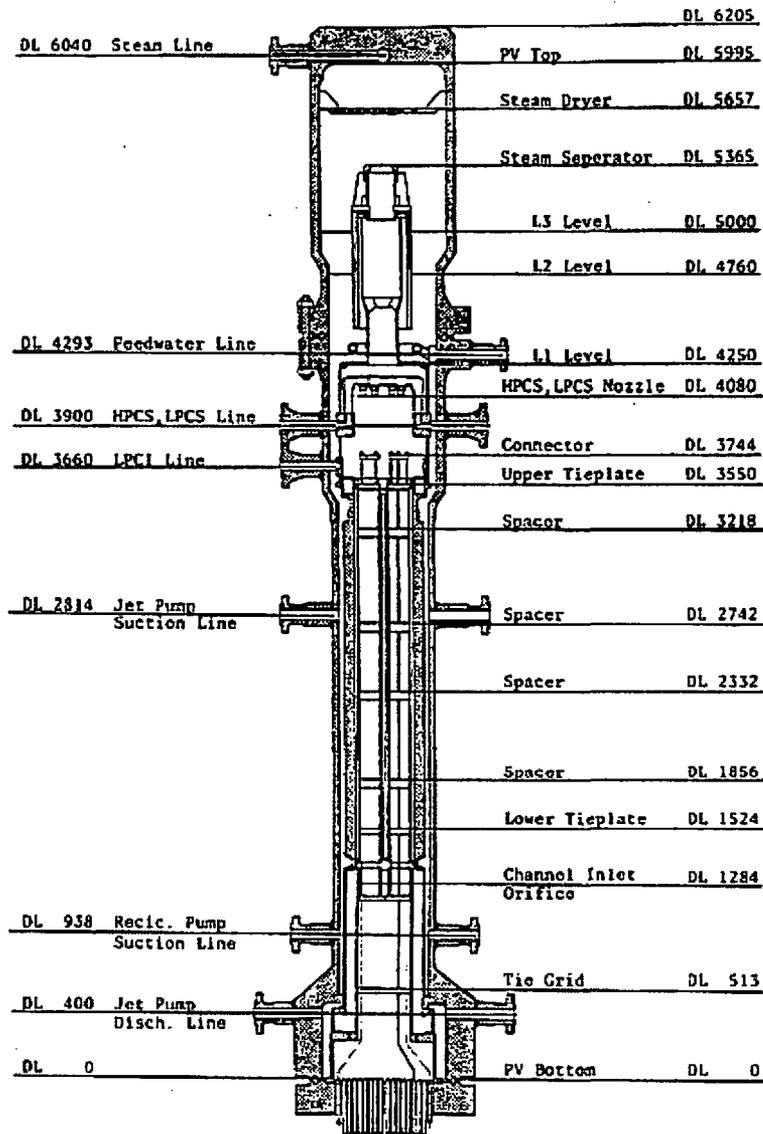
Figure 5.4-2. ROSA-III Pressure Vessel Internals Arrangement

✩ Indicates position of thermocouple.   • Axial Peaking Factor
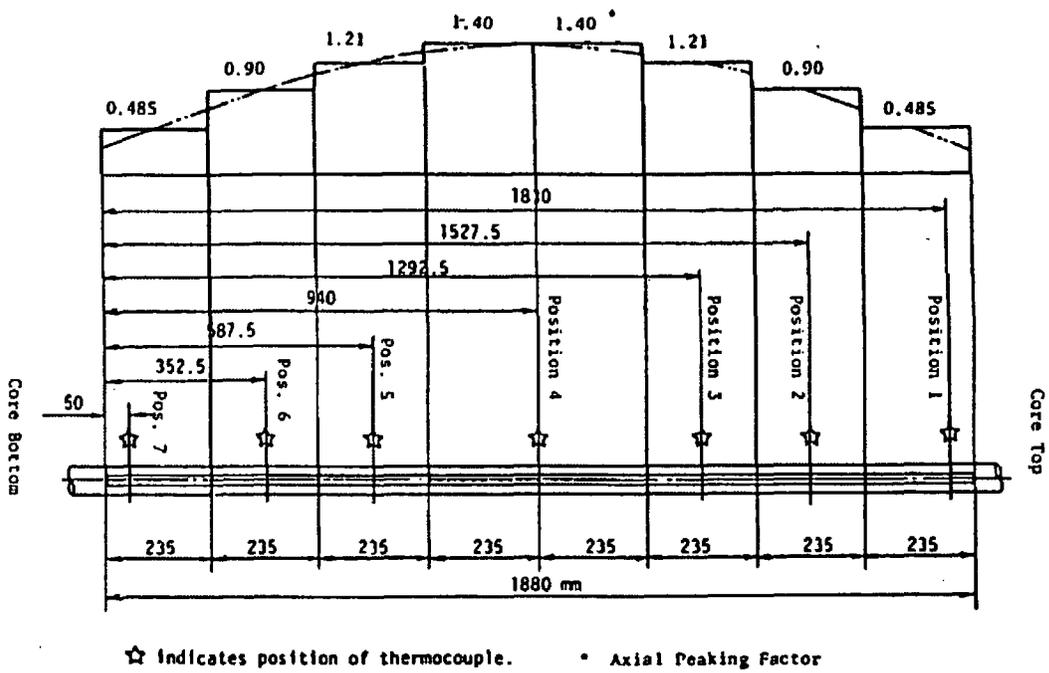
Figure 5.4-3. ROSA-III Heater Rod Axial Power Distribution

Figure 5.4-4. ROSA-III Core Radial Power Distribution
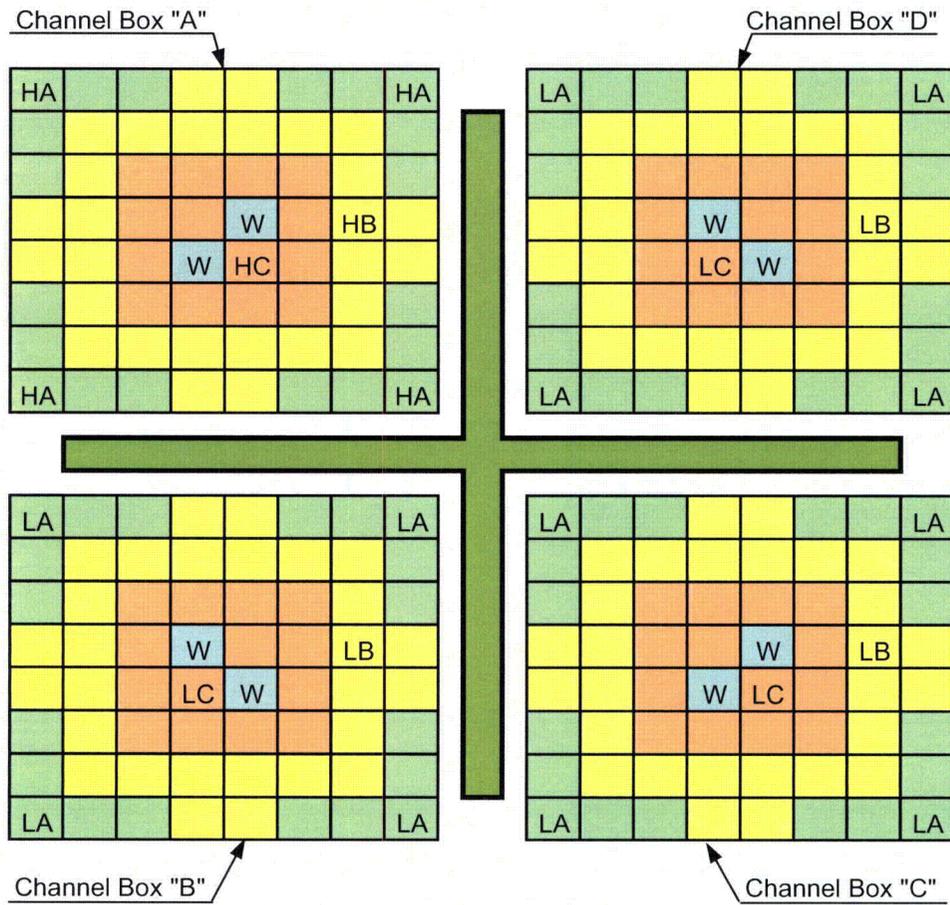
Region	HA	HB	HC	LA	LB	LC	W
Radial Peaking Factor	1.4	1.4	1.4	1.0	1.0	1.0	0
Local Peaking Factor	1.1	1.0	0.875	1.1	1.0	0.875	0
No. of Rods	20	28	14	60	84	42	8

R1 Hot Channel Area

R2 Core Shroud

R3 Pressure Vessel
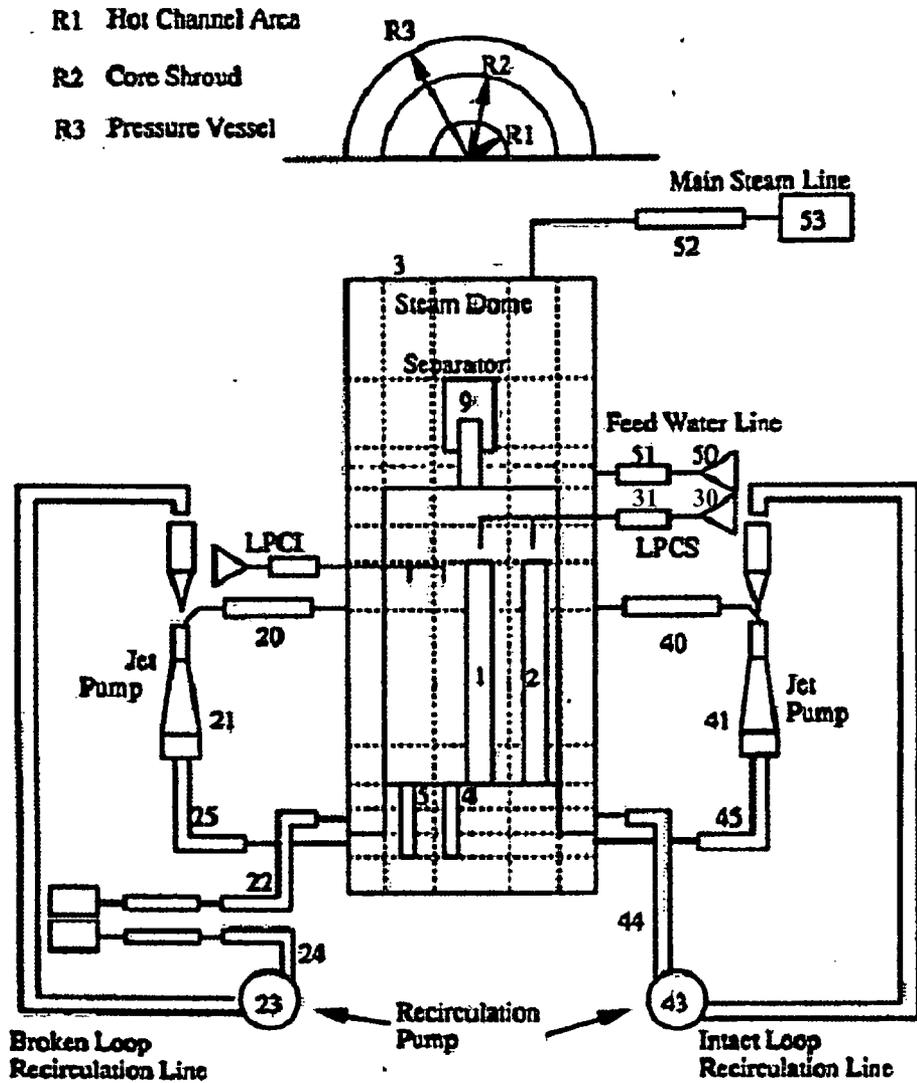
Figure 5.4-5. TRACG Model of ROSA-III Test Facility Configured for Large Break
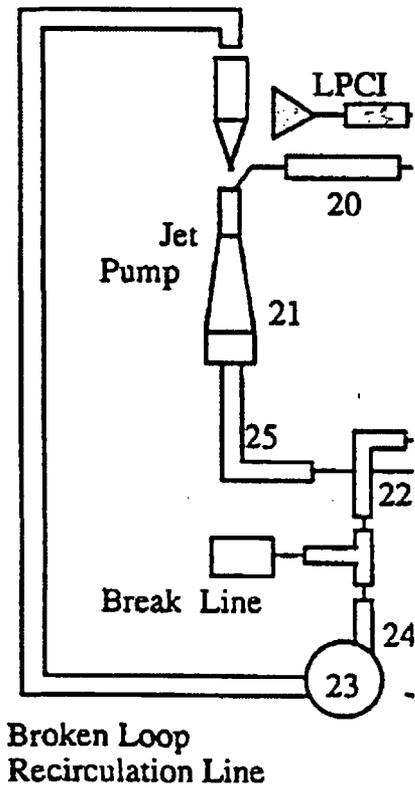
Figure 5.4-6. TRACG Model of Recirculation Line for Small Break
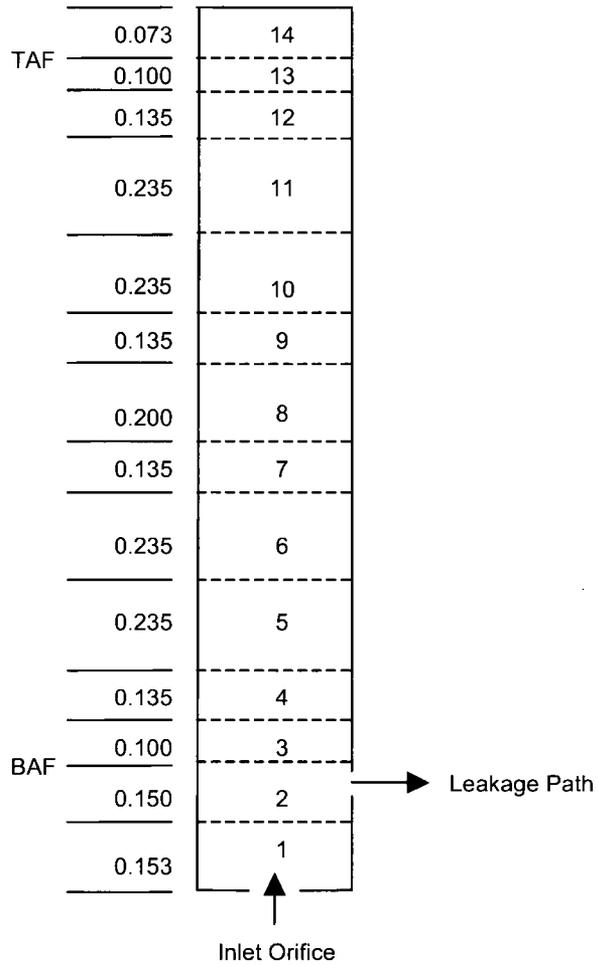
Figure 5.4-7. TRACG Model of ROSA Fuel Bundle (cell heights in m)

[[

]]

Figure 5.4-8. Comparison of Measured and Calculated Pressure for Test 926

[[

]]

Figure 5.4-9. Comparison of Measured and Calculated PCT for Test 926

[[

]]

Figure 5.4-10. Comparison of Measured and Calculated Pressure for Test 912

[[

]]

Figure 5.4-11. Comparison of Measured and Calculated Downcomer Level for Test 912

[[

]]

Figure 5.4-12. Comparison of Measured and Calculated PCT for Test 912

5.5 FIX-II

5.5.1 FIX-II Test Facility and Test Matrix

The FIX-II test facility was a 1:777 scaled representation of the Swedish Oskarsham-2 external-pump BWR. The FIX-II test program provided experimental data on LOCAs and other transients included in the safety design basis of Swedish BWRs [5-14 to 5-16]. Figure 5.5-1 shows a schematic of the FIX-II test facility. The pressure vessel included a lower plenum, core region, upper plenum, steam separator and a steam dome. There were two recirculation loops. An "intact" loop provided 75% of the total recirculation flow and loop volume and a "broken" loop provided 25% of the recirculation flow and loop volume. The downcomer, bypass and guide tube were simulated by individual pipes outside the pressure vessel.

The core was simulated by an electrically heated 6x6 rod bundle. The rods were constructed with an Inconel-600 cladding surrounding a core of compacted magnesium oxide. Rod heating was simulated by direct current heating of the Inconel-600 cladding. The cladding thickness was varied along the length of the rods to provide a centrally peaked axial power profile. Integrated rod powers varied from 0.957 to 1.034 of the average value for the bundle. There were five thermocouples in each rod to measure the clad temperature. The rod bundle was surrounded by an insulating Teflon sleeve through which measurement lines were inserted. Coolant water circulated through the gap between the sleeve and the vessel wall to prevent flashing in the measurement lines. The bypass walls were electrically heated to simulate the bundle-to-bypass heat transfer. During a simulated LOCA transient, the bundle and bypass powers followed programmed power decay curves.

The initial conditions for a LOCA simulation were established by connecting the pressure vessel to a heat-exchanger loop. A pump in the heat exchanger loop took suction from the lower end of the downcomer. The flow passed through the heat exchanger and discharged to the steam dome through the feedwater and spray lines. The system pressure and core inlet subcooling were controlled by the amount of heat removal in the heat exchanger. The heat exchanger loop was isolated during the LOCA simulation. The two types of recirculation-line breaks considered in this study were simulated by the break arrangements shown in Figure 5.5-2. The break flow limiter in these arrangements consists of a conical nozzle followed by a 0.213 m run of tubing with the same diameter as the nozzle throat. The break flow discharged into water-filled tanks that condensed the steam. The tanks were equipped with standpipes to measure the break flow.

FIX-II tests 5052 (large break) [5-15] and 3025 (intermediate break) [5-16] were selected for TRACG qualification. The initial conditions and important test parameters for both tests are shown in Table 5.5-1. Both tests simulated breaks in a single recirculation line in a plant with four recirculation loops. Test 5052 simulated a guillotine rupture and Test 3025 simulated a break characterized by an intermediate size split. Test 5052 was initiated by opening valves V117 and V120 and simultaneously closing valve V103 between the two ends of the break (Figure 5.5-2). Test 3025 was initiated by opening valve V120. Test initiation was also marked by the initiation of power decay in the bundle and bypass, and coastdown of the pump in the intact loop. Neither test involved ECCS actuation.

5.5.2   TRACG Model for Simulation of FIX-II Tests

The two-ring TRACG model of the FIX-II vessel is shown in Figure 5.5-3. The radius of the outer ring corresponds to the inner radius of the pressure vessel and the radius of the inner ring is one-half of the diagonal dimension of the rod bundle. The TRACG VSSL component is divided into fifteen axial cells. This nodalization provides appropriate geometric definition of the principal regions of the vessel (e.g., lower plenum) and correspondence with elevations where flows are entering or leaving the vessel. It also facilitates association of axial levels with measurement locations.

An overview of the model including the components that represent the bundle, bypass, guide tube, external downcomer and recirculation loops and pumps is shown in Figure 5.5-4. Additional one-dimensional components model the external piping for systems such as feedwater and spray and the piping used to simulate the break. The configuration of the recirculation line components in Figure 5.5-4 is for a large (guillotine) break on the discharge side of the pump. Break flow is directed to BREK components C60 and C71 on the pump and lower plenum sides of the break, respectively. (The zero-flow FILL component, C70, seals off the flowpath that would be used to simulate a break on the suction side of the pump.) For the simulation of the intermediate discharge break, the flow path to the BREK component on the lower plenum side of the break (C71) is set to zero, as shown in Figure 5.5-5.

The nodalization of the CHAN component that represents the rod bundle is shown in Figure 5.5-6. The CHAN is located between Levels 2 and 6 in the VSSL and has 11 cells, the top ten of which are heated. Within the CHAN, the heater rods are divided into five TRACG rod groups in accordance with their power peaking factors. Rod Group 4, representing three rods in the center of the bundle, has the highest average power peaking. Rod Group 5 represents the rod with the highest local peaking factor in the bundle and is used as input for the TRACG Hot Rod Model. Ten radial nodes are used to model the heater rods as shown in Figure 5.5-7. Node 7 is associated with the rod thermocouple location. The heat capacity and thermal diffusivity of the rod are accurately represented by appropriate selection of the nodal properties from the TRACG materials property library.

The gap between the Teflon instrumentation sleeve and the vessel wall is represented by the VSSL outer ring between Levels 3 and 6. A FILL and PIPE combination is used to supply cooling water to Level 3 and a PIPE and BREK combination is used to extract it from Level 6. With this configuration, the TRACG test section heat loss of 204 kW matches closely with the measured heat loss. Vessel wall stored energy is modeled with double-sided heat slabs between the vessel interior and the environment. Metal masses within the lower plenum are modeled by lumped-parameter heat slabs. Heat losses from components outside the vessel (e.g., downcomer, bypass and recirculation loops) were modeled by outside surface heat transfer coefficients that were chosen by calibrating the model heat losses to steady-state heat loss measurements.

Feedwater flow, spray flow and flow to the heat exchanger loop were modeled as boundary conditions using FILL components with input parameters based on test measurements. Flow through the SRV was modeled by a velocity versus pressure boundary condition.

5.5.3   Calculation Results

[[

]]

5.5.4 Conclusions

TRACG satisfactorily predicts the system responses to large and intermediate recirculation-line break LOCAs in the FIX-II test facility. For both break configurations, the calculated pressures, break flows and bundle temperatures are in good agreement with the corresponding measurements. [[

]]

Table 5.5-1
FIX-II Test Conditions

Parameter	Test 3025	Test 5052
Break Type	Split-Ended	Guillotine
Break i.d. (mm.)	12	21.6 + 21.6
Relative Break Area	31%	200%
Decay Power	ANS+ 0%	ANS+0%
ECCS	None	None
Initial Conditions		
Bundle Power (MW)	3.385	3.356
Steam Dome Pressure (MPa)	6.997	6.90
Power to Bypass Heaters (kW)	57.4	56.5
Intact Loop Pump Flow (kg/s)	4.56	4.40
Broken Loop Pump Flow kg/s)	1.55	1.68
Bundle Flow (kg/s)	5.51	5.51
Bypass Flow (kg/s)	0.6	0.57
Feedwater Flow kg/s)	2.49	2.30
Spray Flow (kg/s)	5.36	5.10
Spray Temperature ($^\circ$C)	180.9	181.3
Feedwater Temperature ($^\circ$C)	180.9	181.3
Spray Condenser Level (m)	6.34	6.223
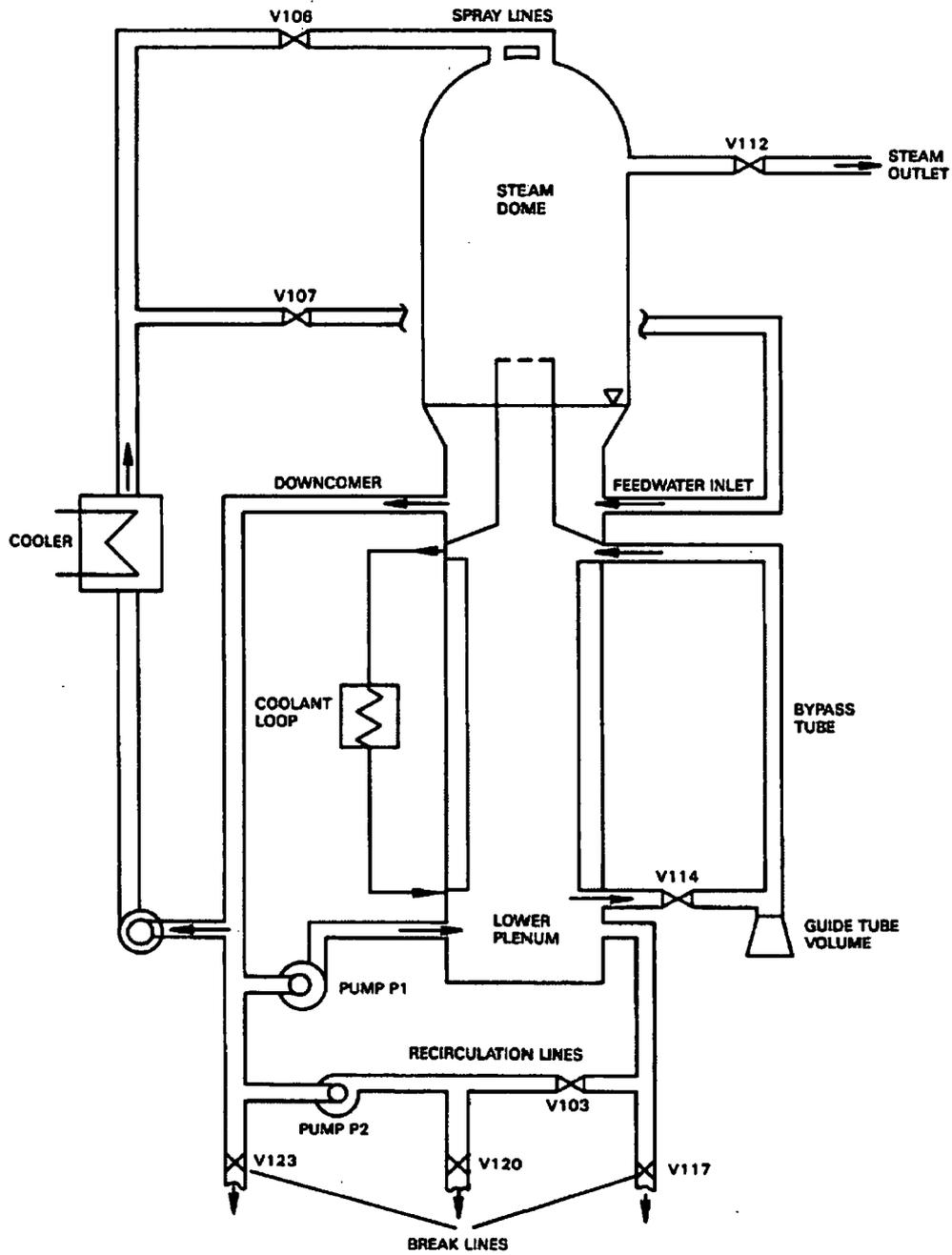
Figure 5.5-1. Schematic Diagram of FIX-II Test Facility
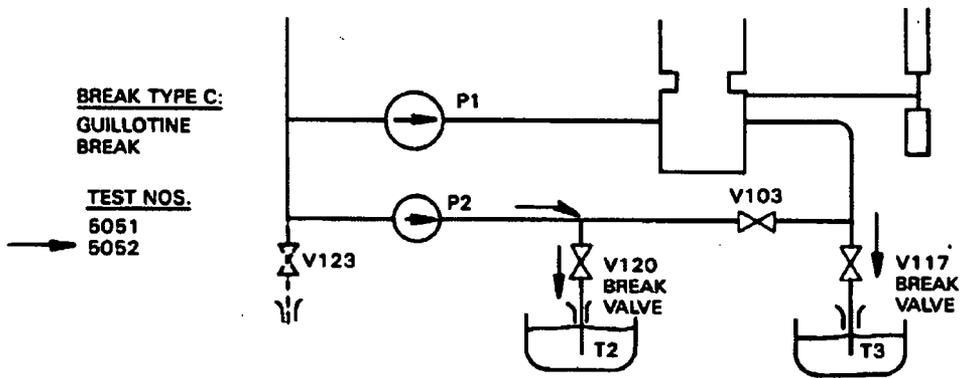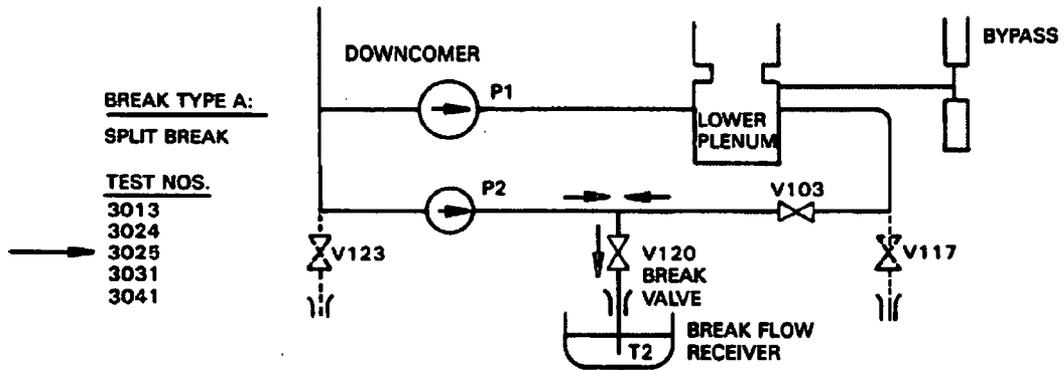
Figure 5.5-2. FIX-II Recirculation Line Configurations for Tests 5052 and 3025
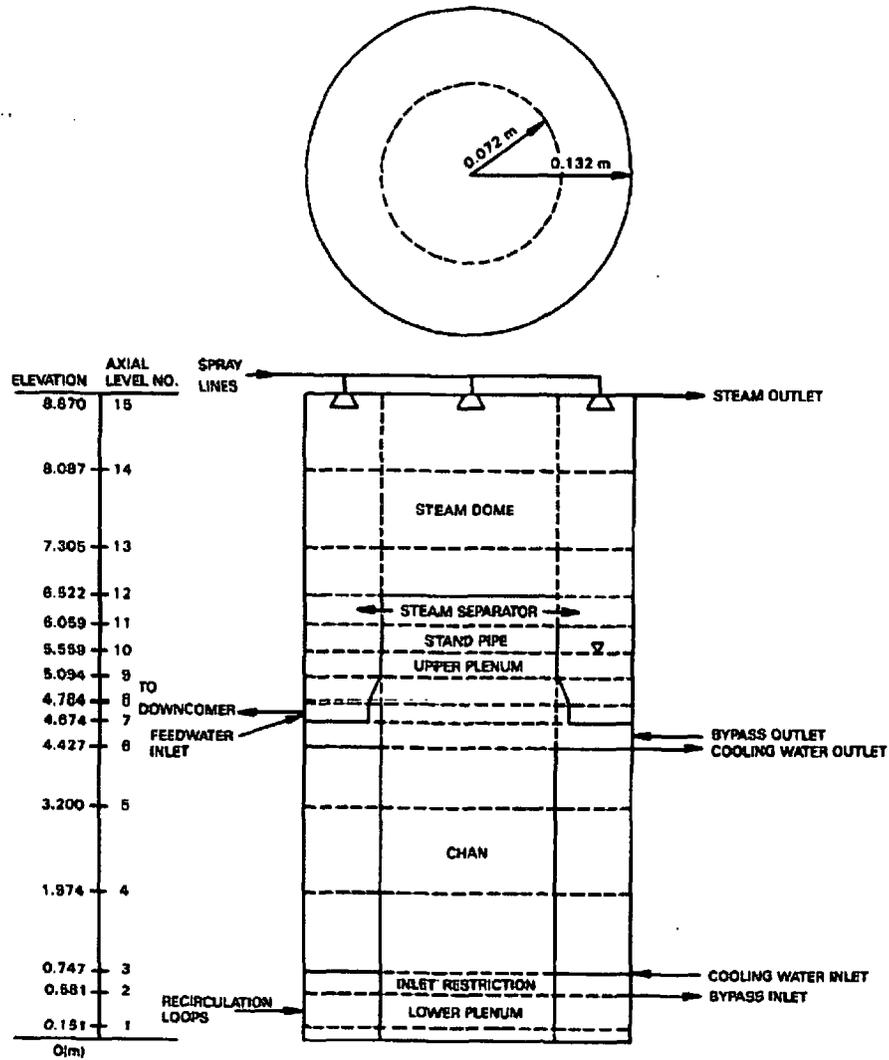
Figure 5.5-3. Nodalization of VSSL Component for TRACG Model of FIX-II Test Facility
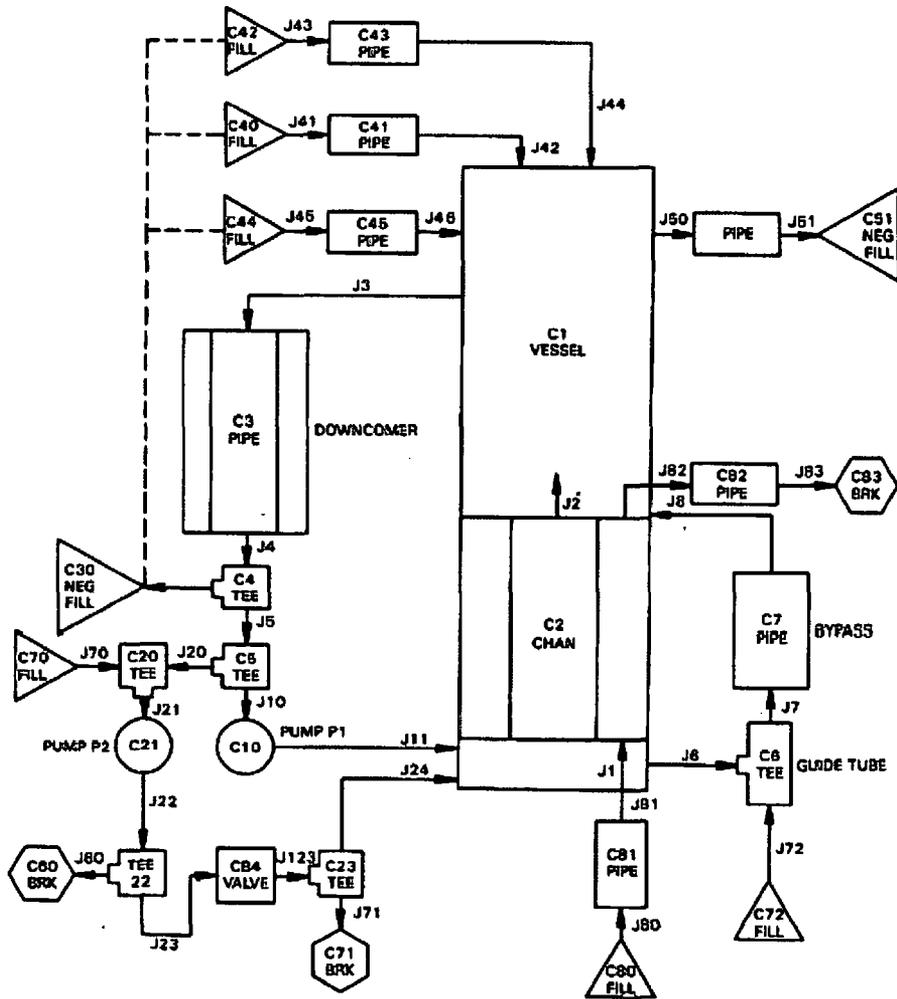
Figure 5.5-4. Component Arrangement for TRACG Model of FIX-II Test Facility
Configured for Large Recirculation Line Break

INTEGRAL SYSTEM EFFECTS TESTS
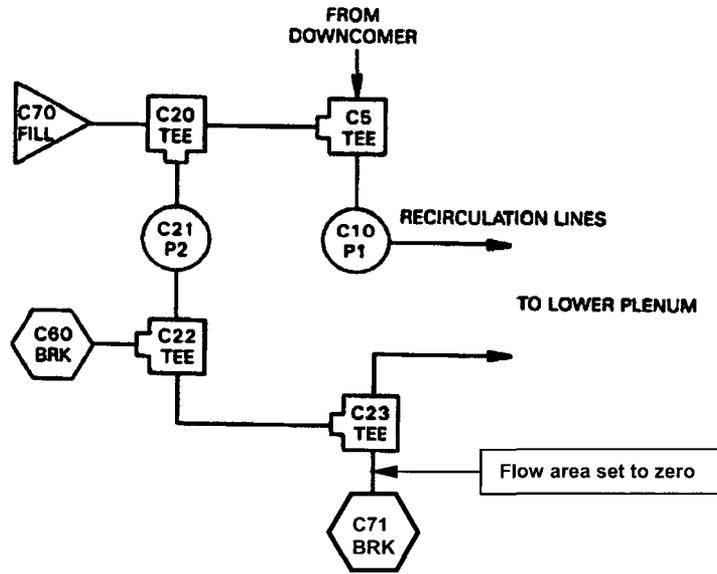
Figure 5.5-5. TRACG FIX-II Recirculation Line Configuration for Intermediate Break

FIX II BUNDLE TC	THERMOCOUPLE LOCATION (mm)	HEATER ROD ELEVATION (mm)	CHAN CELL NO.	DIFFERENTIAL PRESSURE MEASUREMENT	AXIAL POWER FACTOR
T16	3660	3680	11	dpt12	0.484
T15	3496				
T14	3297	3312	10		0.868
T13	3082				
T12	2810	2944	9	dpt11	1.033
T11	2550				
T10	2313	2576	8	dpt10	1.144
T9	2088	2208	7		1.144
T8	1816	1840	6	dpt9	1.210
T7	1592				
T6	1367	1472	5	dpt8	1.210
T5	1319				
T4	1130	1104	4	dpt7	1.144
T3	870	736	3	dpt6	1.033
T2	598	368	2	dpt5	0.730
T1	184	0	1		

Figure 5.5-6. TRACG CHAN Nodalization with Measurement Locations and Axial Peaking Factors
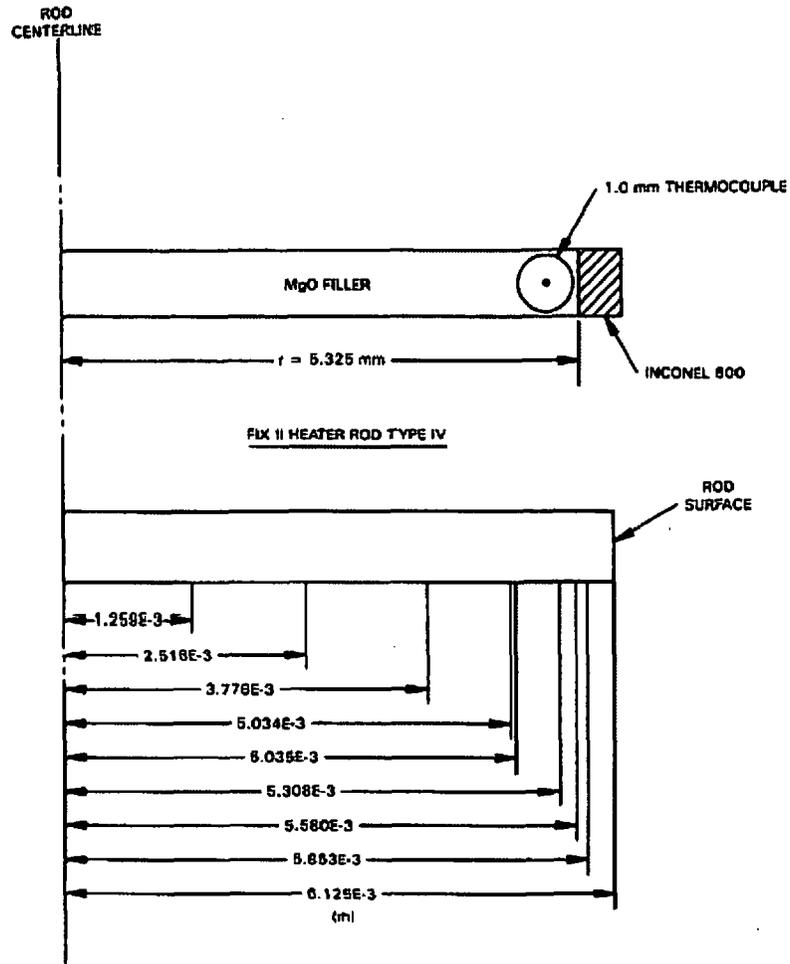
Figure 5.5-7. TRACG Heater Rod Nodalization

[[

]]

Figure 5.5-8. Steam Dome Pressure for FIX-II Test 5052

[[

]]

Figure 5.5-9. Integrated Break Flow for FIX-II Test 5052

[[

]]

Figure 5.5-10. Lower Bundle Rod Temperatures (0.60 m) for FIX-II Test 5052

[[

]]

Figure 5.5-11. Midplane Bundle Rod Temperatures (1.59 m) for FIX-II Test 5052

[[

]]

Figure 5.5-12. Upper Bundle Rod Temperatures (2.81 m) for FIX-II Test 5052

[[

]]

Figure 5.5-13. Maximum Measured Temperature vs. TRACG Hot Rod for Test 5052

[[

]]

Figure 5.5-14. Steam Dome Pressure for FIX-II Test 3025

[[

]]

Figure 5.5-15. Integrated Break Flow for FIX-II Test 3025

INTEGRAL SYSTEM EFFECTS TESTS

[[

]]

Figure 5.5-16. Lower Bundle Rod Temperatures (0.60 m) for FIX-II Test 3025

[[

]]

Figure 5.5-17. Midplane Bundle Rod Temperatures (1.59 m) for FIX-II Test 3025

[[

]]

Figure 5.5-18. Upper Bundle Rod Temperatures (3.30 m) for FIX-II Test 3025

5.6 GIST

The GDCS (Gravity-Drain Cooling System) Integrated Systems Test (GIST) facility was built at the GE Nuclear Energy site in San Jose, California with the objective of demonstrating the performance of the SBWR GDCS for refill of the reactor vessel following a LOCA. The test results and data evaluations were first reported in References 5-17 through 5-19. Five tests from the GIST test matrix were selected for TRACG qualification. The objective of the qualification task is to assess the capability of TRACG to predict the response of the GDCS to the depressurization of the RPV and the concurrent pressurization of the containment in the late blowdown and refill period of a LOCA transient. The qualification consists of comparisons of TRACG calculations of RPV and containment pressures, GDCS flow rate and regional RPV inventories with the corresponding GIST measurements.

5.6.1 GIST Test Facility and Test Matrix

The GIST facility (Figures 5.6-1 through 5.6-3) was based on an early version of the SBWR design that has since evolved into the current ESBWR design. The facility included representations of the basic features of the design that could significantly affect the performance of the GDCS. Specifically, since the containment pressure affects GDCS initiation, the containment drywell and wetwell were simulated in the facility. The focus of the tests was the GDCS system performance and the RPV/containment integrated system response for the low pressure (1.07 MPa and below) range of the LOCA blowdown (Figure 5.6-4).

The GIST facility was a full-height, 1:508 volumetric scale model of the March 1987 SBWR conceptual design [5-17, 5-18]. As depicted in Figures 5.6-2 and 5.6-3, GIST had cylindrical vessels simulating regional volumes of the SBWR with interconnecting piping that was scaled to simulate the Automatic Depressurization System (ADS), the GDCS lines and a range of LOCA conditions, including a Main Steamline Break (MSLB), a GDCS Line Break (GDLB), and a vessel Bottom Drain Line Break (BDLB). Simulated decay heat was supplied to the RPV via electrically heated coils. The GIST facility was well-scaled for simulation of the real-time response of the key LOCA parameters of pressure; temperature, velocity and level change [5-20].

Section 3.4 of Reference 5-18 provides a detailed description of all the GIST facility tests. The tests selected for the TRACG qualification study (Table 5.6-1) represent a spectrum of break types, initial RPV liquid inventories, containment initial conditions and postulated single failures. These tests provide a meaningful challenge to TRACG for prediction of the blowdown rate, the integrated vessel-containment system response, the GDCS response, the vessel reflood and the core thermal-hydraulic response under low pressure natural circulation conditions. Table 5.6-1 lists the key features of each of the tests selected for the TRACG qualification task.

Figure 5.6-4 shows the progression of a typical GIST test. The GIST facility was designed to pick up the SBWR late blowdown transient starting from 1.07 MPa and, accordingly, the initial thermal-hydraulic test conditions in the GIST RPV corresponded to 1.07 MPa. The containment vessels were initialized to pressures and temperatures corresponding to the time at which the RPV pressure reaches 0.79 MPa. This was considered to be the "official" start of the test. The drywell air was purged with steam to simulate the effect of the carryover of noncondensable into the wetwell during the early stages of the blowdown. The RPV blowdown from 1.07 MPa to 0.79 MPa was directed to the atmosphere. During this time interval, the RPV regional water

levels and void fractions adjusted as the system locked in to the SBWR depressurization curve. The blowdown flows through the LOCA and ADS lines were switched from the atmosphere to the drywell and the suppression pool, respectively, when the RPV pressure reached 0.79 MPa. The transition was smooth because there was no change in blowdown area. Subsequent to the opening of the low pressure depressurization valves (DPVs), the head of water in the suppression pool became sufficient to overcome the RPV pressure and open the GDCS check valves. GDCS flow entered the annulus of the RPV and reflooded the vessel.

The key measurements in the GIST tests were the RPV, drywell and wetwell pressures, the collapsed level in the RPV annulus and the GDCS flow rate. The estimated uncertainties in these measurements are shown in Table 5.6-2.

5.6.2 TRACG Input Model for Simulation of GIST Tests

Schematics of the TRACG input model of the GIST facility are shown in Figures 5.6-5 through 5.6-8. The GIST RPV is simulated by the first 16 axial levels of a TRACG VSSL component with one radial ring and one 360-degree azimuthal sector (Figure 5.6-5). Levels 1 through 5 represent the lower plenum and Levels 8 through 10 represent the upper plenum. Levels 6 and 7 have no function other than to provide the axial span between the top and bottom of the heated rod bundle and the bypass. Levels 11 through 15 represent the portion of the downcomer that surrounds the standpipe (chimney) and Level 16 represents the steam dome. The annulus portions of the downcomer in the GIST facility are modeled with 9-cell 1-D TEE components that connect the bottom of the downcomer region of the VSSL component to the lower plenum. The secondary branches of these TEE components provide the entry points for the GDCS lines. The guide tube, bypass and standpipe are modeled with 1-D TEE or PIPE components. The assemblage of electrically heated rods is modeled with a CHAN component that connects to the lower plenum and the bypass at the bottom and to the upper plenum at the top. The GIST RPV wall is modeled as a double-sided heat slab that responds to the fluid and heat transfer conditions on the inside and outside. Heat losses from the RPV to the environment are modeled by specifying an outside heat transfer coefficient calculated from GIST system heat loss data.

The GIST wetwell is simulated with five levels of the TRACG VSSL component. (Figure 5.6-6). This nodalization is adequate to capture the temperature profile in the suppression pool with inflows through the DPVs and the drywell-to-wetwell vents. The GDCS flow is drawn from the bottom level of the wetwell. The upper and lower drywells are modeled with one-dimensional TEE components that provide inflow/outflow junctions for break, vent and vacuum breaker flows. One-dimensional PIPE, TEE and VLVE components are used in various combinations to represent the DPV/steam lines, the GDCS lines, drywell-to-wetwell vents and the vacuum breaker. The configuration of the DPV/steam line and GDCS line components are adjusted, as necessary, to represent the different break types simulated by the GIST TRACG qualification tests. The TRACG representations of the main steamline and the DPV lines for the different break types are shown in Figure 5.6-7. These lines take their flow from the steam dome region (Level 16) of the TRACG VSSL component.

The flow characteristics of the GDCS lines were measured before each of the GIST tests. With a nominal driving head equivalent to 7.01 m of water, the single-line flow rate was 0.082 liters/s. This flow rate was measured at the downstream end of the GDCS line using a 0.0048 m diameter venturi connected through a tube to the 0.011 m inner diameter GDCS line. To calibrate

the flow characteristics of the GDCS lines in the TRACG model, a separate input model representing a single GDCS line was prepared. This model consisted of a VLVE component for the GDCS line and BREK components at the upstream (wetwell) and downstream (annulus) ends to maintain the upstream and downstream pressures. With an appropriate nodalization and choice of the GDCS local line losses, TRACG reproduced the measured flow rate of 0.082 liters/s with a driving head of 7.01 m of water. This nodalization and set of loss coefficients were used for the GDCS line portions of the GIST/TRACG input decks. This calibration does not influence the calculated GDCS initiation time, which is determined by the calculated pressure difference across the GDCS line.

In addition to the GIST facility geometry, the thermodynamic conditions in the system prior to initiation of the transient tests form a part of the GIST/TRACG input model. A set of initial conditions, characterizing the thermodynamic state of each of the GIST vessels, was prescribed for the tests in the qualification matrix. The initial conditions measured by the test facility instrumentation were used to initiate the transient TRACG simulations. These conditions have been summarized for each of the five qualification tests in Table 5.6-3. The data shown in this table can be used directly to prescribe the initial thermodynamic parameters (pressures, temperatures, and liquid, vapor and air inventories) for each of the TRACG cells in the portions of the model that represent the GIST vessels. Initial conditions for the lines interconnecting the vessels were specified by appropriate extensions of the vessel conditions into the adjacent lines. The TRACG simulation followed the startup trajectory of the tests from the initial RPV pressure of 1.07 MPa. in accordance with the procedure described above for the GIST facility.

5.6.3 Results and Discussion

As stated above, five GIST tests were selected for TRACG analysis (Table 5.6-1). It can be seen from Table 5.6-1 that the selected GIST tests provide a comprehensive qualification basis for TRACG. Key variations among the tests include: (1) break location and type (liquid vs. steam); (2) DPV availability; (3) initial vessel inventory and (4) containment pressurization. The qualification tests had the common feature of an assumed failure to open the valve in one of the GDCS lines. Test B01 is the reference MSLB case. It was characterized by a rapid RPV blowdown and inventory loss and is the most limiting break for containment pressure. Test B07 is an MSLB with low initial RPV inventory. It resulted in uncovery and subsequent heatup of the rods simulating the core. Test C01A is a GDLB test. This test has the minimum availability of GDCS - one line broken and a second line unavailable due to valve failure. The flow from the broken GDCS line was discharged into the drywell. Test A07 (BDLB) simulates a small break at the bottom of the RPV and represents the largest LOCA below the elevation of the core. The break flow discharged to the lower drywell. In addition to the failure of one of the GDCS lines, failure to open one of the low-pressure DPVs was assumed. Test A07 is characterized by the slowest blowdown and longest delay in the initiation of GDCS flow. Test D03A is a no-break test with steam discharge through the DPV lines to the suppression pool. The test was run with a high decay heat. With no break, there is no containment back pressure to aid the GDCS flow. Details of the comparisons between the TRACG calculations and the test measurements for the five GIST tests are presented below.

5.6.3.1 TRACG/GIST Comparisons for BDLB LOCA (Test A07)

[[

]]

5.6.3.2 TRACG/GIST Comparisons for Other LOCA Types

[[

]]

5.6.3.3 Margin to Boiling Transition

[[

]]

5.6.4 Conclusions

TRACG calculates the performance of the GIST facility with acceptable accuracy over the range of break sizes and initial conditions tested. The calculations included system pressures, regional inventories of the two-phase fluid within the annulus and core, GDCS onset time and the GDCS flow rate. The key parameters of RPV pressure and core inventory were calculated accurately.

Table 5.6-1
GIST Facility Tests Selected for TRACG Qualification

I	B01 Main Steamline Break	
	A	Rapid RPV Blowdown
	B	Rapid RPV Inventory Loss
II	**B07 Main Steamline Break with Low Water Level**	
	A	Lowest Initial RPV Inventory
	B	Core Uncovery and Subsequent Heatup
III	**C01A GDCS Line Break**	
	A	Minimum Availability of GDCS
	B	Drywell Depressurization
	C	Wetwell-to-Drywell Vacuum Breaker Operation
IV	**A07 Bottom Drain Line Break**	
	A	Slowest Blowdown and Recovery
	B	Largest LOCA Below the Core
	C	No Low Pressure DPVs
V	**D03A No Break**	
	A	No Containment Backpressure to Aid GDCS
	B	High Decay Heat

Table 5.6-2
Measurement Uncertainties for GIST Tests

Measurement	Uncertainty
RPV Pressure	$\pm$ 14 kPa
Drywell Pressure	$\pm$ 7 kPa
Wetwell Pressure	$\pm$ 6 kPa
Annulus Pressure Drop	$\pm$ 0.85 kPa
GDCS Mass Flux	$\pm$ 9.5 kg/m^2-s

Table 5.6-3
GIST Initial Conditions Used in TRACG Input

Test	A07	B01	B07	C01A	D03A
Drywell Pressure (MPa)	0.196	0.198	0.199	0.198	0.101
Drywell Water Level (meters above bottom)	0.132	0.127	0.142	0.140	0.150
Wetwell Pressure (MPa)	0.138	0.150	0.150	0.150	0.101
Wetwell Water Level (meters above bottom)	5.974	5.974	6.014	6.014	5.982
RPV Dome Pressure (MPa)	1.060	1.060	1.057	1.058	1.065
RPV Level (meters above bottom)	8.814	8.636	7.620	8.814	8.814
Available GDCS Lines	3	3	3	2	3
Low-Pressure DPVs Available	No	Yes	Yes	Yes	Yes

INTEGRAL SYSTEM EFFECTS TESTS
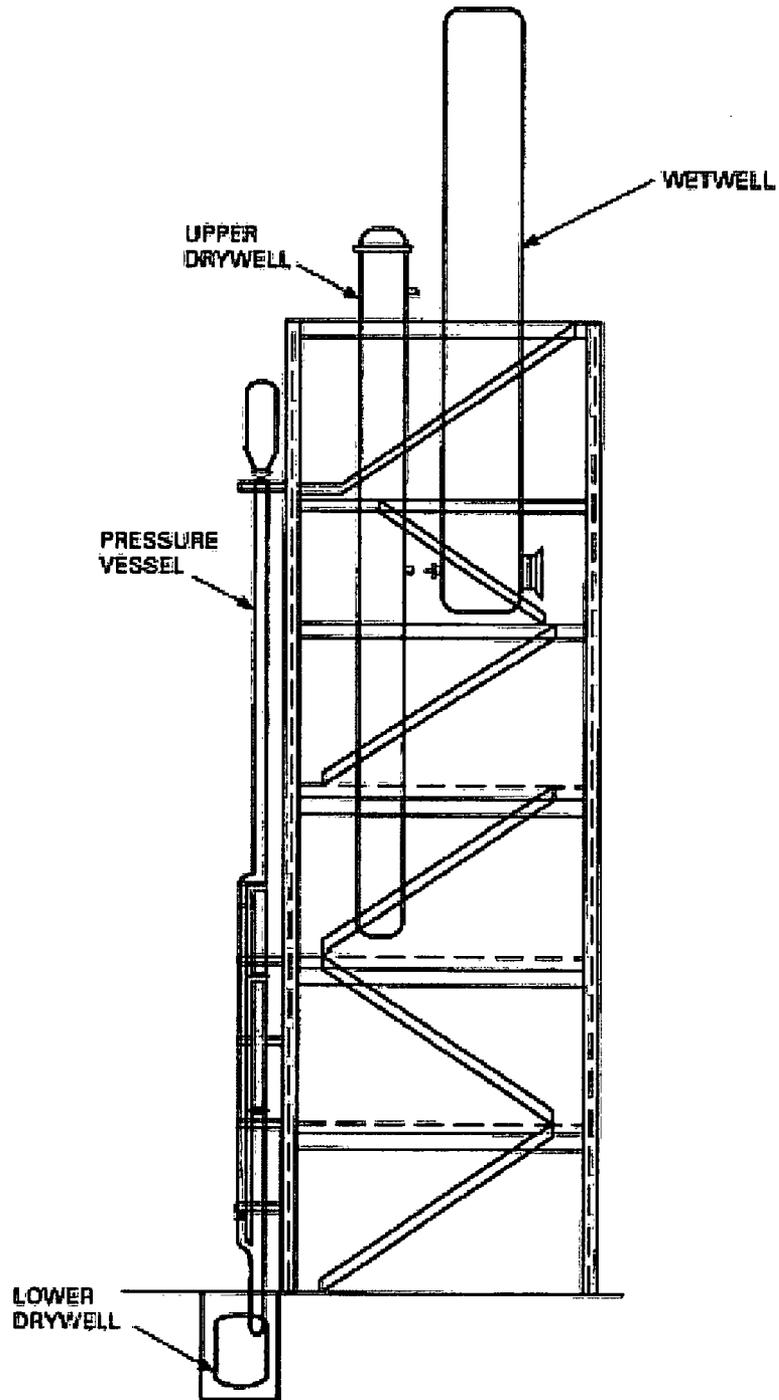
Figure 5.6-1. GIST Facility
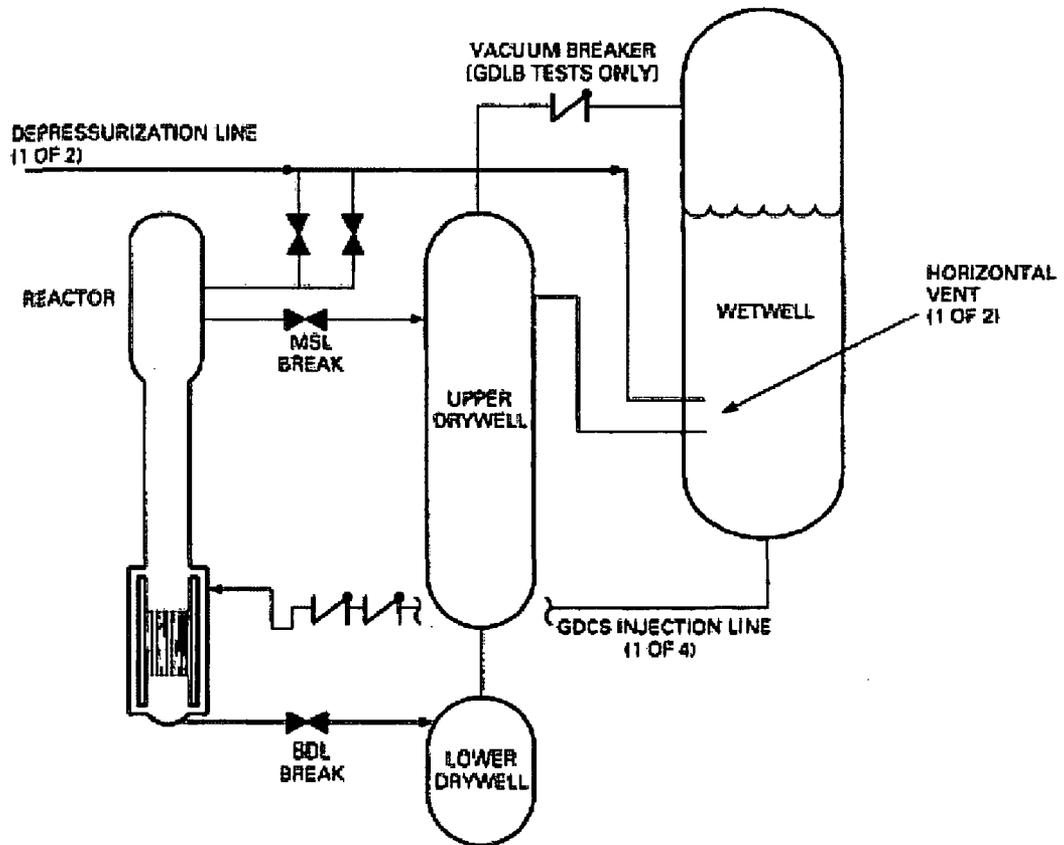
Figure 5.6-2. GIST Facility – Major Flow Paths
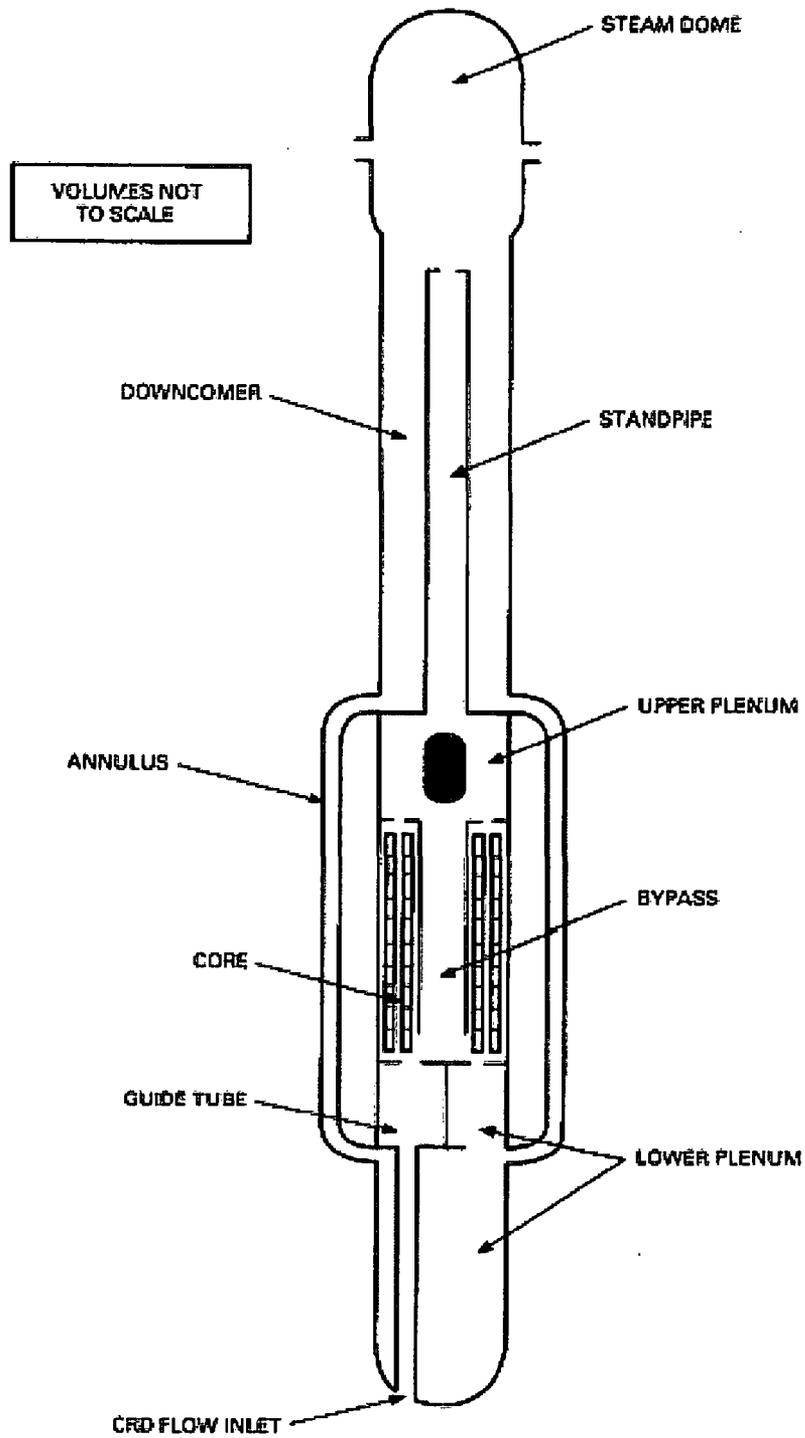
Figure 5.6-3. GIST Facility – Pressure Vessel
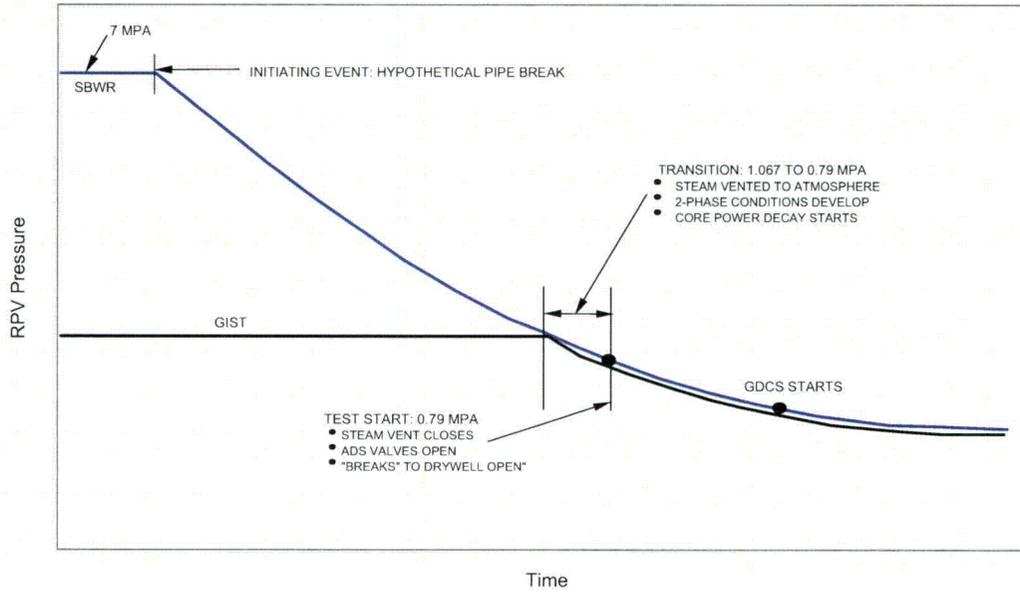
Figure 5.6-4. Schematic Representation of GIST RPV Blowdown
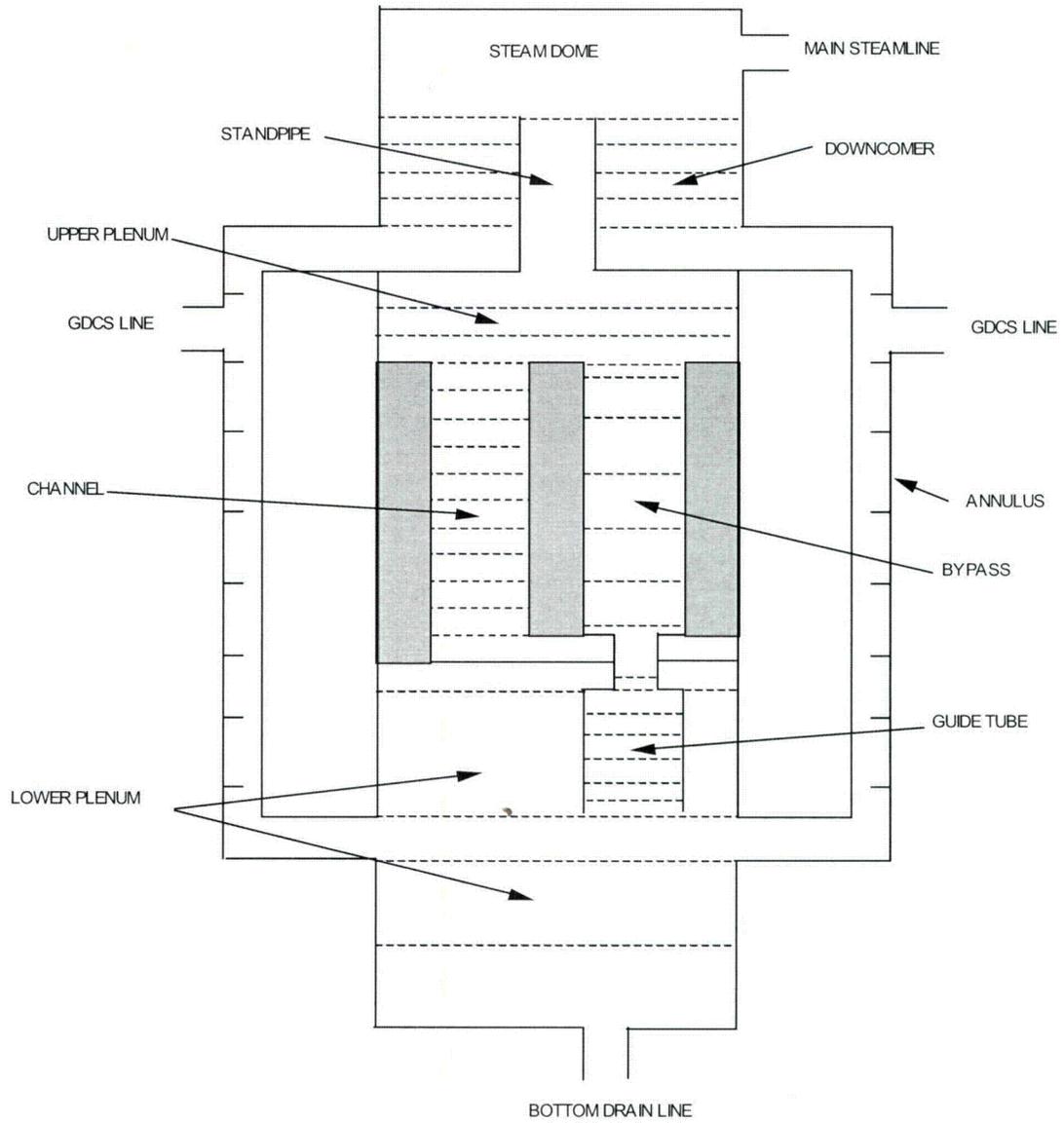
Figure 5.6-5. TRACG Nodalization of GIST RPV
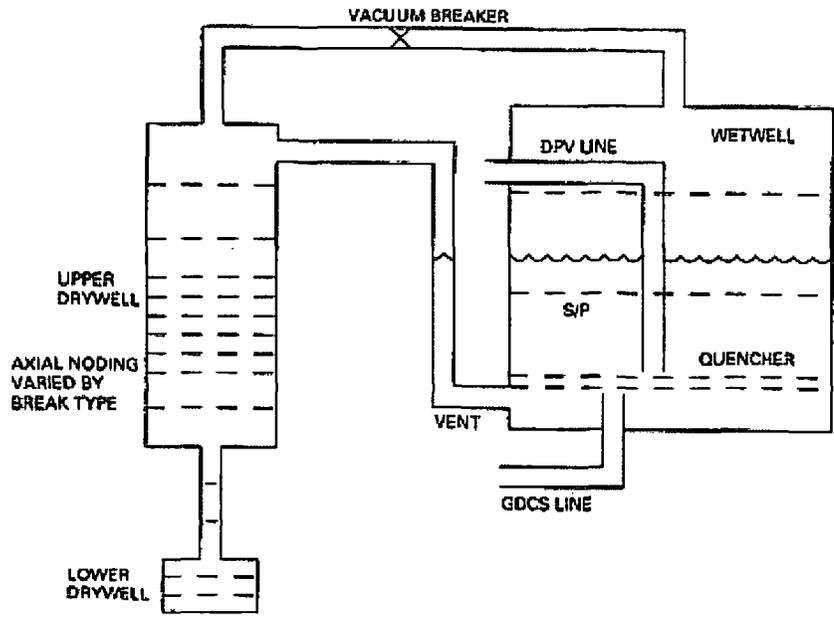
Figure 5.6-6. TRACG Nodalization of GIST Containment
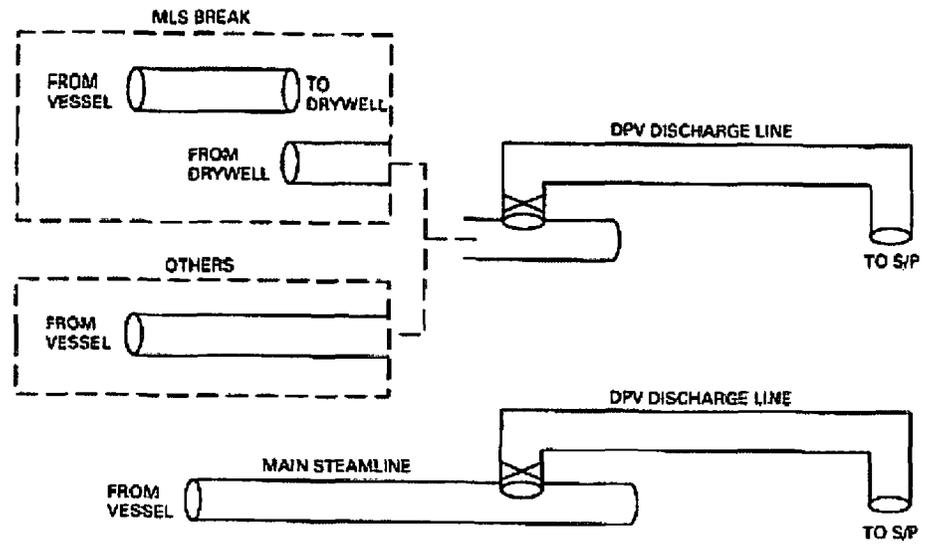
Figure 5.6-7. TRACG Modeling of GIST Steamlines

[[

]]

Figure 5.6-8. Comparison of RPV Pressures (Test A07 - BDLB)

[[

]]

Figure 5.6-9. Comparison of Upper Drywell Pressures (Test A07 - BDLB)

[[

]]

Figure 5.6-10. Comparison of Wetwell Pressures (Test A07 - BDLB)

[[

]]

Figure 5.6-11. Comparison of GDCS Flow Rates (Test A07 - BDLB)

[[

]]

Figure 5.6-12. Comparison of Annulus Pressure Drops (Test A07 - BDLB)

[[

]]

Figure 5.6-13. Comparison of Core Pressure Drops (Test A07 - BDLB)

[[

]]

Figure 5.6-14. Comparison of Bypass Pressure Drops (Test A07 - BDLB)

[[

]]

Figure 5.6-15. Comparison of Standpipe Pressure Drops (Test A07 - BDLB)

[[

]]

Figure 5.6-16. Comparison of RPV Pressures (Test B01 - MSLB)

[[

]]

Figure 5.6-17. Comparison of RPV Pressures (Test B07 – MSLB w/LWL)

[[

]]

Figure 5.6-18. Comparison of RPV Pressures (Test C01A - GDLB)

[[

]]

Figure 5.6-19. Comparison of RPV Pressures (Test D03A – No Break)

[[

]]

Figure 5.6-20. Comparison of GDCS Flows (Test B01 - MSLB)

[[

]]

Figure 5.6-21. Comparison of GDCS Flows (Test B07 – MSLB w/LWL)

[[

]]

Figure 5.6-22. Comparison of GDCS Flows (Test C01A - GDLB)

[[

]]

Figure 5.6-23. Comparison of GDCS Flows (Test D03A – No Break)

[[

]]

Figure 5.6-24. Comparison of Annulus Pressure Drops (Test B01 - MSLB)

[[

]]

Figure 5.6-25. Comparison of Annulus Pressure Drops (Test B07 – MSLB w/LWL)

[[

]]

Figure 5.6-26. Comparison of Annulus Pressure Drops (Test C01A - GDLB)

[[

]]

Figure 5.6-27. Comparison of Annulus Pressure Drops (Test D03A – No Break)

[[

]]

Figure 5.6-28. Comparison of Core Pressure Drops (Test B01 - MSLB)

[[

]]

Figure 5.6-29. Comparison of Core Pressure Drops (Test B07 – MSLB w/LWL)

[[

]]

Figure 5.6-30. Comparison of Core Pressure Drops (Test C01A - GDLB)

[[

]]

Figure 5.6-31. Comparison of Core Pressure Drops (Test D03A – No Break)

[[

]]

Figure 5.6-32. Comparison of Rod Temperatures for Test B07

5.7 REFERENCES

[5-1] W. J. Letzring, Preliminary Facility Description Report for the BD/ECC 1A Test Phase, GEAP-23592/NRC-2, December 1977.

[5-2] D. Seely, and R. Muralidharan, *BWR Low Flow Bundle Uncovery Test and Analysis*, General Electric Company, (GEAP-24964, NUREG/CR-2231, EPRI NP-1781), August 1981.

[5-3] L. S. Lee, G. L. Sozzi and S. A. Allison, *BWR Large Break Simulation Tests – BWR Blowdown/Emergency Core Cooling Program*, Volumes 1 & 2, General Electric Company, (GEAP–24962-1, NUREG/CR–2229, EPRI NP–1783), March 1981.

[5-4] A. G. Stephens, BWR Full Integral Simulation Test (FIST) Program Facility Description Report, (GEAP-22054, NUREG/CR-2576, EPRI NP-2314), December 1982.

[5-5] W. S. Hwang, Md. Alamgir and W. A. Sutherland, *BWR Full Integral Simulation Test (FIST) Phase I Test Results*, (GEAP-30496, NUREG/CR-3711, EPRI NP-3602), November 1983.

[5-6] W. A. Sutherland et al., BWR Full Integral Simulation Test (FIST) Phase II Test Results and TRAC-BWR Model Qualification, (GEAP-30876, NUREG/CR-4128, EPRI NP-3988), October 1985.

[5-7] W. A. Sutherland and W. S. Hwang, *BWR FIST Test and Analysis*, Proceedings of the USNRC 12th Water Reactor Safety Research Information Meeting (NUREG/CP-0058, Vol. 1), October 22-26, 1984, Gaithersburg, Maryland.

[5-8] J. E. Barton et al., *BWR Refill-Reflood Program Task 4.4 – 30° SSTF Description Document*, (GEAP-24939, NUREG/CR-2133, EPRI NP-1584), May 1982.

[5-9] D. G. Schumacher, T. Eckert and J. A. Findlay, BWR Refill–Reflood Program Task 4.4 – CCFL/Refill System Effects Tests (30° Sector) SSTF System Response Test Results, (GEAP–22046, NUREG/CR–2568, EPRI NP-2374), March 1982.

[5-10] J. A. Findlay, BWR Refill-Reflood Program Task 4.4 – CCFL/Refill System Effects Test (30° Sector) Evaluation of ECCS Mixing Phenomena, (GEAP-22150, NUREG/CR-2786, EPRI NP-2542), December 1982.

[5-11] J. A. Findlay, BWR Refill-Reflood Program Task 4.4 – CCFL/Refill System Effects Test (30° Sector) Evaluation of Parallel Channel Phenomena, (GEAP-22044, NUREG/CR-2566, EPRI NP-2373), December 1982.

[5-12] H. Nakamura et al., ROSA-III 200% Double-Ended Break Integral Test Run 926 (HPCS Failure), JAERI-M 84-008, February 1984.

[5-13] Y. Anoda et al., Experiment Data of ROSA-III Integral Test Run 912 (5% Split Break Test without HPCS Actuation), JAERI-M 82-010, February 1982.

[5-14] L. Nilsson and PA Gustafson, *FIX-II – LOCA Blowdown and Pump Trip Heat Transfer Experiments*, Summary Report for Phase 2: Part 1, Studsvik Technical Report NR-83/238, February 1983.

[5-15] L. Nilsson et al., FIX-II – LOCA Blowdown and Pump Trip Heat Transfer Experiments; Experimental Results from LOCA Test No. 5052, Studsvik Technical Report NR-83/323, March 1984.

[5-16] O. Sandervag and D. Wennerberg, , *FIX-II Experimental Results of Test 3025 (ISP-15)*, Studsvik Technical Report NR-83/283, July 1983.

[5-17] J.M. Mross, Final Test Report: Testing of the Gravity-Driven Cooling System for the Simplified Boiling Water Reactor, GE Nuclear Energy, NEDO-31680, July 1989.

[5-18] P.F. Billig, Simplified Boiling Water Reactor (SBWR) Program Gravity-Driven Cooling System (GDCS) Integrated Systems Test - Final Report, GE Nuclear Energy, GEFR-00850, October 1989.

[5-19] Md. Alamgir et al., TRACG prediction of Gravity-Driven Cooling System Response in the SBWR/GIST Facility LOCA Tests, ANS Transactions, 62, pp. 665-668, November 1990.

[5-20] B.S. Shiralkar, et al., *SBWR Test and Analysis Program Description*, NEDC-32391P, Rev. C, August 1995.

6.0 BWR PLANT NODALIZATION

This section describes the details of the standard TRACG nodalization used for BWR plant performance simulations. The description of the standard nodalization is followed by Sections 6.9.1 and 6.9.2 that discuss the nodalization sensitivity of the TRACG calculations for plant transient and LOCA simulations. Deviations from the standard nodalization for specific applications (e.g., adding the capability to simulate various break locations for LOCA analyses) are (or will be) addressed in the appropriate application methodology reports.

The BWR reactor system is represented by a standard set of TRACG components. The reactor components in the BWR TRACG model are:

- Reactor vessel
- Fuel channels
- Guide tubes
- Steam separators
- Steamlines (up to the turbine bypass and stop valves)
- Jet pumps and recirculation loops
- Feedwater lines
- Piping associated with the ECCS
- Control system

The containment structure is not represented for the operating BWR plants. The containment pressure, temperature and heat transfer coefficients on the outside of the reactor vessel are used as boundary conditions for the thermal-hydraulic calculations. For the ESBWR, the containment is part of the overall TRACG model. The basic principles underlying the modeling of the ESBWR containment are described in Reference 6-1. The specific application of these principles to the modeling of the ESBWR containment is described in the ESBWR application LTR [6-2].

The standard BWR nodalization has been developed based on experience from the qualification against separate effects tests (Section 3), the component performance tests (Section 4) and the integral system effects tests (Section 5). As stated above, sensitivity studies supporting the nodalization are documented in Section 6.9. The nodalization described in the subsequent sections is considered adequate for BWR transient and accident analyses. A more detailed nodalization may be used whenever special needs arise.

6.1 REACTOR VESSEL

The reactor vessel is represented by a TRACG three-dimensional (3-D) VSSL component (Figure 6.1-1). The axial nodalization of the VSSL component, described in TRACG convention by the locations of a sequence of level boundaries, is largely dictated by the positions of specific reactor hardware. The refinement of the VSSL axial nodalization used for BWR plant performance simulations is consistent with that used in Section 5 for the simulation of the integral system tests. The relationship between the level boundaries and the corresponding physical locations in the reactor vessel is shown in the following table:

BWR PLANT NODALIZATION   6-1

Table 6.1-1
Locations of Level Boundaries in TRACG VSSL Component

[[	
	]]

The core region is modeled using three radial rings inside the core shroud. The outer core ring includes all of the fuel channels with the more restrictive flow orificing used for the channels near the core periphery. The inner core ring is sized to include the same number of channels as the peripheral ring. The remaining channels are placed in the central core ring. The diameter of each of the three concentric core regions is determined by the number of bundles in the region. The use of three core rings is consistent with the results of SSTF testing (Section 5.3) where three channel flow modes were observed during the refill-reflood portion of a simulated LOCA. Additional studies [6-3] have confirmed that three core rings provide sufficient detail to capture parallel channel phenomena. A fourth (outer) ring is required to represent the reactor downcomer annulus. Typically, the reactor vessel is modeled as a 2-D axisymmetric region by using one $360°$ azimuthal sector. Multiple azimuthal sectors can be used for situations in which the representation of azimuthal asymmetry in the vessel is judged to be important. The leakage loss coefficients between the core and the lower plenum are consistent with the current design methods.

Heat transfer to the vessel structure is modeled using vessel heat slabs. Structures located on cell boundaries such as the core shroud, core support plate or vessel outer wall are modeled as double-sided heat slabs. Structures such as in-core monitor equipment that are contained within a cell are modeled as lumped parameter heat slabs. Heat transfer between the vessel fluid and the structural boundaries of other components with which the vessel communicates (e.g., the fuel channels) is provided by the TRACG component-to-component heat transfer capability.

Table 6.1-2 shows a comparison of the nodalization used for TRACG qualification based on the integral system tests in Section 5 with that used for the BWR plant. It can be seen that the nodalization for the test facilities and the plant are quite similar when the geometrical characteristics of the facilities are taken into account. The minor differences that remain result from the need to capture the locations of specific instrumentation in the test facilities. The similarity of the nodalizations for the integral system test facilities and the BWR plant provides

confidence that the agreement demonstrated between the TRACG calculations and the integral facility test data can be extrapolated to provide confidence in the plant calculations. It may be noted that the number of cells shown for the recirculation line is for the intact loop. Cells are added as necessary to model the breaks for LOCA simulations.

Sensitivity studies supporting the vessel nodalization were conducted in which the number of axial levels, radial regions and azimuthal sectors were varied. Additionally sensitivity studies on the number of nodes in the vessel heat slabs were performed. These studies, described in Section 6.9, demonstrate the adequacy of the standard BWR nodalization.

Table 6.1-2
Comparison of BWR Nodalization with Test Facility Nodalization

	TLTA		FIST		SSTF		ROSA		BWR	
3-D Regions	Rings	Levels	Rings	Levels	Rings	Levels	Rings	Levels	Rings	Levels
Vessel Overall	2	16	2	19	4	14	3	13	[[	
Lower Plenum	2	5	2	6	3	5	3	4		
Bypass	1	5	1	4	3	4	2	3		
Upper Plenum	1	3	1	3	3	4	2	2		
Stand Pipes	1	1	1	2	N/A	N/A	3	2		
Steam Separator	1	1	1	1	N/A	N/A	2	1		
Dryer	N/A	N/A	1	2	N/A	N/A	N/A	N/A		
Steam Dome	2	1	2	1	N/A	N/A	3	1		
Downcomer[a]	1	8	1	10	1	9	1	5		
1-D Components	Cells		Cells		Cells		Cells			
Jet-Pump	6		6		NA		5			
Recirculation Line	15		20		NA		16 + 7[b]			
Separator	1		2		NA		1			
Standpipe	1		5		NA		4			
Channel	26		21		11		14			
Guide Tube	6		6		5		2		]]	

[a] The top of the downcomer is defined as the top of the upper plenum
[b] In the ROSA test facility there are 16 cells in the recirculation line itself; the jet pumps are external to the pressure vessel and the seven additional cells are in the pipe segments connecting the suction inlet (3 cells) and the jet pump discharge (4 cells) to the vessel.

[[

]]

Figure 6.1-1. BWR Reactor Vessel Nodalization

BWR PLANT NODALIZATION

6.2 FUEL CHANNELS

[[

]]

Sensitivity studies supporting the channel nodalization described above were conducted in which the numbers of axial channel cells, rod groups and radial nodes in the fuel rods and channel wall were varied. In addition a sensitivity study was performed on the effect of the

number of channel groups. These studies, documented in Section 6.9, demonstrate the adequacy of the standard BWR channel grouping and nodalization.

[[

]]

Figure 6.2-1. BWR Fuel Channel Nodalization

6.3   CONTROL ROD GUIDE TUBES

[[

]]

6.4   STEAM SEPARATORS

[[

]]

6.5   STEAMLINES

[[

•

]]

A sensitivity study supporting the steam line nodalization was conducted in which the number of cells in the steam line was varied. This study, described in Section 6.9, demonstrates the adequacy of the standard BWR steam line nodalization.

[[

]]

Figure 6.5-1. BWR Steam Line Nodalization

6.6   RECIRCULATION LOOPS

[[

[[

]]

A sensitivity study supporting the recirculation line nodalization was conducted in which the number of nodes in the recirculation line was varied. This study, documented in Section 6.9, demonstrates the adequacy of the standard BWR recirculation line nodalization.

[[

]]

Figure 6.6-1. BWR Recirculation Line Nodalization

6.7   FEEDWATER PIPING

[[

]]

6.8   CONTROL SYSTEMS

[[

• ,

• ,

• ,

• ,

• ,

]]

6.9   SENSITIVITY STUDIES

This section describes two sets of sensitivity studies conducted in support of the standard TRACG BWR nodalization. The sensitivity studies evaluate the impact of variations in the standard BWR nodalization and variations in the time step size and convergence criteria. Separate studies, described below, were conducted for the class of plant transients characterized as AOOs (Anticipated Operational Occurrences) and for LOCAs (Loss-of-Coolant Accidents). Typical scenarios from these two categories were selected and evaluated on the basis of their respective figures of merit, most notably ΔCPR (change in critical power ratio) and PCT (peak cladding temperature).

6.9.1   Sensitivity Studies for AOOs

The sensitivity studies were done for a typical BWR/4 turbine trip without bypass transient. The impact of variations in nodalization and timestep control was evaluated for the transient $\Box$CPR, the minimum water level in the downcomer, the peak vessel pressure and the maximum fuel temperature. The cases executed for the sensitivity study are shown in Table 6.9-1.

Table 6.9-1
Sensitivity Studies for AOOs

[[	
	]]

[[

]]

[[

]]

Figure 6.9-1. Impact of Sensitivity Studies on Minimum Water Level

[[

]]
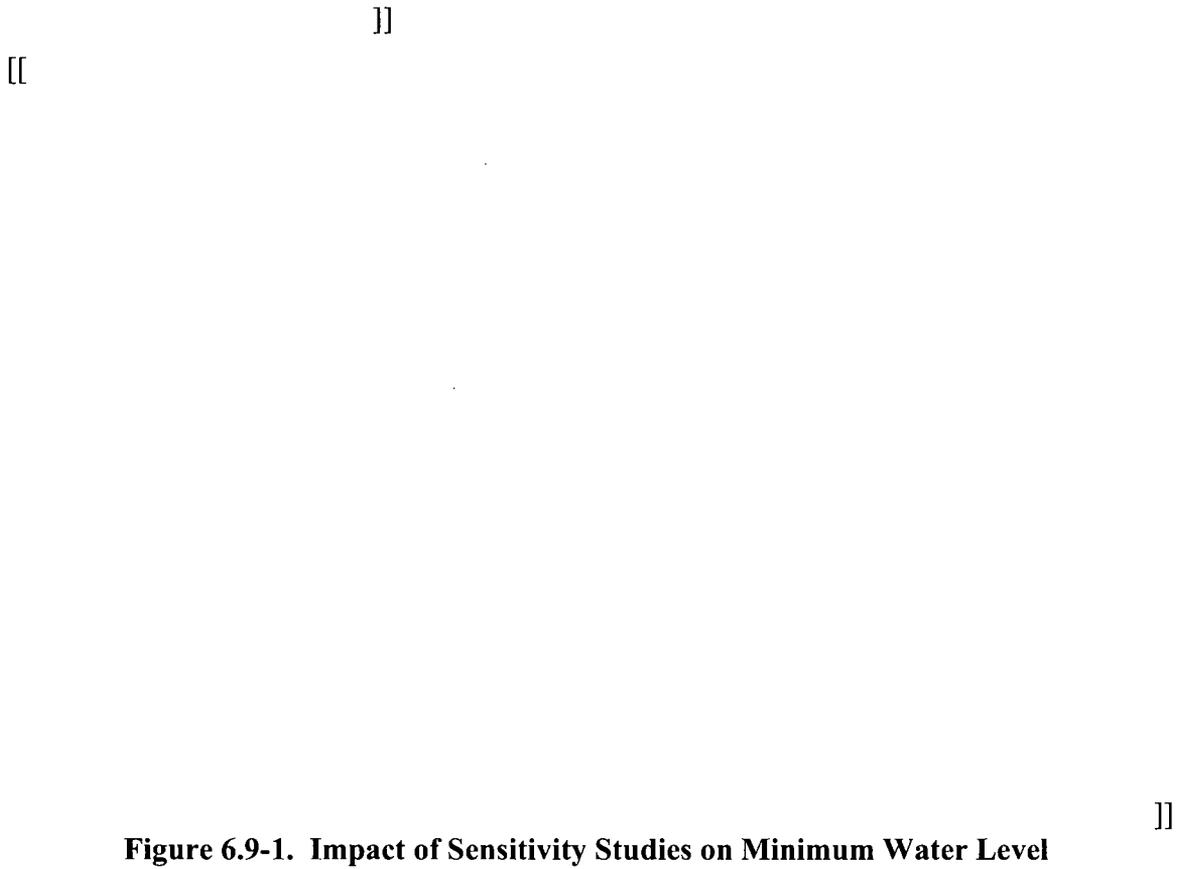
Figure 6.9-2. Impact of Sensitivity Studies on Transient ΔCPR/ICPR

[[

]]

Figure 6.9-3. Impact of Sensitivity Studies on Peak Vessel Pressure

[[

]]

Figure 6.9-4. Impact of Sensitivity Studies on Peak Fuel Temperature Increase

6.9.2 Sensitivity Studies for Loss of Coolant Accident

[[

]]

Table 6.9-2
Sensitivity Studies for ECCS/LOCA

[[	
	]]

[[

]]

Figure 6.9-5. Timestep Sensitivity for BWR/4 Suction DBA

[[

]]

Figure 6.9-6. Nodalization Sensitivity for 1st Peak PCT for Suction DBA

[[

]]

Figure 6.9-7. Nodalization Sensitivity for 2nd Peak PCT for Suction DBA

6.10 REFERENCES

[6-1] J. G. M. Andersen et al., *TRACG Model Description*, NEDE-32176P, Rev. 3, April 2006.

[6-2] B. S. Shiralkar and Y. K. Cheung, *TRACG Application for ESBWR*, NEDC-33083P-A, March 2005.

[6-3] Md. Alamgir, BWR Refill-Reflood Program, Task 4.8: TRAC-BWR Model Qualification for BWR Safety Analysis Final Report, NUREG/CR-2571, 1983.

[6-4] S. P. Congdon, et al., Harmonic Modes of the Neutron Diffusion Equation: Application to BWR Stability, International Workshop on BWR Stability, Brookhaven National Laboratory, October, 1990.

[6-5] Steady State Nuclear Methods, NEDE–30130PA, April 1985.

[6-6] S. Richards (NRC) to G. Watford (GE), Amendment 26 to GE Licensing Topical Report NEDE-24011-P-A, "GESTAR II" - Implementing Improved GE Steady State Methods (TAC No. MA6481), MFN-035-99, November 10, 1999.

7.0 PLANT DATA

The final step in the qualification of TRACG is the comparison to integral BWR plant data. This qualification, when combined with the separate effects, component, and system effects testing in the previous sections, provides an excellent basis for the application of TRACG to BWR plant transient evaluation. The following plant data comparisons are included:

- The simulation of the Peach Bottom turbine trip tests is discussed in Section 7.1. The Peach Bottom tests provide valuable data for comparison of pressure response to a turbine stop valve closure. The effect of the resultant void collapse in the core region and power increase is also assessed.

- The simulation of the Hatch two pump trip test is discussed in Section 7.2. This test provides data for assessment of the level and core flow response to a recirculation pump trip.

- The simulation of the Hatch MSIV closure test is discussed in Section 7.3. This test provides data for assessment of the level and pressure response to a steam line valve closure.

- The simulation of the LaSalle Instability event is discussed in Section 7.4. This event provides an assessment of the prediction of corewide oscillations. The simulation of the transient response of the event is also assessed.

- The simulation of the Leibstadt stability tests is presented in Section 7.5. These tests provide data to assess the prediction of regional oscillation characteristics.

- The simulation of an unplanned transient at the Nine Mile Point-2 reactor that led to a slowly growing power oscillation and a system-initiated scram is presented in Section 7.6. Data from this event are used to assess code capability for the prediction of the observed power oscillation.

- The simulation of four low-flow stability tests conducted at Peach Bottom Unit 2 is presented in Section 7.7. These tests provide a comprehensive data set for assessment of core stability design methods.

- The simulation of the Nine Mile Point 2 Pump Upshift test is discussed in Section 7.8. This test provides data for assessment of the power and flow response to a change in recirculation loop conditions.

- The simulation of the Leibstadt Loss of Feedwater test is discussed in Section 7.9. This test provides data for assessment of the level and pressure response to a loss of coolant inventory.

7.1 PEACH BOTTOM TURBINE TRIP TESTS

Three specially instrumented turbine trip with bypass tests at reduced power level were performed in Unit 2 at the Peach Bottom Atomic Power Station in April 1977 [7-3]. The tests, which were designed to obtain qualification data for transient analysis codes, were sponsored by the Electric Power Research Institute and performed by GE and Philadelphia Electric Company. The test conditions were selected to ensure fuel operation within acceptable design values while maximizing the amount of model qualification data. The main focus of the tests was to obtain high quality test data on the effects of steam line dynamics during rapid pressurization events. The tests were conducted with the direct scram (the scram that would be initiated by the turbine stop valve position switches) disabled so that the scram would initiate on high neutron flux. This departure from the normal reactor operation was required to obtain a sufficiently large neutron flux increase to provide for a meaningful model–data comparison.

7.1.1 Test Summary

The initial conditions and scram setpoints for the three turbine trip test are shown in Table 7.1–1. The initial test conditions were selected in a sequence of increasing power along a rod line near rated core flow. A xenon transient prior to the second test made it necessary to reduce core flow to hold the power to within 1% of the planned power level. A total of 153 signals, as listed in Table 7.1-2, were recorded by a digital data acquisition system. Eighty channels were allocated to record a sample of the total of 172 LPRMs. The total number of viable LPRM signals for each test and the number at each of the four LPRM axial levels are shown in Table 7.1-2.

Figures 7.1-1 through 7.1-3 show comparisons between the initial TRACG axial power shapes calculated by PANAC11 [7-1 and 7-2] and data from two sources in Reference 7-3. One data source is the process computer calculations [7-3; Appendix C]. The second data source is the recorded (viable) LPRM signals [7-3; Section 6 and Appendix D]. The average and ±one-sigma ranges of the LPRM signals at each of the four axial levels are plotted in Figures 7.1-1 through 7.1-3. Before averaging, the raw LPRM signals were calibrated with gain factors that account for the relative importance of each signal to the calculation of the average power at a given elevation. The importance of a raw LPRM signal depends on the location of the instrument and the number of neighboring LPRMs that are also sampled.

Table 7.1-1
Peach Bottom Turbine Trip Test Conditions

| Condition | Core Power | | Core Flow | | Flux Scram Setting |
	(MWt)	(% of Rated)	(kg/s)	(% of Rated)	(% of Rated Power)
Rated	3293	100.0	12,915	100.0	125
TT1	1562	47.4	12,764	98.8	85
TT2	2030	61.6	10,445	80.9	95
TT3	2275	69.1	12,839	99.4	77

PLANT DATA

Table 7.1-2
Peach Bottom Dynamic Test Signals

No. of Signals Recorded	Test Signal Description					
80	Number of Viable Recorded LPRM Signals by Axial Level Test	Total	A	B	C	D
	TT1	76	19	18	20	19
	TT2	75	19	17	20	19
	TT3	74	19	17	20	18
4	APRM Signals					
2	TIP Signals					
4	Jet Pump (Calibrated) ΔPs					
1	Core ΔP					
2	Steamline Nozzle ΔPs					
2	Steamline Nozzle Upstream Pressures					
2	Turbine Inlet Pressures					
1	Reactor Vessel Pressure					
1	Core Exit Pressure					
2	Reactor Feedpump Flows					
1	Reactor Feedwater Temperature					
2	Recirculation Loop Flows					
2	Recirculation Pump Inlet Temperatures					
2	Reactor Water Level					
31	Control Rod Drift Relays					
1	Scram Solenoid Relay					
4	Turbine Stop Valve Position Switches (2 at 10% and 2 at 90%)					
4	Turbine Bypass Valve Position Switches (2 at 10% and 2 at 90%)					
1	Turbine Bypass Position					
4	Turbine Stop Valve Position					

7.1.2 Model Inputs

The TRACG analysis of the Peach Bottom Unit 2 turbine trip tests was performed using the standard BWR/6 plant nodalization scheme described in Section 6. At the time the tests were conducted, there were 576 7x7 and 188 8x8 fuel bundles loaded in the core. The accumulated average core exposure was 12.7 GWd/T. In the TRACG calculations, the bundles were simulated by eight CHAN components. Each CHAN component represented a group of bundles of the same type (i.e., 7x7 or 8x8), similar power and similar radial location (radial ring in the TRACG VSSL component). The bundle groupings varied for the three test simulations as shown in Table 7.1–3. The core power during the transient simulations was calculated using the TRACG 3-D neutron kinetics package. The kinetics model was initialized to a wrap-up file from the GE 3-D BWR Core Simulator [7-1, 7-2] at the initial test conditions. As described above, the initial axial power distributions for the three turbine trip tests are shown in Figures 7.1-1 through 7.1-3.

7.1.3 Data Comparisons

[[

]]

7.1.4 Conclusions

TRACG simulations of three turbine trip tests at Peach Bottom Unit 2 resulted in satisfactory predictions of the reactor pressurization and the neutron flux response. The integrated neutron flux, which is a key variable for the calculation of the MCPR, was accurately predicted. These results provide strong support for the use of TRACG to predict the transient behavior of operating BWRs.

Table 7.1-3
Peach Bottom 2 Turbine Trip Tests Bundle Grouping for TRACG Analyses

[[								
								]]

Table 7.1-4
Neutron Flux Comparisons for Peach Bottom Turbine Trip Tests

[[						]]
						]]

[[

]]

Figure 7.1-1. Peach Bottom Turbine Trip 1 – Initial Axial Power Shape

[[

]]

Figure 7.1-2. Peach Bottom Turbine Trip 2 – Initial Axial Power Shape

[[

]]

Figure 7.1-3. Peach Bottom Turbine Trip 3 – Initial Axial Power Shape

[[

]]

Figure 7.1-4. Peach Bottom Turbine Trip 1 – Fission Power Response

[[

]]

Figure 7.1-5. Peach Bottom Turbine Trip 2 – Fission Power Response

[[

]]

Figure 7.1-6. Peach Bottom Turbine Trip 3 – Fission Power Response

[[

]]

Figure 7.1-7. Peach Bottom Turbine Trips 1, 2 and 3 Integrated Fission Powers

[[

]]

Figure 7.1-8. Peach Bottom Turbine Trip 1 – Average LPRM Responses

[[

]]

Figure 7.1-9. Peach Bottom Turbine Trip 2 – Average LPRM Responses

[[

]]

Figure 7.1-10. Average LPRM Responses by Level for Peach Bottom Turbine Trip 3

[[

]]

Figure 7.1-11. Change in Dome Pressure for Peach Bottom Turbine Trips 1, 2 and 3

7.2 HATCH TWO–PUMP TRIP TEST

The two–pump trip test at Hatch Unit 2 was conducted on November 18, 1978 as one of a series of startup tests. The fuel loading was the GE6 design with an 8x8 lattice consisting of 62 fuel rods and two small water rods. The initial core power and flow rate were 74 and 102% of rated, respectively. The transient was initiated by tripping both recirculation pump motors. The action of tripping the recirculation pumps initiated a specific sequence of events starting with a sharp decrease in core flow. The reduced core flow caused an increase in the core voids and a reduction in power and steam flow. In response, the downcomer water level rose and the feedwater control system reacted by cutting back feedwater flow to reduce the water level. As expected, the level increase caused by the two–pump trip was not large enough to set off a high–level scram.

7.2.1 TRACG Model

The TRACG analysis was performed with the standard BWR plant nodalization scheme described in Section 6. The transient core power was calculated with the TRACG 3–D neutron kinetics package initialized to a wrap-up file from the GE 3–D BWR Core Simulator [7–1, 7-2] at the test conditions. The 560 fuel bundles in the core were represented by [[   ]] TRACG hydraulic channel (CHAN) components. The inputs for the CHAN components were chosen to characterize the thermal–hydraulic behavior of groups of bundles. The bundle grouping was chosen based on bundle power and radial location (Figure 7.2–1). For example, the CHAN20 component was used to represent the 76 low-power peripheral bundles.

7.2.2 Results and Discussion

[[

]]

7.2.3 Conclusions

The following conclusions can be made on the basis of the comparison of TRACG results and test measurements described in Section 7.2.2.

[[

•

]]

[[

]]

Figure 7.2-1. TRACG Channel Grouping for Hatch Two-Pump Trip Test

[[

]]

Figure 7.2-2. Hatch 2 Pump Trip Level Response

[[

]]

Figure 7.2-3. Hatch 2 Pump Trip Total Core Flow

PLANT DATA

[[

]]

Figure 7.2-4. Hatch 2 Pump Trip Fission Power

7.3   HATCH MSIV CLOSURE TEST

The MSIV closure test at Hatch Unit 2 was conducted on June 27, 1979 as one of a series of startup tests following a lengthy outage for plant repairs. As stated in Section 7.2, the fuel loading was the GE6 design with an 8x8 lattice consisting of 62 fuel rods and two small water rods. The initial core power and flow rate were 90.7% and 99.6%, respectively, of their rated values at the time of the test. The transient was initiated by closing the main steam isolation valves (MSIVs). The MSIV closure immediately triggered a scram on valve position. The steamline isolation initiated a rise in the dome pressure due to the reduction in steam outflow from the vessel. The combination of decreasing power and increasing pressure reduced the void fraction in the core and upper plenum. In response, the water inventory in the subcooled downcomer and the saturated bulkwater region inside the shroud head decreased to compensate for the increased liquid content of the core and upper plenum. In addition, the reduced steam flow caused a reduction in the pressure drop through the dryer assembly. The combination of liquid transfer to the core and upper plenum, and decreased dryer pressure drop, substantially decreased the reactor water level outside the separator skirt where the level is measured. When the feedwater sparger was uncovered by the falling level at about 6 seconds, steam quenching by subcooled water occurred and substantially reduced the pressurization rate. The level increased after about 8 seconds due to the continued addition of feedwater.

7.3.1   TRACG Model

As discussed in Section 7.2.1, the TRACG analyses of the Hatch transient tests were performed using the standard plant nodalization scheme described in Section 6. The core power during the transient was calculated by the three–dimensional neutron kinetics package available in TRACG. The kinetics model was initialized to a wrapup file from the GE 3–D BWR Core Simulator [7–1, 7-2] at the test initial conditions.

As in the case of the TRACG simulation of the two-pump trip test (Section 7.2.1), the 560 fuel bundles in the core were represented by [[   ]] hydraulic channel (CHAN) components. The channel grouping was chosen on the basis of bundle power and radial location (Figure 7.3–1) such that each CHAN component characterized the thermal–hydraulic behavior of the corresponding group of bundles. The channel grouping differed slightly from that used for the two-pump trip simulation because of the higher initial power for the MSIV closure test and the corresponding difference in radial power distribution.

The average of the closure times for the eight MSIVs in the Hatch Unit 2 plant is 3.72 s with a standard deviation of 0.33 s. On this basis, a closure time of 3.72 s was used for the TRACG simulation.

7.3.2   Results and Discussion

[[

]]

7.3.3 Conclusions

The following conclusions can be made on the basis of the comparison of TRACG results and test measurements described in Section 7.3.2.

[[

•

]]

[[

]]

Figure 7.3-1. TRACG Channel Grouping for Hatch MSIV Closure Test

PLANT DATA

[[

]]

Figure 7.3-2. Hatch MSIV Closure Dome Pressure Response

[[

]]

Figure 7.3-3. Hatch MSIV Closure Level Response

PLANT DATA

7.4 LASALLE INSTABILITY EVENT

The March 1988 LaSalle–2 instability event [7-5] provided useful qualification data for corewide oscillation stability analysis and plant transient response. The plant conditions at the time of the event are summarized in Table 7.4–1. The reactor was operating at 84% of rated power and 76% of rated flow. The event was initiated by a trip of both recirculation pumps that caused a flow coastdown to natural circulation conditions. The reduction in core flow caused a decrease in the core average power to near 40% and the reduced steam flow caused a reduction in feedwater heating. The reduction in feedwater heating caused the average power to increase to 45% and increased the power peaking at the bottom of the core. Corewide oscillations were detected at approximately 5 minutes following the pump trip and a high APRM scram occurred at about 7 minutes (410 seconds).

The data used to assess the TRACG simulation of the event fall into two categories. The steamline flow, core flow, dome pressure, water level and feedwater flow and temperature were recorded at one-minute intervals over the first six minutes. The second category included continuous recordings of power, core flow, water level and feedwater flow over a one-minute period prior to the scram. Following the event, it was discovered that the feedwater actuator valve had malfunctioned. This is consistent with the large 35-second period swings in feedwater flow observed during the event and the corresponding fluctuations in power, core flow and water level that were recorded during the one-minute period leading up to the reactor scram.

7.4.1 TRACG Model

The TRACG analysis of the LaSalle–2 BWR/5 instability event was performed with the standard plant nodalization described in Section 6. The fuel channel nodalization was modified for stability application by subdividing each of the bottom four heated nodes into four smaller nodes. This modification provides greater resolution of the density wave near the boiling boundary. The channel grouping for the test simulation is shown in Figure 7.4–1. Each of the 764 fuel bundles in the core is assigned to one of eight representative hydraulic channels (CHAN components). The fuel bundles were grouped on the basis of type and power peaking. APRM and LPRM responses were simulated using the TRACG control system to access the 3D power distribution.

[[

]]

7.4.2 Results

[[

]]

7.4.3 Discussion of the Results

[[

]]

7.4.4 Conclusions

The following conclusions can be drawn from the TRACG simulation of the LaSalle instability event:

[[

•

]]

PLANT DATA

Table 7.4-1
Initial Conditions for LaSalle Instability Event

Power (MW)	Flow (kg/s)	Dome Pressure (MPa)	Feedwater Temperature (K)	Feedwater Flow (kg/s)
2801	10332	6.878	478	1460

Table 7.4-1
APRM Comparison

[[		
		]]

[[

]]

[[

]]

Figure 7.4-1. TRACG Channel Grouping for Analysis of LaSalle-2 Instability Event

PLANT DATA

[[

]]

Figure 7.4-2. Reactor Power Prediction without Imposed Pressure Perturbations

[[

]]

Figure 7.4-3. Reactor Power Prediction with Imposed Pressure Perturbations

[[

]]

Figure 7.4-4. APRM Prediction

[[

]]

Figure 7.4-5. Core Flow Comparison

[[

]]

Figure 7.4-6. Dome Pressure Comparison

[[

]]

Figure 7.4-7. Feedwater Temperature Comparison

[[

]]

Figure 7.4-8. Feedwater Flow Comparison

[[

]]

Figure 7.4-9. Steam Line Flow Comparison

[[

]]

Figure 7.4-10. Water Level Comparison

[[

]]

Figure 7.4-11. Detailed APRM Comparison

[[

]]

Figure 7.4-12. Detailed Feedwater Flow Comparison

[[

]]

Figure 7.4-13. Detailed Core Flow Comparison

[[

]]

Figure 7.4-14. Detailed Water Level Comparison

[[

]]

Figure 7.4-15. Core Inlet Temperature Prediction

7.5 LEIBSTADT STABILITY TESTS

The Leibstadt stability tests, conducted during the first cycle of operation, provide Local Power Range Monitor (LPRM) and Average Power Range Monitor (APRM) data during limit cycle regional oscillations at several power/flow conditions. In this section, four of these tests (Tests 4, 4A, 5 and 5A) are analyzed with the objective of evaluating the capability of TRACG to predict the occurrence and characteristics of regional oscillations. The basis for the selection of these four tests is that they provide high quality data for oscillation amplitude. Table 7.5-1 shows the matrix of test conditions. All of the tests were performed at the minimum recirculation pump speed. The key test variables were the position of the flow control valve and the feedwater temperature. Tests 4 and 5 were performed with the flow control valve open and Tests 4A and 5A were performed with the flow control valves at their minimum position. The measured core flows for these two conditions are 31% and 29%, respectively, of the rated core flow. Tests 4 and 4A were performed with normal feedwater temperature and Tests 5 and 5A were performed with a reduced feedwater temperature. Figure 7.5–1 shows a portion of the Leibstadt power/flow map with the four test points indicated. A sample of the LPRM recordings for Test 4, showing the out–of–phase regional oscillation, is presented in Figure 7.5–2.

7.5.1 TRACG Model

[[

]]

7.5.2 Results and Discussion

[[

]]

7.5.3 Conclusions

The following conclusions are supported by the comparison of the results of TRACG simulations of four Leibstadt stability tests with the behavior observed at the plant:

[[

•

]]

Table 7.5-1
Test Conditions

[[						
						]]

Table 7.5-2
TRACG vs. Leibstadt Peak-to-Peak LPRM Amplitude Comparison

[[								]]
								]]

Table 7.5-3
TRACG vs. Leibstadt Peak-to-Peak APRM Amplitude Comparison

[[								
								]]

Table 7.5-4
TRACG vs. Leibstadt Frequency Comparison

[[								
								]]
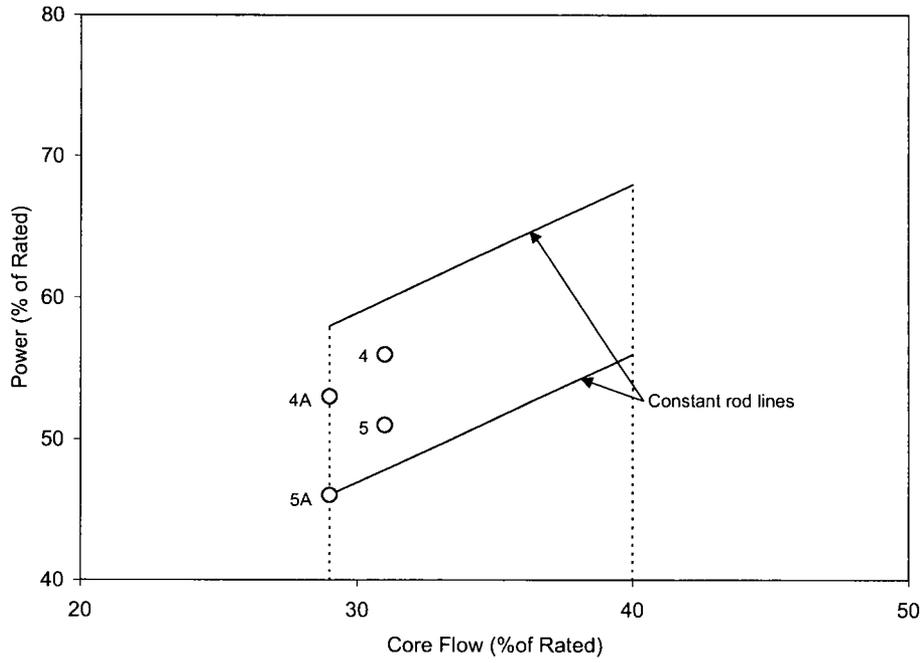
Figure 7.5-1. Power/Flow Test Conditions for Leibstadt Stability Tests

[[

]]

Figure 7.5-2. Sample Leibstadt Regional Oscillation LPRM Test Data

[[

]]

[[

]]

Figure 7.5-3. TRACG Channel Grouping and Radial Peaking for Leibstadt Test 4

[[

]]

Figure 7.5-4. Test 4 Power Response Prediction at 32.5% Flow

[[

]]

Figure 7.5-5. Test 4 Peak LPRM Prediction at 32.5% Flow

[[

]]

Figure 7.5-6. Test 4 APRM Prediction at 32.5% Flow

[[

]]

Figure 7.5-7. Test 4 Peak LPRM Prediction vs. Core Flow

[[

]]

Figure 7.5-8. Test 4 APRM Prediction vs. Core Flow

[[

]]

Figure 7.5-9. Test 4A Peak LPRM Prediction vs. Core Flow

[[

]]

Figure 7.5-10. Test 5 Peak LPRM Prediction vs. Core Flow

[[

]]

Figure 7.5-11. Test 5A Peak LPRM Prediction vs. Core Flow

[[

]]

**Figure 7.5-12. Variation of LPRM Oscillation with Axial Position
for Test 4 at 32.5% Flow**

[[

]]

**Figure 7.5-13. Variation of LPRM Amplitude with Radial Position
for Test 4 at 32.5% Flow**

7.6   NINE MILE POINT-2 STABILITY EVENT

On July 24, 2003, the Nine Mile Point-2 (NMP-2) reactor underwent a transient that included an unplanned flow runback and recirculation pump downshift, accompanied by an adjustment in feedwater temperature, that took the plant from 99.9% to 47.1% of rated power and from 93.3% to 28.0% of rated flow. At these conditions, a slowly growing core instability developed and was subsequently terminated by an Oscillation Power Range Monitor (OPRM) system-initiated scram. The qualification study documented in this section examines the capability of TRACG to predict the power oscillation observed during the NMP-2 instability event.

7.6.1   NMP-2 Stability Detection and Suppression

The NMP-2 plant has implemented the Boiling Water Reactor Owners Group (BWROG) Long Term Stability Solution Option III [7-6]. Under this protocol, the (OPRM) system monitors core power oscillations by real-time processing of a large number of signals, each of which is the average of signals from a number of neighboring LPRM detectors. The set of LPRM detectors used to produce each OPRM signal is referred to as an OPRM cell. The OPRM signals are analyzed by three separate detection algorithms that test for neutron flux oscillations. These algorithms are the Period Based Detection Algorithm (PBDA), the Amplitude Based Algorithm (ABA), and the Growth Rate Algorithm (GRA). Automatic protection is actuated if any one of the three algorithms meets its trip conditions.

The NMP-2 OPRM system uses a configuration (designated 4P) with 4 LPRMs assigned to each OPRM cell. There are 120 OPRM cells with 30 cells assigned to each of four Reactor Protection System (RPS) channels. An RPS channel trip will occur when any OPRM signal in the channel meets its trip condition. The LPRM to OPRM assignment for one of the four NMP-2 RPS channels (Channel 2) is shown in Figure 7.6-1. Along each of 43 plumb-line locations within the core, there is a set of 4 LPRMs at elevations designated A, B, C and D. Typically, Level A is 0.457 m (18 in.) above the bottom of the core and Levels B,C and D are separated from the level below by 0.914 m (36 in.). A 3-digit OPRM notation is used in the discussion that follows. The first digit designates the instrumentation channel (1 to 4) and the second two digits designate the OPRM cell within the channel (01 to 30).

7.6.2   TRACG Simulation of the NMP-2 Instability Event

[[

]]

7.6.3 Results and Discussion

[[

]]

7.6.4 TRACG Sensitivity Studies

[[

]]

7.6.5   Conclusions

[[

]]

Table 7.6-1
Estimated Growth Rate and Frequency of NMP-2 and TRACG OPRM Signals

[[				
				]]

Figure 7.6-1. NMP-2 OPRM Channel 2 Assignment

[[

]]
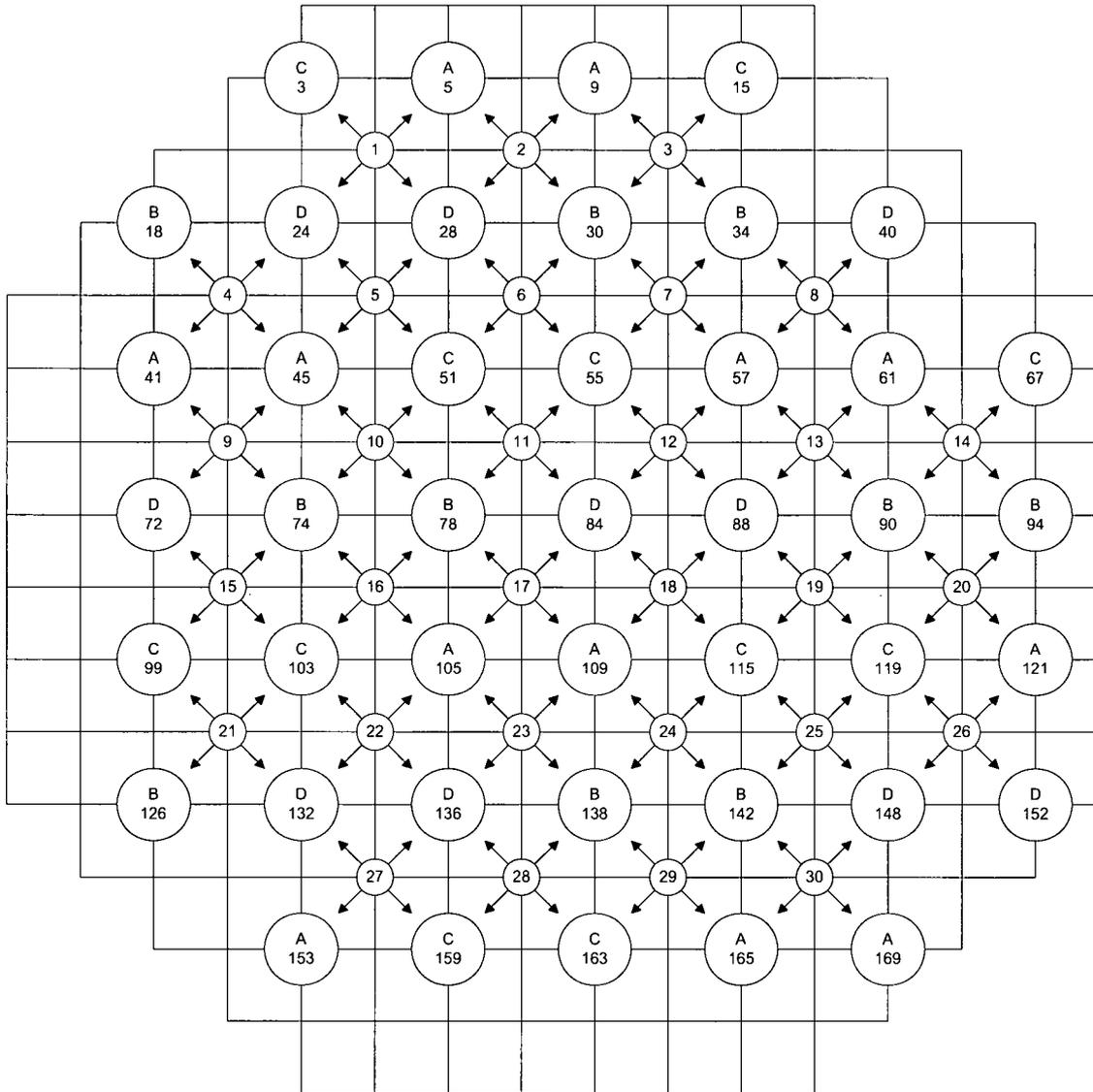
Figure 7.6-2. TRACG Channel Grouping for NMP-2 Stability Analysis
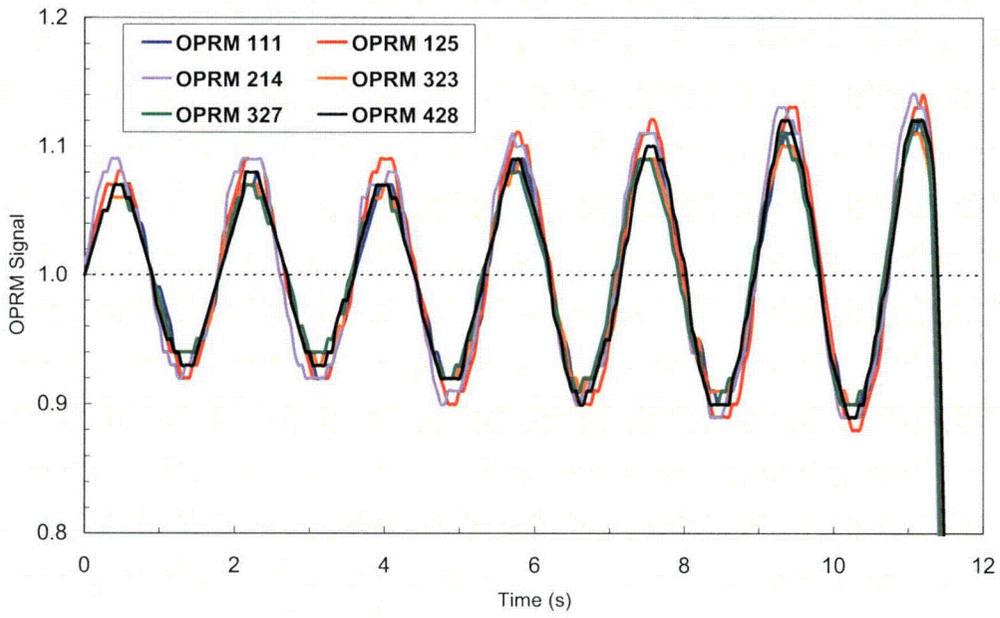
Figure 7.6-3. NMP-2 OPRM Data

[[

]]

Figure 7.6-4. TRACG Core Power

[[

]]
Figure 7.6-5. Comparison of Power Signals from OPRM111

[[

]]
Figure 7.6-6. Comparison of Power Signals from OPRM125

PLANT DATA

[[

]]

Figure 7.6-7. Comparison of Power Signals from OPRM214

[[

]]

Figure 7.6-8. Comparison of Power Signals from OPRM323

[[

]]

Figure 7.6-9. Comparison of Power Signals from OPRM327

[[

]]

Figure 7.6-10. Comparison of Power Signals from OPRM428

[[

]]

Figure 7.6-11. CPR for TRACG Hot Channel (CHAN81)

[[

]]

Figure 7.6-12. Sensitivity of Oscillation Growth Rate to Initial Power

[[

]]

Figure 7.6-13. Sensitivity of Oscillation Growth Rate to Circulation Flow

[[

]]

Figure 7.6-14. Sensitivity of Oscillation Growth Rate to Feedwater Temperature

7.7 PEACH BOTTOM UNIT 2 STABILITY TESTS

Four low-flow stability tests (designated PT1 through PT4) were conducted at Peach Bottom Unit 2 (PB2) at the end of Cycle 2 on April 14, 15 and 16, 1977 [7-3]. The stability tests were performed during the same period as the turbine trip tests (Section 7.1) and, specifically, between Turbine Trip 1 on April 9 and Turbine Trip 2 on April 23. The stability tests were conducted along the low-flow end of the rated power-flow line and along the power-flow line corresponding to minimum recirculation pump speed. The objectives of the stability tests were: (1) to demonstrate that the stability margin of a BWR can be determined by means of small pressure perturbation tests; (2) to increase the data base for qualification of core stability design methods; and (3) to demonstrate safe operation at low flow conditions above the rated power/flow rod line. The reactor core stability margin was determined from an empirical model fitted to transfer function data between the core pressure measurement and the APRM (Average Power Range Monitor) neutron flux signal. Both periodic and pseudo-random binary signals were applied to the pressure regulator setpoint as the input signal. The pseudo-random binary perturbation technique has been found to be an operationally simple and precise technique for measuring BWR core stability margins. The tests demonstrated large stability margins (low decay ratios) for the Peach Bottom 2 Cycle 2 core design. (Note: The discussion in this paragraph and Section 7.7.1 was paraphrased from material in Reference 7-3.)

7.7.1 Test Conditions and Test Results

The operating conditions at which the low flow stability tests were conducted are listed in Table 7.7-1 and the test points are shown on the power-flow map in Figure 7.7-1. The minimum core flow that could be achieved at test conditions PT2, PT3 and PT4 was about 20% of rated recirculation pump speed rather than natural circulation core flow, as originally planned. The experimentally obtained transfer function between the APRM and core pressure was fit to a second order function with one real zero and two complex poles. In the Laplace domain the transfer function is of the form:

$$G(s) = \frac{K_P(\tau_1 s + 1)}{s^2/\omega_1^2 + 2\delta_1 s/\omega_1 + 1}$$

where δ_1 is the damping ratio, ω_1 the natural frequency, K_p the gain and τ_1, by definition, the negative reciprocal of the zero. The decay ratio is then calculated as:

$$\ln DR = \frac{-2\pi\delta_1}{\sqrt{1-\delta_1^2}}$$

Data for resonant frequency, damping ratio and decay ratio are presented in Table 7.7-2 for the four tests.

7.7.2 TRACG Input Model and Analysis Procedure

[[

]]

7.7.3 Results and Discussion

[[

]]

7.7.4 Sensitivity Studies

[[

]]

7.7.5 Channel Decay Ratio

[[

]]

7.7.6 Summary and Conclusion

[[

]]

Table 7.7-1
PB2 Operating Conditions for Stability Tests [7-3]

Test Number	Reactor Power		Core Flow Rate		Core Pressure	Core Inlet Enthalpy
	MWt	% Rated	kg/s	% Rated	MPa	kJ/kg
PT1	1995	60.6	6627	51.3	6.895	1184
PT2	1702	51.7	5418	42.0	6.839	1175
PT3	1948	59.2	4901	38.0	6.929	1158[a]
PT4	1434	43.5	4901	38.0	6.888	1180

[a] Value given in Reference 7-3 (1229 kJ/kg) is believed to be in error as it does not satisfy the reactor heat balance.

Table 7.7-2
PB2 Stability Test Results

Test Number	Closed Loop Resonant Frequency (Hz)	Damping Coefficient	Decay Ratio
PT1	0.44	0.318	0.12
PT2	0.47	0.319	0.12
PT3	0.44	0.168	0.34
PT4	0.40	0.190	0.30

Table 7.7-3
TRACG Channel Grouping for PB2 Core

[[				
				]]

Table 7.7-4
Comparison of TRACG Predictions with Test Data

[[					
					]]

Table 7.7-5
Sensitivity to Form of Applied Pressure Perturbation (Test PT1)

[[				
				]]
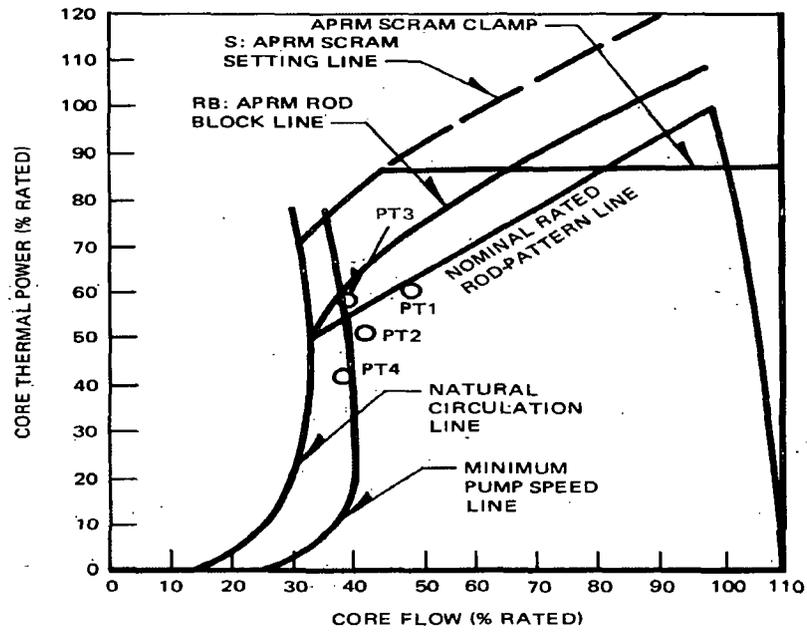
Figure 7.7-1. Test Conditions on PB2 Power/Flow Map [7-3]

[[

]]

Figure 7.7-2. Average Axial Power Shapes for Peach Bottom Stability Tests

[[

]]

Figure 7.7-3. TRACG Power Response to Pressure Perturbation for Test PT1

[[

]]

Figure 7.7-4. TRACG Power Response to Pressure Perturbation for Test PT2

[[

]]

Figure 7.7-5. TRACG Power Response to Pressure Perturbation for Test PT3

[[

]]

Figure 7.7-6. TRACG Power Response to Pressure Perturbation for Test PT4

[[

]]

Figure 7.7-7. TRACG Predictions of Decay Ratio versus Peach Bottom Data

[[

]]

**Figure 7.7-8. Sensitivity of TRACG Power Response
to No. of Channel Groups (Test PT2)**

[[

]]

Figure 7.7-9. TRACG Channel Decay Ratios for Test PT3

7.8   NINE MILE POINT PUMP UPSHIFT TEST

The Nine Mile Point 2 (BWR/5) pump speed upshift test was performed on November 4 1996 [7-7]. The initial core power and flow rates were approximately 30% and 31% of rated, respectively. Nine Mile Point 2 has a two-speed motor that is used in conjunction with a flow control valve to regulate core flow. The initial pump speed in both loops was 25% with pump power supplied by the MG set. The position of the flow control valve was 16.7% open in loop A and 95.6% open in loop B. During the transient the pump speed was changed from the initial value of 25% to high (grid synchronous) speed in loop A. The speed change was accomplished by switching from the 15-Hz MG set power to 60-Hz power from an internal equipment bus. The pump speed in loop B was not changed. The core flow increase was accompanied by a power increase to a maximum of 52% of rated at 15 seconds from the beginning of the transient. The power and flow at the end of the transient were 37% and 44% of rated, respectively.

7.8.1   TRACG Model

[[

]]

7.8.2   Results and Discussion

[[

]]

7.8.3   Conclusion

[[

]]

[[

]]

Figure 7.8-1. Nine Mile Point Cycle 6 Core Loading

[[

]]

Figure 7.8-2. Loop A Pump Speed

[[

]]

Figure 7.8-3. Loop A Flow

[[

]]

Figure 7.8-4. Loop B Flow

[[

]]

Figure 7.8-5. Core Flow

[[

Figure 7.8-6. Core Power   ]]

PLANT DATA

7.9 LEIBSTADT LOSS OF FEEDWATER WITH HPCS UNAVAILABLE TEST

7.9.1 Test Description

The Leibstadt loss of feedwater (LOFW) test was performed as part of a series of plant startup tests. The LOFW test, designated Startup Test Number STP-2001, was performed on October 14, 1984. The initial core loading was entirely made up of GE7 bundles. The GE7 bundle has an 8x8 lattice with two water rods. The initial core power was 3007 MWth (99.8% of rated) and the initial core flow was 8994 kg/s (80.6% of rated). The High Pressure Core Spray (HPCS) system was disabled so that only the Reactor Core Isolation Cooling (RCIC) system and Control Rod Drive (CRD) flow were available to supply makeup water to the reactor pressure vessel (RPV). The test was initiated by simultaneously tripping the two operating feedwater pumps. All level related automatic initiations and actions were allowed to occur normally. The timing of significant events during the test is shown in Table 7.9-1.

7.9.2 TRACG Model

[[

]]

7.9.3 Results and Discussion

[[

PLANT DATA

]]

7.9.4 Conclusions

A TRACG simulation of the Leibstadt loss-of-feedwater test (STP-2001) was performed. Based on the comparisons between the TRACG predictions and the test measurements presented above, the following conclusions can be drawn:

[[

•

]]

Table 7.9-1
Event Timing During Leibstadt Loss-of-Feedwater Test

Event	Time (s)
Level 4 / low feedwater flow recirculation flow control valve runback	6.0
Level 3 scram	14.7
Level 3 recirculation pump trip	16.5
Level 2 RCIC initiation	19.4
RCIC at full flow	42.0

[[

]]

[[

]]

Figure 7.9-1. TRACG Channel Grouping for Leibstadt LOFW Analysis

[[

]]

Figure 7.9-2. Water Volume Added to Bypass by Leibstadt CRD System

[[

]]

Figure 7.9-3. Leibstadt LOFW Short-Term Level Response

[[

]]

Figure 7.9-4. Leibstadt LOFW Long-Term Level Response

[[

]]

Figure 7.9-5. Leibstadt LOFW Feedwater Flow Response

[[

]]

Figure 7.9-6. Leibstadt LOFW RCIC Flow Response

[[

]]

Figure 7.9-7. Leibstadt LOFW Dome Pressure Response

PLANT DATA

[[

]]

Figure 7.9-8. Leibstadt LOFW Sensitivity of Wide-Range Water Level to Decay Heat

7.10 REFERENCES

[7-1]   Steady State Nuclear Methods, NEDE–30130PA, April 1985.

[7-2]   S. Richards (NRC) to G. Watford (GE), Amendment 26 to GE Licensing Topical Report NEDE-24011-P-A, "GESTAR II" - Implementing Improved GE Steady State Methods (TAC No. MA6481), MFN-035-99, November 10, 1999.

[7-3]   Transient and Stability Tests at Peach Bottom Atomic Power Station Unit 2 at End of Cycle 2, EPRI NP-564, June 1978.

[7-4]   R. W. Turkowski and W. Yee, Final Summary Report Edwin I. Hatch Unit 2 Startup Test Results, NEDO-24734, October 1979.

[7-5]   USNRC, AEOD Concerns Regarding The Power Oscillation Event at LaSalle 2 (BWR–5), AEOD Special Report S803, 1988.

[7-6]   C. R. Lehmann et al., Internal Pump Reactor Stability Detect and Suppress Solutions Licensing Basis Methodology for Reload Applications, NEDO-32465-A, August 1996.

[7-7]   Qualification of the One-Dimensional Core Transient Model (ODYN) for Boiling Water Reactors, Supplement 1 – Volume 4, NEDC-24154P-A, Revision 1, February 2000.

8.0 CONCLUSIONS

TRACG has been extensively qualified against data from test facilities and BWR plants. On the basis of the qualification studies documented in this report, the following conclusions can be stated:

- *Separate effects tests*: The performance of the fundamental models and correlations in TRACG has been assessed with reference to a broad spectrum of separate effects tests that directly address the basic thermal-hydraulic and reactor kinetics phenomena in a BWR. The thermal-hydraulic phenomena include interfacial shear and heat transfer, wall friction and heat transfer and density wave propagation. Based on these comparisons, it can be concluded that TRACG simulates the basic BWR thermal–hydraulic and kinetics phenomena very well.

- *Component performance tests*: The performance of TRACG has been assessed with reference to test data from scaled and full-scale BWR components. These components include the jet pump, steam separator, BWR upper plenum and the upper plenum spray distribution. The jet pump, steam separator and upper plenum comparisons justify the conclusion that TRACG simulates the performance of these BWR components very well. The upper plenum spray distribution comparisons support the spray allocation procedure that has been implemented for TRACG LOCA applications.

- *Integral system effects tests*: The performance of TRACG has been assessed with reference to LOCA/ECCS tests from a range of test facilities representing scaled simulations of various BWR product lines. Based on these comparisons, it can be concluded that TRACG simulates the basic phenomena, component interactions and integral system performance with sufficient accuracy to justify its application for transient and accident evaluations in operating and design-stage BWRs.

- *BWR plant tests:* The performance of TRACG has been assessed with reference to transient and stability data from BWR plants. Based on these comparisons, it can be concluded that TRACG simulates the thermal-hydraulic and neutronic phenomena and their interactions with sufficient accuracy to justify its application for evaluations of plant transient and stability performance in operating and design-stage BWRs.

In summary, it can be stated that the TRACG qualification studies documented in this report demonstrate that the code is capable of simulating the thermal-hydraulic and kinetics-related phenomena that govern the behavior of a BWR for steady-state operation, reactor transients, reactor stability and LOCA. In conjunction with the evolving set of TRACG application reports [8-1 through 8-4] the qualification studies support the application of the code to the performance evaluation of a BWR plant for steady-state operation, abnormal operational occurrences (AOOs), ATWS, reactor instability, LOCAs and rod-drop accidents.

8.1 REFERENCES

[8-1]   B. S.Shiralkar and Y. K. Cheung, *TRACG Application for ESBWR*, NEDC-33083P-A, March 2005.

[8-2]   B. S.Shiralkar, L. A.Klebanov and Y. K.Cheung, *TRACG Application for ESBWR Stability Analysis*, NEDE-33083P, Supplement 1, December 2004.

[8-3]   W. Marquino, S. Sitaraman and B. S. Shiralkar, *TRACG Application for ESBWR Anticipated Transient Without Scram Analysis*, NEDE-33083P, Supplement 2, January 2006.

[8-4]   Rod Drop Accident Analysis for KKM, Global Nuclear Fuel 0038-4878 (Class III), June 2005.